

**Investigations of bridged bis(cyclopentadienyl)- and  
pnictogenyl-substituted aluminum compounds**

**Dissertation**

Zur Erlangung des Grades

Des Doktors der Naturwissenschaften

Der Naturwissenschaftlich-Technischen Fakultät

Der Universität des Saarlandes

Von

**Dipl.-Chem.**

**Wasim Haider**

Saarbrücken

2021



Tag des Kolloquiums:	08.06.2022
Dekan:	Univ.-Prof. Dr. Jörn Walter
Berichterstatter:	Dr. André Schäfer Prof. Dr. David Scheschkewitz
Vorsitz:	Prof. Dr. Christopher Kay
Akademischer Mitarbeiter:	Dr. Bernd Morgenstern



*Für Nesrin*



The present dissertation was prepared in the time between Jan. 2017 and Aug. 2020 in the Emmy Noether Junior Research Group Inorganic Chemistry at the Department of Chemistry at the Faculty of Natural Science and Technology at Saarland University under the supervision of Dr. André Schäfer.

Die vorliegende Dissertation wurde in der Zeit zwischen Jan. 2017 and Aug. 2020 in der Emmy Noether Nachwuchsgruppe Anorganische Chemie im Fachbereich Chemie der Naturwissenschaftlich-Technischen Fakultät an der Universität des Saarlandes unter der Anleitung von Dr. André Schäfer erstellt.





بِسْمِ اللَّهِ الرَّحْمَنِ الرَّحِيمِ

وَقَالَ رَبِّ زِدْنِي عِلْمًا



## Abstract

The present work demonstrates the findings on the synthesis and characterization of the first bis(aluminocenophane), which has two  $\eta^5$ -bonded cyclopentadienyl rings and the shortest Al-Al single bond of all acyclic dialanes. Furthermore, the results of donor stabilized aluminocenophane derivatives with different donor ligands as well as different *ansa*-bridging motifs such as sila[2] and carba[1] are presented. The new complexes are characterized in the solid state and in solution. In addition, quantum chemical studies were carried out on these new molecules. The synthesis of bis(aluminocenophane) as well as donor stabilized aluminocenophane derivatives started from the corresponding magnesocenophanes as powerful cyclopentadienyl transfer agents with aluminum(III)halide.

Furthermore, the synthesis of monomeric, dimeric and trimeric pnictogenylalanes and their reactivity towards carbon dioxide is presented. The bonding situations of the monomeric and oligomeric as well as donor-stabilized aminoalane and phosphanylalane could be illuminated by NBO and EDA analysis. Furthermore, the mechanism of the carbon dioxide insertion reaction into the Al-N-, Al-P- and Al-D-bonds could be illustrated.

Since the popular synthesis strategy for ferrocene-containing polymers (ring-opening polymerization) starts from the isolation of the monomer precursor (ferrocenophane), polyferrocenylmethylene (PFM) was previously unknown because carba[1]ferrocenophanes have not been reported. In this thesis, a new synthesis route of polyferrocenylmethylene (PFM) starting from carba[1]magnesocenophane is described. In addition to the characterization of the polymer, a crystal structure of a cyclic hexamer of polyferrocenylmethylene was obtained.



## Zusammenfassung

Die vorliegende Arbeit befasst sich mit der Synthese und Charakterisierung des ersten Bis(aluminocenophans), welches zwei  $\eta^5$ -gebundene Cyclopentadienyl-ringe und die kürzeste Al-Al-Einfachbindung aller acyclischen Dialane aufweist. Darüber hinaus werden donor-stabilisierte Aluminocenophan-Derivate mit unterschiedlichen Donor-Liganden sowie unterschiedlichen *ansa*-Verbrückungsmotiven wie Sila[2] und Carba[1] vorgestellt. Die neuen Komplexe wurden sowohl im Festkörper als auch in Lösung charakterisiert. Darüber hinaus, wurden quantenchemische Untersuchungen zu diesen neuen Molekülen angestellt. Die Synthese des Bis(aluminocenophans) sowie der donor-stabilisierten Aluminocenophan-Derivate gingen von den entsprechenden Magnesocenophanen als gute Cyclopentadienyl-transferreagenzien und Aluminium(III)halogeniden aus.

Außerdem wird die Synthese von monomeren, dimeren und trimeren Pnictogenylalanen und deren Reaktivität gegenüber Kohlenstoffdioxid beschrieben. Quantenchemische Untersuchungen an diesen neuen Molekülstrukturen wurden angestellt. Durch NBO und EDA-Analyse konnten die Bindungssituationen der monomeren und oligomeren sowie donor-stabilisierten Aminoalane und Phosphanylalane beleuchtet werden. Des Weiteren, konnte der Mechanismus der Kohlenstoffdioxid-Insertionsreaktion in die Al-N-, Al-P- und Al-D-Bindungen aufgeklärt werden.

Da die bekannte Synthesestrategie ferrocenhaltiger Polymere (Ringöffnungspolymerisation) von der Isolierung des Monomersprecursors (Ferrocenophan) ausgeht, war die Synthese von Polyferrocenylmethylen bisher unbekannt, da Carba[1]ferrocenophane nicht beschrieben sind. In dieser Arbeit wird ein neuer Syntheseweg für Polyferrocenylmethylen ausgehend von Carba[1]magnesocenophan beschrieben. Neben der Charakterisierung des Polymers wurde auch die Kristallstruktur eines cyclischen Hexamers von Polyferrocenylmethylen erhalten.









## List of Publications

- Lewis base complexes of sila[2]aluminocenophanes; **Wasim Haider**, Volker Huch and André Schäfer, *Dalton Trans.*, 2018, **47**, 10425–10428.
- A bis(aluminocenophane) with a short aluminum–aluminum single bond; **Wasim Haider**, Diego M. Andrada, Inga-Alexandra Bischoff, Volker Huch and André Schäfer, *Dalton Trans.*, 2019, **48**, 14953–14957; (Cover).
- Donor-Stabilized Monocarpa-Bridged Bis(cyclopentadienyl)alanes; **Wasim Haider**, Volker Huch, Bernd Morgenstern and André Schäfer, *ChemistryOpen*, 2020, **9**, 1095–1099; (Cover).
- Magnesocenophane-Catalyzed Amine Borane Dehydrocoupling; Lisa Wirtz, **Wasim Haider**, Volker Huch, Michael Zimmer and André Schäfer, *Chem. Eur. J.*, 2020, **26**, 6176–6184; (Cover).
- Rings and Chains: Synthesis and Characterization of Polyferrocenylmethylene; **Wasim Haider**, Tamara Winter, Alexander Schießer, Volker Presser, Markus Gallei and André Schäfer, *Macromol. Rapid Commun.*, 2021, **42**, 2000738.
- Diarylpnictogenyldialkylalanes – Synthesis, Structure, Bonding Analysis, and CO<sub>2</sub> Capture, **Wasim Haider**, Marces Calvin-Brown, Inga-Alexandra Bischoff, Volker Huch, Bernd Morgenstern, Carsten Müller, Tetiana Sergeieva, Diego M. Andrada, and André Schäfer; (in preparation).



## Acknowledgement/Danksagung

“He who does not thank the people has not thanked Allah”.

Hadeeth

I would like to thank several peoples who had an important influence on my Ph.D. journey. First of all, I am deeply indebted to my supervisor **Dr. André Schäfer**. He made my Ph.D. thesis possible by adopting me scientifically and allowing me to work on interesting projects. I am indebted to him for his excellent supervision and for consistently motivating me to pursue my ideas and conduct my research.

I would like to express my deepest gratitude to **Prof. Dr. David Scheschkewitz**, for being my scientific companion for the past four years, for his patience, and thoughtful review of my work.

A very special thank you goes to my research group colleagues **Carsten Müller**, **Sergej Lauk**, and **Lisa Wirtz** for the very pleasant work atmosphere, meaningful discussions, trusting work relationships, and the barbecue parties. I also had a great pleasure of working with our scientific coworkers **Inga Bischoff**, and **Joshua Warken**.

Moreover, I would like show my appreciation to the research group of **Prof. Dr. Guido Kickelbick** for the outstanding work atmosphere in the lab.

Special thanks to **Pit Ries** and **Alisa Gläser**, whom I was honored to supervise their practical work and for their engagement and diligence. I very much appreciate **Marcus Calvin-Braun** for conducting his successful Bachelor thesis under my supervision. He made my task easy with his dedication, diligence, humor, and curiosity.

I gratefully acknowledge the assistance of **Dr. Volker Huch** and **Dr. Bernd Morgenstern** for the XRD measuring, **Dr. Michael Zimmer** for NMR-measurments, **Bastian Oberhausen** for IR- measurments, and **Susanne Harling** for elemental analysis. Many thanks also to **Susanne Limbach** for her helpfulness in bureaucratic matters.

Certainly, my deep and sincere gratitude to my family for their continuous and unparalleled love, help, and support. I am indebted to my parents for giving me the opportunities and experiences that have made me who I am. This journey would not have been possible if not for them.

Last but not least, my success and the completion of my dissertation would not have been possible without the support and nurturing of my wife **Nesrin Mawas**; thank you and I  
*LOVE YOU.*



## **Content**

List of Abbreviations	1
1. Introduction	4
1.1. Natural Occurrences of Aluminum	4
1.2. Applications of Organoaluminum Compounds	4
1.3. Magnesocenes & Magnesocenophanes	5
1.4. Ferrocenophanes & Ferrocene-based Polymers	11
1.5. Cyclopentadienyl Aluminum Compounds	15
1.6. Dialanes	42
1.7. Amino- and Phosphanylalane	55
<b>2. Motivation</b>	<b>64</b>
3. Results & Discussion	66
3.1. Synthesis and Characterization of Magnesocenophanes	66
3.2. Donor-stabilized Aluminocenophane derivatives	71
3.3. A Bis(aluminocenophane)	86
3.4. Monomeric and Oligomeric Amino- and Phosphanylalanes	100
3.5. Polyferrocenylmethylene	123
<b>4. Summary</b>	<b>132</b>
<b>5. Experimental Details</b>	<b>135</b>
5.1. General Information	135
5.2. Synthesis and Reactivity Studies	137
5.3. Computational Details	195
<b>6. Appendix</b>	<b>203</b>
6.1. List of Compounds	203
6.2. List of Schemes	229
6.3. List of Figures	233

6.1. List of Tables	239
<b>7. References</b>	<b>240</b>

## List of Abbreviations

Ad	1-Adamantyl
Ar	Aryl
BbP	2,6-[(Me <sub>3</sub> Si) <sub>2</sub> CH] <sub>2</sub> -C <sub>6</sub> H <sub>3</sub>
biph	Biphenyl
Bu	Butyl
Cp	Cyclopentadienyl
°C	degree Celsius
CAAC	Cyclic alkyl amino carbene
CV	Cyclic Voltammetry
CVD	Chemical Vapor Deposition
Cp*	Pentamethylcyclopentadienyl
d	Distance
d (NMR)	doublet
D	Donor
Dip	2,4-Diisopropylphenyl
dme	1,2-Dimethoxyethane
dmsO	Dimethyl Sulfoxide
DSC	Differential Scanning Calorimetry
EDA	Energy Decomposition Analysis
Et	Ethyl
g	Gas
g·mol <sup>-1</sup>	gram per mole
h	Hour
sept. (NMR)	Septet
HOMO	Highest Occupied Molecular Orbital
Hz	Hertz
IR	Infrared Spectroscopy

<sup>t</sup> Bu	<i>iso</i> -Butyl
<sup>i</sup> Pr	<i>iso</i> -Propyl
kJ	Kilojoule
LUMO	Lowest Unoccupied Molecular Orbital
MALDI-ToF	Matrix Assisted Laser Desorption Ionization-time of flight
<sup>Me</sup> Cp	Methylcyclopentadienyl
Mes	Mesityl
NBO	Natural Bond Orbital
NHC	N-Heterocyclic Carbene
NMR	Nuclear Magnetic Resonance
Ph	Phenyl
Pm	Picometre
ppm	Part per million
Py	Pyridine
R	Universal Substituent
ROP	Ring Opening Polymerization
r.t.	Room temperature
s (NMR)	Singlet
SEC	Size exclusion chromatography
<i>sec</i> -Bu	Secondary Butyl
Tip	2,4,6-Triisopropylphenyl
TGA	Thermogravimetric Analysis
tmp	<i>Tetra</i> -methylpipyridin
TMEDA	Tetra-methylethylenediamine
thf	Tetrahydrofuran
tmeda	Tetramethylethylenediamine
<sup>t</sup> Bu	<i>Tert</i> -butyl
UV-VIS	Ultraviolet-visible spectroscopy



XRD

X-ray diffraction

### 1. Introduction

#### 1.1. Natural Occurrences of Aluminum

Aluminum is one of the most abundant naturally existing elements on earth's surfaces. In the earth's crust, aluminum is the most prevalent metallic element, and is the third-most abundant of all elements, after oxygen and silicon.<sup>1</sup> Aluminum is a component of most silicate minerals and is primarily sourced from bauxite. Furthermore, aluminum is the twelfth-most common element in the solar system.<sup>2</sup> Therefore, aluminum is a very valuable and available element for a wide variety of investigations and applications.

#### 1.2. Applications of Organoaluminum Compounds

Organoaluminum compounds have many interesting applications in industry. They play an important role in several technical processes like *Ziegler* process, which uses an organoaluminum compound to produce fatty alcohols.<sup>3-6</sup> On the other hand, organoaluminum compounds are utilized not only in the catalysis to polymerize alkenes into plastic product, but also as co-catalyst – for instance, in the oligomerization of ethylene as well as in the olefin metathesis in homogeneous and heterogeneous catalysis.<sup>7</sup>

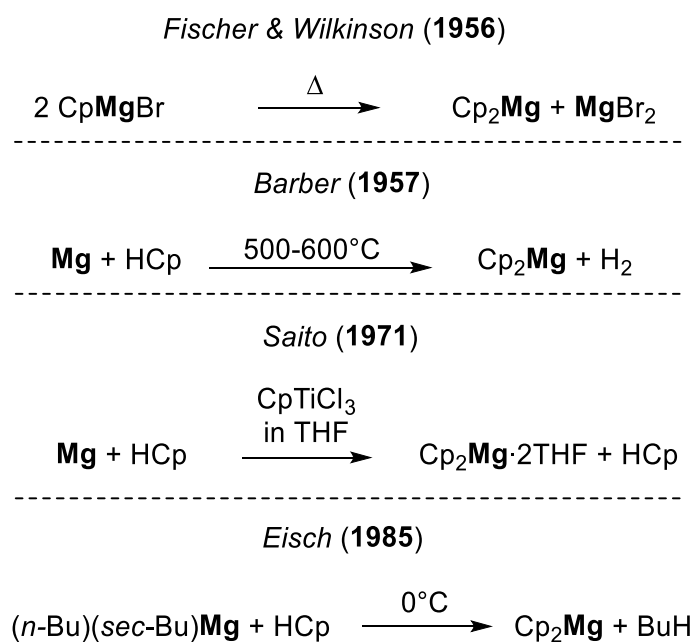
Organoaluminum compounds represent a major ingredient in the synthesis of ceramics which have many applications in different fields. Organoaluminum compounds also have an indispensable role when they are utilized as thin film coating so that they can be applied in different domains like optics,<sup>8</sup> electronics,<sup>9</sup> and mechanics.<sup>10-13</sup>

Since the trivalent organoaluminum compounds are deficient to electron density, these compounds represent Lewis acids, which allows them to be able to form Lewis acid/base adducts with  $\sigma$  donor ligands like  $\text{NR}_3$ ,  $\text{PR}_3$ , and NHCs etc..<sup>14,15</sup> Such complexes have many applications; for instance, in the catalysis of terminal alkynes by hydroalumination and cross-coupling of the derived alanes,<sup>16</sup> in lactide ring-opening polymerization,<sup>17</sup> and the polymerization of Michael-Type monomers.<sup>18,19</sup> The catalysis is not the only application field for these donor-stabilized organoaluminum compounds; however, they are widely used in chemical vapor deposition processes.<sup>20,21</sup>

## 1.3. Magnesocenes &amp; Magnesocenophanes

After the first report of ferrocene by *Kealy* and *Pauson* in 1951, magnesocene was published by *Fischer* and *Wilkinson* independent from each other.<sup>22–24</sup> It took few years until the structure of magnesocene was completely characterized.<sup>25–31</sup>

The synthesis routes of magnesocene were varied over time (Scheme 1). Initially, *Fischer* and coworkers obtained it from the Grignard compound CpMgBr by heating and subsequent sublimation. The second route starts from magnesium metal and cyclopentadiene at 500–600°C.<sup>23,24,27</sup> The third method of synthesizing magnesocene is by utilizing CpTiCl<sub>3</sub> as a catalyst at room temperature instead of heating to 500–600°C as in the second route; and the fourth way, which is currently the most used, is the reaction between cyclopentadiene and dialkylmagnesium such as (*n*-Bu)(*sec*-Bu)Mg or more commonly (*n*-Bu)<sub>2</sub>Mg.<sup>32,33</sup>



Scheme 1: Synthesis of magnesocene 2 via different routes.

In 1956, *Weiss* and *Fischer* determined the structure of magnesocene by radiographic examinations.<sup>25</sup> About twenty years later, in 1975, *Bründer* and *Weiss* determined the exact structure in the crystalline state by single crystal X-ray diffraction so that bonds and distances were defined.<sup>30</sup>

## 1. Introduction

The structure of magnesocene **2** is isotype to ferrocene **1** (Figure 1);<sup>34</sup> the Mg-atom is positioned between the cyclopentadienyl rings which are parallel to each other and possess a staggered conformation, with a Mg-Cp<sub>centroid</sub> distance of 198.1 pm,<sup>30</sup> while the Fe-Cp<sub>centroid</sub> distance is 166.1 pm.<sup>34</sup> The difference in the bond lengths of Mg-Cp<sub>centroid</sub> and Fe-Cp<sub>centroid</sub> probably traces back to the nature of the bonding of Mg/Fe-Cp. The Mg-Cp<sub>centroid</sub> has more ionic character, while Fe-Cp<sub>centroid</sub> has more covalent character with the participation of the iron *d*-orbitals in the bonding, which is not the case in magnesocene.

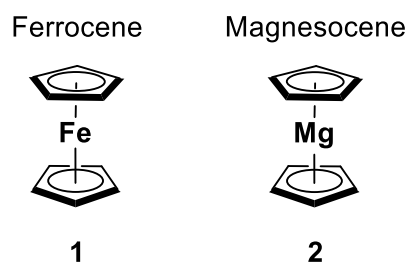
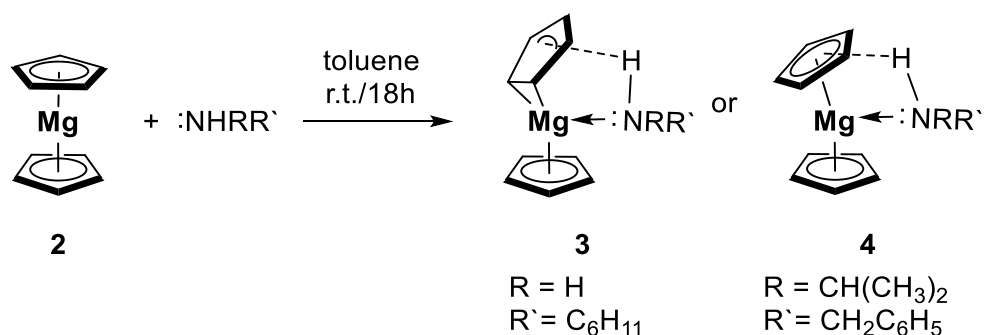


Figure 1: Structures of ferrocene **1** and magnesocene **2**.

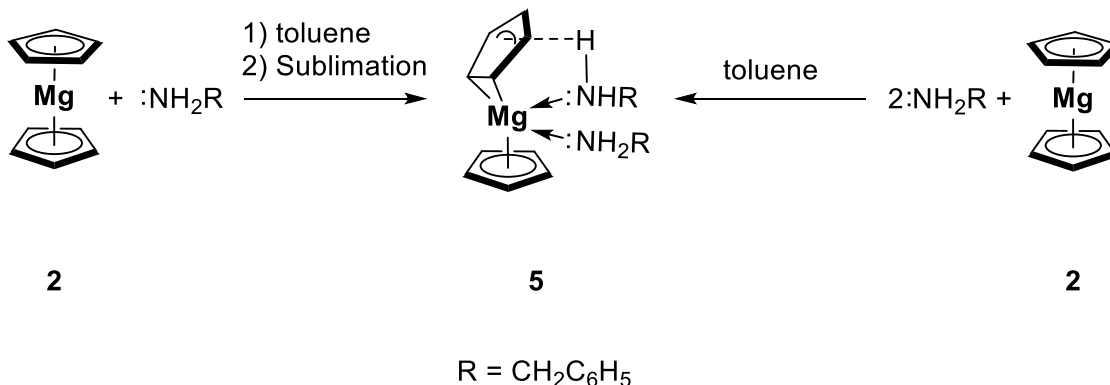
Magnesocene **2** has many properties, thus giving it a broad bandwidth of applications. For instance, the magnesium center possesses a high degree of Lewis acidity that leads to the isolation of Lewis acid/base adducts with different  $\sigma$ -donor ligands like amines. In 2003, *Winter* et al. reported magnesocene amine adducts. These compounds exhibit a ring slippage of the magnesium atom and one of the bonded cyclopentadienyl rings from  $\eta^5$  to  $\eta^2$  in many cases in the solid state (Scheme 2).<sup>35</sup> These complexes exhibit high thermal stability so that most of these adducts can be sublimated, which can be explained by the N-H $\cdots$ C<sub>5</sub>H<sub>5</sub><sup>-</sup> interaction.<sup>35</sup>



Scheme 2: Reactions of magnesocene **2** and different amines to give **3** or **4**.

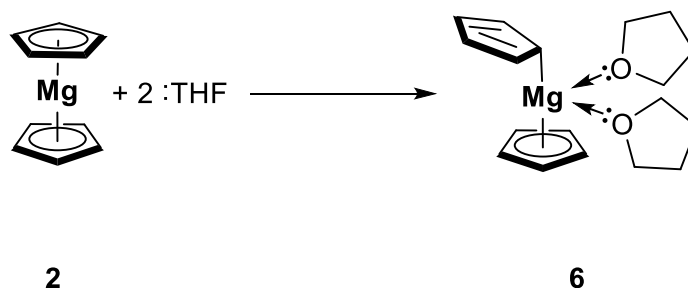
## 1. Introduction

Magnesocene **2** forms with benzylamine a Lewis acid/base adduct that undergoes a ligand exchange by sublimation to give magnesocene **2** and magnesocene bis(amine) complex **5** with  $\eta^5/\eta^2$  bonded cyclopentadienyl rings (Scheme 3).<sup>35</sup>



Scheme 3: Synthesis of **5**.

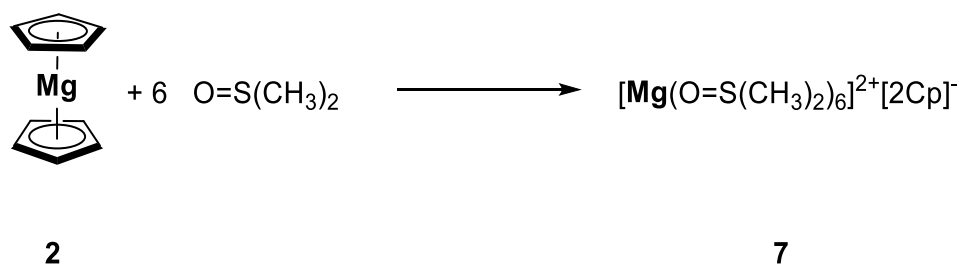
In 2003, *Behrens et al.* demonstrated that magnesocene is able to coordinate two molecules of tetrahydrofuran (thf) **6** with one difference to the structure **5**; one of the cyclopentadienyl ligands is  $\eta^1$  bonded to the magnesium atom in the solid state probably because thf is the stronger  $\sigma$ -donor compared to the benzylamine (Scheme 4).<sup>36</sup>



Scheme 4: Synthesis of **6**.

The reaction between dimethyl sulfoxide (dmsO) and magnesocene **2** afforded an ionic structure with two uncoordinated cyclopentadienyl rings as counterions **7**, which was unknown before in alkaline earth chemistry (Scheme 5). Generating such a complex of magnesium dication illustrates the ionic character of the Mg-Cp bond, making it able to dissociate in a magnesium dication coordinated by six molecules dmsO and two Cp ligands as uncoordinated bare counteranion **7**.

## 1. Introduction



Scheme 5: Reaction of magnesocene **2** with dmsol to give **7**.

Recently, *Wachtler* et al. demonstrated a new application domain for magnesocene **2** as electrolyte in batteries<sup>39</sup>. Because magnesocene **2** dissociates to a certain extent in ethereal solvents like diethyl ether, thf or 1,2-dimethoxyethane (dme) (Figure 2), it became the first example as halide-free electrolyte with an anodic stability average between 1,5 V at platinum and 1,8 V at Mg/Mg<sup>2+</sup>. Furthermore, *Wachtler* et al. proved that this electrolyte is stable for prolong cycling.<sup>37</sup>

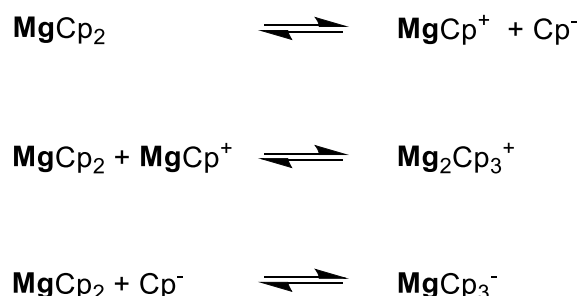
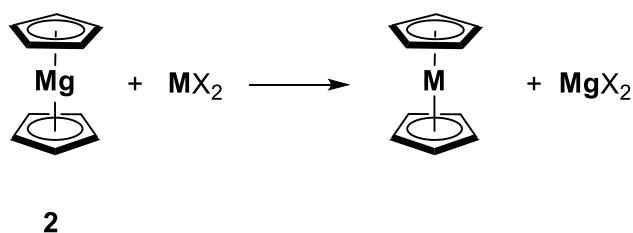


Figure 2: Dissociation of magnesocene **2** in ethereal solution.

Because of this property (low conductivity in ethereal solvent), magnesocene is appropriate as a semiconductor, which makes it applicable as a starting material in CVD and doping processes.<sup>38,39</sup>

Another application is the use of magnesocene in transmetalation reactions depending on the formation of MgX<sub>2</sub> (Scheme 6)<sup>40</sup>. In 1966, *Hull* et al. reported that the formation of MgX<sub>2</sub>, accompanied with a high free energy (supposedly because of lattice energy) makes the metathesis possible – this means that the formation of the magnesium dihalide is the driving force of the reaction.<sup>40</sup>

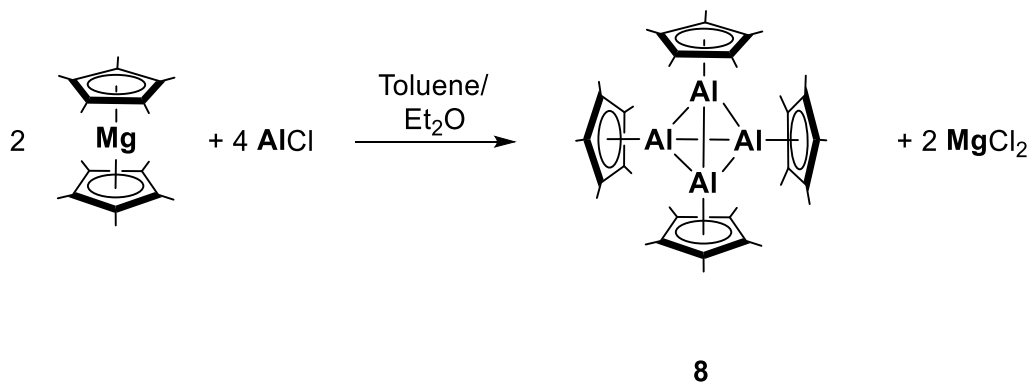
## 1. Introduction



M: transition metal  
X: halide

**Scheme 6: General metathesis reaction of magnesocene **2** as transmetalation reagent.**

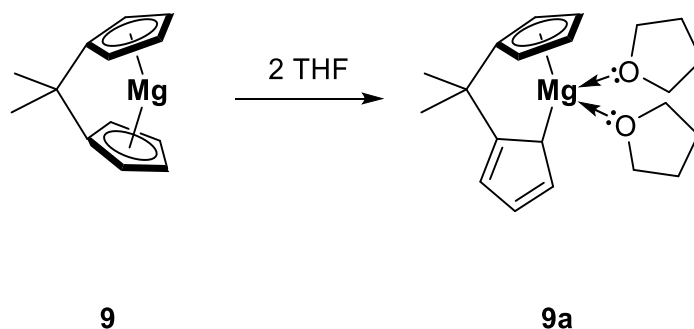
Moreover, the application of magnesocene **2** as a transmetalation agent is not only relevant to the synthesis of metallocenes of transition metals but also to the *p*-block elements such as aluminum. In 1991, *Schnöckel* et al. published the synthesis of low-valent compound **8** starting from Mg(Cp\*)<sub>2</sub> as transmetalation reagent with AlCl<sub>3</sub> in a metathesis reaction (Scheme 7).<sup>41–44</sup>



**Scheme 7: Synthesis of **8** by transmetalation reaction.**

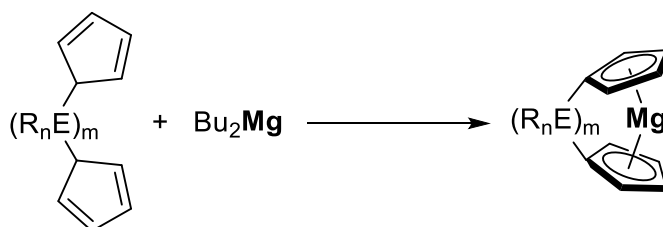
Magnesocene and ferrocene were discovered in the same decade; however, the first reported ferrocenophane was synthesized few years after ferrocene in 1957.<sup>45</sup> On the other hand, the first reported magnesocenophane, carba[1]magnesocenophane **9**, was published by *Burger* et al. and isolated as a Lewis acid/base adduct with tetrahydrofuran (thf) **9a**, in 1997 (Scheme 8).<sup>46,47</sup>

## 1. Introduction



**Scheme 8:** Reaction of the C[1]magnesocenophane 9 with THF to give 9a.

One of the most acquainted synthesis routes of ferrocenophane is the lithiation of ferrocene **1** followed by the integration of the bridge with different motifs as a second step by a salt elimination. On the other hand, the synthesis of magnesocenophane started with the synthesis of the *ansa*-ligand followed by the deprotonation of the ligand as a second step with  $\text{Bu}_2\text{Mg}$  (Scheme 9).<sup>48–53</sup>



**Scheme 9:** General synthesis of magnesocenophanes.

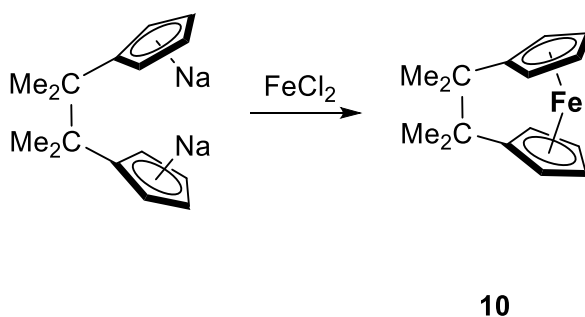
The synthesis route in Scheme 9 is not the only one known; magnesocenophanes with different cyclopentadienyl ligands, as well as different bridges, can be also achieved by nucleophilic addition, or C-C coupling reaction. These results were reported by *Westerhausen* and *Antiñolo*.<sup>54,55</sup>

The main application of the magnesocenophanes is still as Cp transfer reagents in transmetalation reactions mostly throughout the synthesis of metallocenophanes of *d*- or *p*-block elements.<sup>54–56</sup>



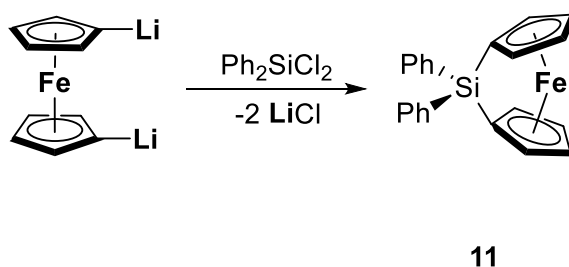
## 1.4. Ferrocenophanes &amp; Ferrocene-based Polymers

The fly-trap approach is a common synthesis route of ferrocenophanes; for instance, compound carba[2]ferrocenophane is synthesized by the treatment of  $\text{Me}_4\text{C}_2\text{Cp}_2\text{Na}_2$  with iron dichloride (Scheme 10), which was reported by *Rinehart Jr.* et al. in 1960.<sup>56</sup>



Scheme 10: Synthesis of the first ferrocenophane 10.

Another main route to synthesize a ferrocenophane involves the salt metathesis of dilithioferrocene with an organoelement dihalide, which was the method used to synthesize the first sila[1]ferrocenophane by *Osborne* in 1975 (Scheme 11).<sup>57</sup>



Scheme 11: Synthesis of ferrocenophane 11.

The metallocenophanes of transition metals have been widely investigated. One of the most essential studied domains is the influence of the linkage between both cyclopentadienyl rings, which can affect the overall geometry and is characterized by different angles (Figure 3).<sup>58</sup>

## 1. Introduction

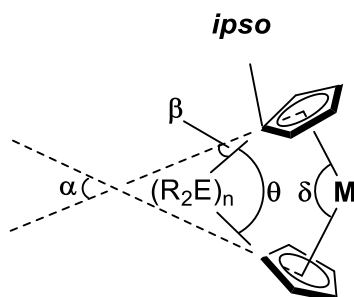


Figure 3: General illustration of a metallocenophane with a definition of the related angles.

The variety in the bridge in metallocenophanes, such as Si, S, P, Al, Ga, can affect the general properties of metallocenophanes due to the variation of the dihedral angle between the two cyclopentadienyl ring units ( $\alpha$  angle). The generation of such a ring-tilted structure not only gives up more sphere to coordinate an additional ligand to the metal center but also increases the Lewis acidity/basicity of the metal center of the metallocenophane.<sup>59,60</sup> However, *Manners* et al. explained in details the influence of the  $\alpha$ -angle on the UV-VIS property of a ferrocenophane. A trend in the disturbance of molecular orbital energies was observed by an increase of the  $\alpha$ -angle which leads to a decrease of the HOMO-LUMO-gap with the tilting of the cyclopentadienyl ligands.<sup>61</sup> Figure 4 shows different [1]ferrocenophanes with the measured  $\lambda_{\max}$  and  $\alpha$ -angle (in the solid state) in comparison to ferrocene.<sup>58</sup>

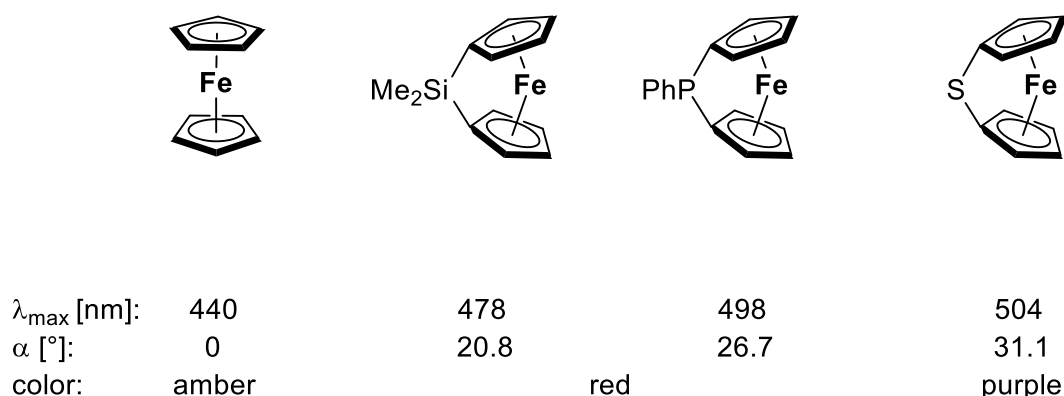


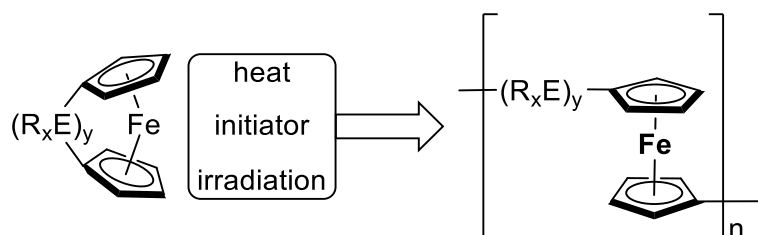
Figure 4: Colors in solution (hexane) of ferrocene and different [1]ferrocenophanes with the corresponding  $\lambda_{\max}$  and  $\alpha$ -angle.

## 1. Introduction

Notably, the size of the  $\alpha$ -angle is related to the ring strain in the ferrocenophane. Thus, the larger the  $\alpha$ -angle becomes (the stronger the cyclopentadienyl rings are tilted), the more ring-strain the system possesses. This is believed to be the reason why the C[1]ferrocenophane is unknown.<sup>50,58,62–64</sup>

Metallocenophanes of transition metals have important applications in homogenous catalysis<sup>59,62</sup> and in material science it has been discovered in the 1990s that ferrocenophanes have high ring strain and undergo ring opening polymerization (ROP) to afford high-molecular-weight ferrocene containing polymers.<sup>65</sup> Such ferrocene containing polymers have attracted much attention because of their diverse applications regarding redox activity, magnetic and catalytic properties, etch resists, self-organized materials, mechanical, electrochemical, opto-electronic, and magnetic properties.<sup>66–80</sup>

For the synthesis of such a ferrocene-based polymer by anionic, cationic, thermal, and transition metal catalyzed ring-opening polymerization (ROP), the isolation of the corresponding ferrocenophane is mandatory.<sup>65,81–91</sup>



**Scheme 12: General ring opening polymerization reaction starting from a strained ferrocenophane.**

For the ROP reactions, many examples of ferrocenophanes are reported in the literature with different motifs in the bridge leading to different properties (Figure 5). The ring opening polymerization is not the only synthetic route for polyferrocene, but it can also be synthesized by polycondensation – for instance, by treating  $PPhCl_2$  with dilithioferrocene to afford a high-molecular-weight of ferrocenylphosphine polymers reported by *Seyferth* et. al in the early 1980s (Scheme 13).<sup>92</sup>

## 1. Introduction

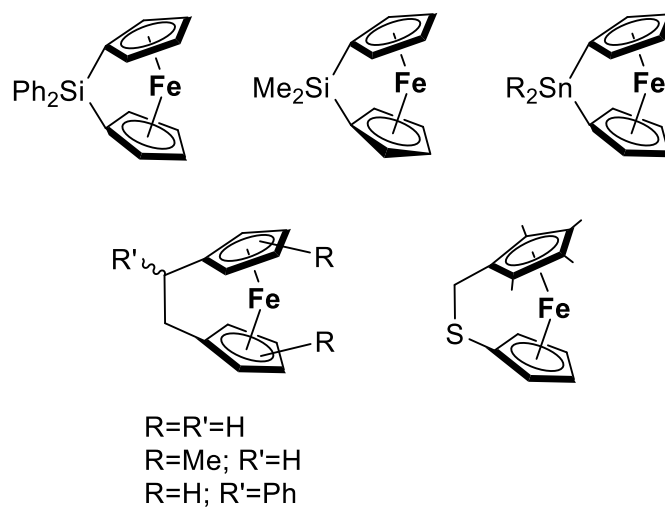
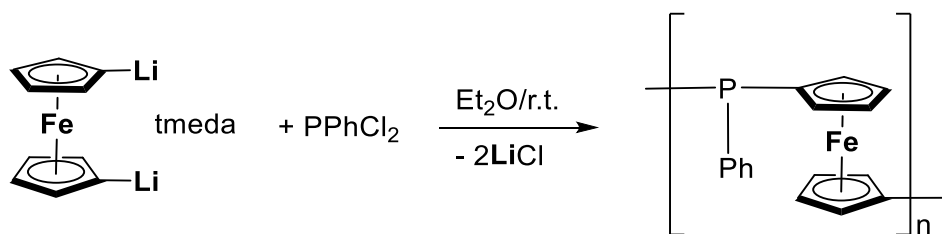


Figure 5: Various examples of different ferrocenophanes that undergo ROP.



Scheme 13: Synthesis of ferrocenylphosphine polymer by polycondensation reaction.

## 1.5. Cyclopentadienyl Aluminum Compounds

The first cyclopentadienyl aluminum compound,  $\text{Et}_2\text{AlCp}$ , dates back to 1961.<sup>93</sup> Since then, this class of compounds has garnered broad attention in organometallic chemistry. The bonding nature between the aluminum atom and the cyclopentadienyl ring is very complex due to the electronic nature of aluminum (*inter alia* the aluminum oxidation state), the variation of bonding arrangements of the cyclopentadienyl ring (the hapticity), and the ability of cyclopentadienyl ligand to build various bonds to the aluminum atom from ionic to  $\pi$ -covalent and  $\sigma$ -covalent; this ability can be influenced by the steric demand of the cyclopentadienyl ligand (Figure 6).<sup>94,95</sup>

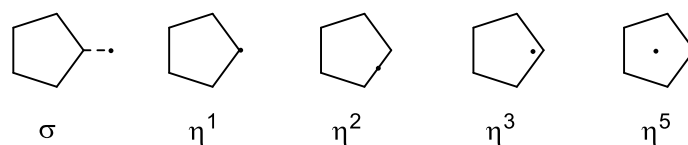


Figure 6: General presentation of the bonding mode between aluminum atom and cyclopentadienyl ligand.

Compared with main group elements, cyclopentadienyl ligands bind to transition metals mostly strong covalently in an  $\eta^5$  fashion.<sup>96–103</sup> There are few examples in transition metal chemistry in which the cyclopentadienyl ligand is not  $\eta^5$  bonded, which can be clarified by the rule of electron-counting.<sup>103</sup> In general, for main group of metals, such uniform electron counting rules do not exist. This is evident when the structures of metallocenium cations of group 13 metals ( $[\text{MCp}_2]^+$ ) are compared in the solid state.<sup>102,104–110</sup> The hapticities of the bonded cyclopentadienyl ligands differ from  $\eta^5/\eta^1$  in case of boron to  $\eta^5/\eta^5$  in case of aluminum and  $\eta^1/\eta^3$  in case of gallium (Figure 7).

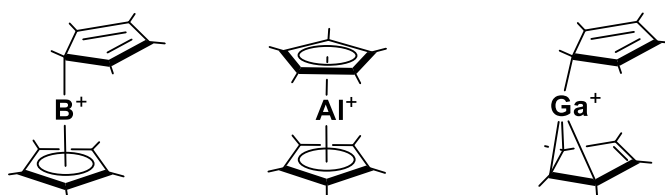


Figure 7: Structures of the metallocenium cations of boron, aluminum and gallium.

## 1.5.1. Mono Cyclopentadienyl Aluminum Compounds

In  $\sigma$ -bonded cyclopentadienyl compounds of transition metals and main group elements,<sup>111,112</sup> sigmatropic rearrangements can occur. The migration of the element around cyclopentadienyl ligands is described by many authors and was discussed in details by *Sergeyev and Abel* in 1973, *Larrabee* in 1974, *Cotten* in 1975, *Spangler* in 1976 and summarized by *Jutzi* in 1986.<sup>113–118</sup>

*Jutzi* elucidated that the fluxional behaviour occurring in cyclopentadienyl compounds of main group elements are influenced by (i) the nature of the main group element, (ii) the substituents at the main group element, (iii) the other bonded substituent to the cyclopentadienyl ligand or the steric demand of the cyclopentadienyl ligand<sup>127</sup>. This sigmatropic rearrangement can be identified by NMR, IR and Raman spectroscopy in solution and by X-ray crystal structure analysis in the solid state.<sup>119–121</sup> The influence of the main group element on the isomer ratio in  $C_5H_5E$  (E: main group element) compounds can be highlighted in two different sigmatropic processes, which may arise in these compounds (Figure 8).

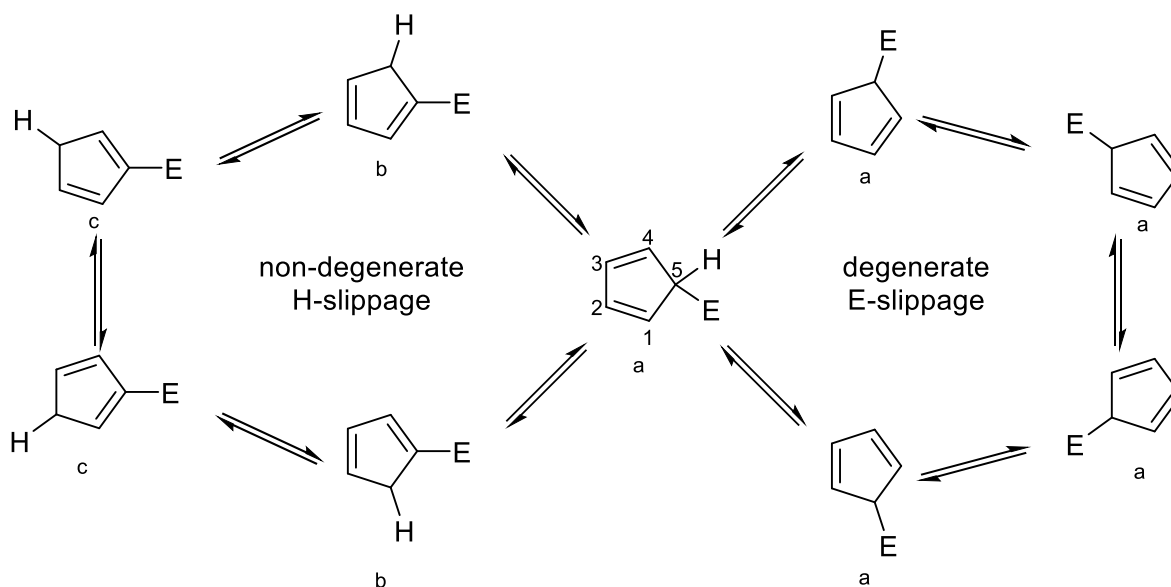


Figure 8: The dynamic sigmatropic rearrangement process in  $C_5H_5E$  compounds.

## 1. Introduction

The first process is a non-degenerate 1,2-slippage of the hydrogen, which is related to 1,5-sigmatropic rearrangement, accompanied by the formation of isomers where the element is located either allylic (a) or vinylic (b, c) to the cyclopentadienyl ring. The second process is a degenerate 1,2-slippage of the element moiety accompanied by the formation of one structure where the element is allylic (a) positioned. From the dynamic of these processes, three situations can be derived regarding the thermodynamic data of the investigations taking into account both 1,2 H and 1,2 E slippages (Figure 9):

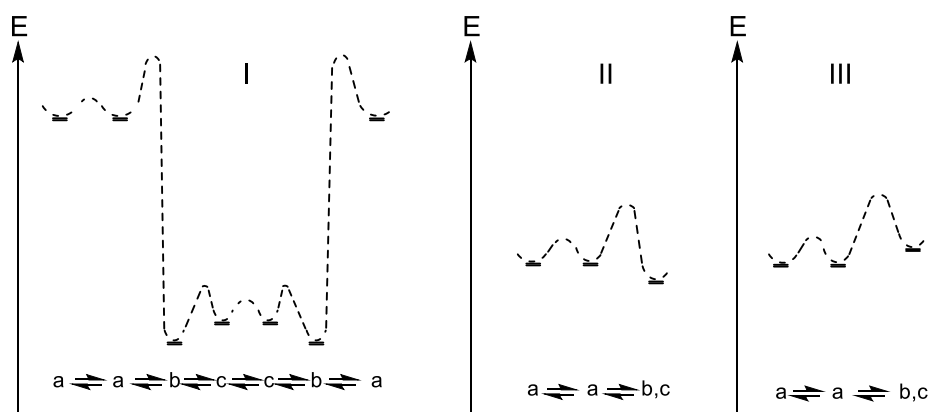


Figure 9: Representation of energy of the sigmatropic rearrangement in  $C_5H_5E$  compounds.

Situation I: the energy of allylic isomer (a) is clearly higher than the vinylic (b, c) because of the strong back-bonding from the vinylic  $\pi$  system into a vacant orbital at the main group element. Furthermore, the activation energy of 1,2-H slippage is higher than the activation energy of 1,2-E slippage. An example for this is  $CpBMe_2$ .<sup>122</sup>

Situation II: the vinylic and the allylic isomers are nearly energetically similar. The vinylic isomer could be energetically preferred when the bonded metal moiety possesses an electron-acceptor character. The degenerate and non-degenerate slippages have almost the same activation energies; nevertheless, the rate of 1,2-E slippage is higher than the rate of 1,2-H slippage in most cases. This is the typical behaviour for all cyclopentadienylsilanes and has been studied in details for  $CpSiMe_3$ .<sup>123–125</sup>

Situation III: energetically, the situation III looks like situation II with one difference: the activation energy of 1,2-H slippage is higher than the activation energy of 1,2-E slippage. Accordingly, only the highly fluxional allylic isomers are observable under normal conditions. This behaviour has been proven by X-ray crystallography in many compounds such as  $CpAlMe_2$ ,  $CpGaMe_2$  and  $CpPbPh_3$ .<sup>121,126,127</sup>

## 1. Introduction

As mentioned before, the first reported cyclopentadienyl aluminum compound was a monocyclopentadienyl diethylaluminum by *Giannini & Cesca* in 1961 (Figure 10).<sup>93</sup> They suggested a dimeric structure with two bridging ethyl groups and  $\sigma$ -bonded cyclopentadienyl rings.

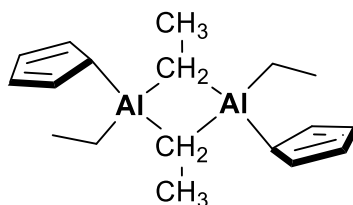
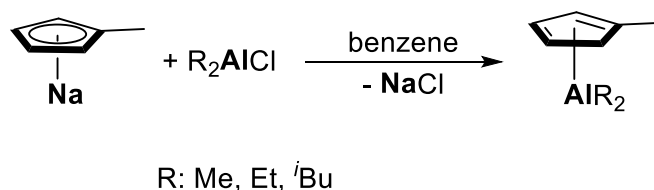


Figure 10: Presentation of the dimeric structure of  $\text{Et}_2\text{AlCp}$  as suggested by *Giannini & Cesca*.

In 1969, *Kroll et al.* reported an NMR study of cyclopentadienyldialkylaluminum compounds ( $\text{R}_2\text{AlCp}$  with  $\text{R} = \text{Me}, \text{Et}$  and  $i\text{Bu}$ ) and displayed that only one signal for the protons in the Cp-ring for all compounds is detected in  $^1\text{H}$  NMR spectra contrary to the suggestion of *Gianinni*.<sup>128</sup> Furthermore, even at  $-91^\circ\text{C}$  only one signal is detected in  $^1\text{H}$  NMR spectra. One explanation for that is a rapid 1,2- or 1,3-rearrangement, which means that the activation energy for this rearrangement process must be very low. Thus, such a migration of aluminum atom around the ring according to  $^1\text{H}$  NMR data is postulated by *Kroll et al.* for the first time for non-rigid behaviour of organoaluminum compounds containing a cyclopentadienyl ligand.<sup>128</sup>

In order to collect more information about the stereochemically non-rigid organoaluminum compounds containing cyclopentadienyl ligand, *Kroll* investigated new mono substituted cyclopentadienyl dialkylaluminum compounds with the form  $\text{R}_2\text{Al}^{\text{Me}}\text{Cp}$  ( $\text{R} = \text{Me}, \text{Et}, i\text{Bu}$ ;  $^{\text{Me}}\text{Cp}$ : methylcyclopentadienyl ligand) (Scheme 14) at the end of 1969. He hoped that the methyl group bonded to the cyclopentadienyl ring would slow down the rearrangement so that it could be observed on the  $^1\text{H}$  NMR time scale and make the solubility of these compounds in the non-polar solvent higher so that the  $^1\text{H}$  NMR study in low temperature will be better detected.<sup>129</sup>



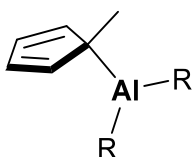
Scheme 14: Synthesis of compounds  $\text{R}_2\text{Al}^{\text{Me}}\text{Cp}$  ( $\text{R} = \text{Me}, \text{Et}, i\text{Bu}$ ).



## 1. Introduction

The  $^1\text{H}$  NMR spectrum of the  $\text{R}_2\text{Al}^{\text{Me}}\text{Cp}$  with  $\text{R} = \text{Me}$  displayed one signal for all four cyclopentadienyl protons and one signal for the cyclopentadienyl bonded methyl group at room temperature. However, upon cooling a solution of this compound in toluene- $d_8$  to  $+10^\circ\text{C}$  a splitting of the signal of the cyclopentadienyl protons into two singlets (1:1) was observed. Further cooling to  $-40^\circ\text{C}$  only led to broadening the signals. Analogous  $^1\text{H}$  NMR results were detected by *Fritz* et al. in cases of tetramethylcyclopentadienyl stannane and triethylmethylcyclopentadienyl plumbane at ambient temperature.<sup>130,131</sup> These NMR results as well as the high electron density at the carbon carrying the methyl group as an electron-donating group can be interpreted as arguments for a static structures of the tetramethylcyclopentadienyl stannane and triethylmethylcyclopentadienyl plumbane.

In case of  $\text{R}_2\text{Al}^{\text{Me}}\text{Cp}$ , there are two indicators against a static structure as to be seen in Figure 11. Namely, the cyclopentadienyl bonded methyl group signal showed no changing in the  $^1\text{H}$  NMR spectrum upon cooling of the investigated sample to  $+10^\circ\text{C}$ ; and the broadening of the signals of cyclopentadienyl protons and the methyl group protons signals bonded to aluminum atom upon cooling of the investigated sample to  $-40^\circ\text{C}$  indicated a dynamic behaviour.



$\text{R} = \text{Me}, \text{Et}$

**Figure 11: A static structure of  $\text{R}_2\text{Al}^{\text{Me}}\text{Cp}$  ( $\text{R} = \text{Me}, \text{Et}$ ) analogous to the suggestion of *Fritz* for stannane and plumbane based on V T- $^1\text{H}$ -NMR.**

In 1972, *Haaland* and *Weidlein* argued, according IR and Raman spectroscopy investigations, that the structure of  $\text{CpAlMe}_2$  in the solid state includes  $\pi$ -bonded cyclopentadienyl rings and has a  $\text{D}_{5h}$  symmetry.<sup>120</sup> They also showed evidence against a methyl group bridged dimer structure or a  $\sigma$ -bonded cyclopentadienyl ligand. Furthermore, they suggested a polymeric structure (Figure 12) throughout a  $\eta^5$  bonded cyclopentadienyl ligand to aluminum atom in the solid state, which is known for main group cyclopentadienyl compounds such as  $\text{PbCp}_2$  and  $\text{InCp}$  compounds.<sup>132,133</sup> *Haaland & Weidlein* also suggested that the polymer existed in solution and in gas phase as monomeric and oligomeric structures maintaining the  $\pi$ -bonded cyclopentadienyl ring.<sup>120</sup>

## 1. Introduction

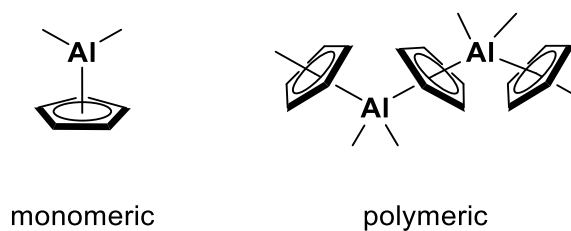
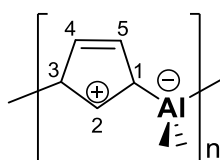


Figure 12: Suggested structures of  $\text{Me}_2\text{AlCp}$  as monomer and polymer by *Haaland* and *Weidlein*.

One year later, *Haaland & Drew* demonstrated, by electron scattering pattern from the gaseous monomeric  $\text{Me}_2\text{AlCp}$ , models with  $\eta^1$  ( $\sigma$ -bond) or  $\eta^5$  ( $\pi$ -bond) bonded cyclopentadienyl ligands.<sup>134</sup> Using CNDO/2 calculations, the internal rotation barrier of cyclopentadienyl ring is of the order of  $20.9 \text{ kJ}\cdot\text{mol}^{-1}$  and the perpendicular distance between the aluminum atom and the Cp-ring is  $210.0 \text{ pm}$ , the C-C bond in the ring is  $142.2 \text{ pm}$  and the distance of Al-C(Me) is  $195.2 \text{ pm}$ .

In 1982, *Oliver et. al.* elucidated the structure of cyclopentadienyl dimethylaluminum in the solid state by crystal structure.<sup>121</sup> *Oliver et al.* demonstrated the structure of  $(\mu\text{-Cp})\text{AlMe}_2$  consisting of a cyclopentadienyl-bridged polymer in the solid state without an interaction between chains (Figure 13). The chain consists of dimethylaluminum groups bridged by cyclopentadienyl rings. The distance of the Al-C in the dimethylaluminum unit is  $195.9$  and  $194.7 \text{ pm}$ , which is characteristic for terminal alkyl groups bonded to aluminum atom,<sup>135</sup> with a C-Al-C angle of  $121.8^\circ$ . The aluminum carbon bond distances to both  $\sigma$  bonded cyclopentadienyl rings are not of equal length indicating that one bond suffers an electron deficiency. The C-C bond distances in the cyclopentadienyl ring exhibit one short distance  $\text{C}_4\text{-C}_5 = 135.6 \text{ pm}$  suggesting a double bond and two pairs which are substantially identical. *Oliver* tends to a localized interaction for this compound in the solid state.



12

Figure 13: Structure of  $[(\mu\text{-Cp})\text{AlMe}_2]_n$  12 in the solid state as cyclopentadienyl bridged polymeric.

## 1. Introduction

As mentioned above, the electronic situation of the aluminum atom actually influences the bonding mode to the cyclopentadienyl ligand. According to this fact, *Schnöckel* et. al revolutionized the cyclopentadienyl aluminum chemistry by synthesizing an aluminum(I) compound containing a pentamethylcyclopentadienyl ligand (Scheme 7).<sup>41-44</sup> This important compound was synthesized by the reaction of low valent  $\text{AlCl}^{136}$  with decamethylmagnesocene to yield pentamethylcyclopentadienyl aluminum(I) **8** which was isolated as a tetramer in the solid state in which the aluminum atoms built a tetrahedron with a  $\eta^5$  bonded pentamethylcyclopentadienyl ligands coordinated to each aluminum atom. Every two bonded  $\text{Cp}^*$  ligands ( $\text{Cp}^*$ : pentamethylcyclopentadienyl ligand) are parallel to each other with a  $\text{Al}-\text{Cp}^*_{\text{centroid}}$  distance of  $d_{\text{max}} = 203.2 \text{ pm}$ ,  $d_{\text{min}} = 199.7 \text{ pm}$ ,  $d = 201.5 \text{ pm}$ ;  $\text{Al}-\text{Al}$ -distances of  $d_{\text{max}} = 277.3 \text{ pm}$ ,  $d_{\text{min}} = 276.7 \text{ pm}$ ,  $d = 276.9 \text{ pm}$  and an  $\text{Al}-\text{Al}-\text{Al}$ -angle of  $60.1^\circ$ . The  $^{27}\text{Al}$  NMR spectrum at room temperature displayed one signal around  $-80.8 \text{ ppm}$  with  $\omega_{1/2} = 170 \text{ Hz}$ . *Schnöckel* et al. also demonstrated an equilibrium related to temperature (Figure 14) so that at high temperature the existing structure was the monomer **8a** which is detectable by  $^{27}\text{Al}$  NMR with a shift at  $-150 \text{ ppm}$  with  $\omega_{1/2} = 180\text{-}100 \text{ Hz}$  and forms tetramer **8** at room temperature.<sup>43,44</sup>

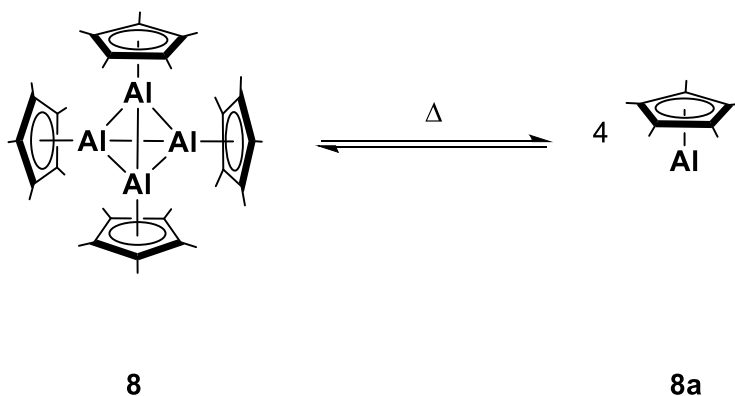
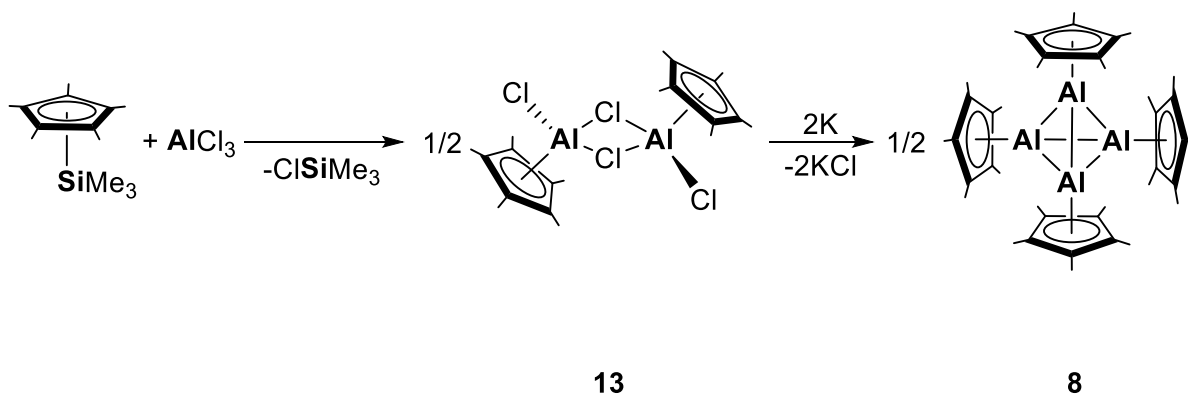


Figure 14: Representation of the equilibrium between **8** and **8a**.

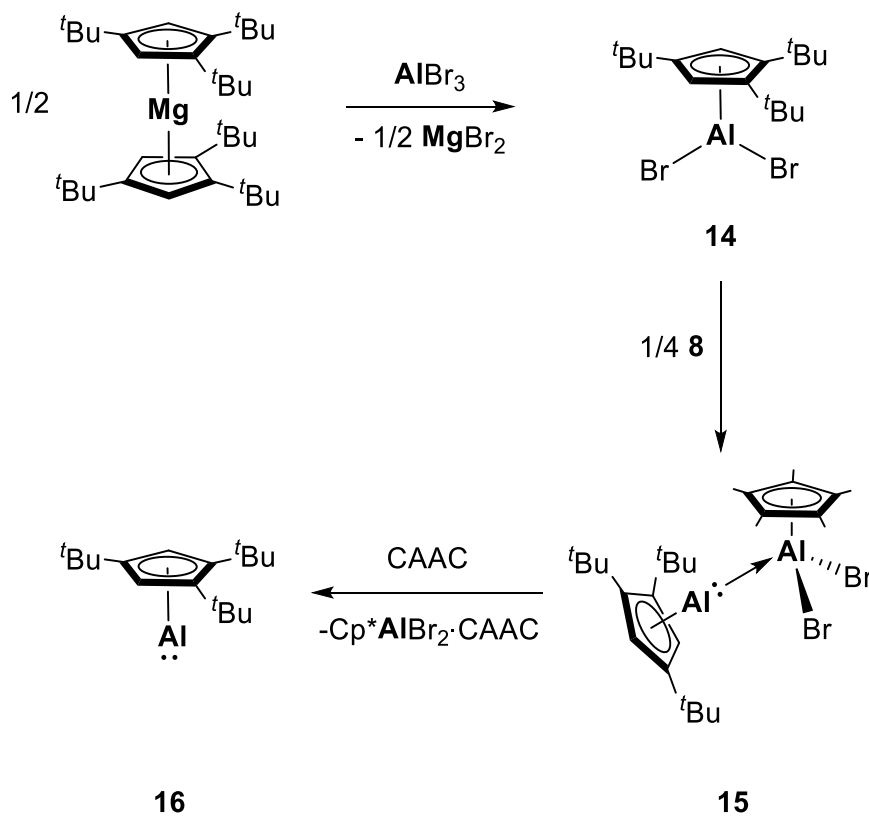
In 1992, another synthesis route of **8** was reported by *Roesky* et. al by the reduction of the corresponding dihalides compound **13** with potassium (Scheme 15).<sup>137,138</sup>

## 1. Introduction



Scheme 15: Synthesis of compounds **8** and **13**.

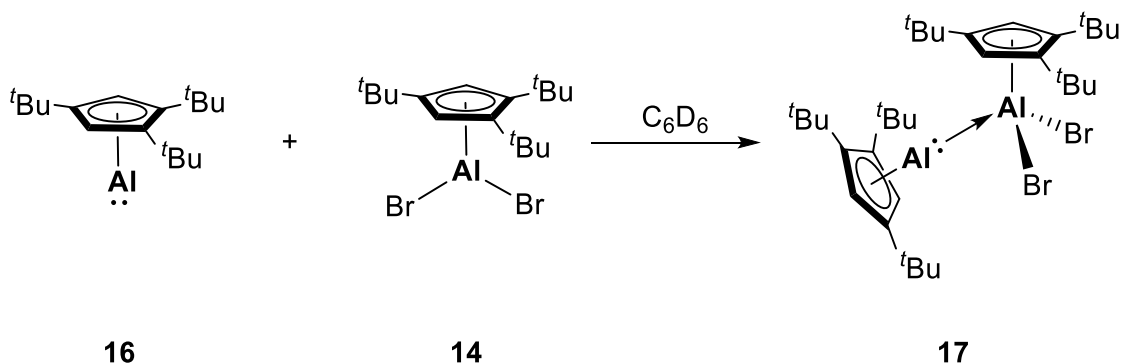
In 2019, *Braunschweig* et. al. reported the first isolated monomeric cyclopentadienyl aluminum(I) compound with an elevated sterically demanding cyclopentadienyl ligand (Scheme 16).<sup>139</sup>



Scheme 16: Synthesis of compound **16**.

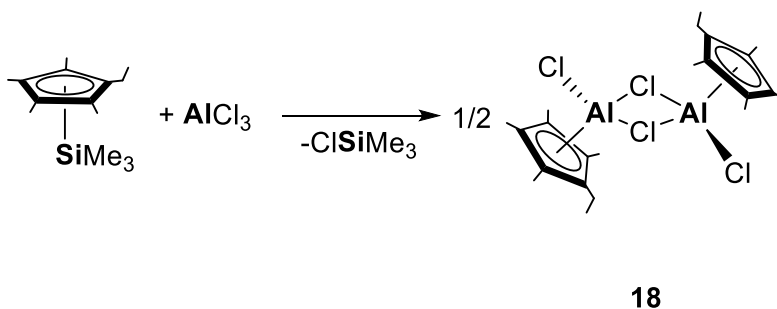
## 1. Introduction

The synthesis of **16** takes place via a three-step reaction (Scheme 16). As expected, the half sandwich aluminum complex **14** is isolated as a monomer compared to compound **13** which is a dimer due to the less elevated steric demanding of Cp\*. Furthermore, compound **16** shows Lewis base property so that a Lewis acid/base adduct could be isolated with two different aluminum species (Scheme 17).<sup>139</sup> Compound **16** features very interesting properties which will be discussed in chapter 1.6.



Scheme 17: Representation of the Lewis basicity of **16**.

In addition to compound **13**, Roesky et al. have synthesized a compound with bulky cyclopentadienyl ligand (Scheme 18) demonstrating that both compounds with the form Cp<sup>B</sup>AlCl<sub>2</sub> (Cp<sup>B</sup>: pentamethylcyclopentadienyl ligand in **13** and 1,2,3,4-tetramethyl-5-ethylcyclopentadienyl ligand in **18**) can be isolated as dimers.<sup>137</sup>

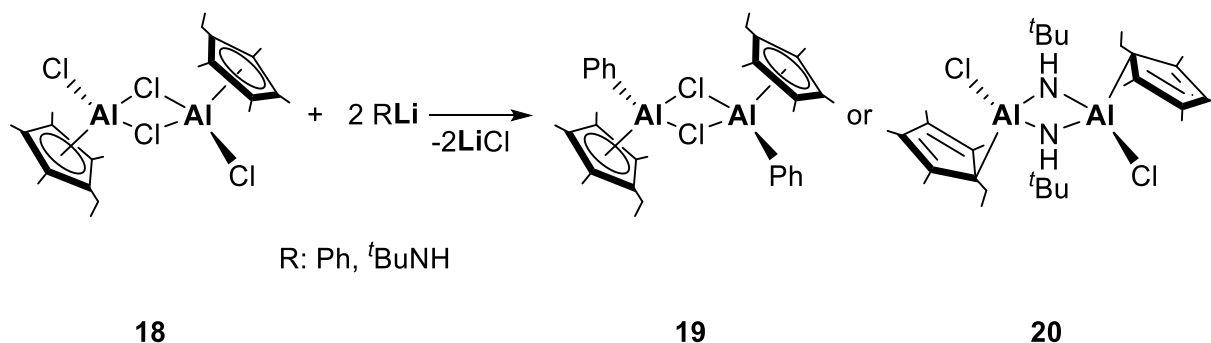


Scheme 18: Synthesis of compound **18** by Me<sub>3</sub>SiCl elimination.

Both complexes **13** and **18** exhibit dimeric structures in the solid state with two bridging chlorine ligands and an η<sup>5</sup> bonded cyclopentadienyl ligand. The distance between the aluminum atom and the bridged chlorine atoms is longer than the distance between aluminum atom and the

## 1. Introduction

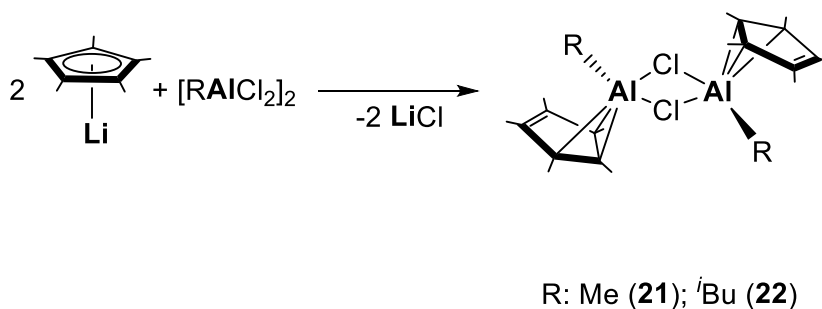
terminal chlorine atom. The substitution on compound **18** is possible and the bonding mode of the cyclopentadienyl ligand can change depending on the substituent (Scheme 19).<sup>140</sup>



Scheme 19: Synthesis of compounds 15 and 16.

The (tetramethyl)(ethyl)cyclopentadienyl ligand is  $\eta^1$ -bonded to aluminum atom in compound **20** due to the electronic property of the amino group (as an electron donating group and strong  $\sigma$ -donor) and the steric shielding of *t*Bu-group while the phenyl group in compound **19** is an electron withdrawing group and less demanding so that the hapticity of the bonded (tetramethyl)(ethyl)cyclopentadienyl ligand remains  $\eta^5$ . Furthermore, amino group in **20** is a stronger  $\sigma$ -donor than chlorine so that the dimerization of compound **20** occurs throughout the amino-group and the chlorine ligands are bonded terminal.

In 1979 and 1982, *Paine* et al. demonstrated that not only the steric shielding of the second bonded substituent to the aluminum atom determined the bonding nature of aluminum atom to the cyclopentadienyl ligand but also the electronic nature of this substituent. *Paine* et. al. synthesized several (pentamethylcyclopentadienyl)(alkyl)aluminum chloride compounds and characterized them (Scheme 20).<sup>141,142</sup>



Scheme 20: Synthesis of compounds 21 and 22.

## 1. Introduction

In compound **21**, the Cp\* is  $\eta^3$  bonded to aluminum atom in the solid state while in compound **22**, the hapticity of the bonded Cp\* is between  $\eta^2$  and  $\eta^3$  according to the C-C bond distances in the ring. The theoretical nonparameterized MO calculations on a model compound [CpAl(CH<sub>3</sub>)Cl]<sub>2</sub> have determined the  $\eta^3$  structures. The distortion in the hapticity of the bonded Cp\* in compound **22** can be attributed to the steric demand or to nonbonding interactions.

Compounds **21** and **22** are isolated in the solid state as doubly chloride bridged dimers. The chloride atoms build a square planar ring with both aluminum atoms. Protons of Cp bonded methyl groups indicate one signal in <sup>1</sup>H NMR spectrum at 32°C; in <sup>13</sup>C spectrum, only two signals were detected demonstrating that the structure in the solid state does not correspond the structure in solution at 32°C. A reason for this behaviour is most likely a 1,2 or 1,3 sigmatropic rearrangement between  $\eta^1$ ,  $\eta^2$  or  $\eta^3$  structures or a rapid ring slippage.

It is unquestionable that the electronic factor of aluminum atom plays an enormous role on the bonding situation between aluminum atom and the cyclopentadienyl ligand. This factor can be controlled via the second substituent on aluminum atom. This was proved by synthesizing new tetramethylcyclopentadienyl ligand with a linked arm occupied with a donor group (tertiary amine) at the end of the chain by *Jutzi* et al. in 1993 and 1996 (Figure 15).<sup>143,144</sup>

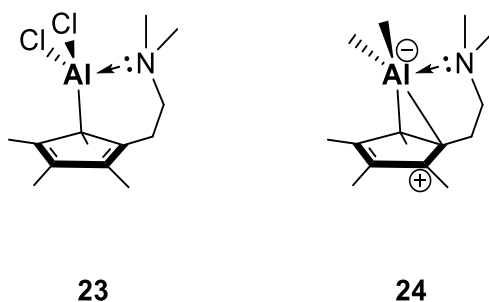
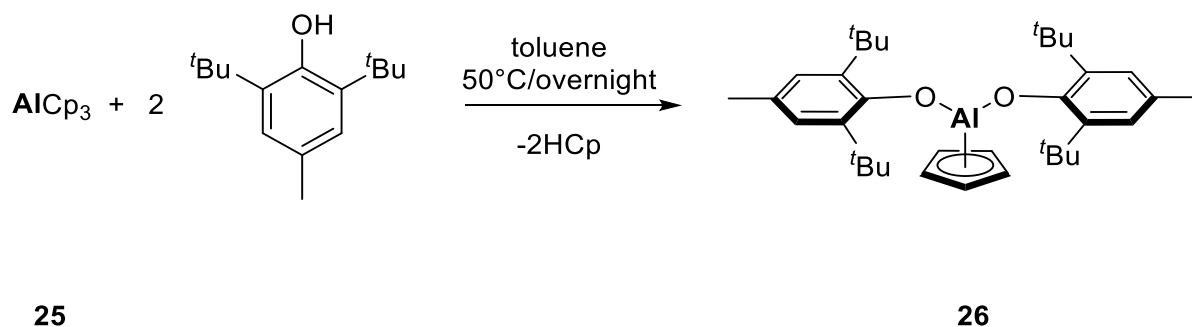


Figure 15: Representation of structures 19, 20.

*Jutzi* showed that compound **23** exists as a monomer in the solid state with an  $\eta^1$  bonded Cp ligand in the allylic position to the aluminum atom. The aluminum atom became tetracoordinated via the intramolecular interaction of the nitrogen atom with the aluminum center. Changing of substituents on aluminum atom from methyl group, electron-donating group, in compound **23** to chlorine, an electron-withdrawing group, in compound **20** led to a change in the coordination fashion from  $\eta^1$  to  $\eta^2$  between aluminum atom and the Cp ligand. A similar effect was observed in compounds **13** with a chlorine ligand; this led to a change in the hapticity of aluminum atom from  $\eta^5$  to  $\eta^3$ .

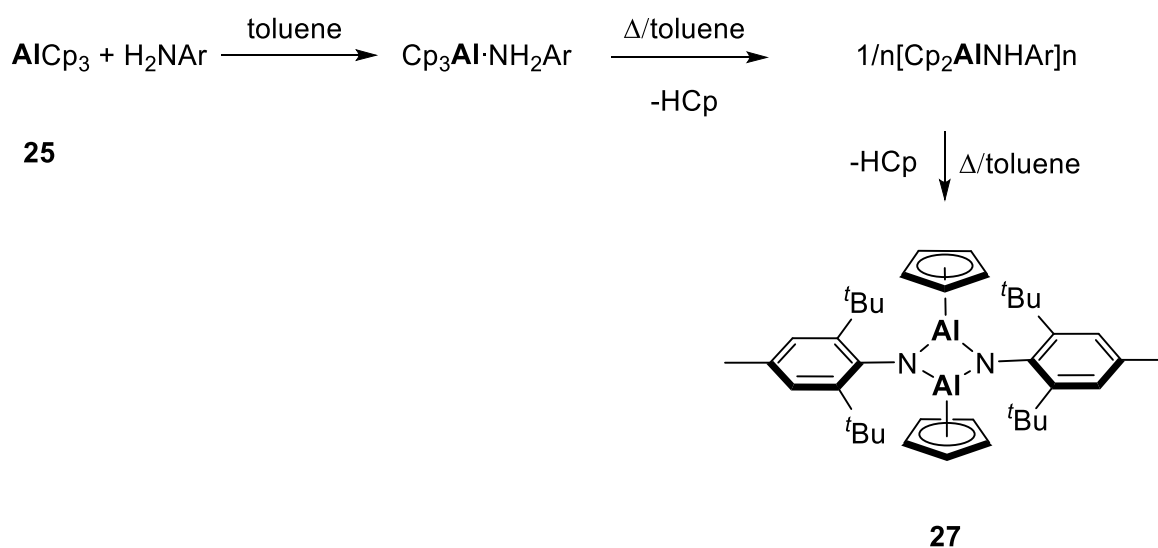
## 1. Introduction

Exchanging the substituent on aluminum from a weak  $\sigma$ -donor group like chlorine by a stronger  $\sigma$ -donor group like alkoxy or aryloxy group with an elevated steric demand should be shielding enough to discourage a dimer formation as well as to permit the  $\eta^5$  bonding mode to the cyclopentadienyl ligand. This scenario has been realized by *Shapiro & Budzelaar* by alcoholysis of  $\text{AlCp}_3$  **25** with two equivalent of 2,3-di-*tert*-butyl-4-methylphenol to afford compound **26** in 1998 (Scheme 21).<sup>145</sup>



Scheme 21: Synthesis of compound **26** by alcoholysis of **25**.

Compound **26** is isolated as a monomer with a  $\eta^5$  bonded cyclopentadienyl ring. The bonding nature of the cyclopentadienyl ligand in compound **26** resembles the bonding arrangement of the Cp ring in the dimeric cyclopentadienyl iminoalane **27** which was synthesized by the elimination of cyclopentadiene by *Shapiro et al.* in 1996 (Scheme 22).<sup>146</sup>

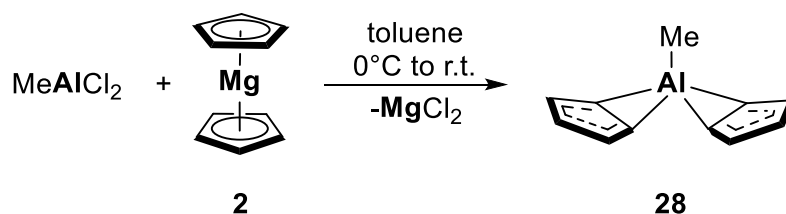


Scheme 22: Synthesis of **27**.



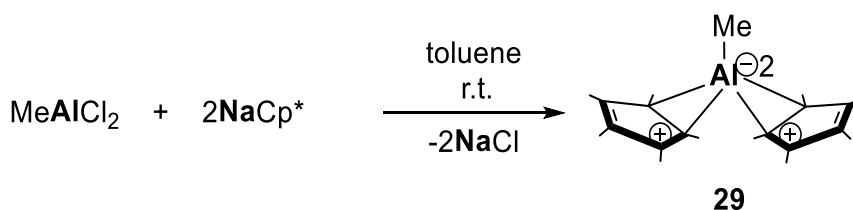
## 1.5.2. Bis(cyclopentadienyl) Aluminum Compounds

Previously, compound  $\text{Me}_2\text{AlCp}$  **12** was isolated as a polymer in the solid state,<sup>121</sup> while in 1994, *Shapiro* et al. isolated compound  $\text{MeAlCp}_2$  **28** as a monomer in the solid state (Scheme 23).<sup>147,148</sup>



Scheme 23: Synthesis of compound **28**.

*Shapiro* et al. used magnesocene **2** as a convenient cyclopentadienyl transfer agent with methyldichloroalane to produce dicyclopentadienylmethylaluminum complex **28** as the first isolated aluminum compound with two cyclopentadienyl ligands. Compound **28** was isolated as a monomeric aluminum compound with two  $\eta^2$  coordinated cyclopentadienyl ligands, which satisfy the electronic deficiency of aluminum atom. The non-coordinated C-C bonds in the cyclopentadienyl rings are approximately 135.0-137.5 pm, indicating a delocalized double bonds in the rings, whereas the coordinated C-C bonds are longer measuring 138.6 pm and 143.7 pm. Compared with  $\text{Me}_2\text{AlCp}$  **12**, the C-C bonds are more localized in the ring due to the binding nature between aluminum atom and the cyclopentadienyl ligand.<sup>121</sup> Even when the steric demand increases in the cyclopentadienyl ligand, the bonding nature to aluminum atom does not change as *Shapiro* et al. demonstrated by the synthesis of compound **29** in 2000 (Scheme 24).<sup>149</sup>

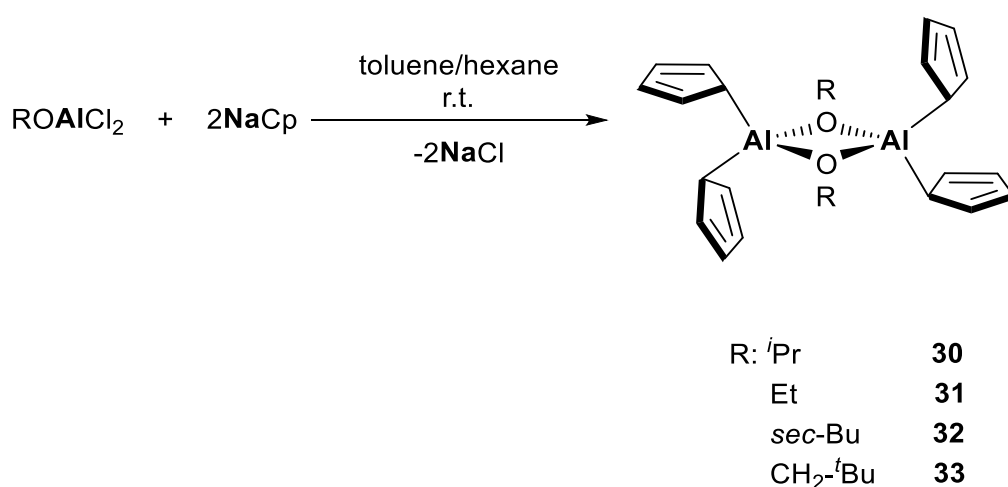


Scheme 24: Synthesis of compound **29**.

## 1. Introduction

Compound **29** displayed a more localized double bond in the ring of pentamethylcyclopentadienyl ligands compared with compound **28** where the double bonds were delocalized in both cyclopentadienyl ligands.

The influence of the substituent at aluminum atom on the bonding between the aluminum atom and the cyclopentadienyl ligand is obvious and leads, in many cases, to dimerizing of aluminum compounds. In 1996 and 2003, *Kunicki et al.* investigated the influence of the alkoxy ligands OR (R = *i*-Pr, Et, CH<sub>2</sub>-*t*Bu, *sec*-Bu) on the aluminum cyclopentadienyl bonding nature in solution by <sup>27</sup>Al NMR studies and in solid state via X-ray crystallography (Scheme 25).<sup>150,151</sup>

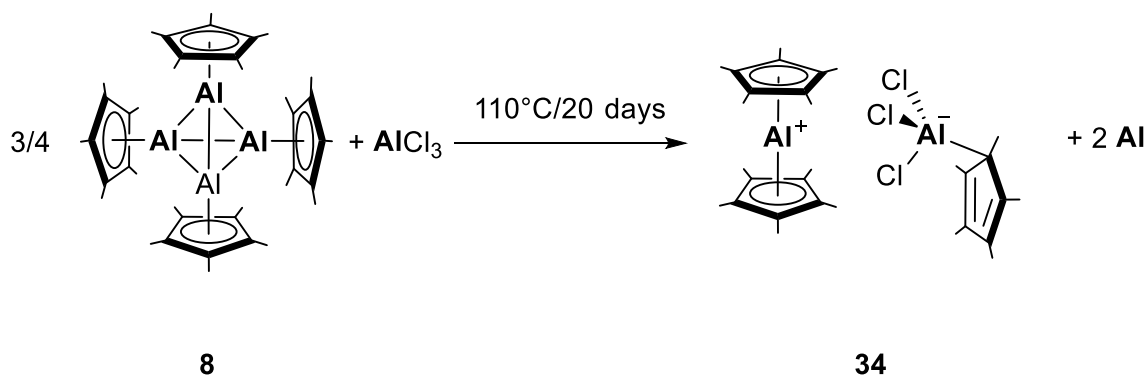


Scheme 25: Synthesis of compounds 30-33.

All compounds **30-33** are isolated as alkoxy-bridged centrosymmetric dimers in the solid state. The center of the dimer is a four membered ring of the Al<sub>2</sub>(μ-O)<sub>2</sub> unit with 2 pm difference between the Al-O bonds. The cyclopentadienyl rings are bonded in η<sup>1</sup> coordination fashion to aluminum atoms, which have a tetrahedral environment. The effect of the alkoxy ligands in compounds **30-33** resemble the effects of amino groups in monocyclopentadienylaluminum compound **20**. Furthermore, the electronic properties of heteroatoms in complexes **20** and **30-33** versus the alkylgroups in complexes **21**, **22**, **28** and **29** have enormous influence on the ability of the aluminum atom to build a σ-bond to the cyclopentadienyl ligand. Although the symmetry of these compounds **20**, **21**, **28** and **29** is low in the solid state, they undergo a very rapid sigmatropic rearrangement in solution so that only one signal for the cyclopentadienyl protons is detected in the <sup>1</sup>H-NMR spectra, giving evidence for a fluxional behaviour.<sup>141,142,147,149-152</sup>

## 1. Introduction

However, when aluminum atom gives up the third substituent, a biscyclopentadienyl aluminumocenium cation can be generated. In 1993, *Schnöckel & Ahlrichs* demonstrated this by synthesizing the decamethyl aluminumocenium cation compound **34** by reacting pentamethyl cyclopentadienyl aluminum(III) tetramer with aluminum trichloride (Scheme 26).<sup>105–107</sup>



Scheme 26: Synthesis of complex **34**.

Compound **34** was characterized in solution so that in the  $^{27}\text{Al}$ -NMR spectrum, a signal was detected at  $\delta = -114.5$  ppm ( $\omega_{1/2} = 50$  Hz) corresponding to the aluminumocenium fragment  $[\text{Cp}^*_2\text{Al}]^+$ . This signal is very highfield-shifted for an Al(III) compound because of the diamagnetic ring current effect of the aromatic rings. In the crystal structure, two staggered  $\eta^5$  bonded pentamethylcyclopentadienyl rings were observed which makes this compound isostructural to decamethylferrocene. It also demonstrated that the pentamethylcyclopentadienyl ligand is able to stabilize the  $\text{R}_2\text{Al}^+$  fragment. Since the central aluminum atom in compound **34** exhibits a positive charge, the  $p$ -orbital participation increases in Al-Cp\* bonding leading to the highest possible hapticity ( $\eta^5$ ). The electron deficiency of aluminum atom is compensated by two  $\pi$ -coordinated pentamethylcyclopentadienyl ligands with a distance of 184.3 pm to aluminum atom, which is not only longer than  $\text{Fe-Cp}^*_{\text{centroid}} = 165.6$  pm<sup>153</sup> in  $\text{Cp}^*_2\text{Fe}$  due to the covalent nature of the Fe-Cp\* with the participation of the  $d$ -orbitals, but also shorter than the bond length of  $\text{Mg-Cp}^*_{\text{centroid}} = 196.8$  pm in  $\text{Cp}^*_2\text{Mg}$ <sup>154</sup> and the bond length of  $\text{Si-Cp}^*_{\text{centroid}} = 211.9$  pm in  $\text{Cp}^*_2\text{Si}$ .<sup>155,156</sup>

This decamethylaluminumocenium cation compound can be synthesized with various counteranions, such as a borate-bridged *ansa*-zirconocene anion or a borate anion. Both aluminumoceniums salts **35** and **36** were synthesized by *Shapiro* et al. (Figure 16).<sup>108,157</sup>

## 1. Introduction

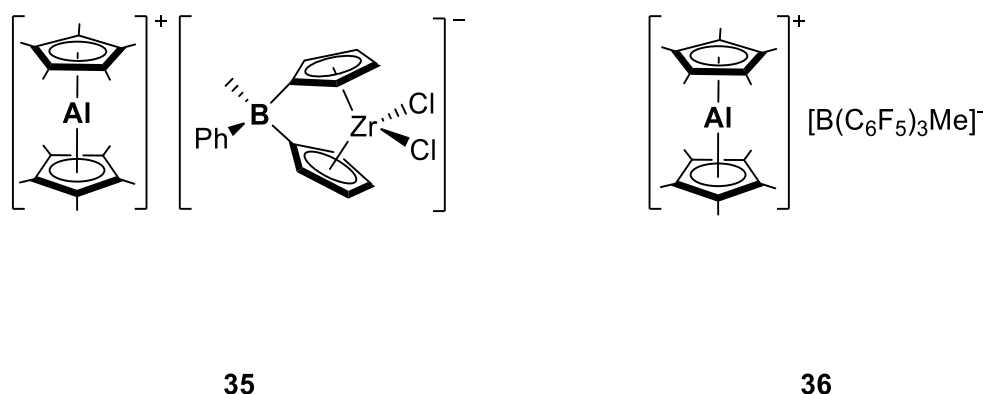
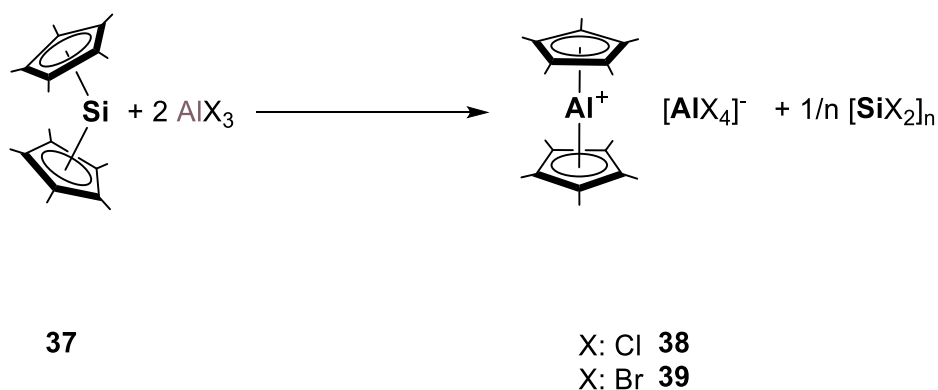


Figure 16: Representation of compounds **35** and **36**.

*Shapiro* et al. demonstrated in both compounds **35** and **36** that there is no interaction between the metal center (Al) and the halides atoms of the counteranions (Cl or F) (the closest distances are Al-F: 507 pm and Al-Cl: 580 pm). The stability of decamethylaluminocenium cation compounds **34-36** at an ambient temperature is not surprising due to the strong  $\sigma$ -donor property and the steric demand of the pentamethylcyclopentadienyl ligand.

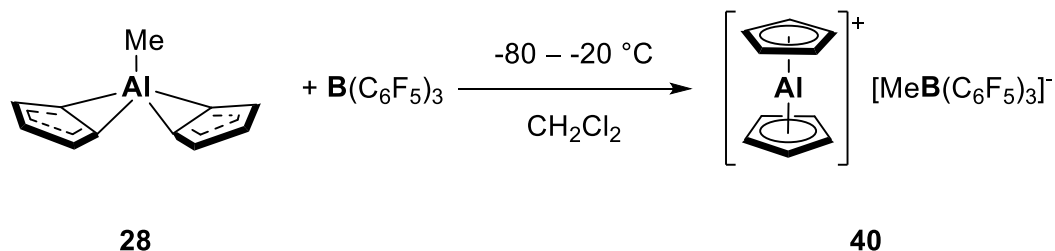
In 1999, *Jutzi* et al. synthesized decamethylaluminocenium cation via a different route using a silicocene as transmetalation reagent (Scheme 27).<sup>158</sup> The treatment of decamethylsilicocene **37** with two equivalent  $\text{AlX}_3$  (X: Cl, Br) afforded compounds **38** and **39**.



Scheme 27: Synthesis of **34** and **35**.

## 1. Introduction

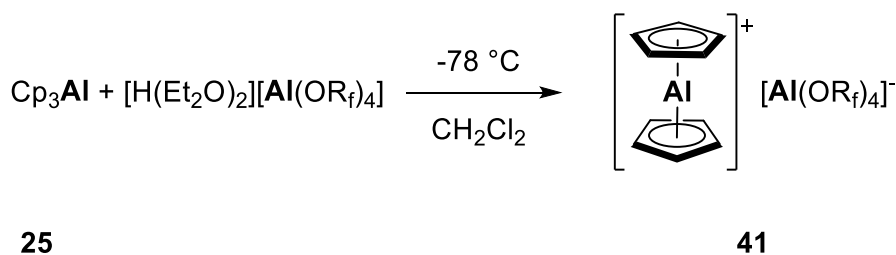
On the other hand, the aluminocenium cation **40** rapidly decomposes at 20°C as reported by *Bochmann et al.* in 1996 (Scheme 28).<sup>109,110</sup>



Scheme 28: Synthesis of compound **40**.

Salt **40** displayed two signals in proton NMR spectrum in temperature range from -80 to -20°C, and one sharp signal at -126.4 ppm ( $\omega_{1/2} = 50$  Hz) in the  $^{27}\text{Al}$  NMR at -60°C, which is more highfield shifted than the signal of decamethylaluminocenium cation. This  $^{27}\text{Al}$  NMR signal is in line with the calculated shift of aluminocenium cation at -130 ppm.<sup>107</sup> *Bochmann et al.* demonstrated that compound **40** contains a highly Lewis acidic metal center, which was utilized as an initiator for carbocationic polymerization of isobutene and isobutene-isoprene copolymerization.<sup>108</sup>

The tuning of the stability and activity of aluminocenium cation, which is a part of compound **40**, can be achieved when a large WCA (weakly coordinated anion) such as  $[\text{Al}(\text{OR}_f)_4]^-$  with ( $\text{R}_f$ :  $\text{C}(\text{CF}_3)_3$ ) that is utilized as a counteranion as demonstrated by *Schnöckel et al.* in 2009 (Scheme 29).<sup>159</sup>



Scheme 29: Synthesis of **41**.

Compound **41** exhibits weak contact between the counteranion and the aluminocenium cation in the solid state (Al-F: 527.8 pm). The aluminium atom is  $\eta^5$  bonded to the cyclopentadienyl rings with an Al-Cp<sub>centroid</sub> distance of 178.9 pm. Aluminocenium cation in compound **41**

## 1. Introduction

indicates a higher activity than in compound **40** with respect to the polymerization of isobutene in solution. Furthermore, compound **42** can also be isolated as a Lewis acid/base adduct of **41** with two molecules of diethylether demonstrating two  $\sigma$ -bonded cyclopentadienyl ligands to aluminum cation center (Figure 17).<sup>159</sup>

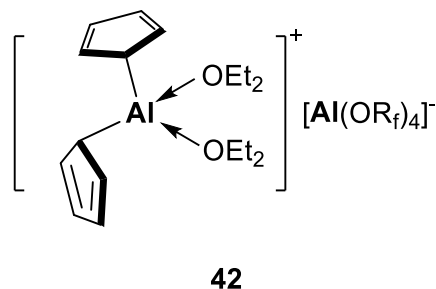


Figure 17: Projection of Compound 42.

Moreover, according to the <sup>1</sup>H NMR investigation, a dynamic temperature dependent equilibrium can be shown and is supported by quantum chemical calculation in the gas phase to determine the  $\Delta_r H^0$  of 97.2 kJ·mol<sup>-1</sup> by the coordination of both diethyl ether molecules (Figure 18).<sup>159</sup>

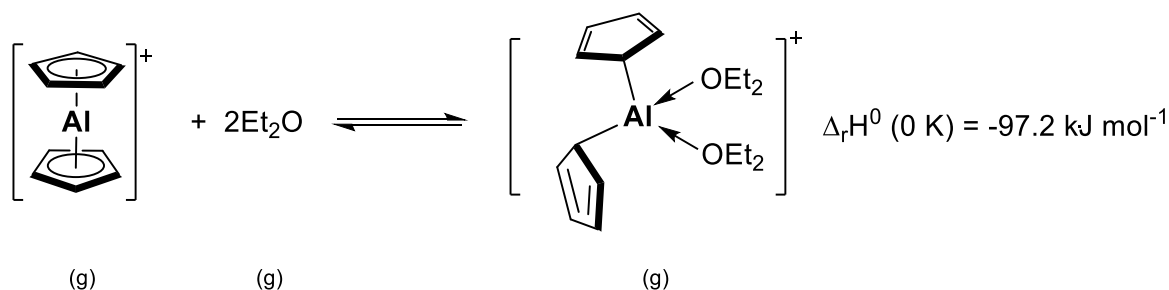
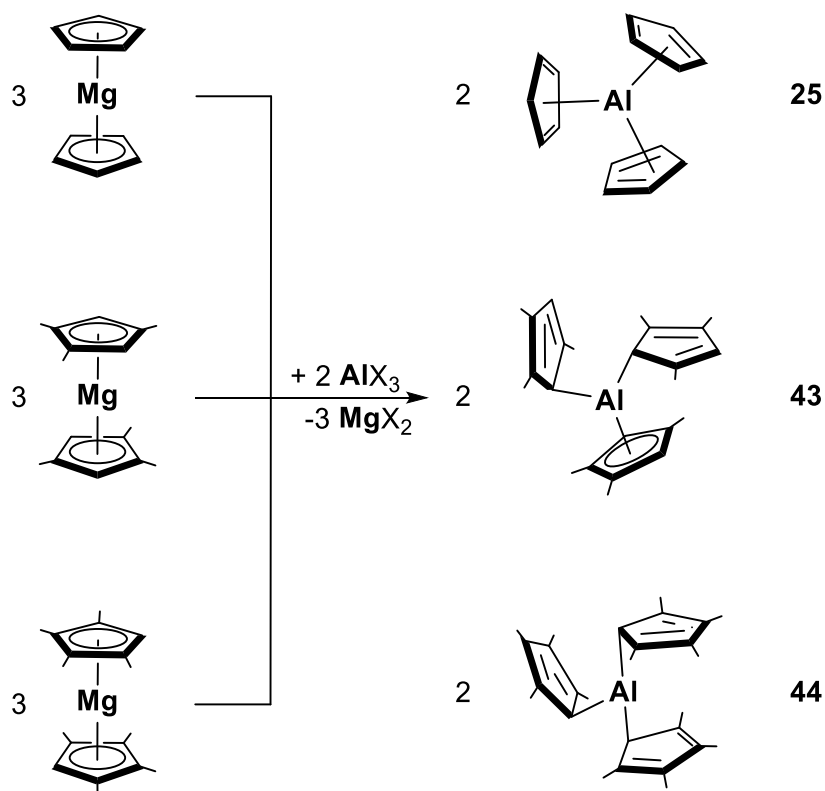


Figure 18: A dynamic and temperature dependent equilibrium between the cations in compounds **41** and **42**.

In conclusion, the higher activity of aluminumcenium cation in compound **41** with respect to the polymerization of isobutene in solution is due to the weaker coordinated counteranion  $[Al(OR_f)_4]^-$  compared with  $[Me(B(C_6F_5)_3)]^-$  in compound **40**, which is able to form a  $Cp_2Al-Me-B(C_6F_5)_3$  ion pair.

## 1.5.3. Tricyclopentadienyl Aluminum Compounds

The tricyclopentadienylaluminum compounds can be synthesized by similar method utilizing the corresponding magnesocene as a transmetalation reagent with aluminum(III) halides (Scheme 30), as reported by *Shapiro et al.*<sup>160–163</sup>



Scheme 30: Synthesis of compound 25, 43 and 44.

Compounds **25**, **43** and **44** reflect the tremendous influence of the steric demand of the cyclopentadienyl ligand on the bonding mode between aluminum atom and the cyclopentadienyl ring in the crystal structure. The steric effect of the cyclopentadienyl ligand is clearly illustrated in these compounds simply because there is no other substituent bonded to aluminum atom except the cyclopentadienyl ring. The steric effect increases when the cyclopentadienyl ligand possesses a substituent such as in compounds **43** and **44**. In compound **25**, two different coordination-isomers exist in the asymmetric unit (**25a** with three

## 1. Introduction

$\eta^2$  bonded Cp; **25b** with two  $\eta^2$  and one  $\eta^1$  bonded Cp) (Figure 19) suggesting a very small energy difference between them.<sup>161,163</sup>

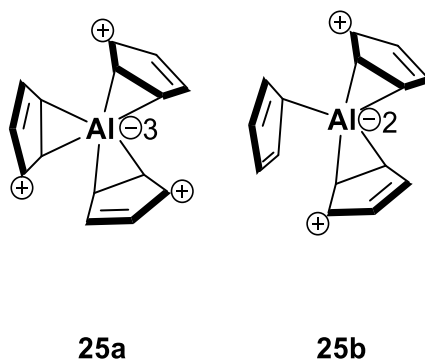


Figure 19: Representation of the two coordination isomers of compound **25** in the crystal.

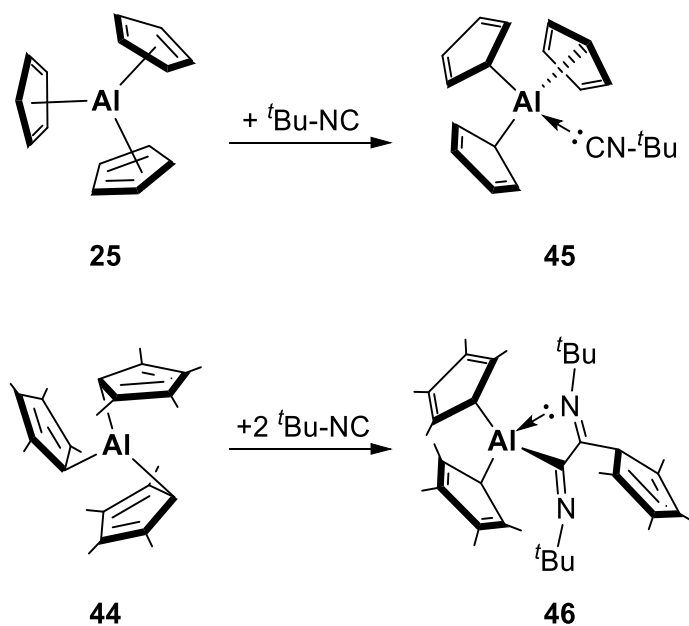
The  $\eta^2$  bonding arrangement of aluminum atom to cyclopentadienyl ligands could be explained electronically in compound **25** so that the aluminum atom compensates the electron deficiency with the increasing of the hapticity to the cyclopentadienyl ligands.

The aluminum center in compound **43** compensates the electron deficiency in another way so that a compromise between the steric and the electronic effects can be found in  $\eta^5$  and two  $\eta^1$  cyclopentadienyl rings; making this arrangement energetically a ground state for this structure. While in compound **44**, the steric effects might be more pronounced than the electronic effects so that the aluminum center avoids the repulsion with the adjacent methyl group of the cyclopentadienyl rings and minimizes it by the  $\eta^1$  arrangement of all bonded cyclopentadienyl rings. The binding between aluminum atom and cyclopentadienyl ligands occurs at the methyl-group-free carbon atom of the cyclopentadienyl ring. The methyl groups also have an electronic effect since they are electron-donating groups so that they destabilize the concentration of negative charge in the region occupied by the aluminum fragment pushing the bonding fashion to cyclopentadienyl ring presumably towards  $\eta^1$ ; in other words, the methyl groups make the cyclopentadienyl ligand a stronger  $\sigma$ -donor.

Interestingly, the tricyclopentadienyl aluminum compounds showed different chemical property with respect to  $\sigma$ -donor ligands such as *tert*-butyl isocyanide (Scheme 31).



## 1. Introduction

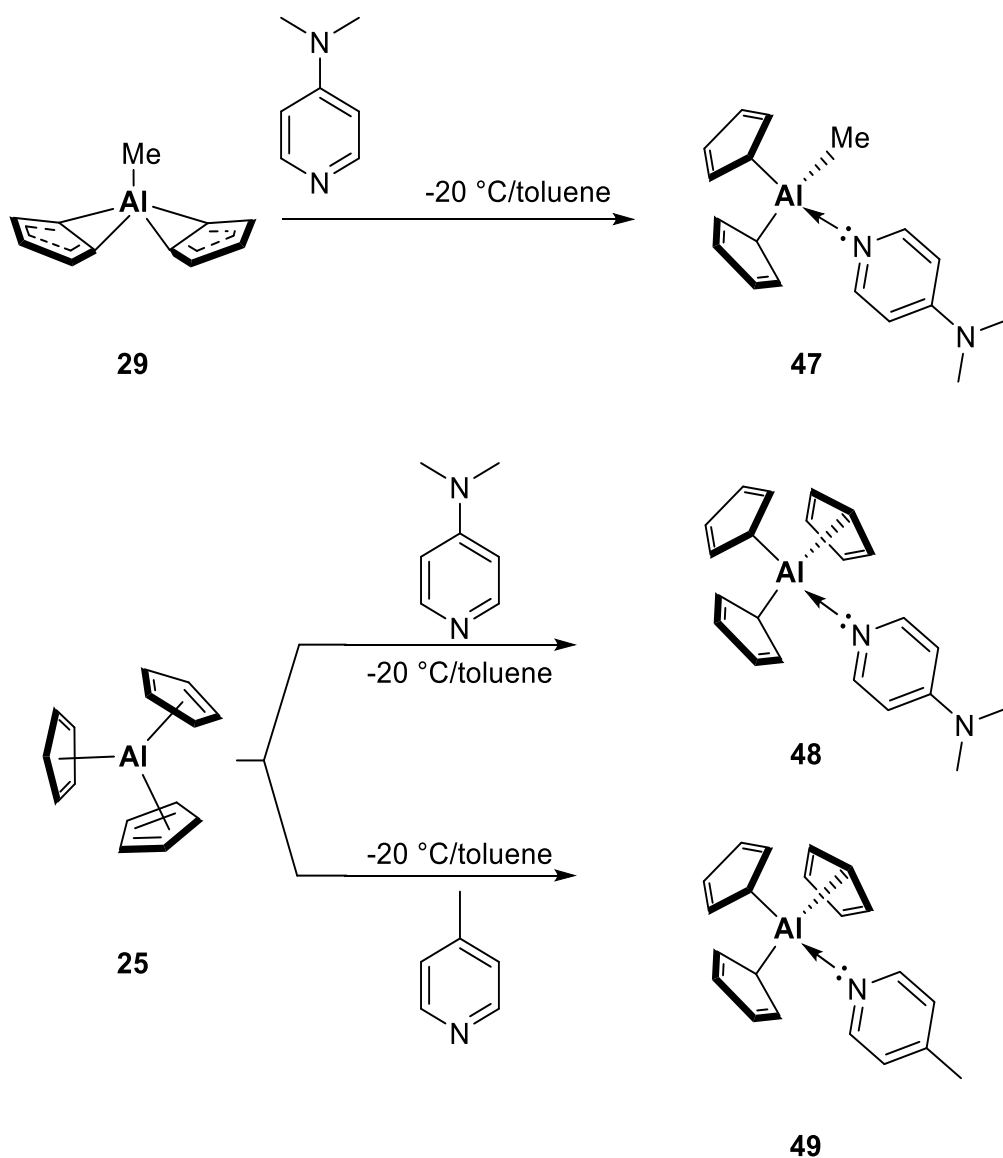


**Scheme 31:** Reaction of compounds **25** and **44** with *tert*-butyl isocyanide to afford compounds **45** and **46**.

While compound **25** reacts with *tert*-butyl isocyanide to afford a Lewis acid base adduct **45**, compound **44** inserts two *tert*-butyl isocyanide molecules between aluminum center and one of the bonded cyclopentadienyl ligands to afford compound **46**.<sup>162,164</sup> The aluminum cyclopentadienyl bond cleavage also occurs in the reaction of compound **21** with an amine or alcohol (Scheme 21 and 22) but under elimination of cyclopentadiene molecule.

## 1.5.4. Donor Stabilized di- and Tricyclopentadienyl Aluminum Compounds

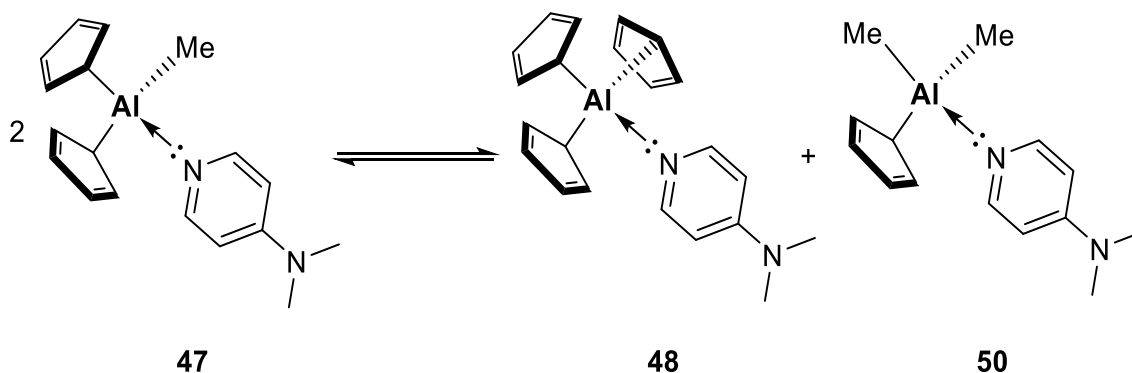
In the case of electronic saturated di- and tricyclopentadienyl aluminum compounds in form of a Lewis acid/base adducts, the hapticity of the bonded cyclopentadienyl ligands to aluminum is almost  $\eta^1$  in the solid state. Many examples in literature are known; for instance, *Kunicki & Zachara* reported di- and tricyclopentadienyl aluminum donor-acceptor complexes in 2006 (Scheme 32).<sup>165</sup>



Scheme 32: Synthesis of compounds 47-49.

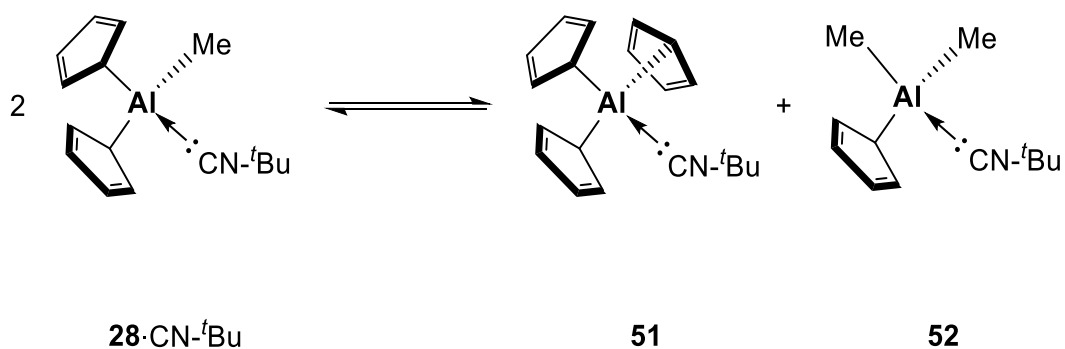
## 1. Introduction

*Kunicki & Zachara* illustrated that cyclopentadienyl rings in compounds **47-49** possess an  $\eta^1$  arrangement to the aluminum center in the solid state. Using multinuclear NMR spectroscopy, an equilibrium of compound **47** in solution was revealed (Scheme 33) such that signals of both compounds **48** and **50** were detected in proton NMR.



Scheme 33: Equilibrium of compound **47** in solution.

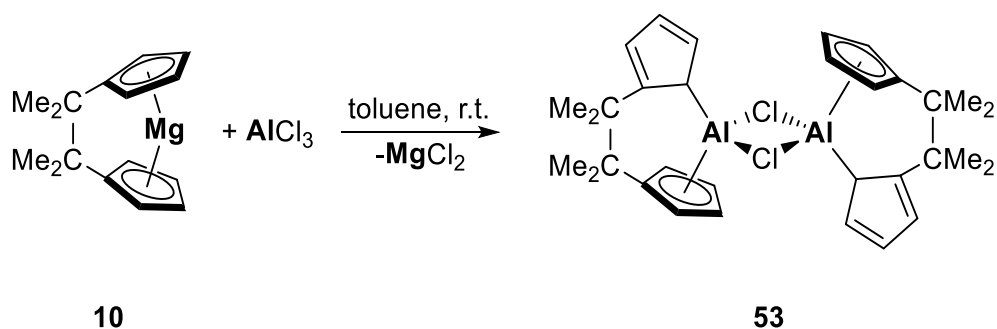
*Shapiro et al.* have also shown such an equilibrium of compound **28** with *tert*-butyl isocyanide (Scheme 34) so that a tricyclopentadienyl aluminum *tert*-butyl isocyanide (Lewis acid/base adduct) **51** can be isolated in the solid state. It should be mentioned that compound **28** without a Lewis base does not undergo a redistribution reaction at ambient conditions.<sup>147,148</sup>



Scheme 34: Equilibrium of compound **28** in the presence of Lewis base like *tert*-butyl isocyanide.

## 1.5.5. Ansa-Aluminocene derivatives

An aluminum complex with interlinked cyclopentadienyl ligands was unknown until 2005 when *Shapiro* et al. synthesized the first carba[2]aluminocenophane derivative and isolated it as a dimer (Scheme 35).<sup>53</sup> The motivations of the synthesis of such complexes was that the handle (*ansa*) between the cyclopentadienyl rings could slow down the fluxional process of the compound in solution so that it will be detectable on the NMR time scale. The second was that the bridge can influence the Lewis acidity of the *ansa*-aluminocene which was observed for *ansa* metallocene of transition metals.<sup>166–169</sup> Finally, if a chiral *ansa*-aluminocene compound could be produced, it might be applicable as an asymmetric catalyst of Lewis acid activated reactions.



Scheme 35: Synthesis of compound 53.

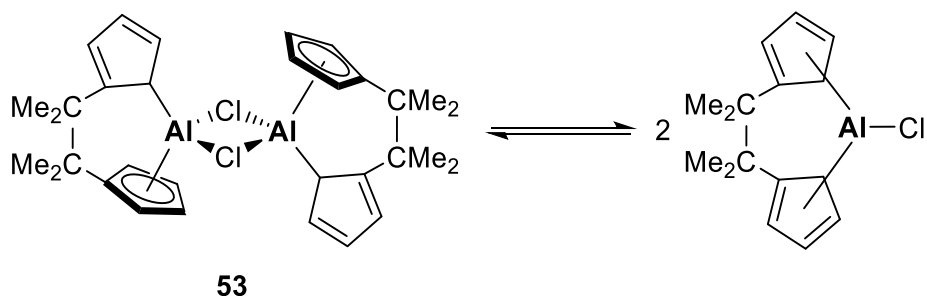
Compound **53** possesses two differently bonded cyclopentadienyl rings in the crystal. The first cyclopentadienyl ring is  $\eta^1$  coordinated to aluminum atom and the second is  $\eta^5$  in the solid state. The C-C bonds of the  $\eta^1$  bonded cyclopentadienyl rings are localized so that two bonds are short and three are long. The aluminum center indicates a distorted tetrahedral geometry, which is analogous to that in the dimeric structure of **19**<sup>140</sup> with a distance of 193.9 pm to  $Cp_{\text{centroid}}$  of the  $\eta^5$  bonded cyclopentadienyl ring, which is longer than the Al- $Cp_{\text{centroid}}$  distances in compounds **26**<sup>145</sup> and **27**.<sup>146</sup> The distance between aluminum atom and the carbon atom of the  $\eta^1$  bonded cyclopentadienyl ring of 198.9 pm is within the range 198.1–208.0 pm of the following compounds **20**,<sup>140</sup> **30–33**,<sup>150,151</sup> **43** and **44**<sup>161,162</sup> and **47–52**.<sup>147,148,165</sup>

The cyclopentadienyl rings are  $\eta^1/\eta^5$  coordinated to aluminum atom in compound **53** in the solid state. This indicates that the dimerization alone did not compensate the electron

## 1. Introduction

deficiency of the aluminum center, which could be traced back to the weak  $\sigma$ -donor property of the chlorine ligand resembling with this behaviour the Al-Cp bonding mode in compounds **18**, **19**, **21** and **22**, which tend to build an Al-Cp bond with higher hapticities than  $\eta^1$ , while the dimerization throughout an alkoxy ligand led to  $\eta^1/\eta^1$  coordination of the cyclopentadienyl rings to aluminum center in compounds **30-33**.

A  $^1\text{H}$  NMR spectroscopic study of the **53** in toluene- $d_8$  indicated two signals of the bonded cyclopentadienyl ring protons at 6.16 and 5.13 ppm and one signal of the methyl group protons in the bridge at 1.01 ppm, which means that compound **53** undergoes a dynamic process in solution. The  $^1\text{H}$  NMR spectrum of **53** at  $-94^\circ\text{C}$  illustrated that the signal of 5.13 ppm splits up into two new signals; one is upfield shifted at 4.36 ppm, which is a characteristic for a bonded proton to  $\text{sp}^3$  hybridized  $\sigma$ -coordinated carbon to aluminum atom, and the second signal is downfield shifted at 6.15 ppm, which is assigned to a bonded proton to non-coordinated  $\text{sp}^2$ -hybridized vinylic carbon. Furthermore, the signal of 6.16 ppm splits into two adjacent signals at 6.33 ppm and 6.40 ppm. Moreover, the methyl group signal of the bridge started to separate by a concentration of the measured solution of 46 mM. This separation increased by minimizing the concentration, which could be explained via a monomer-dimer equilibrium (Scheme 36).



Scheme 36: Monomer-dimer equilibrium of compound **53**.

Due to the four signals in  $^1\text{H}$  NMR spectrum of compound **53** in toluene- $d_8$  at  $-94^\circ\text{C}$ , it can be interpreted as if both of cyclopentadienyl rings are bonded to aluminum atom with an  $\eta^1$  bonding mode. This arrangement at this temperature could be represented in two possible depictions (Figure 20).

## 1. Introduction

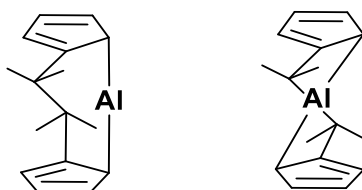
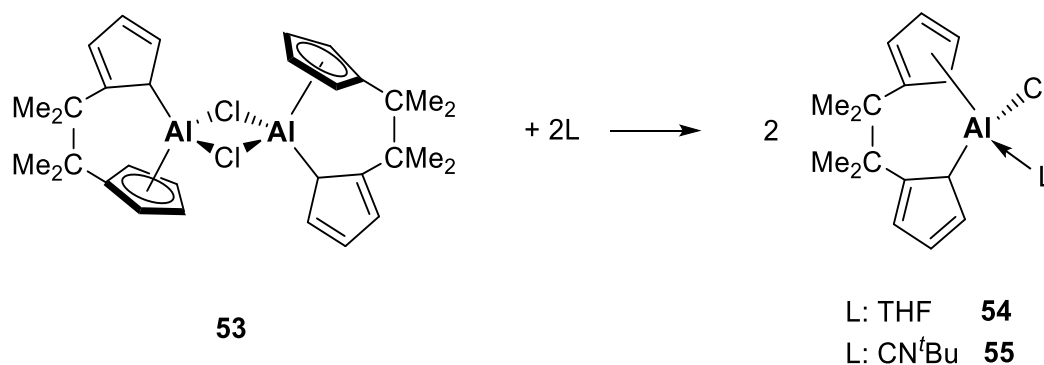


Figure 20: Representation of the two possible depictions of *ansa*-ligand in compound **53**.

Possible rearrangement pathways could involve  $\eta^1$ - $\eta^5$  shifts,  $\eta^1$ - $\eta^3$  shifts, and 1,3-migration of the aluminum atom between the two  $\alpha$ -carbons of the ring. Nevertheless, a stereochemical inversion at aluminum atom could also influence the arrangement of these complexes. The  $^{27}\text{Al}$  NMR spectrum showed a signal at -2 ppm at room temperature in toluene- $d_8$  and it broadened to the baseline by cooling to  $-50^\circ\text{C}$ . The  $^{27}\text{Al}$  signal of -2 ppm is strongly upfield shifted compared to di- and tricyclopentadienyl aluminum compounds (e.x.;  $\delta_{\text{Al}} = 81$  ppm in compound **25**,<sup>161</sup>  $\delta_{\text{Al}} = 72$  ppm in compound **28**,<sup>164</sup>  $\delta_{\text{Al}} = 65$  ppm in compound **43** and  $\delta_{\text{Al}} = 64$  ppm in compound **44**).<sup>161</sup> The  $^{27}\text{Al}$  shift of -2 ppm resembles the detected signal of unbridged di(pentamethylcyclopentadienyl)aluminum chloride with  $\delta_{\text{Al}} = -3$  ppm in  $\text{C}_6\text{D}_6$  at 297 K.<sup>157</sup> Shapiro et al. synthesized also Lewis base adducts of compound **53** (Scheme 37).<sup>53</sup>



Scheme 37: Synthesis of compounds **54** and **55**.

Complex **54** possesses one  $\eta^1$  bonded cyclopentadienyl ring to aluminum atom and one  $\eta^3$ , while both cyclopentadienyl rings in compound **55** are  $\eta^1$  bonded. Because of the epimerizing of the aluminum center and the rearrangement of the cyclopentadienyl ring, the  $^1\text{H}$  NMR spectra of compound **54** displays only two signals for the cyclopentadienyl protons and one

## 1. Introduction

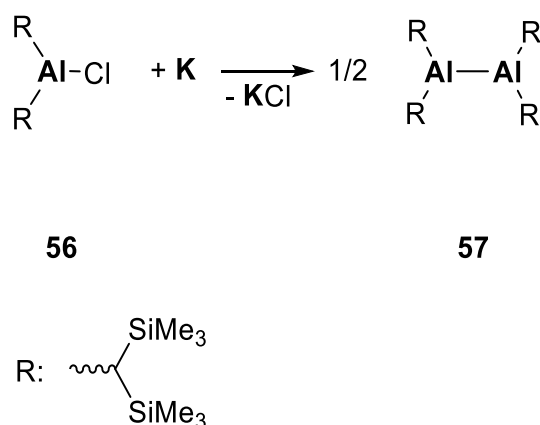
signal for the methyl group protons of the bridge at 43°C and 30°C, respectively. At -99°C, the signals of cyclopentadienyl protons split up into eight signals, and the signal of the methyl group of the bridge splits into four signals. On the other hand, <sup>1</sup>H NMR spectrum of compound **55** exhibits four signals for the cyclopentadienyl moieties and two for the methyl group of the bridge at temperature of -40°C, and further cooling of compound **55** to a temperature of -94°C only leads to broadening the signals.

In conclusion, the NMR investigation of compounds **54** and **55** indicate that both structures undergo a rapid sigmatropic rearrangement with very low energy barriers that are frozen out in solution at low temperatures.

## 1.6. Dialanes

Aluminum atom possesses the oxidation state +II in dialanes. In contrast to triorganyl aluminum compounds which have been recognized for decades, organoaluminum compounds with aluminum centers in low oxidation states were unknown for a long time because of their disproportionation mostly into Al(III), Al(I) or Al(0). Therefore, to give these compounds kinetic stability, most of the work groups have utilized bulky substituents so that the steric shielding would prevent the decomposition of these compounds.<sup>170-174</sup> According to the bound substituents to aluminum atoms, dialanes could be divided into the following sections: acyclic symmetrically substituted dialane, acyclic asymmetrically substituted dialane, and cyclic dialane. The substituents bound to aluminum atom have an enormous influence not only on the kinetic stability of the dialanes, but also on the bond lengths of the Al-Al. This is due to the electronic property and the steric demand of the substituent so that, for instance, additional van der Waals attraction forces (attractive dispersion interactions) increase. In this chapter, different dialanes will be presented and discussed.

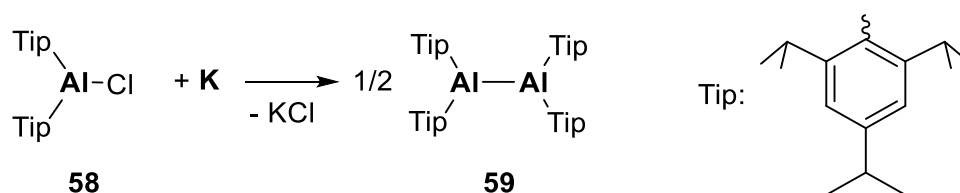
The first isolated and characterized dialane was synthesized by *Uhl* et al. in 1988 by the reduction of bis[bis(trimethylsilyl)methyl]chloroalane **56** with potassium to give tetrakis[bis(trimethylsilyl)methyl]dialane **57** (Scheme 38).<sup>175</sup> Two molecules of compound **57** existed in asymmetrical unit. Each aluminum center possesses a trigonal planar coordination sphere. The aluminum-aluminum bond is 266.0 pm long.

Scheme 38: Synthesis of **57**.

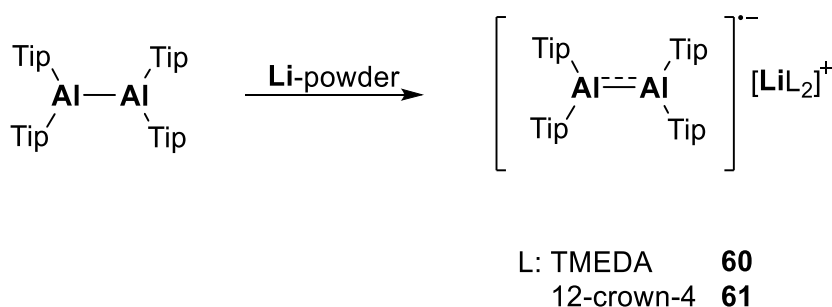


## 1. Introduction

A related complex was obtained by *Power et al.* with Tip (2,4,6- *tri-isopropylphenyl*) as a substituent in 1993 (Scheme 39).<sup>176</sup> *Power et al.* conducted the reduction of compound **58**<sup>177</sup> with one equivalent of potassium to yield compound **59** with an aluminum-aluminum bond length 264.7 pm, which is shorter than the Al-Al bond of **57**. Furthermore, compound **59** can be reduced by single electron transfer (SET) with lithium powder into radical anion **60** (Scheme 40). Compound **60** possesses a shorter aluminum-aluminum distance of 247.0 pm as compound **59**. This is in line with the analogous compound of gallium.<sup>178,179</sup>



**Scheme 39: Synthesis of 59.**



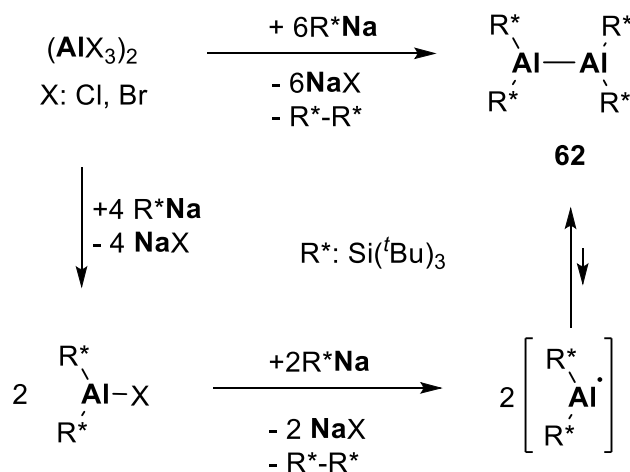
**Scheme 40: Synthesis of compounds 60 and 61.**

All spectroscopic investigations and available structural data illustrate that one electron  $\pi$ -bond between the aluminum atoms is formed in compound **60**. The reduction of compound **59** to compound **60** shortens the Al-Al bond by ca 17 pm and lengthens the Al-C<sub>Tip</sub> distances. The addition of one electron to the bimetallic moiety placed in a  $\pi$ -orbital increases the Al-Al bond order due to partial double bond character which leads to the shortening the Al-Al bond seen in compound **60**. Similar behaviour also occurs when compound **57** is reduced with one electron to yield the radical anion **57<sup>•-</sup>**.<sup>180-182</sup>

In 1998, *Wiberg et al.* presented a dialane compound using a radical reaction (Scheme 41).<sup>183</sup> The first step is the preparation of disupersilylchloroalane which is treated with R<sup>\*</sup>Na to produce the disupersilylalanyl radical. This radical cannot react with another R<sup>\*</sup>Na molecule

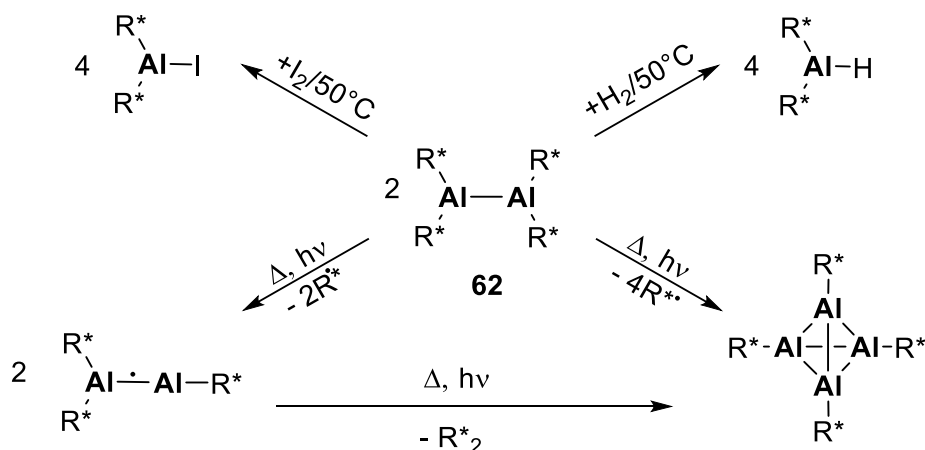
## 1. Introduction

because of the steric demand so that the radical is instead recombined to the dialane **62** and superdisilane.



Scheme 41: Synthesis of compound **62**.

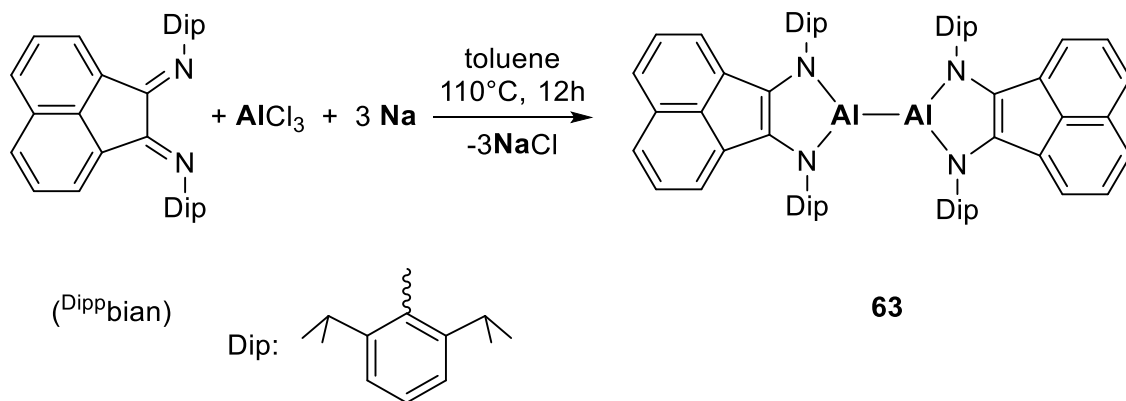
Compound **62** structurally resembles compounds **57** and **59** with the longest aluminum-aluminum distance of 275.1 pm for any acyclic dialane so far. Compared with compounds **57** and **59**, compound **62** is thermally less stable and it decomposes at 50°C. Nevertheless, compound **62** demonstrated very interesting chemical reactivity of the Al-Al bond (Scheme 42). Both halves  $\text{R}^*_2\text{Al}$  of compound **62** are bonded not only through a chemical Al-Al bond, but also through an additional van der Waals attractions (attractive dispersion interaction) of the alkyl groups. A similar effect was observed in the bonding between the supersilyl fragments  $\text{R}^*\text{-R}^*$ .<sup>184–186</sup>



Scheme 42: Reactions of **62** with different substrates.

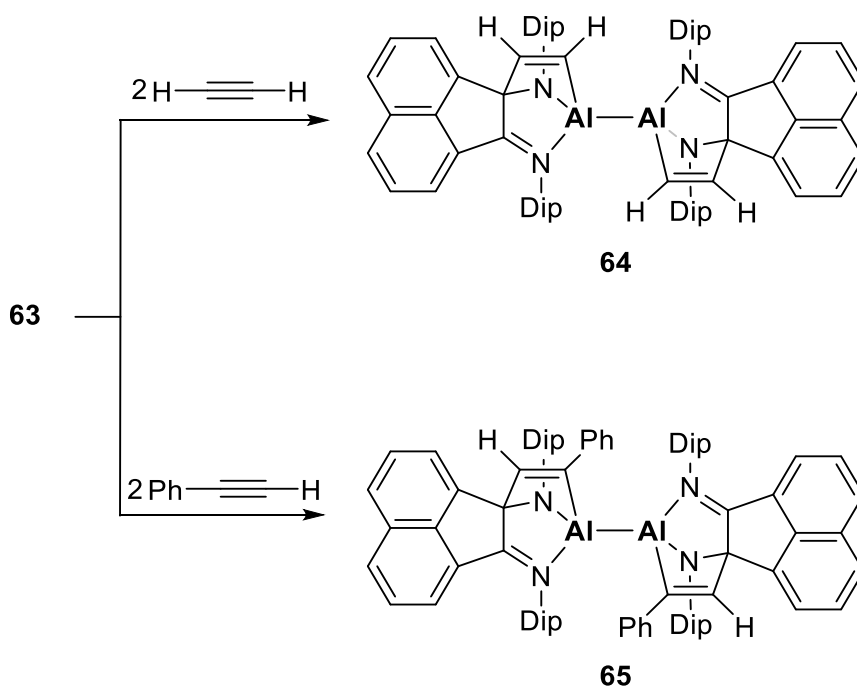
## 1. Introduction

In 2012, Fedushkin & Abakumov et al. reported a dialane **63** with redox-active bis-amido ligand (Scheme 43).



Scheme 43: Synthesis of compound **63**.

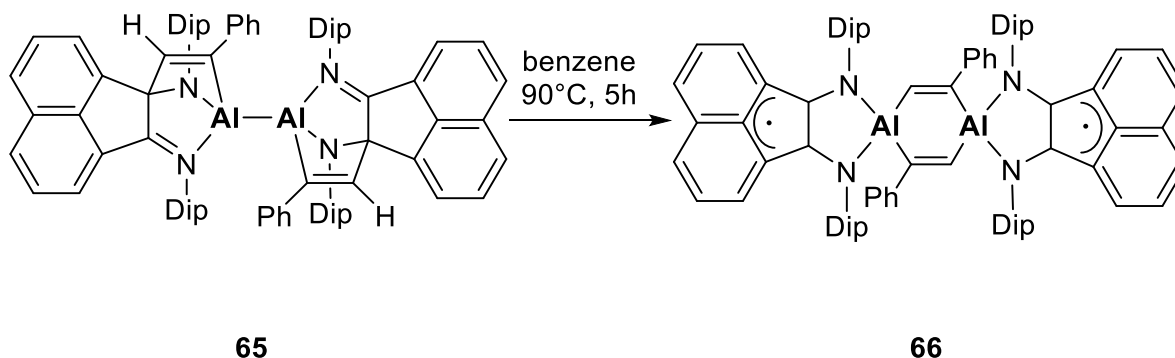
Thus, new reactivities of these compounds could be demonstrated (Scheme 44).<sup>187</sup> Aluminum atoms in compound **63** adopt a trigonal planar geometry with an Al-Al distance of 252.2 pm. This is the shortest Al-Al bond length of any acyclic symmetrical substituted dialane known in literature before 2012. Compound **63** reacts with alkynes in a cycloaddition reaction and inserts two alkyne molecules (Scheme 44).



Scheme 44: Synthesis of compounds **64** and **65**.

## 1. Introduction

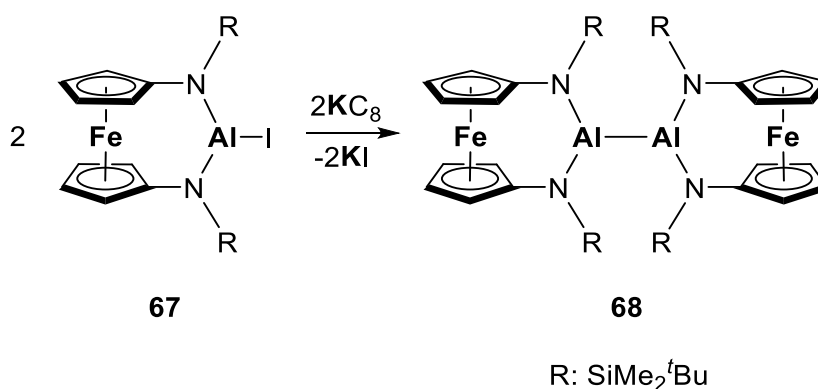
The product of the cycloaddition **65** undergoes a rearrangement reaction, such that a symmetrical structure with two radical-anionic <sup>Dipp</sup>phian ligands and two bridging alken-1,2-diyl moieties can be produced (Scheme 45).



Scheme 45: Rearrangement of compound **65** into compound **66**.

The insertion of the two molecules of acetylene and phenylacetylene into compound **63** leads to the elongation of the Al-Al distance to 254.8 pm and 260.0 pm in compounds **64** and **65**, respectively.

In 2018, *Siemeling* et al. synthesized a dialane **68** with an Al-Al bond length in line with the one observed for compound **63** (Scheme 46).<sup>188</sup>



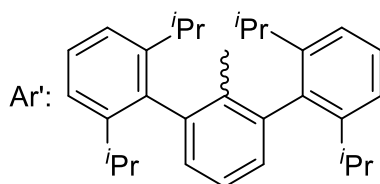
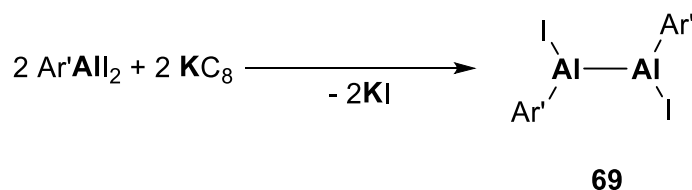
Scheme 46: Synthesis of compound **68**.

Compound **68** was synthesized via the reduction of compound **67** with potassium graphite. The aluminum atoms possess a trigonal planar environment with an Al-Al distance of

## 1. Introduction

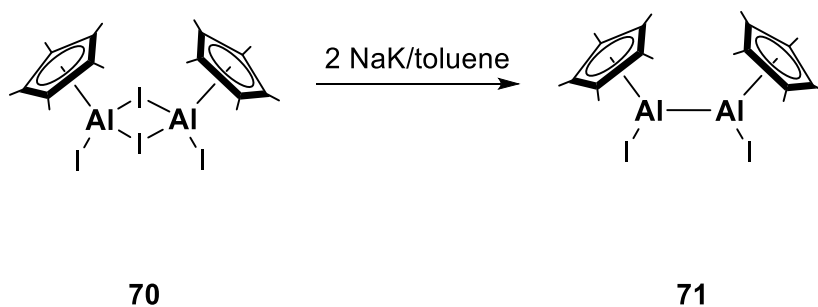
252.6 pm. An explanation for the Al-Al distance could be that the London dispersion forces between the peripheral methyl groups give an additionally stabilizing influence.

In 2003, *Power et al.* managed to synthesize a new asymmetrically substituted dialane **69** with an Al-Al bond of 260.9 pm (Scheme 47).<sup>189</sup> The aryl substituents of each are bonded in *trans* position to one another's in compound **69**. The short Al-Al bond is likely due to the contraction of the effective radius of Al by the iodine substituent.



**Scheme 47: Synthesis of compound 69.**

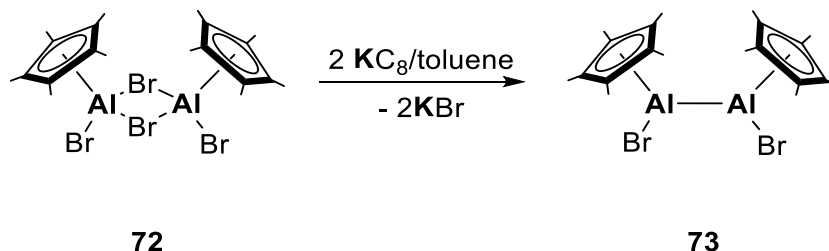
In 2008, *Arnold et al.* synthesized a new complex **71** with pentamethylcyclopentadienyl ligand as a bulky substituent and an Al-Al distance of 253.2 pm. It was produced via a reduction reaction of the monosubstituted pentamethylcyclopentadienyl diiodoalane **70**, which is a dimer with  $\eta^5$  bonded pentamethylcyclopentadienyl ligands to aluminum atom in the solid state, with sodium/potassium alloy (Scheme 48).<sup>190</sup> Compound **71** represents the first acyclic asymmetrical dialane with a  $\eta^5$  bonded pentamethylcyclopentadienyl ligands.



**Scheme 48: Synthesis of complex 71.**

## 1. Introduction

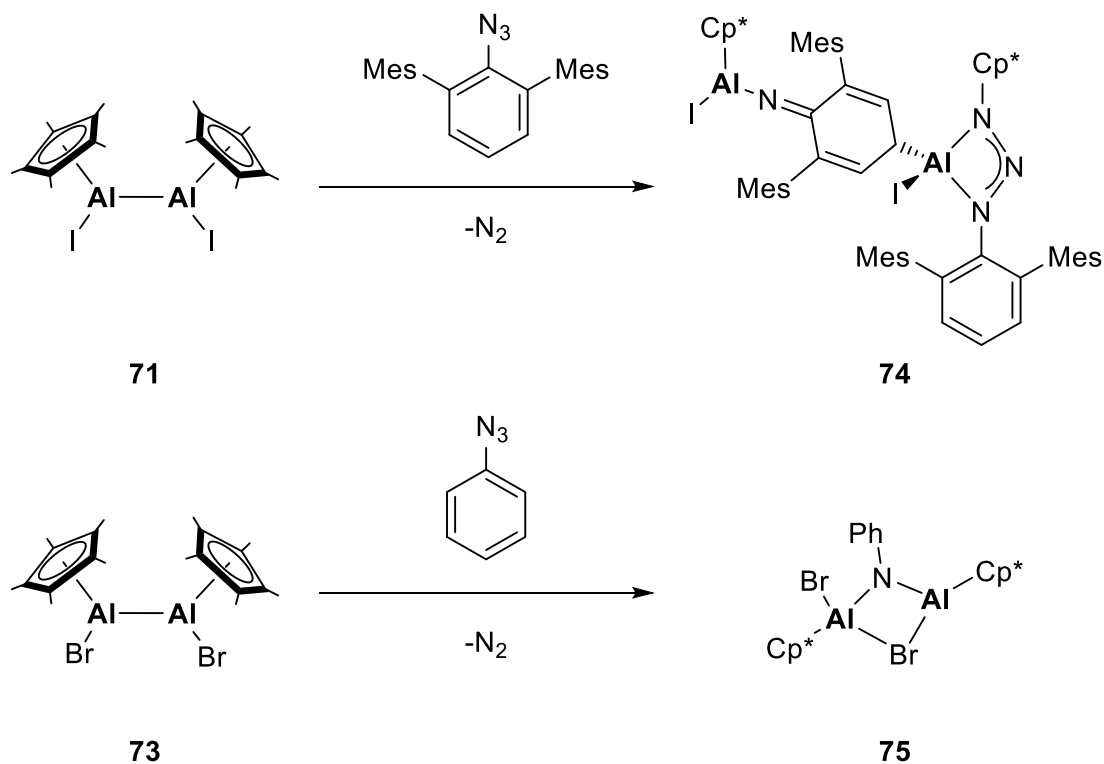
In 2018, *Braunschweig* et al. reported a related complex with bromide instead of iodide substituents (Scheme 49).<sup>191</sup>



Scheme 49: Synthesis of complex **73**.

The Al-Al distance of 253.0 pm in compound **73** is approximately identical to that of compound **71**, indicating no influence of the halide on the Al-Al bond length. The reduction of the chlorinated precursor only led to compound [Cp\*Al]<sub>4</sub> **8** and unreacted [Cp\*AlCl<sub>2</sub>]<sub>2</sub>.

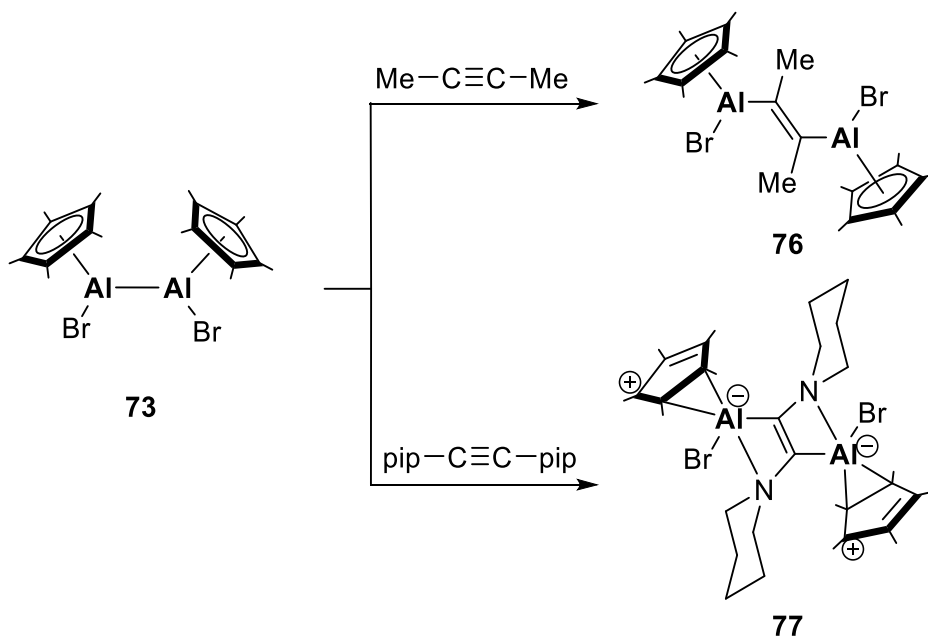
Both groups studied the reactivity of these dialanes, **71** and **73**, for example with arylazides, and they observed different products in an oxidative cleavage of the Al-Al bond (Scheme 50).<sup>189,191</sup>



Scheme 50: Reaction of different azide substrates with compounds **71** and **73**.

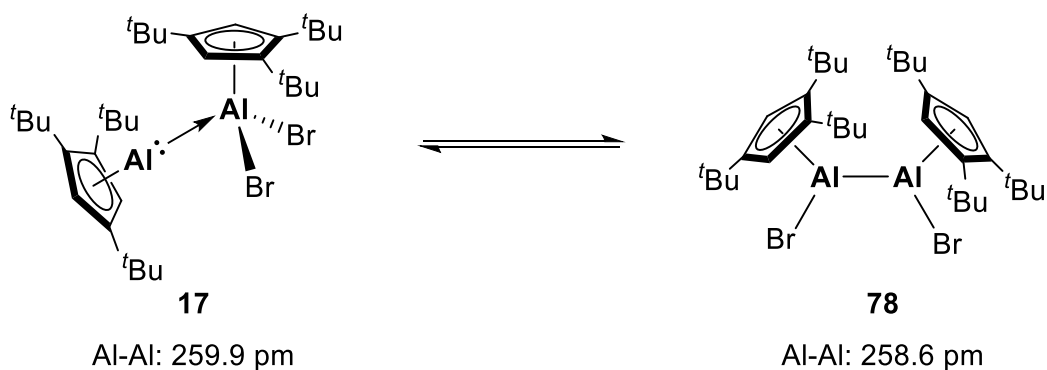
## 1. Introduction

*Arnold* also found that compound **71** could be iodinated to yield compound **70** again. *Braunschweig* reported that the Al-Al bond could allow insertion of unsaturated substrates like substituted acetylene to form new compounds with a change in the hapticity of the bound pentamethylcyclopentadienyl ligand from  $\eta^5$  to  $\eta^2$  in compound **77** (Scheme 51).



**Scheme 51:** Reaction of compound **73** with unsaturated substrates via insertion reaction into the Al-Al bond.

In 2019, *Braunschweig* et. al. also synthesized a new monomeric cyclopentadienyl Al(I) compound **16** featuring Lewis base property (Scheme 16 and 17, chapter 1.5.1.). The Lewis acid/base adduct **17** isomerizes to a dialane **78** indicating approximately similar Al-Al bond length (Scheme 52).<sup>139</sup>

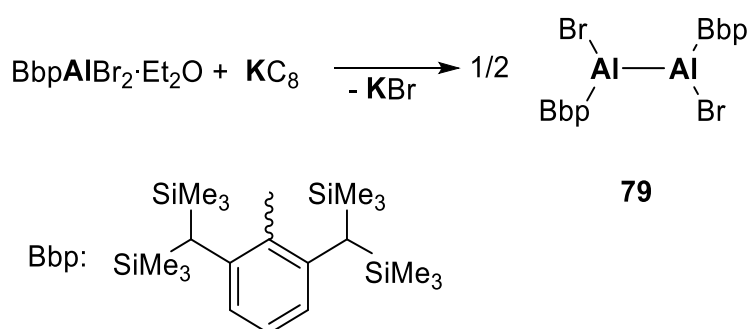


## 1. Introduction

### Scheme 52: Isomerization of 17 to dialane 78.

The comparison between the Al-Al bond lengths of 253.9 pm in compounds **73** and 258.6 pm in **78** indicates the influence of the elevated steric demanding cyclopentadienyl ligand on the Al-Al distances.

Analogous to compound **69**, Tokitoh et al. reported a dialane **79**, which is supported by a bulky aryl substituent (Scheme 53) with an Al-Al bond length of 259.2 pm.<sup>192</sup>



Scheme 53: Synthesis of compound **79**.

In summary, acyclic dialanes differ in the Al-Al bond lengths according to the elevated steric demand of the substituents bound to aluminum atoms (Figure 21 and 22). This influence is clearly observed in compounds **57**, **59**, and **62** with Al-Al bond lengths 263.0 pm, 264.7 pm and 275.1 pm, respectively<sup>175,176,183</sup> as well as in compounds **71**, **73** and **78**.



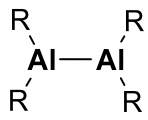
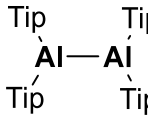
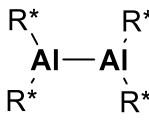
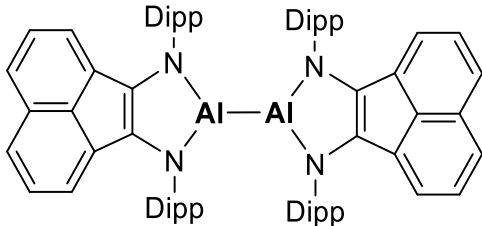
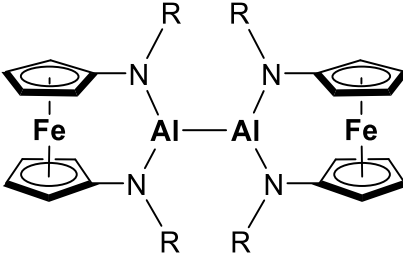
acyclic symmetrical dialane		
<p><b><u>Uhl</u></b></p>  <p>(1988) Al-Al: 263.0 pm <b>57</b></p> <p>R: [(Me<sub>3</sub>Si)<sub>2</sub>CH]</p>	<p><b><u>Power</u></b></p>  <p>(1993) Al-Al: 264.7 pm <b>59</b></p> <p>Tip: 2,4,6-<sup>i</sup>Pr<sub>3</sub>C<sub>6</sub>H<sub>2</sub></p>	<p><b><u>Wiberg</u></b></p>  <p>(1998) Al-Al: 275.1 pm <b>62</b></p> <p>R*: Si(<sup>t</sup>Bu)<sub>3</sub></p>
<p><b><u>Fedushkin &amp; Abakumov</u></b></p>  <p>(2012) Al-Al: 252.2 pm <b>63</b></p> <p>Dipp: 2,6-<sup>i</sup>Pr<sub>2</sub>C<sub>6</sub>H<sub>3</sub></p>	<p><b><u>Siemeling</u></b></p>  <p>(2018) Al-Al: 252.6 pm <b>68</b></p> <p>R: SiMe<sub>2</sub><sup>t</sup>Bu</p>	

Figure 21: Representation of examples for acyclic symmetrically and dialanes.

On the other hand, the highly steric demand of the Si(<sup>t</sup>Bu)<sub>3</sub> group in compound **62** increases the attractive dispersion interaction forces so that the Al-Al bond remains stable below a temperature of 50°C. This weak stability of compound **62** is reflected in its reactivity, such that compound **62** can activate a hydrogen molecule. This means that the bound substituent could also influence the reactivity of these compounds.

Including the dialanes, a substituent that is able to build with the aluminum centers a bond mostly involving *p*-orbitals like Cp\* in compounds **71** and **73** or a bond with double bond

## 1. Introduction

character like an amine in compounds **63** and **68** led to a shortening the Al-Al bond length by ca 7-13 pm, as compared to compounds which include a substituent that lack this ability.<sup>187,188</sup>

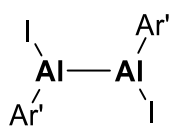
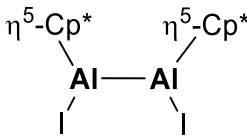
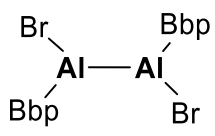
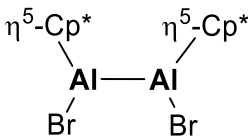
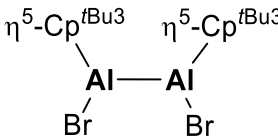
<b>acyclic asymmetrical dialane</b>		
<p><b><u>Power</u></b></p>  <p><b>2003</b> Al-Al: 260.9 pm <b>69</b></p> <p>Ar': 2,6-(Dipp)<sub>2</sub>-C<sub>6</sub>H<sub>3</sub> Dipp: 2,6-<sup>i</sup>Pr<sub>2</sub>C<sub>6</sub>H<sub>3</sub></p>	<p><b><u>Arnold</u></b></p>  <p><b>2008</b> Al-Al: 253.2 pm <b>71</b></p> <p>Cp*:(Me<sub>5</sub>C<sub>5</sub>)</p>	<p><b><u>Tokitoh</u></b></p>  <p><b>2012</b> Al-Al: 259.2 pm <b>79</b></p> <p>Bbp: 2,6-[(Me<sub>3</sub>Si)<sub>2</sub>CH]<sub>2</sub>-C<sub>6</sub>H<sub>3</sub></p>
<p><b><u>Braunschweig</u></b></p>  <p><b>2018</b> Al-Al: 253.0 pm <b>73</b></p> <p>Cp*:(Me<sub>5</sub>C<sub>5</sub>)</p>	<p><b><u>Braunschweig</u></b></p>  <p><b>2018</b> Al-Al: 258.6 pm <b>78</b></p>	

Figure 22: Representation of examples for acyclic asymmetrically and dialanes.

A reason for this could be that the *s*-orbital of the aluminum atoms is more involved in the Al-Al bond, leading to this shortening, whereas the *p*-orbitals of the aluminum atoms are more engaged in the bonding-interaction to the substituents. On the other hand, the highly steric demand of the cyclopentadienyl ligand increases the Al-Al distance in compound **78** so that the repulsion of the substituents <sup>t</sup>Bu on cyclopentadienyl ligand could be minimized as possible.

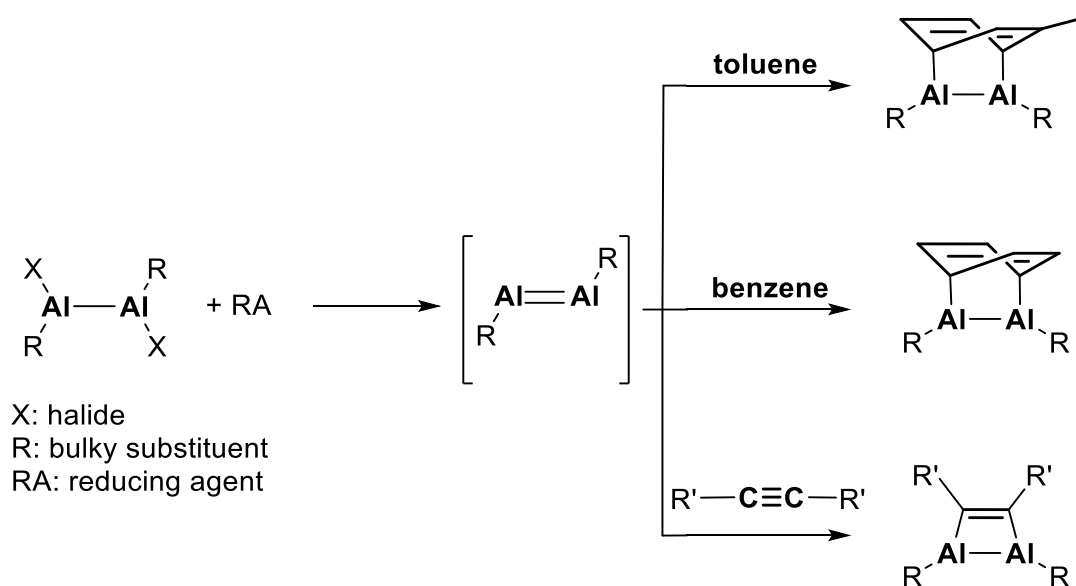
Comparing the Al-Al bond length of compound **71** with that of compound **73** reveals nearly no difference although they differ in the halogenide substituent. This indicates that the halogenide

## 1. Introduction

substituents have a similar influence on the Al-Al bond length but a different influence on the reactivity of the dialanes compound such that compound **73** showed lower reactivity (controllable) towards dialumination of unsaturated species, while compound **71** undergoes further Al-migration and C-H activation.<sup>190,191</sup> This difference in the reactivity between **71** and **73** can be traced back to the fact that Al-Br bond is less labile than Al-I bond.

The influence of the elevated steric demanding cyclopentadienyl ligand on the Al-Al bond length is clearly observed by comparing the Al-Al distances in compounds **73** and **78** due to the repulsion of the bonded substituents to the cyclopentadienyl rings.

In the literature, the acyclic asymmetrically substituted dialane compounds bearing a halide (like compounds **69** and **79**) represent the starting materials for cyclic dialanes. The reduction of these compounds produces very reactive species which are mostly expected to be dialenes or dialumenes. These species will react with a solvent or an alkyne in a cycloaddition reaction to yield a cyclic dialane (Scheme 54, Figure 23). The reduction of compounds **71** or **73** leads to compound **8** [AlCp\*]<sub>4</sub>.



Scheme 54: General representation of the synthesis of cyclic dialanes.

Regarding this, three examples were synthesized by the reduction of the corresponding acyclic asymmetrically substituted dialanes with potassium graphite to yield a cyclic dialane (Figure 23).<sup>189,193–196</sup>

## 1. Introduction

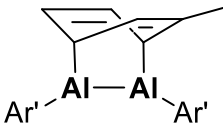
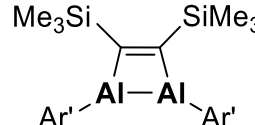
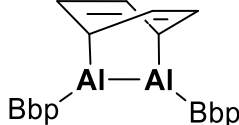
cyclic dialane		
<p><b><u>Power</u></b></p>  <p>Ar'—Al—Al—Ar'</p> <p><u>2003</u> Al-Al: 258.3 pm <b>80</b></p> <p>Ar': 2,6-(Dipp)<sub>2</sub>-C<sub>6</sub>H<sub>3</sub> Dipp: 2,6-<sup>i</sup>Pr<sub>2</sub>C<sub>6</sub>H<sub>3</sub></p>	<p><b><u>Cui</u></b></p>  <p>Me<sub>3</sub>Si—C=C—SiMe<sub>3</sub></p> <p>Ar'—Al—Al—Ar'</p> <p><u>2006</u> Al-Al: 249.5 pm <b>81</b></p> <p>Ar': 2,6-(Dipp)<sub>2</sub>-C<sub>6</sub>H<sub>3</sub> Dipp: 2,6-<sup>i</sup>Pr<sub>2</sub>C<sub>6</sub>H<sub>3</sub></p>	<p><b><u>Tokitoh</u></b></p>  <p>Bbp—Al—Al—Bbp</p> <p><u>2013</u> Al-Al: 259.2 pm <b>82</b></p> <p>Bbp: 2,6-[(Me<sub>3</sub>Si)<sub>2</sub>CH]<sub>2</sub>-C<sub>6</sub>H<sub>3</sub></p>

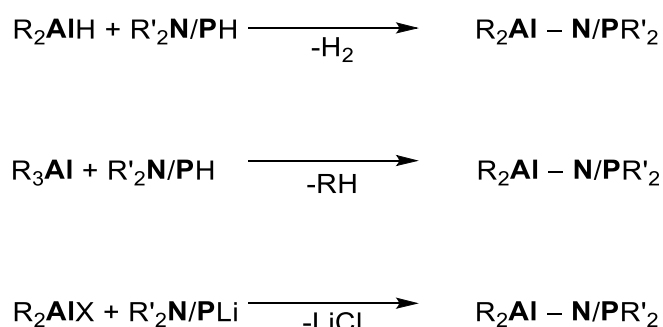
Figure 23: Representation of examples for cyclic dialanes with corresponding Al-Al bond lengths.

The Al-Al bonds are of different distances with regard to the formed ring. Cyclic dialane with four membered ring exhibits shorter Al-Al bond length (249.5 pm in compound **81**) than cyclic dialanes including six membered rings (258.3 and 259.2 pm in compounds **80** and **82**, respectively). The Al-Al bond length of compound **81** has a double bond character which resembles the anion radical dialane compound **60** with Al-Al bond length of 247.0 pm. There is only one example in the literature (by *Inoue* et al. in 2017) of an isolated dialumene with an Al-Al bond length of 239.4 pm.<sup>197</sup> In conclusion, the aluminum-aluminum bond length in a cyclic dialane is mostly influenced by the formed ring.

## 1.7. Amino- and Phosphanalane

Compounds with the form  $R_2E^{13}-E^{15}R'_2$  ( $E^{13}$ : B, Al, Ga, In and Tl;  $E^{15}$ : N, P, As, Sb and Bi), also known as pnictogenyltrielanes, have attracted attention for a long time<sup>198-219</sup> regarding their applications in catalysis,<sup>220-227</sup> as precursors for the generation of thin films of AlN and group 13/15 semiconductors,<sup>228-239</sup> generation of radicals<sup>240</sup> and nanocrystalline materials,<sup>241,242</sup> as precursor sources of micro- and optoelectronic apparatus,<sup>215,243-249</sup> in bond activation processes,<sup>250-267</sup> in C-H metalation reactions,<sup>268-271</sup> and as new precursors of AlP ceramic.<sup>272-275</sup>

Aminoalane and phosphanalane compounds with the form  $R_2Al-(N/P)R'_2$  can be synthesized via different routes (Scheme 55) (i) elimination of  $H_2$ ,<sup>276-283</sup> (ii) elimination of an alkane,<sup>199,207,268,284-287</sup> (iii) and salt metathesis.<sup>199,288-296</sup>



Scheme 55: Representation of the synthesis routes of aminoalane and phosphanalane.

The bond between a pnictogen and a triel in monomeric compounds with the form  $R_2E^{13}-E^{15}R'_2$  ( $E^{15} = N$  and P) can possess a double bond nature depending on the donating of the lone pair of pnictogen into the vacant  $p$ -orbital on the triel (dative  $\pi$ -bonding), as seen in amido boranes (Figure 24).<sup>204,209</sup>

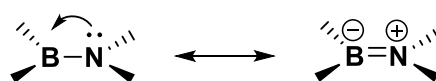


Figure 24: Representation of the lone pair donation of nitrogen into the vacant  $p$ -orbital on boron.

## 1. Introduction

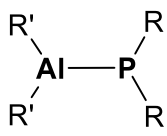
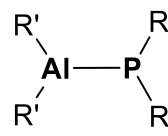
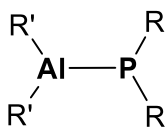
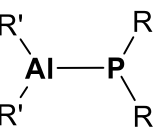
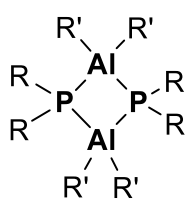
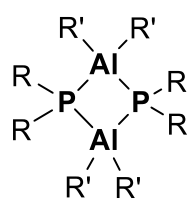
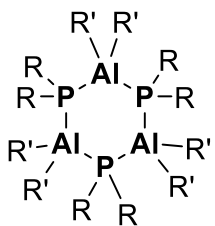
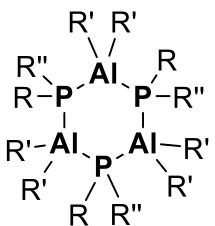
Aminoalane and phosphanylalane compounds possess monomeric or oligomeric structures. Figures 25 and 26 summarize instances of aminoalanes and phosphanylalanes in both forms.<sup>268,276,278,284–286,294,295,297–302</sup>

Monomeric aminoalane				
Al-N: 181.4 pm R: biph R': Cl	Al-N: 184.5 pm R: biph R': Me	Al-N: 182.4 pm R: biph R': Et	Al-N: 181.5 pm R: tmp R': C <sub>6</sub> F <sub>5</sub>	Al-N: 186.9 pm R: Si( <sup>t</sup> Bu) <sub>2</sub> Me R': Me
<b>83</b>	<b>84</b>	<b>85</b>	<b>86</b>	<b>87</b>
Oligomeric aminoalane				
Al-N: 198.3, 200.9 pm R: C <sub>6</sub> F <sub>5</sub> R': Me R'': H	Al-N: 195.3 pm R: Me R': <sup>i</sup> Pr	Al-N: 195.3, 197.9 pm R: Me R': NMe <sub>2</sub>	Al-N: 198.4 pm R: <sup>i</sup> Bu R': Me	Al-N: 199.1, 202.4 pm R: Ph R': Me R'': SiMe <sub>3</sub>
<b>88</b>	<b>89</b>	<b>90</b>	<b>91</b>	<b>92</b>

Figure 25: Presentation of instances of monomeric and oligomeric aminoalane structures with Al-N bond lengths (biph: biphenyl, tmp: *tetra*-methylpyridin, <sup>t</sup>Bu: *tert*-butyl, <sup>i</sup>Bu: *iso*-butyl).

The monomeric structures of the aminoalanes and phosphanylalanes can have similar properties to amido boranes with respect to the bonding arrangement (double bond character throughout a dative  $\pi$ -bonding). The oligomerization of an aminoalane or a phosphanylalane can be controlled via the steric demand of the substituents bound to both atoms (Al and N or P). When the substituent is bulky enough, the compound will be monomeric.

## 1. Introduction

Monomeric phosphanylalane			
 <p>Al-P: 234.2 pm R: Tip R': SiPh<sub>3</sub></p> <p><b>93</b></p>	 <p>Al-P: 233.4 pm R: tmp R': SnMe<sub>3</sub></p> <p><b>94</b></p>	 <p>Al-P: 236.1 pm R: tmp R': SiMe<sub>3</sub></p> <p><b>95</b></p>	 <p>Al-P: 235.4 pm R: Mes R': <sup>t</sup>Bu</p> <p><b>96</b></p>
Oligomeric phosphanylalane			
 <p>Al-P: 247.6 pm R: Ph R': <sup>i</sup>Bu</p> <p><b>97</b></p>	 <p>Al-P: 244.6 pm R: Ph R': SiMe<sub>3</sub></p> <p><b>98</b></p>	 <p>Al-P: 244.6-247.9 pm R: Ph R': Me</p> <p><b>99</b></p>	 <p>Al-P: 244.4 pm R: Ph R': SiMe<sub>3</sub> R'': H</p> <p><b>100</b></p>

**Figure 26: Presentation of instances of monomeric and oligomeric phosphanylalane structures with Al-P bond lengths (Ad: 1-adamantyl, tmp: *tetra*-methylpiperidin, <sup>t</sup>Bu: *tert*-butyl, <sup>i</sup>Bu: *iso*-butyl, Tip: 2,4,6-*tri*-isopropylphenyl).**

The instances in Figures 25 and 26 indicate that the Al-N bond lengths in monomeric aminoalane compounds are shorter by 8.4-21.0 pm than the Al-N bond lengths in the oligomers, while the Al-P bond lengths in monomeric phosphanylalane compounds are shorter by 8.5-14.5 pm than in the oligomeric compounds. This might be an argument for the double bond character of the Al-N bond more than for Al-P bond. Another argument for double bond character of Al-N bond and a single polarized Al-P bond can be that aluminum and nitrogen atoms have trigonal planar arrangements in all monomeric structures of aminoalanes, while phosphorous possesses a pyramidal coordination sphere in monomeric compounds of phosphanylalanes. In order to form a double bond between aluminum atom and nitrogen atom

## 1. Introduction

or phosphorous atom in an aminoalane or a phosphanylalane with the form  $R_2Al-(N/P)R'_2$ , the donation of the lone pair at the pnictogen atom (N and P) has to be efficient, which means that the coordination environment of the pnictogen (N and P) has to be planar and aligned to facilitate the  $p$ -orbital overlap. These conditions (the planarity and alignment) exist more in monomeric aminoalane compounds than phosphanylalane compounds (Figure 27).<sup>210,214</sup>

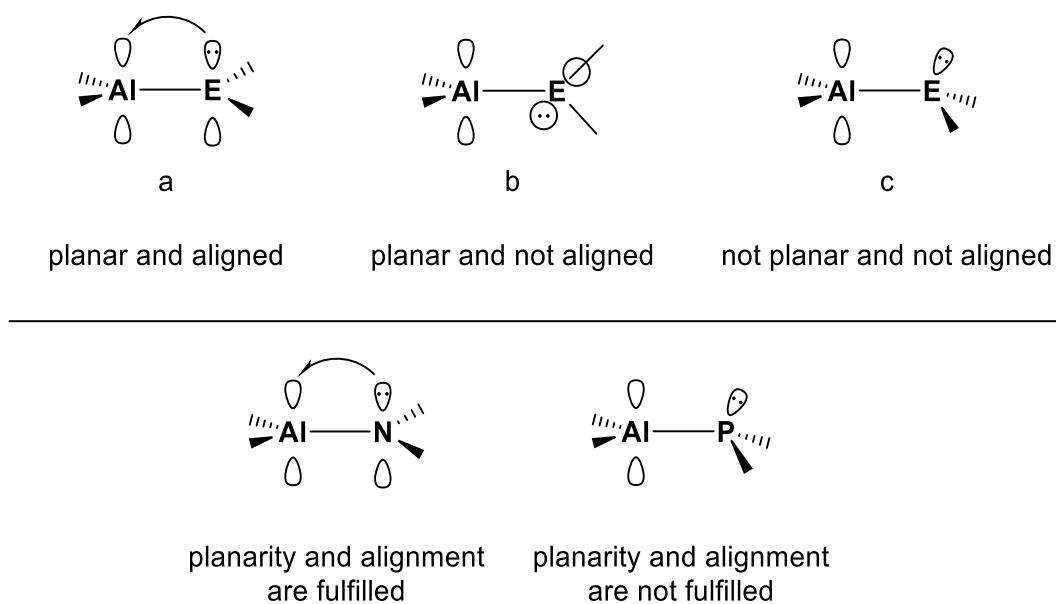


**Figure 27: Orientation of the lone pair in  $R_2Al-ER'_2$  (E: pnictogen) compared with aminoalane and phosphanylalane compounds.**

On the other hand, regarding the inversion barriers of the pnictogen atoms, which can be influenced by the bonded substituent to the pnictogen,<sup>303-307</sup> the heavier pnictogen possesses much higher barriers. For instance,  $\sim 146 \text{ kJ mol}^{-1}$  for  $PH_3$  compared to  $25 \text{ kJ mol}^{-1}$  for ammonia  $NH_3$ , which means phosphorous tends to build a pyramidal geometry (Figure 28).<sup>308-310</sup>

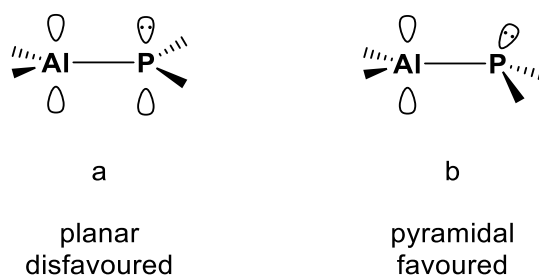


**Figure 28: Geometry of phosphorous in  $R_2Al-PR'_2$  a) planar and b) pyramidal.**



## 1. Introduction

Furthermore, the  $p$ -orbitals of aluminum and pnictogen atoms have to be energetically similar to maximize the overlap and increase the double bond character of Al-E (E: N, P). Figure 29 illustrates that the energy difference between the vacant  $p$ -orbital of aluminum and the lone pair of nitrogen ( $\Delta E_1$ ) is smaller than the energy difference between the vacant  $p$ -orbital of aluminum atom and the lone pair of phosphorous atom ( $\Delta E_2$ ), indicating that a  $p$ -orbital overlap between aluminum atom and nitrogen atom is more feasible than between aluminum atom and phosphorous atom.

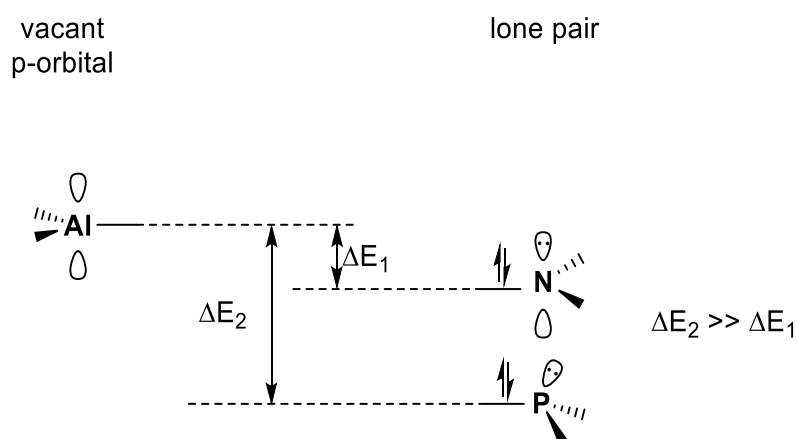
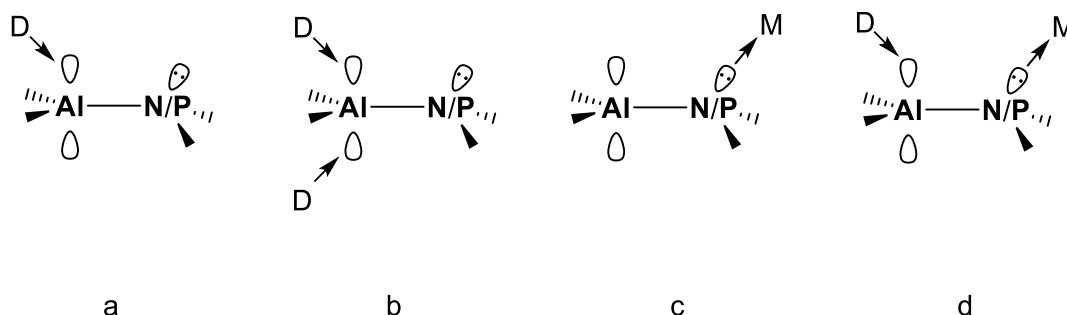


**Figure 29: Qualitative energy diagram of the  $p$  orbitals of the aluminum, nitrogen and phosphorous fragments.**

It is worth mentioning that the shortening of Al-N bond in  $R_2Al-NR'_2$  compounds compared with the sum of the Al-N covalent radii's (the sum of the aluminum and nitrogen covalent radii Al-N: 197 pm)<sup>311</sup> is not necessarily evidence of a multiple bond.<sup>209</sup> Previously, it was suggested that the bond between atoms with a partial ionic character, because of different electronegativities, is shorter than the sum of the covalent atoms radii.<sup>311-313</sup> This shortening of the Al-N bond compared with the sum of the Al-N covalent radii's resulted more from the ionic interaction rather than the Al-N  $\pi$ -bonding throughout the electron-donating via  $p$ - $p$  orbital overlap, which has a maximum value of  $45 \text{ kJ}\cdot\text{mol}^{-1}$  for a structure model with the form of  $H_2Al-NH_2$ .<sup>314</sup>

Amino- and phosphanylalane with the form  $R_2Al-(N/P)R'_2$  possess different chemical properties so that, for instance, they are amphoteric regarding the attendance of a Lewis acid center (Al) and Lewis base center (N/P). This property makes these compound classes very attractive in the coordination chemistry because they are able to associate with a transition metal fragments as well as with  $\sigma$ -donors,<sup>280,281,284,295,296,300,315-321</sup> thereby, aminoalane and phosphanylalane compounds can be stabilized as monomeric structures (Figure 30).

## 1. Introduction

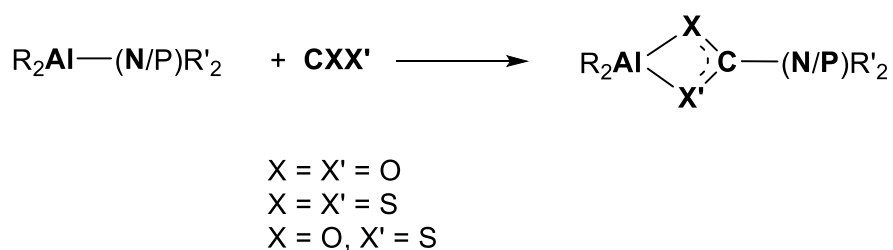


M: transition metal fragment  
D: donor

**Figure 30: Depiction of the amphoteric nature of amino- and phosphanylalane and the possible types of stabilization.**

However, it is known in literature that only phosphanylalane compounds build complexes with transition metal fragments like  $W(CO)_5$  and  $Cr(CO)_5$ .<sup>280,281,316,318</sup> On the other hand, the aminoalane compounds are able to activate the C-H bond of the bonded aryl to nitrogen.<sup>268,270,271</sup> Regarding the polarization of Al-N/P bond in aminoalane and phosphanylalane compounds due to different electronegativities, these compounds possess potential in the activation of small molecules such as  $CO_2$ ,  $CS_2$ , and  $COS$ ; thus, a molecule of these can be inserted between the aluminum atom and the pnictogen atom (Scheme 56).<sup>296,322–</sup>

326



**Scheme 56: Reaction of aminoalane and phosphanylalane compounds with small molecules.**

Such insertion reactions are illustrated by many authors in literature since 1995 and they are summarized in Figure 31.<sup>296,322–326</sup>

## 1. Introduction

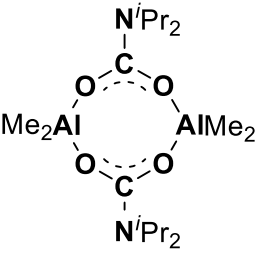
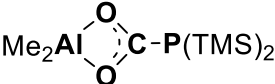
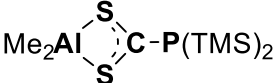
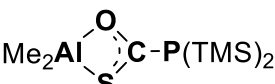
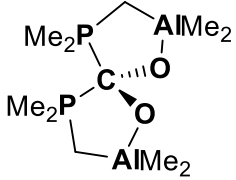
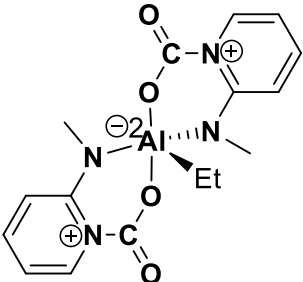
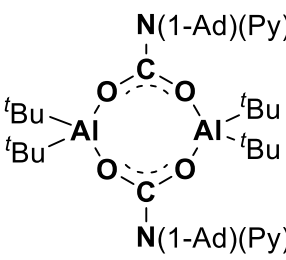
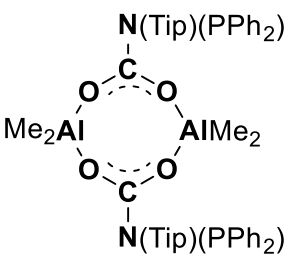
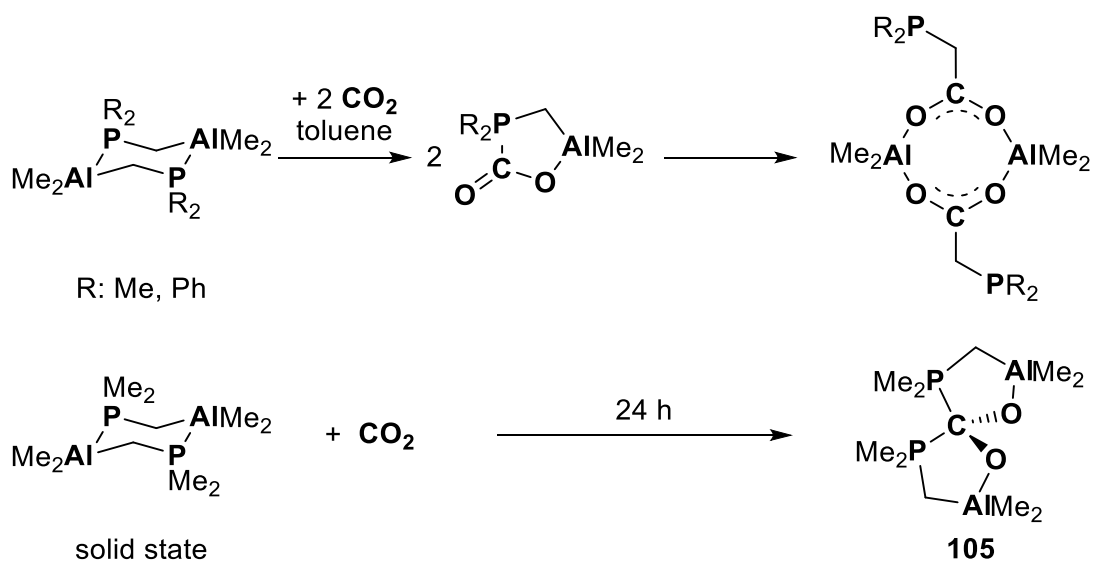
<i>Chang</i>	<i>Nöth&amp;Paine</i>	<i>Fontaine</i>
 <p style="text-align: center;"><b>101</b></p>	 <p style="text-align: center;"><b>102</b></p>  <p style="text-align: center;"><b>103</b></p>  <p style="text-align: center;"><b>104</b></p>	 <p style="text-align: center;"><b>105</b></p>
<i>Brewster</i>	<i>Uhl</i>	<i>Harder</i>
 <p style="text-align: center;"><b>106</b></p>	 <p style="text-align: center;"><b>107</b></p>	 <p style="text-align: center;"><b>108</b></p>

Figure 31: Representation of aminoalane and phosphanylalane compounds with CO<sub>2</sub>-, CS<sub>2</sub>- and COS-insertion.

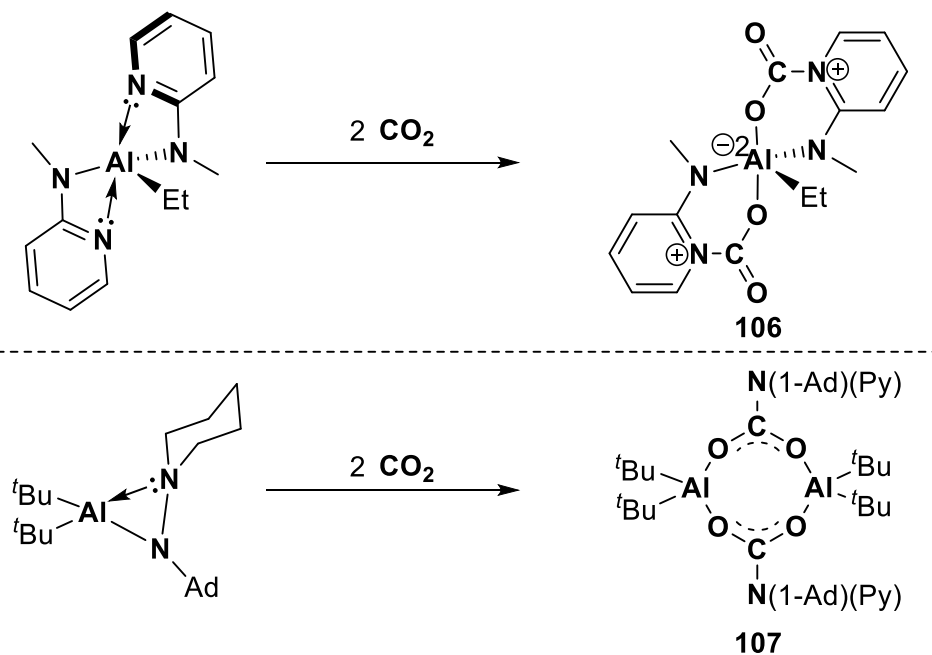
The compounds in Figure 31 differ in the starting materials so that the preparation of compound **101** started with an ethynyl-bridged polynuclear aluminum-magnesium complex, while the synthesis of compounds **102-104** started from monomeric phosphanylalane. Both compounds **105** and **108** are products of the reaction of dimeric starting materials with carbon dioxide. Interestingly, compound **105** was synthesized via a solid state reaction while the same reaction afforded another CO<sub>2</sub> insertion product in solution (Scheme 57).<sup>323</sup>

## 1. Introduction



Scheme 57: Reactivity of  $(\text{R}_2\text{PCH}_2\text{AlMe}_2)_2$  with  $\text{CO}_2$ .

Although the synthesis of both compounds **106** and **107** started from an amine-stabilized aminoalane, the insertion reaction of  $\text{CO}_2$  afforded two different products (Scheme 58).<sup>296,325</sup>

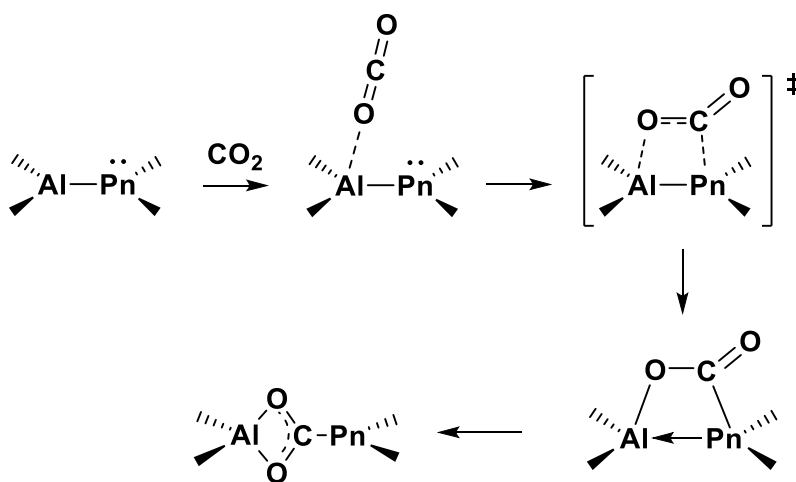


Scheme 58: Synthesis of compounds **101** and **102**.

## 1. Introduction

In compound **106**, the insertion of CO<sub>2</sub> occurs into the aluminum-nitrogen bond of the coordinated nitrogen atom (Al-donor bond) and not between the aluminum atom and the direct covalently bonded nitrogen atom. While in compound **107**, the CO<sub>2</sub> insertion occurred between the aluminum atom and the direct covalently bonded nitrogen atom.

Mechanistically, the insertion reaction of a CO<sub>2</sub> molecule into an aluminum-pnictogen bond occurs in different steps.<sup>327</sup> It starts by the coordination of a CO<sub>2</sub> molecule to aluminum center via the oxygen atom building a transition state with a four membered ring and followed by the rearrangement of the CO<sub>2</sub> moiety and insertion into the aluminum-pnictogen bond (Scheme 59).



Scheme 59: General mechanism of the CO<sub>2</sub> insertion into the Al-Pn bond.

In summary, amino- and phosphanylalanes with the form R<sub>2</sub>Al-(N/P)R'<sub>2</sub> possess an Al-N/P bond with less double bond character compared to those of amino- and phosphanylboranes.<sup>328–332</sup> Amino- and phosphanylalanes possess Lewis acid/base centers as well as very polar bonds (Al-N/P) because of different electronegativities, making them potentially interesting compounds for the activation of small unreactive molecules such as CO<sub>2</sub>.

## 2. Motivation

Metallocenophanes of transition metals were discovered at the end of the 1960s<sup>56</sup> and their chemistry developed rapidly in the last decades with regards to their application as monomer in ring opening polymerization (see chapter 1.4.). Furthermore, metallocenophanes of transition metals are also used in homogeneous catalysis.<sup>59,62,333</sup> However, such compounds of main-group elements, particularly of aluminum, are very rare. Until the beginning of this doctoral thesis in 2016, there was only a single report of aluminocenophane-type compounds **53-55**, published by *Shapiro* et al. in 2005 (Figure 32).<sup>53</sup>

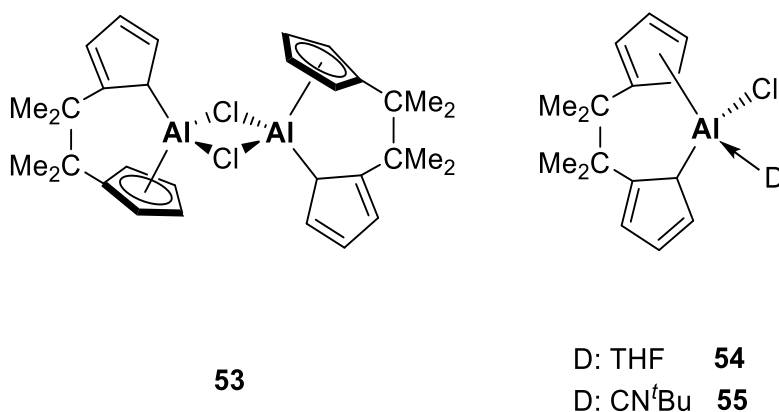


Figure 32: Instances of aluminocenophane derivatives until 2018.

This lack of aluminum complexes with two interlinked cyclopentadienyl ligands became the key motivation for further investigations in the course of this doctoral thesis. As an aim, different aluminum complexes with different linkages between the cyclopentadienyl ligands should be investigated (Figure 33) and new synthesis route were to be developed. Furthermore, the aluminum cyclopentadienyl bonding situation should be studied by the systematic variation of the third substituent. Moreover, aluminum-group 15 compounds substituted with interlinked cyclopentadienyl-groups as well as alkyl groups should be studied.

## 2. Motivation

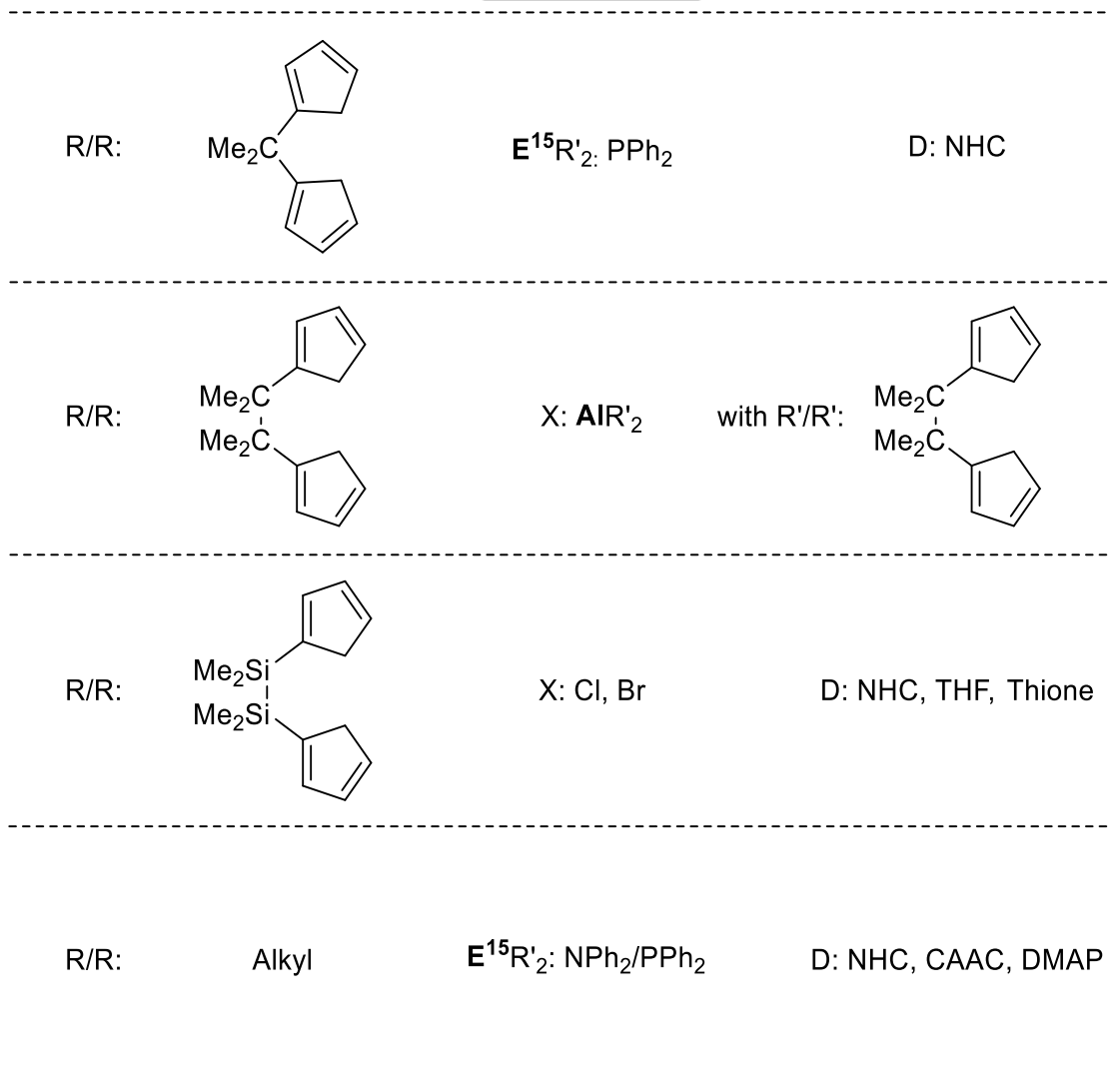
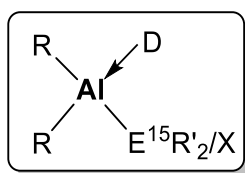


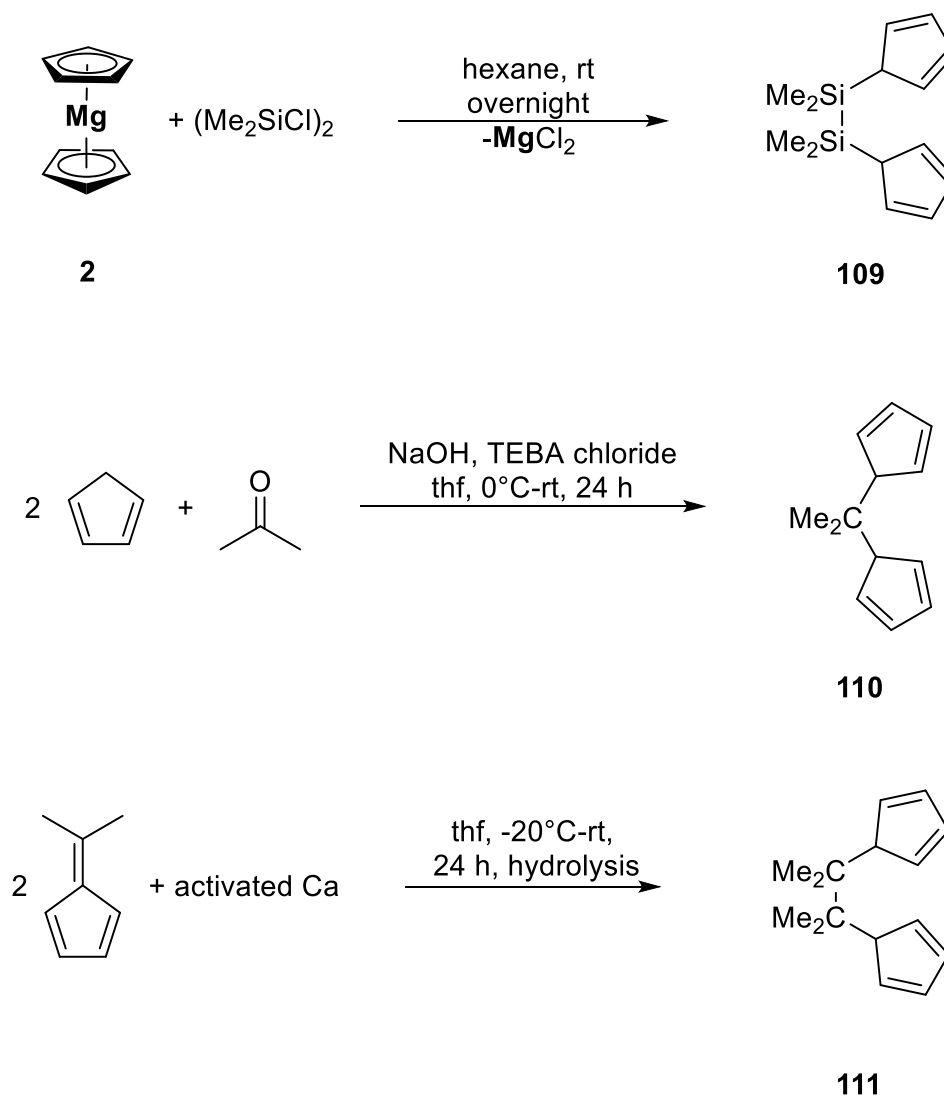
Figure 33: Representation of the scope of this doctoral thesis.

## 3. Results &amp; Discussion

## 3.1. Synthesis and Characterization of Magnesocenophanes

Parts of this chapter have been published in *Dalton Trans.*, 2018, **47**, 10425–10428; and *Chem. Eur. J.*, 2020, **26**, 6176–6184.

The synthesis of magnesocenophanes started with the synthesis of the free *ansa*-ligand as the first step. Scheme 60 explains the synthesis of all *ansa*-ligands which are utilized in this thesis.<sup>46,47,53,334–337</sup>



Scheme 60: Synthesis of the different *ansa*-ligands 109-111.



### 3. Results & Discussion

For compound **109**, other cyclopentadienyl transfer agents can be employed such alkali cyclopentadienide (LiCp). All of the *ansa*-ligands were obtained as a mixture of different isomers. These isomers are result from the fact that the double bonds in the cyclopentadienyl rings can exhibit three bonding modes (allyl, vinyl and allyl-vinyl) with altogether six isomers (Figure 34). The isomers could be clearly observed by  $^{29}\text{Si}$  NMR spectroscopy of compound **109**, which indicated nine signals. Compounds **109** and **110** were isolated as oils, while compound **111** was isolated as a crystalline solid.

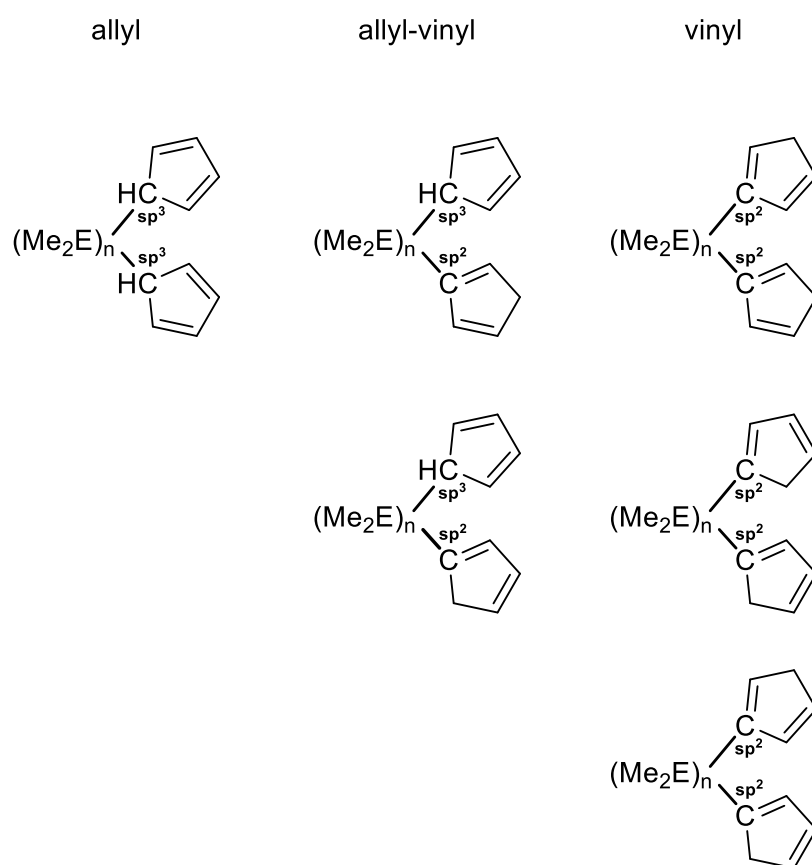
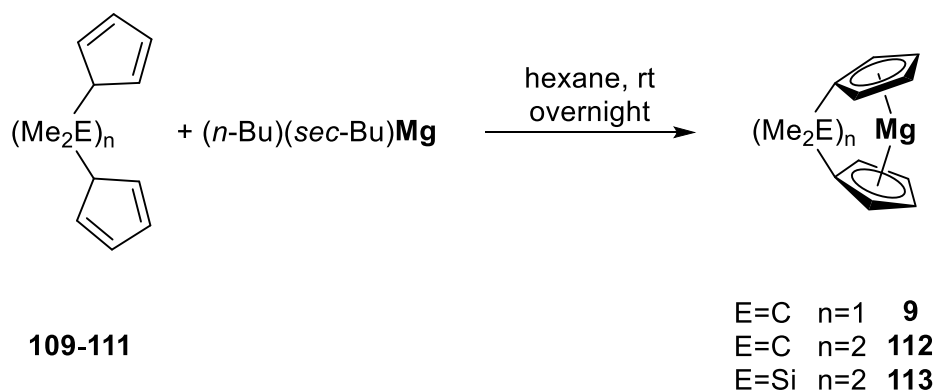


Figure 34: Isomers of the *ansa*-ligands **109-111** (**109**; E = Si, n = 2; **110**: E = C, n = 1; **111**: E = C, n = 2).

The second step in the synthesis of magnesocenophanes is the reaction of the free *ansa*-ligands **109-111** with  $(n\text{-Bu})(\text{sec-Bu})\text{Mg}$  to yield the corresponding magnesocenophanes **9**, **112** and **113** (Scheme 61).<sup>46,47,53,334,335</sup>

### 3. Results & Discussion



**Scheme 61: Synthesis of magnesocenophanes 9, 112 and 113.**

Compounds **9** and **112** are known in the literature and completely characterized.<sup>46,47,53,338</sup> The newly synthesized sila[2]magnesocenophane **113** could be isolated in good yields (54%) and was characterized via NMR spectroscopy in solution and via X-ray diffraction in the solid state. Single crystals of **113** in form of its Lewis acid base adduct **113**·dme, suitable for single crystal X-ray diffraction analysis, could be obtained from a toluene/dme solution at 253 K (Figure 35). In compound **113**·dme, a distorted  $\eta^5$  bonding between cyclopentadienyl rings and the metal center is observed with two different Mg1-Cp<sub>centroid</sub> bond lengths (226.6 pm and 230.8 pm); one longer by 4 pm but still in line with Mg1-Cp<sub>centroid</sub> of 230.5 pm in compound **9**·dme.<sup>334,335</sup>

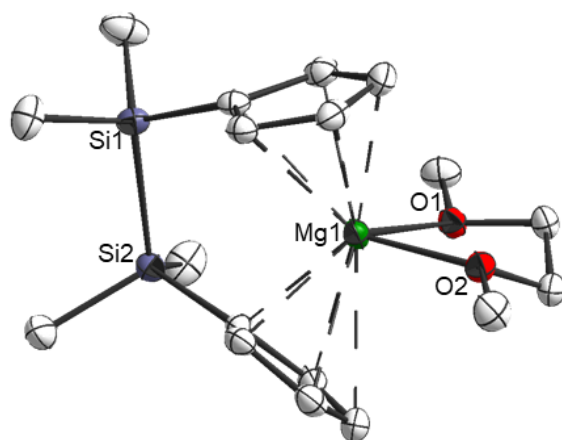


**Figure 35: Molecular structure of 113·dme in the crystal (thermal ellipsoids for 50% probability level, H-atoms were omitted for clarity).**

### 3. Results & Discussion

The distances between Mg1 atom and the oxygen atoms of the dme moiety are similar (Mg1-O1 = 212.5 pm and Mg1-O2 = 210.4 pm) and they are longer than the Mg-O bond length in **9**·dme (205.3 pm).<sup>334</sup> An explanation could be that the  $\alpha$ -angle of **9**·dme is larger than in **113**·dme ( $\alpha_{9\text{-dme}} = 80.1^\circ$ ,  $\alpha_{108\text{-dme}} = 52.7^\circ$ ) which make the magnesium atom more Lewis-acidic and sterically more accessible so that the dme molecule is more strongly bonded to the magnesium atom.

In the  $^1\text{H}$  NMR spectrum of **113**, one signal was detected for the cyclopentadienyl protons in solution compared to the **113**·dme spectrum, which features two signals (Figure 36) due to different vicinities of the cyclopentadienyl rings in **113**·dme. Moreover, the signal in the  $^{29}\text{Si}$  NMR spectrum of **113**·dme is downfield shifted -27.2 ppm compared to the signal of **113** of -24.2 ppm in the  $^{29}\text{Si}$  NMR spectrum.

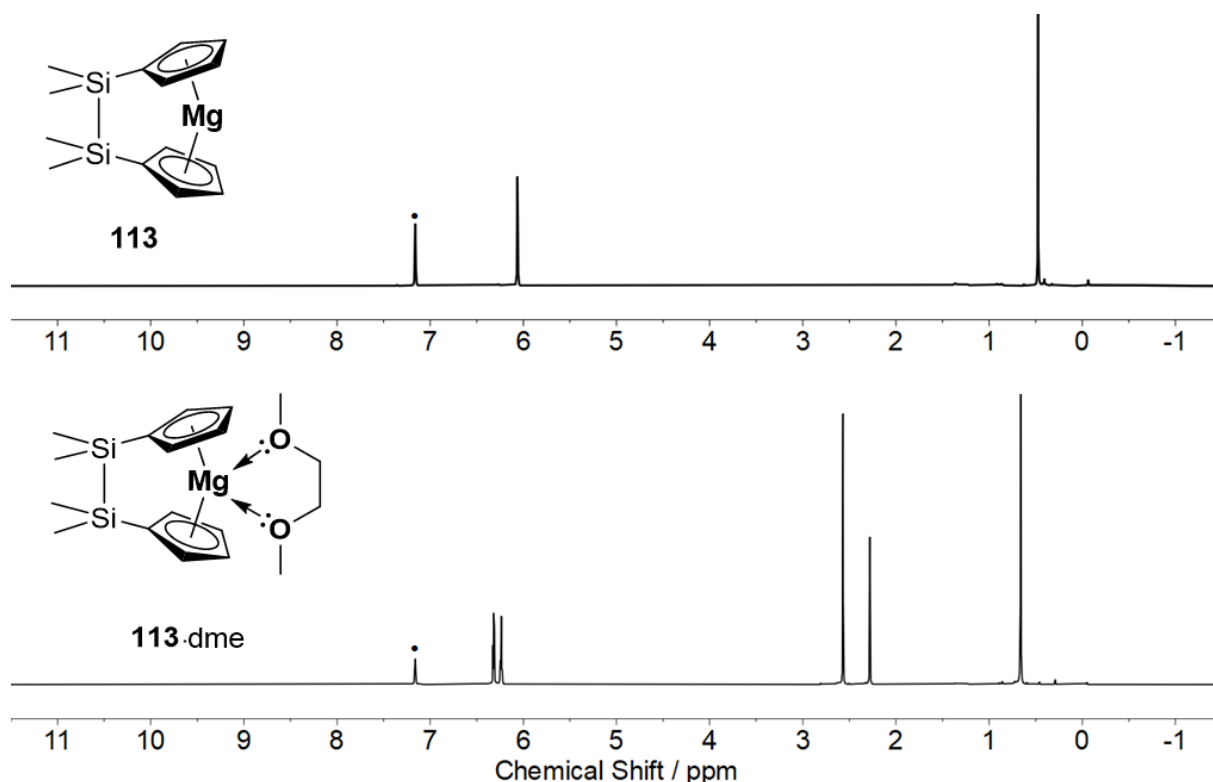
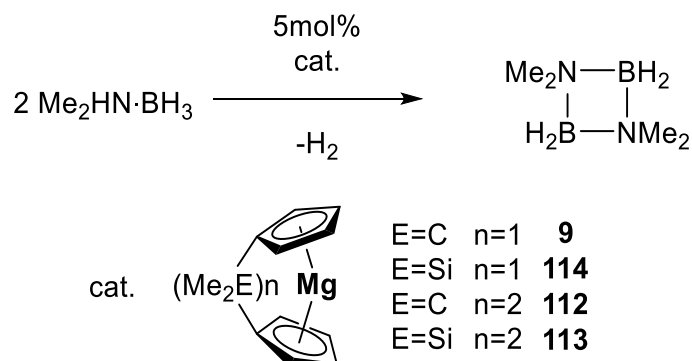


Figure 36:  $^1\text{H}$  NMR spectra of **113** and **113**·dme in  $\text{C}_6\text{D}_6$  by (398 K, 400 MHz)( $\bullet = \text{C}_6\text{HD}_5$  signal).

The main application of the magnesocenophanes is still as a cyclopentadienyl transfer agent in transmetalation reactions throughout the synthesis of metallocenophanes of d-elements or p-block elements.<sup>53-55</sup> In 2020, our group showed that magnesocenophanes are able to catalyze dehydrocoupling reactions of amine boranes (Scheme 62). It could be demonstrated that C[1]magnesocenophanes **9** and Si[1]magnesocenophanes **114** gave the best results

### 3. Results & Discussion

compared with magnesocene **2**, dibutylmagnesium  $n\text{-Bu}_2\text{Mg}$ , C[2]magnesocenophane **112** and Si[2]magnesocenophane **113**.<sup>334</sup>



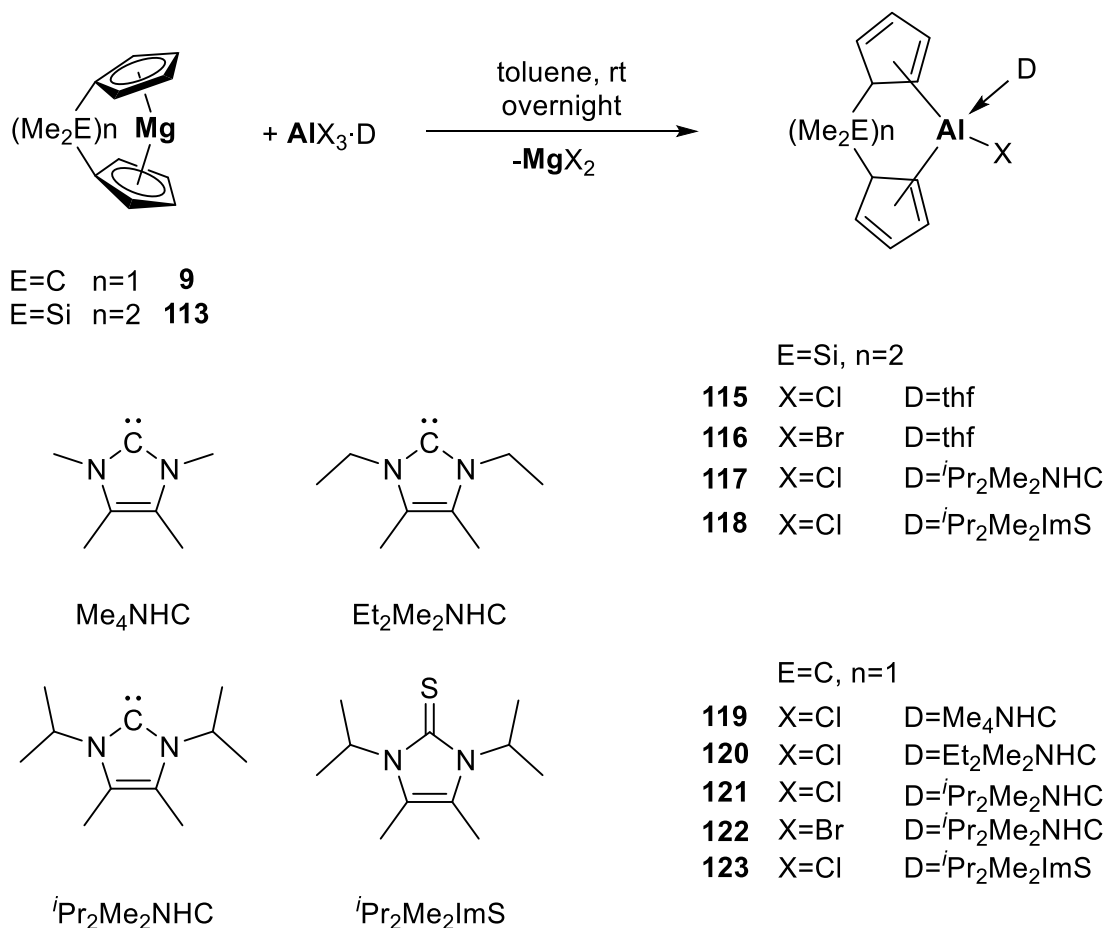
**Scheme 62: Magnesocenophans catalyzed dehydrocoupling reaction of the dimethylamine borane.**

In this work, we also examined the Lewis acidity of compounds **9**, **112-114** computationally and demonstrated it to be a function of the tilting of the cyclopentadienyl rings.

## 3.2. Donor-stabilized Aluminocenophane derivatives

Parts of this chapter have been published in *Dalton Trans.*, 2018, **47**, 10425–10428; and *ChemistryOpen*, 2020, **9**, 1095–1099.

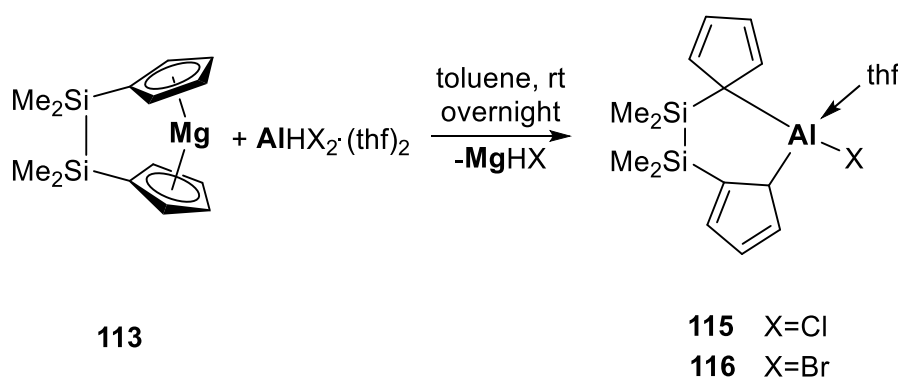
The synthesis of compounds **115–123** started with Lewis acid/base adducts of aluminum(III)halides/donors which were generated *in situ* by the treatment of the aluminum(III)halide with the corresponding donor in toluene at room temperature. The Addition of magnesocenophane **9** or **113** afforded the corresponding donor stabilized sila[2]- or carba[1]bis(cyclopentadienyl)aluminum compounds **115–123** (Scheme 63).<sup>335,339</sup>



Scheme 63: Synthesis of compounds 115-123.

### 3. Results & Discussion

All attempts with sterically more demanding carbenes such as 1,3-bis(2,6-diisopropylphenyl)imidazolin-2-ylidene (SIDipp) and a Cyclic(amino)(alkyl)carbene (<sup>Me</sup>CAAC) indicated no transmetalation reaction at room temperature with C[1]magnesocenophane **9**. Compounds **115** and **116** were synthesized in another way by reacting **113** and  $\text{AlHX}_2 \cdot (\text{thf})_2$ . The aim of this reaction was to generate the thf stabilized sila[2]bis(cyclopentadienyl)-aluminumhydride complexes by the elimination of  $\text{MgX}_2$  with  $\text{X} = \text{Cl}, \text{Br}$ . However,  $\text{MgXH}$  was surprisingly eliminated to yield compounds **115** and **116** (Scheme 64).<sup>335</sup>



**Scheme 64:** Synthesis of compounds **115** and **116** by reacting **113** and dihalogenoalane-2thf.

Analysis of the insoluble by-product by powder diffraction revealed that it was a mixture of magnesium dichloride accompanied with amorphous material. Supposedly, the  $\text{MgClH}$  disproportionated to  $\text{MgCl}_2$  and  $\text{MgH}_2$  that possesses an amorphous structure in the solid state (Figure 37).

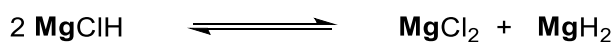
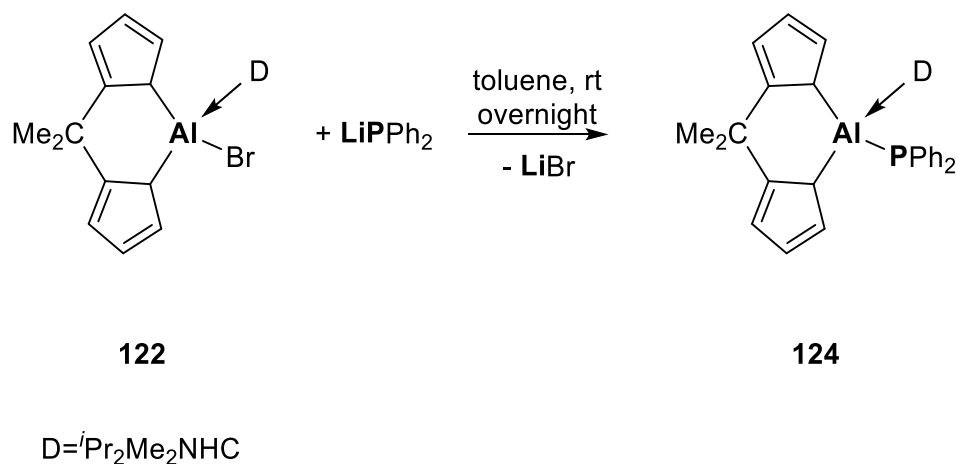


**Figure 37:** Disproportionation of  $\text{MgHCl}$ .

To investigate the possibility of functionalization of compounds **115-123**, compound **122** was treated with lithium diphenylphosphide in toluene. This resulted in a uniform reaction yielding phosphanylalane **124** (Scheme 65).

### 3. Results & Discussion



**Scheme 65: Synthesis of compound 124.**

Complexes **115-124** could be isolated as air and water sensitive colorless solids. Compounds **115-118** are stable at room temperature in solid state for weeks and in solution for several days; while compounds **119-124** are stable at room temperature for months in solid state and in solution. All complexes **115-124** are thermally stable at 50-110°C and they are not sublimable and decompose at 120°C. Compounds **115-118** are soluble in hexane in contrast to compounds **119-124**; but all complexes are soluble in polar solvents.

Compounds **115-124** could be characterized in the solid-state by X-ray diffractometry. Single crystal of complexes **115-124** could be obtained from concentrated hexane solutions at 353 K for **115-118** and from toluene for **119-124** and they were suitable for single crystal X-ray diffraction (Figure 38, 39).

### 3. Results & Discussion

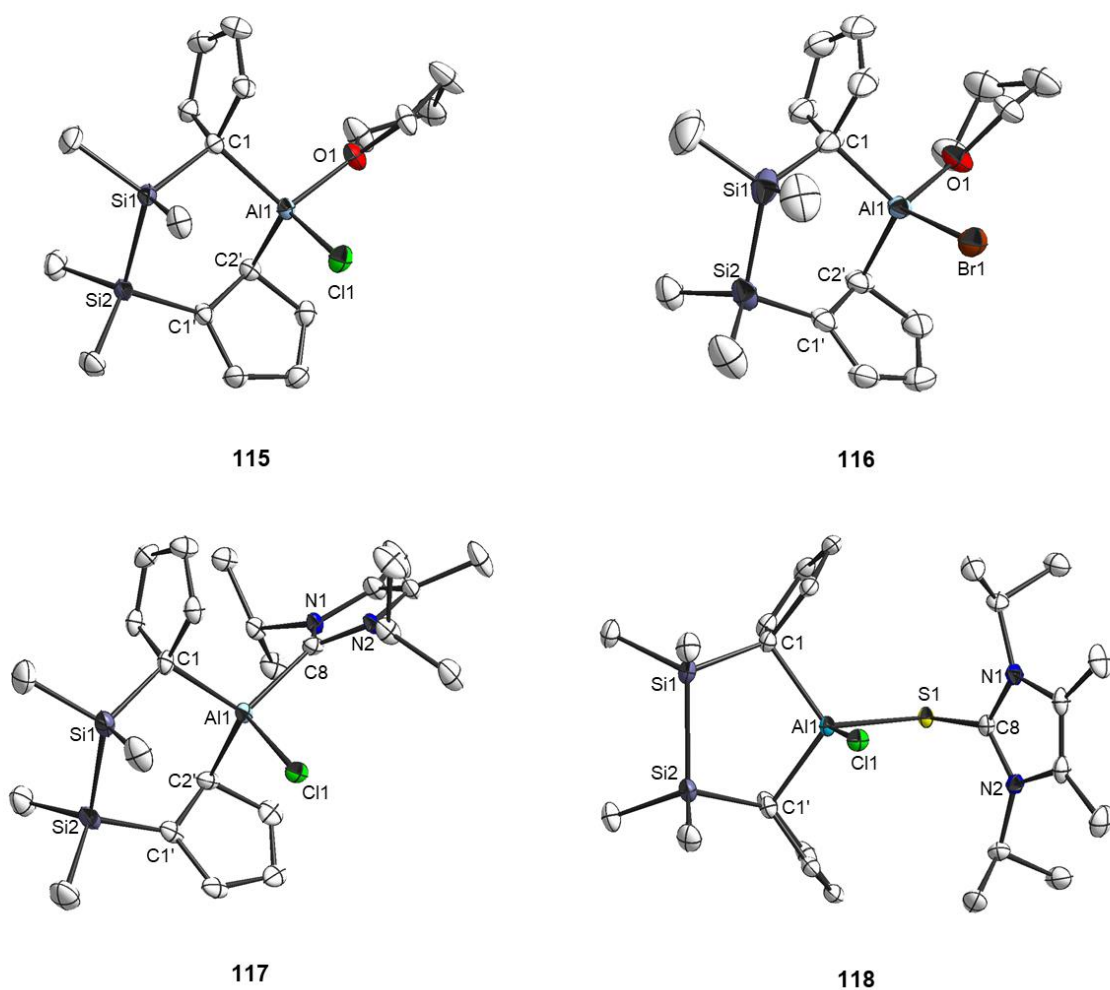


**Figure 38: Molecular structure of compounds 115-118 in the crystals (thermal ellipsoids for 50% probability level, H-atoms were omitted for clarity).**



### 3. Results & Discussion

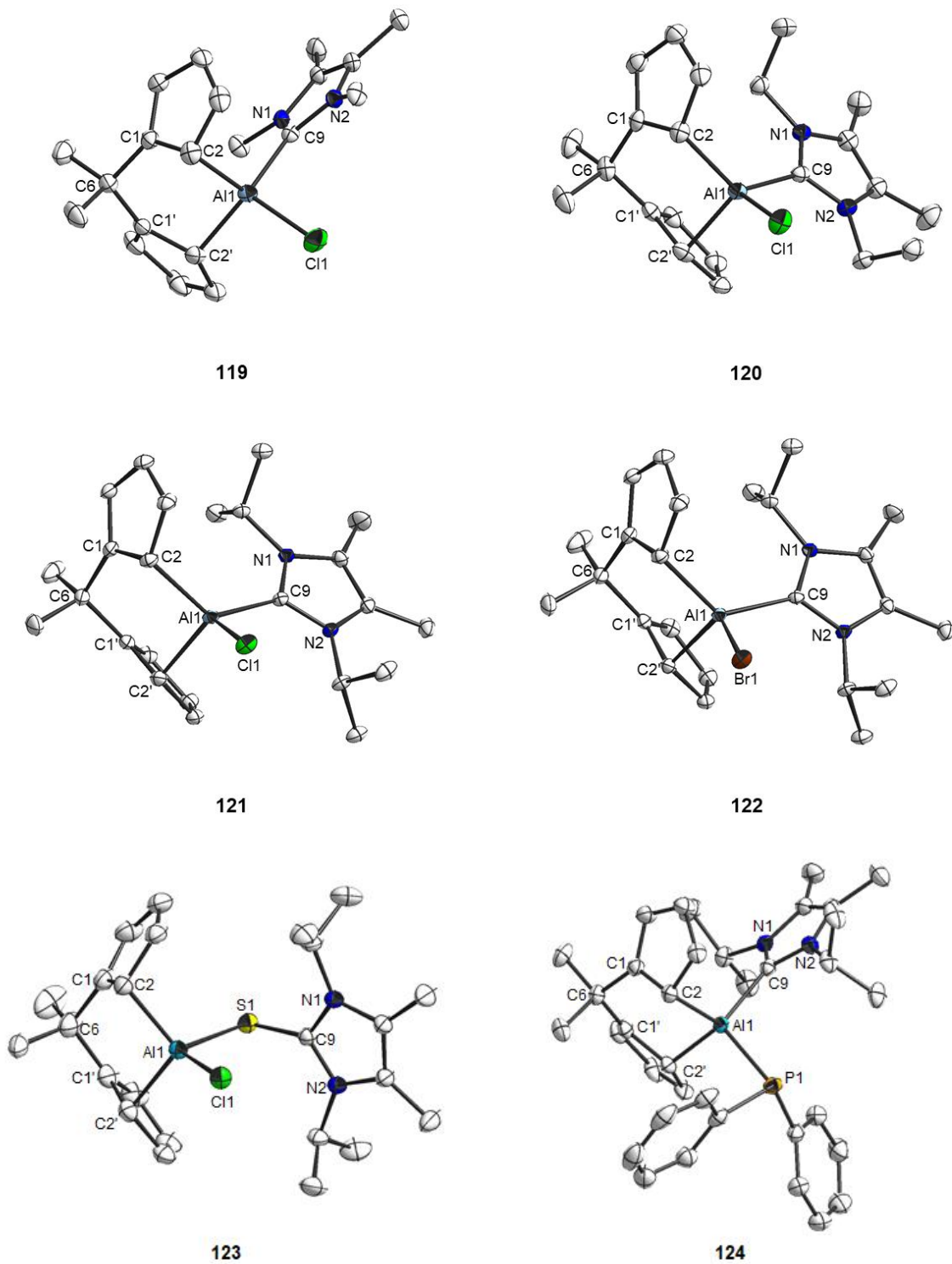


Figure 39: Molecular structure of compounds 119-124 in the crystals (thermal ellipsoids for 50% probability level, H-atoms were omitted for clarity).

### 3. Results & Discussion

The crystal structures of compounds **115-123** indicate that aluminum centers exhibit a slightly distorted tetrahedral geometry. Aluminum atom builds with the *ansa*-ligands a six membered ring chair conformation exhibiting a 1,2'-coordination (Figure 40) of aluminum center to the cyclopentadienyl rings in compounds **115-117** and a 2,2'-coordination in compounds **119-124** where the third aluminum-bonded substituent (halide or diphenylphosphanyl) is bonded in the axial position for compounds **115-117** and in the equatorial position for compounds **119-124** while the donor is positioned in the equatorial plane for compounds **115-117** and in the axial plane for compounds **119-124** (Figure 41).



Figure 40: General representation of carba[1]- and sila[2]bis(cyclopentadienyl)aluminum with numbering on the cyclopentadienyl ligands.

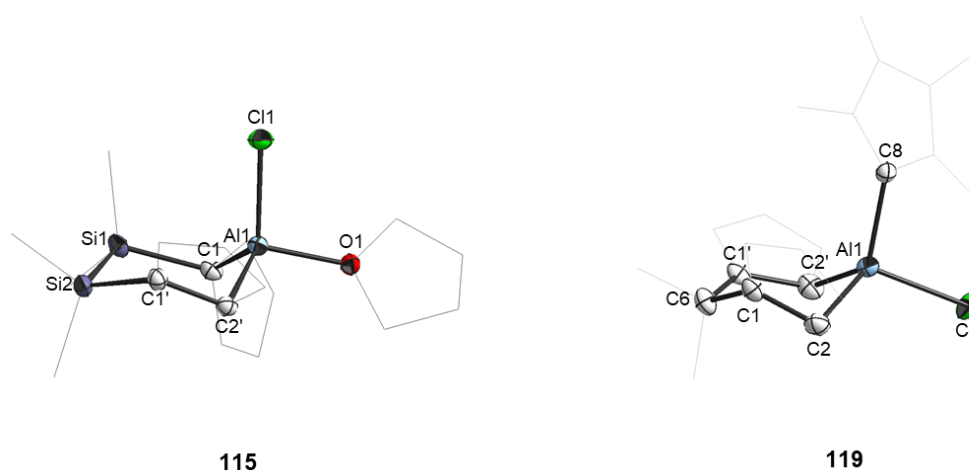
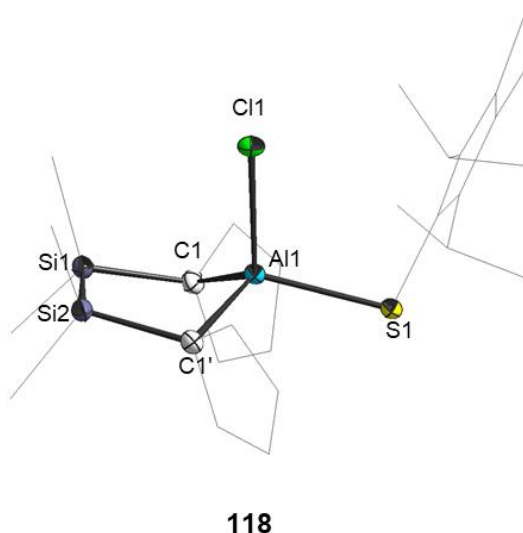


Figure 41: Molecular structure of **115** and **119** in the crystals, highlighting their six membered ring chair conformation (H-atoms were omitted for clarity).

The six membered ring conformation (Figure 41) is believed to be energetically the most favorable conformation in all complexes with an exception in compound **118** where a five membered ring envelope conformation due to a 1,1'-coordination of aluminum atom to the cyclopentadienyl rings is formed and the axial position is occupied by the chlorine atom and

### 3. Results & Discussion

the equatorial by thione ligand (Figure 42). The reason for this exceptional coordination mode might just be the packing effect and electronic reason that is traced back to the donation property of the thione ligand.



**Figure 42:** Molecular structure of **118** in the crystal, highlighting its five-membered ring envelope conformation (H-atoms were omitted for clarity).

In addition, the cyclopentadienyl rings of the *ansa*-ligand in compounds **115-117** are twisted to each other, while the *ansa*-ligand in complexes **118-124** adopts a butterfly-like arrangement. The  $\sigma$  bonding between aluminum centers and the cyclopentadienyl rings in compounds **115-124** led to localized double bonds and single bonds in the cyclopentadienyl rings so that two bonds are short and three bonds are long in the crystal structures (134.7-139.0 pm; 141.0-148.3 pm). Moreover, compounds **115-124** showed two different aluminum cyclopentadienyl distances (Al1-C<sub>Cp</sub>) (Table 1) with one longer than the other by approximately 2-4.6 pm, except for compounds **118** and **123** where both Al1-C<sub>Cp</sub> bond lengths are identical. The bond lengths of Al1-Cl1 elongate with the increase of the steric demand of the coordinated donor to aluminum center which is clearly observed while comparing compounds **115**, **117** and **118**. On the other hand, the halide atoms have almost no influence on the Al-D bond length which can be seen in compounds **115** or **116** and in **121** or **122** where the chlorine atom is exchanged by bromine atom. Moreover, when the steric effect of N-substituted carbene increases from methyl-substituted in compound **119** to ethyl-substituted in compound **120** to *isopropyl*-substituted in compound **121**, the Al-D bond lengths increase from 202.3 pm to 203.2 pm to 204.0 pm, respectively.

### 3. Results & Discussion

**Table 1: Bond lengths<sup>a</sup> of  $\sigma$ -bonds Al-Cp, Al-Cp', Al-D and Al-X in compounds 115-124.**

compound	Compound-number	Bond lengths of Al1-Cp <sup>b</sup> [pm]	Bond lengths of Al1-Cp' <sup>c</sup> [pm]	Bond lengths of Al1-D [pm]	Bond lengths of Al1-X [pm]
Me <sub>4</sub> Si <sub>2</sub> Cp <sub>2</sub> AlCl·thf	<b>115</b>	199.57(10)	201.83(10)	186.59(08)	212.65(04)
Me <sub>4</sub> Si <sub>2</sub> Cp <sub>2</sub> AlBr·thf	<b>116</b>	199.40(03)	202.10(03)	186.35(19)	230.94(08)
Me <sub>4</sub> Si <sub>2</sub> Cp <sub>2</sub> AlCl·iPr <sub>2</sub> Me <sub>2</sub> NHC	<b>117</b>	200.60(03)	205.20(03)	205.80(03)	217.53(12)
Me <sub>4</sub> Si <sub>2</sub> Cp <sub>2</sub> AlCl·ImS	<b>118</b>	204.03(12)	204.03(12)	229.41(06)	217.37(06)
Me <sub>2</sub> CCp <sub>2</sub> AlCl·Me <sub>4</sub> NHC	<b>119</b>	201.67(13)	204.74(13)	202.28(12)	216.96(05)
Me <sub>2</sub> CCp <sub>2</sub> AlCl·Et <sub>2</sub> Me <sub>2</sub> NHC	<b>120</b>	204.72(14)	202.34(14)	203.17(13)	217.12(05)
Me <sub>2</sub> CCp <sub>2</sub> AlCl·iPr <sub>2</sub> Me <sub>2</sub> NHC	<b>121</b>	203.88(13)	201.90(12)	203.98(12)	218.71(05)
Me <sub>2</sub> CCp <sub>2</sub> AlBr·iPr <sub>2</sub> Me <sub>2</sub> NHC	<b>122</b>	203.34(16)	201.32(16)	203.66(14)	235.42(05)
Me <sub>2</sub> CCp <sub>2</sub> AlCl·ImS	<b>123</b>	203.70(13)	203.70(13)	228.87(06)	216.14(06)
Me <sub>2</sub> CCp <sub>2</sub> AlPPh <sub>2</sub> ·iPr <sub>2</sub> Me <sub>2</sub> NHC	<b>124</b>	206.31(01)	202.70(01)	206.18(01)	240.38(01)

<sup>a</sup> The numbering of the atoms corresponds to the labeling of crystal structures in Figures 34 and 35.

<sup>b</sup> Al1-Cp bonds are Al1-C1 in compounds **115-118** and Al1-C2 in compounds **119-124**.

<sup>c</sup> Al1-Cp' bonds are Al1-C2' in compounds **115-117**, **119-124** and Al1-C1' in compound **118**.

Complexes **115-124** were investigated in solution via <sup>1</sup>H-, <sup>13</sup>C-, <sup>29</sup>Si- and <sup>31</sup>P NMR spectroscopy. Regarding the 1-2'-coordination mode of compounds **115-117**, these compounds possess C<sub>1</sub> symmetry in the solid state (Figure 43).

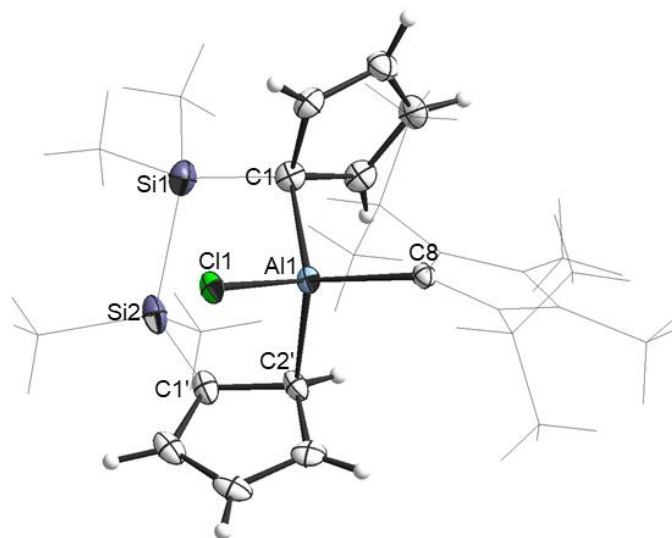


**Figure 43: Molecular structure of 117 in the crystals, highlighting the symmetry of the molecules.**

### 3. Results & Discussion

Due to the  $C_1$  symmetry of compounds **115-117** in the solid state, eight  $^1\text{H}$  signals for cyclopentadienyl protons and ten  $^{13}\text{C}$  signals for cyclopentadienyl carbon atoms and four  $^1\text{H}$  signals and four  $^{13}\text{C}$  signals for the methyl groups in the disilano-bridge as well as two  $^{29}\text{Si}$  signals should be theoretically detected in NMR spectra in solution. Yet, the  $^1\text{H}$  NMR spectra of compounds **115-117** indicate only four signals for cyclopentadienyl protons in solution at room temperature and two signals for the protons of the methyl groups, while  $^{13}\text{C}$  NMR spectra indicate only five signals for the carbon atoms of cyclopentadienyl rings and the  $^{29}\text{Si}$  NMR spectra exhibit one signal (Figure 44).

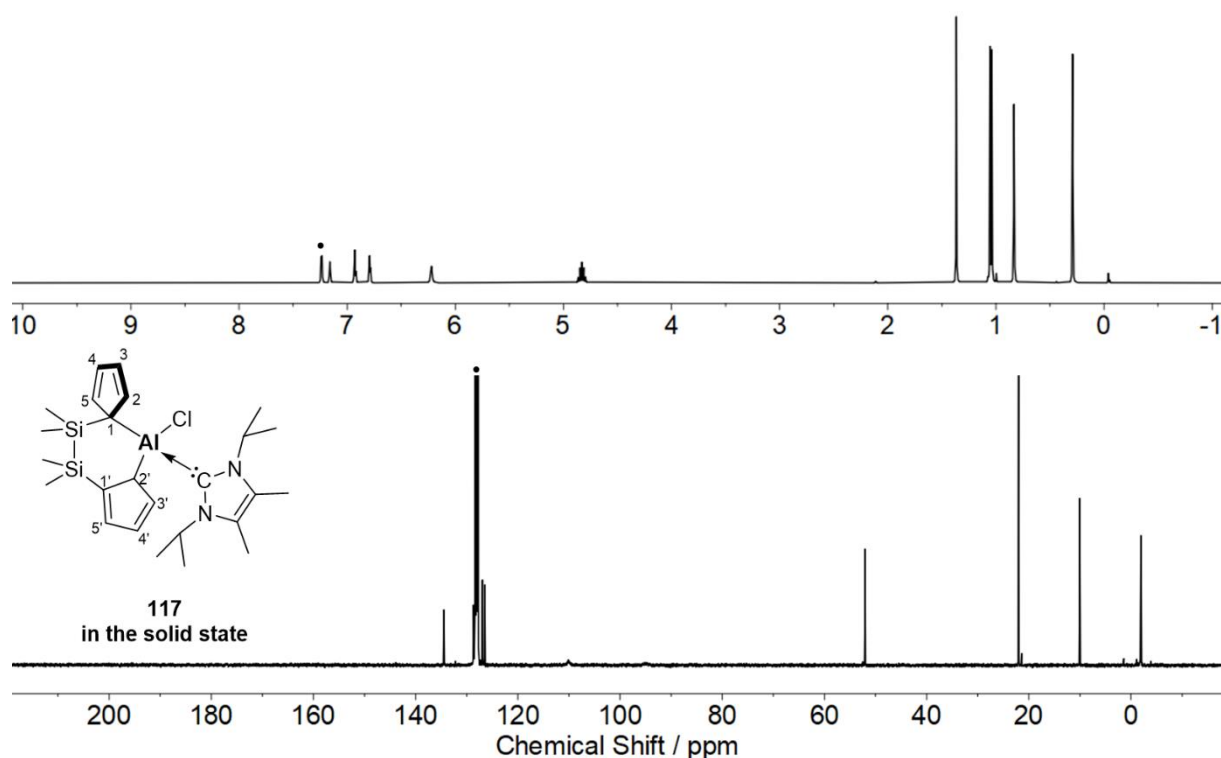


Figure 44:  $^1\text{H}$  NMR spectrum (400.13 MHz,  $\text{C}_6\text{D}_6$ , 298 K) (top) and  $^{13}\text{C}\{^1\text{H}\}$  NMR spectrum (100.62 MHz,  $\text{C}_6\text{D}_6$ , 298 K) (bottom) of **117** ( $\bullet = \text{C}_6\text{HD}_5$  signal).

An explanation for this behaviour is that these compounds undergo aluminum sigma tropic rearrangement in solution. This migration of the aluminum atom around the carbon atoms of cyclopentadienyl rings increases the symmetry of the molecules from  $C_1$  to  $C_s$  in solution reducing the number of the detected signals in  $^1\text{H}$ -,  $^{13}\text{C}$ - and  $^{29}\text{Si}$  NMR spectra of compounds **115-117** (Figure 45) because the protons of the cyclopentadienyl rings as well as of the methyl groups pairwise become homotop.

### 3. Results & Discussion

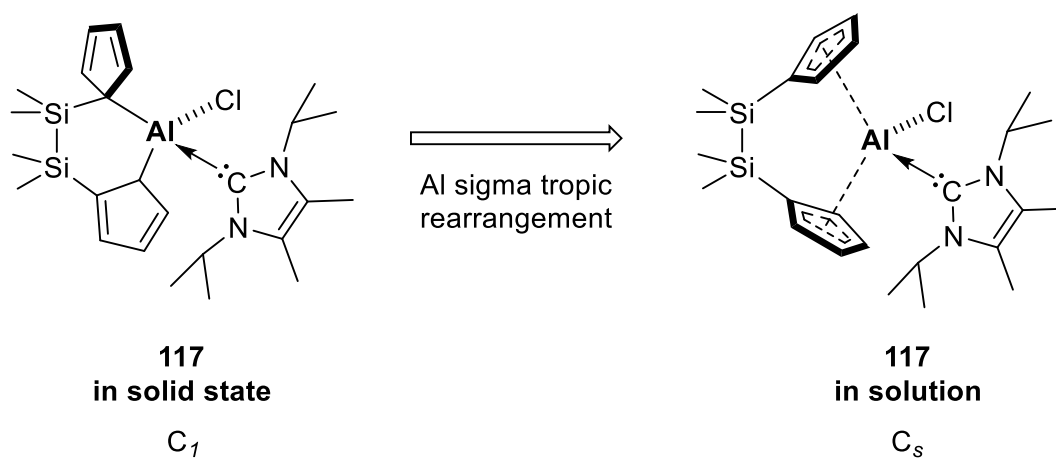


Figure 45: Structure of compound **117** in solid state and in solution containing [1,5] Al sigma tropic rearrangement.

On the other hand, compounds **118-124** possess a  $C_s$  symmetry due to the 1,1'- and 2,2'-coordination modes in the solid state (Figure 46).

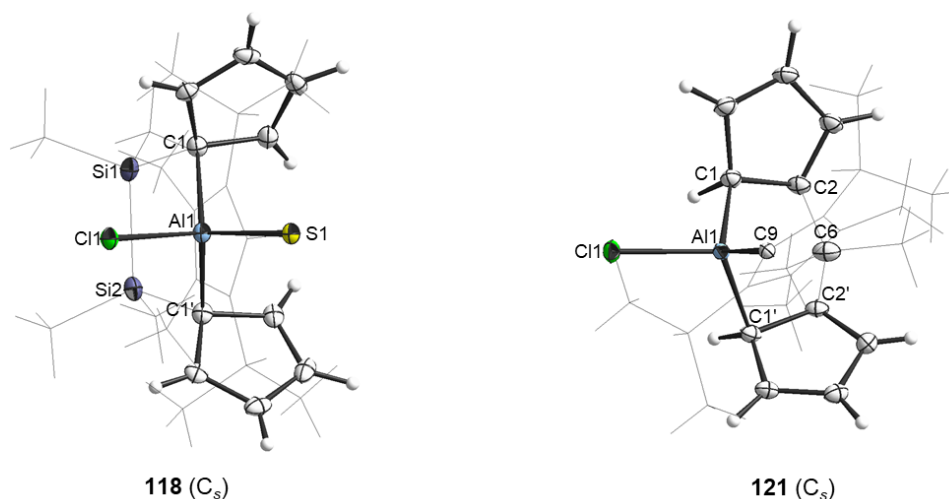


Figure 46: Molecular structure of **118** and **121** in the crystals, highlighting the symmetry of the molecules in the solid state.

Because of the  $C_s$  symmetry of compounds **119-124**, four  $^1\text{H}$  signals for protons of the cyclopentadienyl rings, five  $^{13}\text{C}$  signals for carbon atoms of the cyclopentadienyl rings, two  $^1\text{H}$  signals and two  $^{13}\text{C}$  signal for the methyl group of the methyldiene-bridge and one  $^{13}\text{C}$  signal

### 3. Results & Discussion

for carbon atom of the methyldiene-bridge should theoretically be detected. While compound **118** represents an exception of the sila[2]aluminocenophane compounds with respect to the molecule symmetry ( $C_s$ ) due to the 1,1'-coordination mode in the solid state. Four  $^1\text{H}$  signals for protons of the cyclopentadienyl rings, two  $^1\text{H}$  signals for the methyl groups protons of the disila-bridge, five  $^{13}\text{C}$  signals for the carbon atoms of the cyclopentadienyl rings and one  $^{29}\text{Si}$  signal in the NMR spectra in solution should theoretically be detected. Yet, all complexes **118-124** indicate four signals for cyclopentadienyl protons in the  $^1\text{H}$  NMR spectra in solution at room temperature as well as five signals in  $^{13}\text{C}$  NMR spectra for carbon atoms of cyclopentadienyl rings (Figure 47, 48). Although the number of the detected  $^1\text{H}$  and  $^{13}\text{C}$  signals of the structures **118-124** in solution are in line with the expected signals of these structures in the solid state, it does not mean that no aluminum sigma tropic rearrangement occurs in solution.

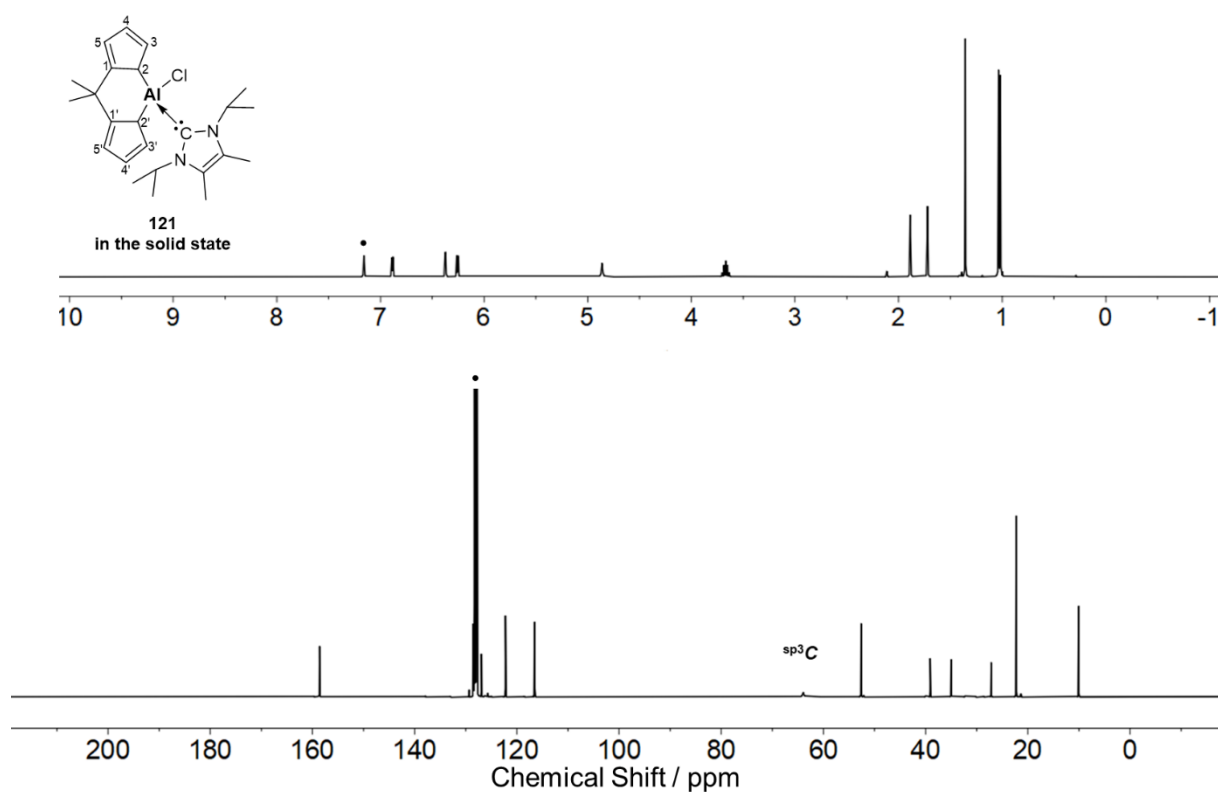


Figure 47:  $^1\text{H}$  NMR spectrum (400.13 MHz,  $\text{C}_6\text{D}_6$ , 298 K) (top) and  $^{13}\text{C}\{^1\text{H}\}$  NMR spectrum (100.62 MHz,  $\text{C}_6\text{D}_6$ , 298 K) (bottom) of **121** in solution ( $\bullet = \text{C}_6\text{HD}_5$  signal).

### 3. Results & Discussion

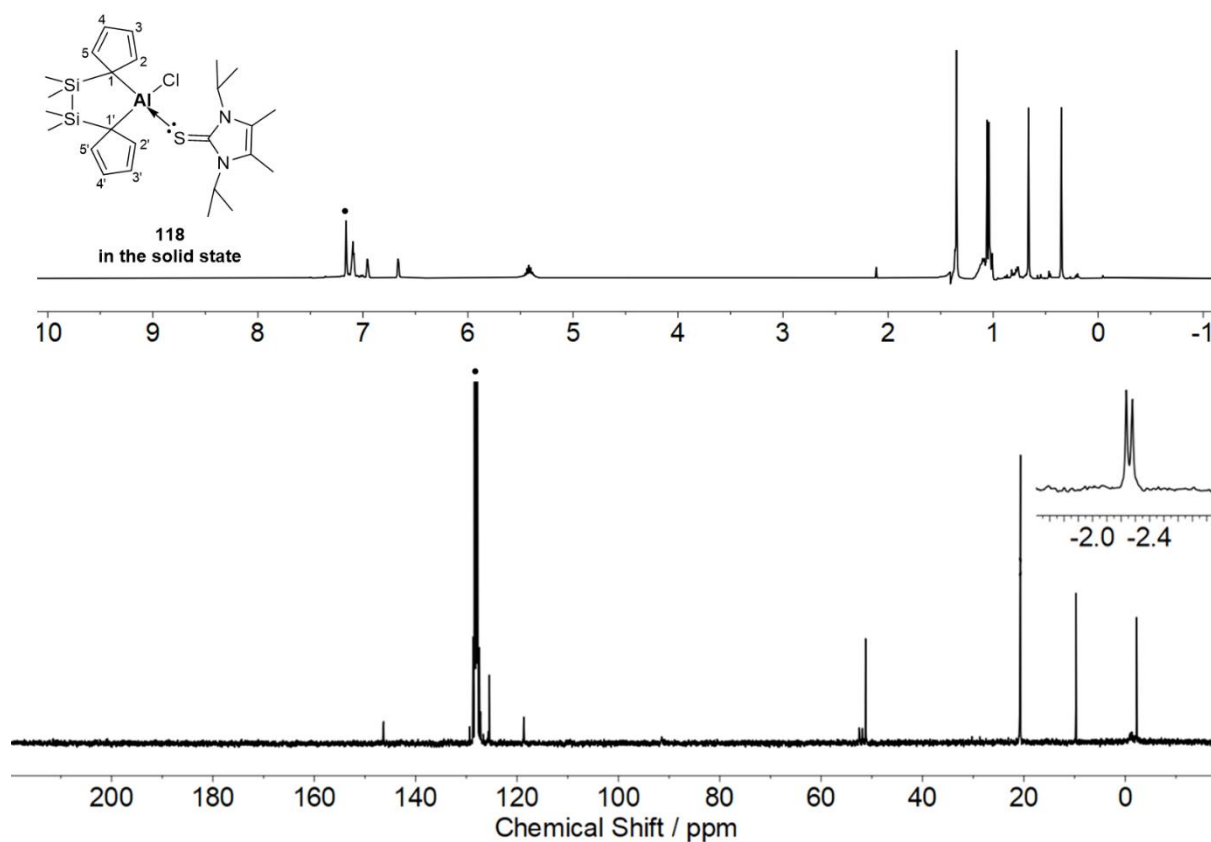


Figure 48:  $^1\text{H}$  NMR spectrum (400.13 MHz,  $\text{C}_6\text{D}_6$ , 298 K) (top) and  $^{13}\text{C}\{^1\text{H}\}$  NMR spectrum (100.62 MHz,  $\text{C}_6\text{D}_6$ , 298 K) (bottom) of **118** in solution ( $\bullet$  =  $\text{C}_6\text{HD}_5$  signal).

The  $^1\text{H}$ - and  $^{13}\text{C}$  NMR data for compounds **119-124** also showed signals in both spectra ( $^1\text{H}$ - and  $^{13}\text{C}$  NMR) which are relatively up-field shifted ( $\delta^1\text{H}$ : 4.61-5.04 ppm;  $\delta^{13}\text{C}$  = 59.2-68.9 ppm) indicating an  $\text{sp}^3$  hybridized  $\sigma$ -coordinated carbon atom of cyclopentadienyl group verified by the  $^1\text{H}$ ,  $^{13}\text{C}$ -HMBC spectrum. These up-field shifted signals could be indicative of rigid structures in solution. Such signals were not detected in all sila[2]aluminocenophane compounds **115-118** indicating a fluxional behaviour of these compounds in solution.

In conclusion, the NMR investigations demonstrated that the aluminum atom undergoes a rapid sigmatropic rearrangement in solution of the structures of sila[2]bis(cyclopentadienyl)-aluminum compounds **115-118**, which has previously been observed for the dicarba-bridged systems.<sup>53</sup> The structures of donor stabilized carba[1]bis(cyclopentadienyl)aluminum derivatives **119-124** in the solid state are in accordance with the detected NMR data in solution and according to this data, the up-field shifted signals in  $^1\text{H}$ - as well as in  $^{13}\text{C}$ -NMR might be indicative of static structures in solution.



### 3. Results & Discussion

To shed light on the bond strength between the aluminum atom and the different donors, DFT calculation at the B3LYP-D3/def2-TZVP<sup>340</sup> level of theory were performed. The calculated bond energy of complexes **115-124** (Figure 49) are summarized in Table 2.

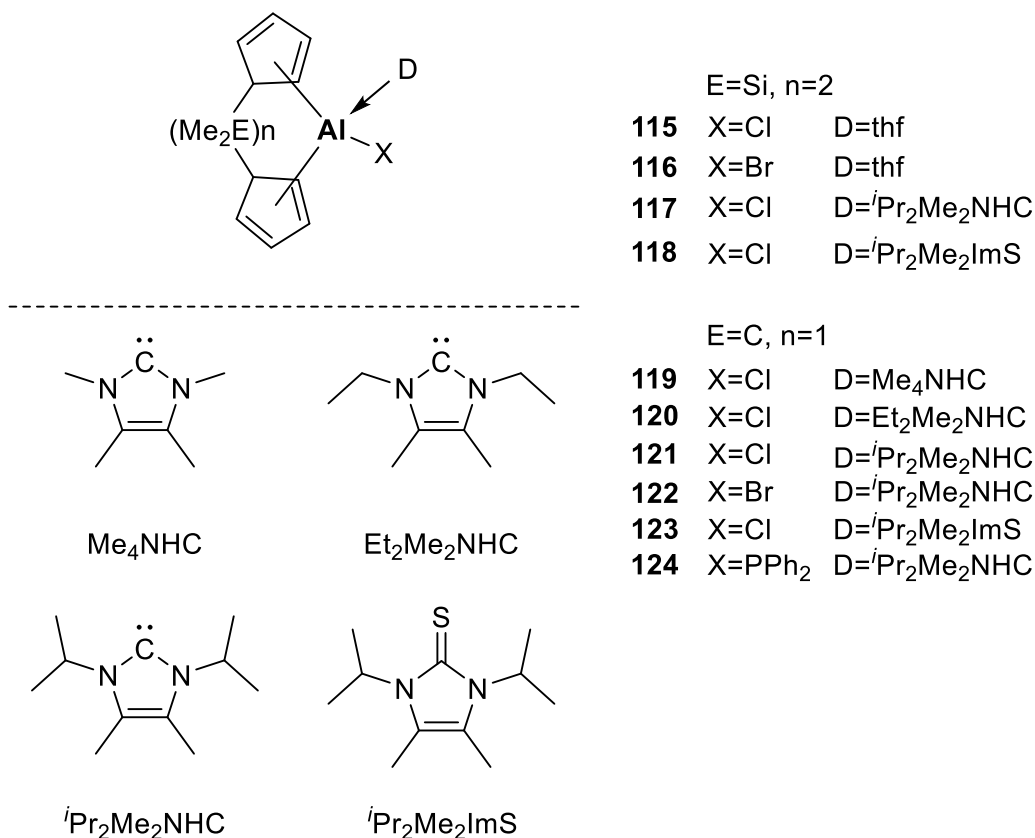


Figure 49: Structures of compounds 115-124.

Table 2: Calculated bond strengths of complexes 115-124.

compound	Compound-number	E(Al-D) [kJ mol <sup>-1</sup> ] <sup>a</sup>
Me <sub>4</sub> Si <sub>2</sub> Cp <sub>2</sub> AlCl·thf	<b>115</b>	124.3
Me <sub>4</sub> Si <sub>2</sub> Cp <sub>2</sub> AlBr·thf	<b>116</b>	124.2
Me <sub>4</sub> Si <sub>2</sub> Cp <sub>2</sub> AlCl· <i>i</i> Pr <sub>2</sub> Me <sub>2</sub> NHC	<b>117</b>	206.6
Me <sub>4</sub> Si <sub>2</sub> Cp <sub>2</sub> AlCl·ImS	<b>118</b>	150.5
Me <sub>2</sub> CCp <sub>2</sub> AlCl·Me <sub>4</sub> NHC	<b>119</b>	233.8
Me <sub>2</sub> CCp <sub>2</sub> AlCl·Et <sub>2</sub> Me <sub>2</sub> NHC	<b>120</b>	239.2
Me <sub>2</sub> CCp <sub>2</sub> AlCl· <i>i</i> Pr <sub>2</sub> Me <sub>2</sub> NHC	<b>121</b>	244.9
Me <sub>2</sub> CCp <sub>2</sub> AlBr· <i>i</i> Pr <sub>2</sub> Me <sub>2</sub> NHC	<b>122</b>	244.4
Me <sub>2</sub> CCp <sub>2</sub> AlCl·ImS	<b>123</b>	176.5
Me <sub>2</sub> CCp <sub>2</sub> AlPPh <sub>2</sub> · <i>i</i> Pr <sub>2</sub> Me <sub>2</sub> NHC	<b>124</b>	222.8

<sup>a</sup> The difference in absolute energies between complexes **115-124** and donor D + donor-free aluminocenophane ([Al]-D vs [Al] + D) represents the Al-D bond strengths computed at the B3LYP-D3/def2-TZVP level of theory.

### 3. Results & Discussion

The calculated bonding energies are in line with the thermal stability of the compounds and when the donor-strength of the Lewis base increases, the bond strength to aluminum center becomes stronger. This is obvious by the increasing bond strength of 124.3 kJ·mol<sup>-1</sup> and 124.2 kJ·mol<sup>-1</sup> for thf in compounds **115** and **116**, respectively, to 150.5 kJ·mol<sup>-1</sup> for thione ligand in compound **118** to 206.6 kJ·mol<sup>-1</sup> for NHC ligand (1,3-diisopropyl-4,5-dimethylimidazolin-2-ylidene) in compound **117** with the consideration that the N-heterocyclic carbenes are significantly stronger  $\sigma$ -donor than an ether or thione.

The steric effect of the Lewis base ligands influences the bonding energies as well so that a light increase of the bond strength is marked by comparing the bonding energy in compound **119** (233.8 kJ·mol<sup>-1</sup>) with less steric demand of N-methyl substituted carbene with the bonding energy in compound **120** (239.2 kJ·mol<sup>-1</sup>) with the more steric shielding of N-ethyl substituted carbene, and with the bonding energy in compound **121** with N-isopropyl substituted carbene (244.4 kJ·mol<sup>-1</sup>). A possible explanation for these increases are the attractive dispersion forces which have been discussed before for main group metallocene NHC complexes.<sup>341–343</sup>

Furthermore, there is almost no change in the bond strength when exchanging the halide from chlorine in compounds **114** and **121** to bromine in compounds **116** and **122**, respectively, which means that the halide has no influence on the coordination strength of the Lewis base to aluminum centers. Moreover, exchanging the third substituent on aluminum (X) from electron withdrawing group (Cl/Br) in compounds **121** and **122** to an electron donating group like PPh<sub>2</sub> in compound **124** leads to a decrease in the bonding energy of the coordinated donor ligand by approximately 22 kJ·mol<sup>-1</sup>. This decrease of the bonding energy in compound **124** is also in line with the bond length of the Al-D which is 3 pm longer than the Al-D in compounds **121** and **122**. An explanation for this decrease in the Al-D bonding energy and the increase of Al-D distance in **124** comparing to compounds **121** and **122** is probably the increase of the electron density on aluminum center resulting from the electron donating character of the PPh<sub>2</sub> group.

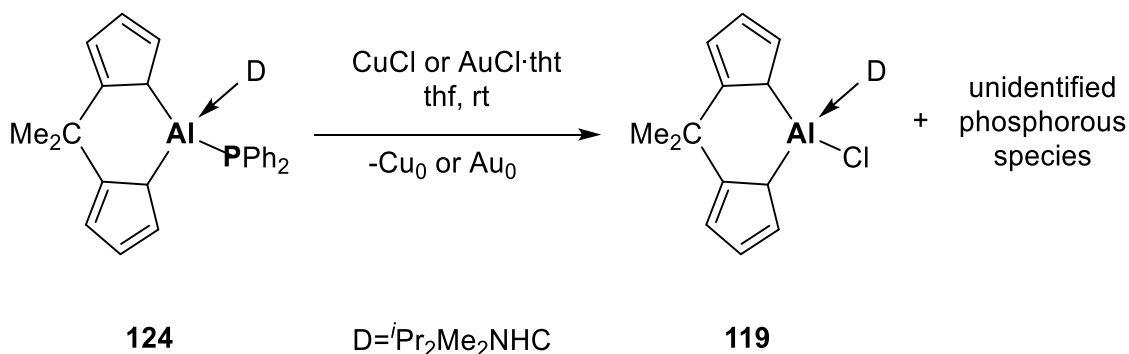
In addition, the influence of the ligand could be observed by comparing the bond strengths and bond lengths of the coordinated thione in compounds **118** and **123** or NHC ligand in compounds **117** and **121** or **122**. The thione ligand in carba[1]bis(cyclopentadienyl)aluminum **123** is bonded to aluminum atom by 26 kJ·mol<sup>-1</sup> stronger than in sila[2]bis(cyclopentadienyl)-aluminum **118**, which is in accordance with the bond lengths (Al-S: 228.8 pm (**118**), Al-S: 229.4 pm (**123**)). Similarly, the NHC in compound **121** or **122** is stronger bonded than in compound **117** by ca -38.3 kJ·mol<sup>-1</sup>.

### 3. Results & Discussion

Phosphanalane **124** is, to the best of my knowledge, the first example of such a compound with two interlinked cyclopentadienyl ligands. Cyclopentadienyl aluminum compounds are mostly substituted by halide or alkyl ligands (see chapter 1.5). Phosphanalane compounds possess very interesting properties depending on the polar aluminum phosphorous bond (see chapter 1.7.) and the phosphorous atom with a trigonal pyramidal geometry and the lone pair represents a coordination site for transition metals in the compound.

Regarding these properties, many attempts to coordinate a transition metal were carried out on compound **124**. The coordination of big transition metal fragments appears to be difficult possibly because of the steric shielding of the coordinated NHC donor in combination with the *ansa*-ligand system making the phosphorus atom sterically overloaded.

Thus, attempts to coordinate a  $W(CO)_5(thf)$  fragment in thf at room temperature led only to a complex mixture of products. On the other hand, treatment with less bulky transition metal fragments like CuCl and AuCl(tht) cleaved the Al-P bond and complex **119** was formed (Scheme 66).



Scheme 66: The reaction of compound **124** with CuCl and AuCl·tht.

## 3.3. A Bis(aluminocenophane) 125

Parts of this chapter have been published in *Dalton Trans.*, 2019, **48**, 14953–14957.

As mentioned before, the first cyclopentadienyl aluminum compound was reported six decades ago in 1961 (chapter 1.5.). None of the published compounds since then contained two  $\eta^5$  bonded cyclopentadienyl ligands coordinated to a neutral aluminum atom. Aluminocenium cations in salts **34-36** and **38-41** are the only aluminum structures exhibiting two  $\eta^5$  bonded cyclopentadienyl ligands making them isostructural to ferrocene. The reason for the two  $\eta^5$  bonded cyclopentadienyl rings in aluminocenium cation is possibly the very high electron deficiency of aluminum atom. Regarding that, it might be possible to produce a compound containing high electron deficient neutral aluminum atom bonded to two cyclopentadienyl ligands in a  $\eta^5$  coordination mode.

Magnesocenophanes are powerful cyclopentadienyl transfer reagents; thus, *Shapiro* et al. utilized C[2]magnesocenophane **112** to synthesize the first aluminocenophane derivative **53** through its treatment with aluminum(III)chloride in toluene in 2005 (Scheme 35).<sup>53</sup> The same reaction in diethyl ether also led to compound **53** on one case isolated as an Al·Et<sub>2</sub>O cocrystal (Figure 50). The crystal structure of compound **53** in Figure 50 shows virtually no differences in bond lengths and hapticities to the previously reported structure of *Shapiro* et al..

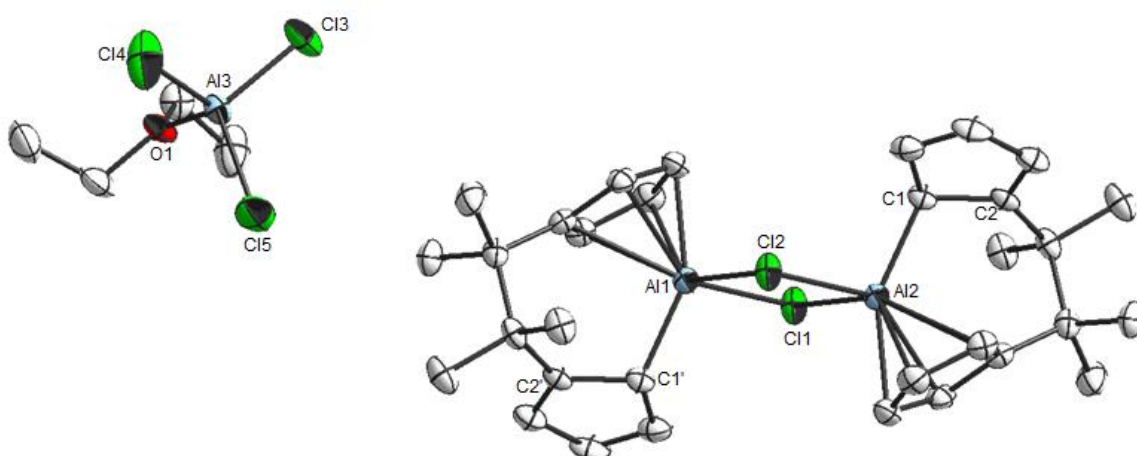
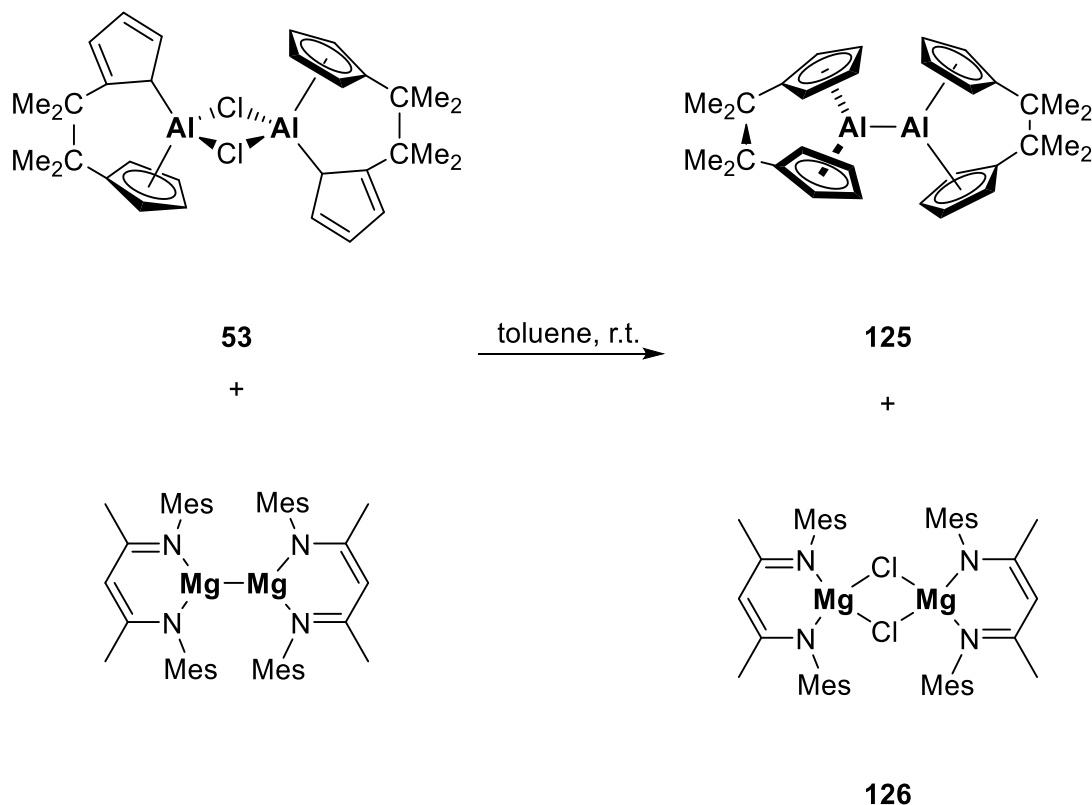


**Figure 50:** Molecular structure of **53**·[AlCl<sub>3</sub>·OEt<sub>2</sub>] in the crystal, (thermal ellipsoids for 50% probability level, H-atoms were omitted for clarity).

### 3. Results & Discussion

The treatment of compound **53** with 1,3- $\beta$ -diketiminate magnesium(I), that was described by Jones et al.<sup>344,345</sup> and represents a very powerful and selective reducing agent for aluminum compounds,<sup>346</sup> afforded bis(aluminocenophane) **125** in a unified reduction (Scheme 67).<sup>347</sup>



Scheme 67: Synthesis of compound **125**.

Compound **125** was isolated as a colorless powder and it is stable under inert gas atmosphere at ambient temperature in the solid state and in solution for several days and at low temperature in the solid state for several weeks. Bis(aluminocenophane) **125** was characterized in solution by  $^1\text{H}$  and  $^{13}\text{C}$  NMR spectroscopy and in the solid state via X-ray crystallography and elemental analysis. Single crystal of compound **125** suitable for x-ray diffraction can be obtained from a concentrated solution of **125** in toluene at 248 K (Figure 51). Compound **126** could also be isolated as a dimer and characterized via X-ray crystallography, with the single crystals obtained from a concentrated solution of 1,2-difluorobenzene at 248 K (Figure 52). It is worth mentioning that a bis(metallocenophane) structural motif is extremely rare. *Manners* et al. reported a bis(carba[2]ruthenocenophanium) dication with a Ru-Ru metal bond in 2012.<sup>348</sup>

### 3. Results & Discussion

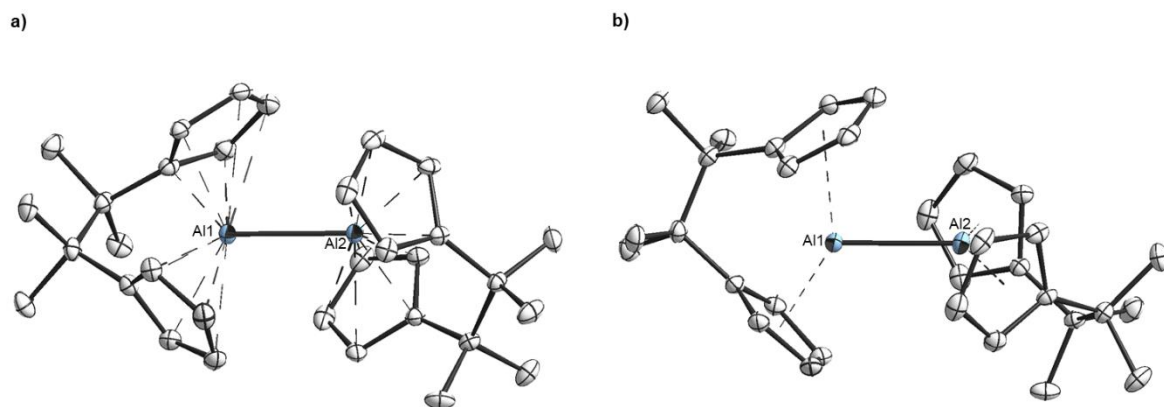


**Figure 51: a) Molecular structure of 125 in the crystal; b) Molecular structure of 125 in crystal highlighting the trigonal planar geometry of aluminum centers, (thermal ellipsoids for 50% probability level, H-atoms were omitted for clarity).**

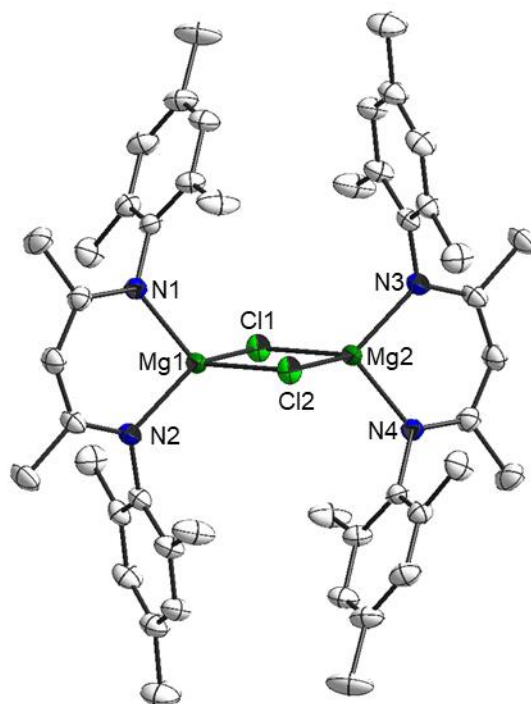


**Figure 52: Molecular structure of 126 in the crystal, (thermal ellipsoids for 50% probability level, H-atoms were omitted for clarity).**

### 3. Results & Discussion

In the solid state, the crystal structure of **125** displayed two aluminum atoms with a bond length of  $d_{\text{Al-Al}} = 250.2$  pm which is the shortest Al-Al bond length of any acyclic dialane known so far (chapter 1.6.; for comparison see Figures 21, 22). Furthermore, the crystal structure indicates that both aluminocenophane moieties are twisted to each other approximately by  $90^\circ$  torsion angle (Figure 51b). Moreover, the cyclopentadienyl rings are bonded to aluminum centers in a distorted  $\eta^5$  geometry with dihedral angle ( $\alpha$ -angle) of  $72.4^\circ$  and  $73.9^\circ$  so that different carbon-carbon bonds in the cyclopentadienyl rings in a range of 139.0-145.6 pm were determined.

The  $^1\text{H}$  NMR spectrum revealed two signals for protons of cyclopentadienyl rings with splitting pattern of triplets and a singlet signal for the protons of methyl group in the ethylidene-bridge; while  $^{13}\text{C}$  NMR spectrum indicated three signals for carbon atoms of cyclopentadienyl rings in aromatic field and two signals in the aliphatic, which means that the structure of compound **125** in solution appears to be symmetrical. The  $^{27}\text{Al}$  NMR spectrum displayed no signals in a range of -200 to +200 ppm at 298 K. Due to the possibility of sigmatropic rearrangements in solution, no statement about the hapticities of the cyclopentadienyl rings can be made based on the NMR data. However, the crystal structure of **125** indicates  $\eta^5$  coordination of all bonded cyclopentadienyl rings to aluminum atoms, which agrees with the  $^1\text{H}$  and  $^{13}\text{C}$  NMR spectra.

Aluminum centers of **125** adopt in the solid state a trigonal planar geometry with respect to the centroids of the bonded cyclopentadienyl rings with torsion angle of  $\text{Cp}_{\text{centroid}}\text{-Al-Al-Cp}_{\text{centroid}}$   $\tau = 84,7^\circ, 81.0^\circ, 95.6^\circ$  and  $98,7^\circ$ . Furthermore, the Al- $\text{Cp}_{\text{centroid}}$  distances are in a range of 204.3-234.1 pm longer than any Al-Cp bond lengths of some known compounds in literature; for instance, 193.9 pm for compound **53**,<sup>53</sup> 203.2 pm for compound **8**<sup>41-44</sup>, 184.3 pm for compound **34**<sup>105,106,108</sup> and 178.9 pm for compound **41**<sup>159</sup> (Figure 53). The bond lengths of Al-Cp in compounds **34** and **41**, which are much shorter than in compound **125**, traced back to the highly Lewis-acidic aluminum centers; while in compounds **8** and **52**, the aluminum centers are neutral and tetracoordinated making them electronically more saturated. On the other hand, the differences in the detected Al-Cp distances in the solid state of **125** are probably attributed to the packing effect in crystal regarding the fact that aluminum cyclopentadienyl bonds are very flexible.

### 3. Results & Discussion

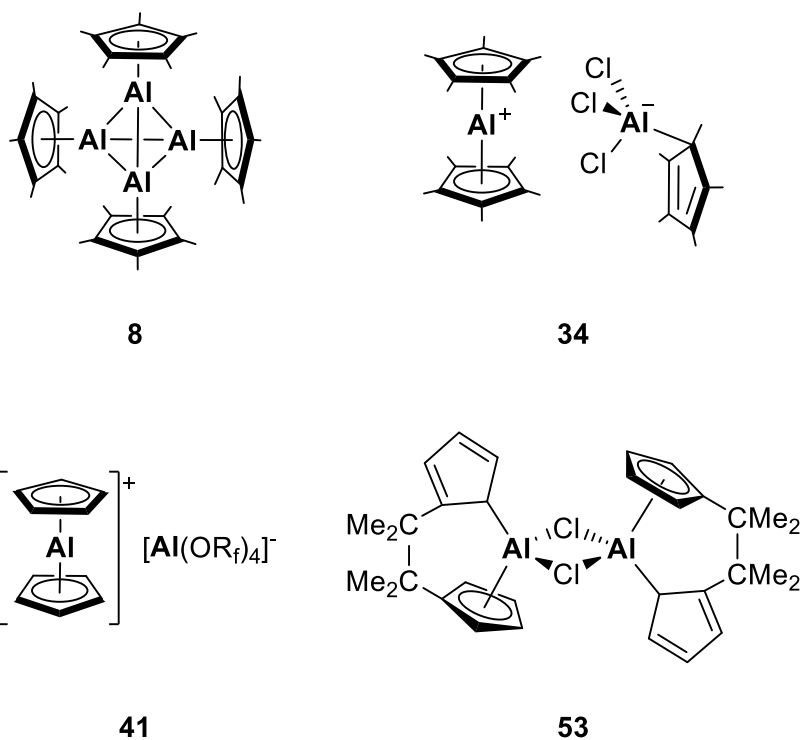
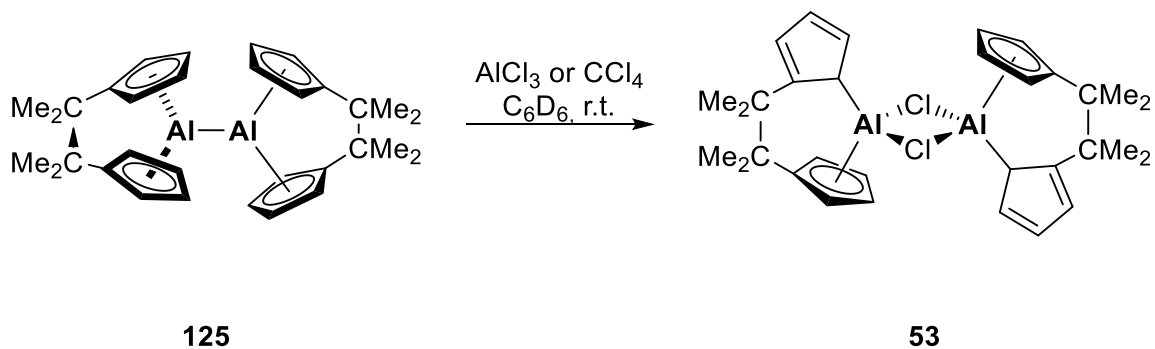


Figure 53: Representation of compounds 8, 34 and 53.

A benzene solution of bis(aluminocenophane) **125** is stable at 333 K for at least two hours. Although the Al-Al bond in compound **125** is the shortest of any acyclic dialane, as mentioned above, it possesses a high reactivity due to the oxidation state of aluminum atom. Therefore compound **125** is oxidized with element chlorides such as  $\text{AlCl}_3$  or  $\text{CCl}_4$  at room temperature to give again compound **53** (Scheme 68).

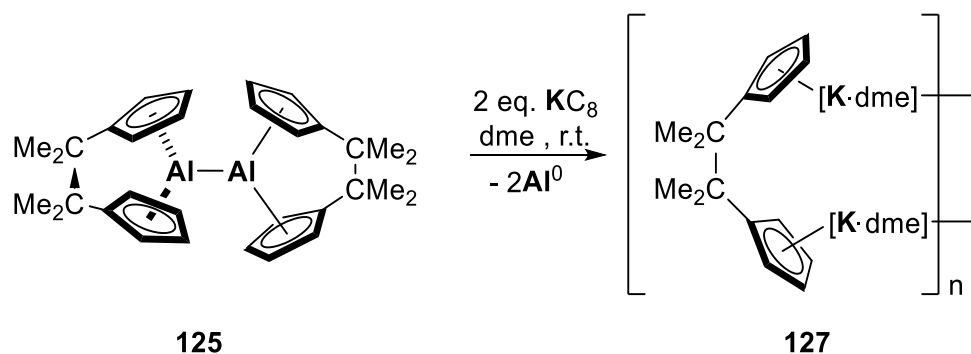


Scheme 68: Reaction of compound 125 with element chloride to yield compound 53.



### 3. Results & Discussion

On the other hand, every attempt to reduce compound **125** to yield a radical anion dialane analogous to compounds **60** and **61** resulted in overreduction. For instance, the reduction with one or two equimolar of potassium graphite in dme yielded the dipotassium salt of the *ansa*-ligand (Scheme 69).



Scheme 69: Reduction of **125** with potassium graphite.

Compound **127** could be obtained in crystalline form from a dme solution, forming a polymeric structure in the solid state (Figure 54). Alkali metal cyclopentadienide complexes tend to form polymeric structures in the solid state.<sup>349</sup> In particular, potassium cyclopentadienide builds a polymeric pattern with cyclopentadienyl anion.<sup>350–352</sup> Analogously, a polymeric pattern structure was also found in compound **127** with a dme molecule coordinated to every potassium atom. Every potassium atom is coordinated to two cyclopentadienyl rings in  $\eta^5/\eta^2$  coordination mode.

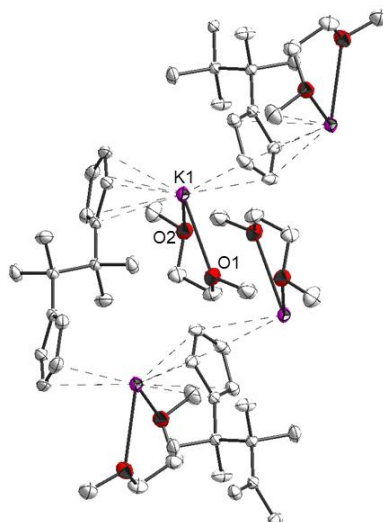


Figure 54: Polymeric Molecular structure of **127** in the crystal, (thermal ellipsoids for 50% probability level, H-atoms were omitted for clarity).

### 3. Results & Discussion

To investigate the Lewis-acidic properties, compound **125** was reacted with two equivalents of *tert*-butyl isonitrile (*t*BuNC) to obtain a Lewis acid/base product of dialanes. Analogous products of dialanes have already been reported before by many authors (Figure 55).<sup>346,353–358</sup>

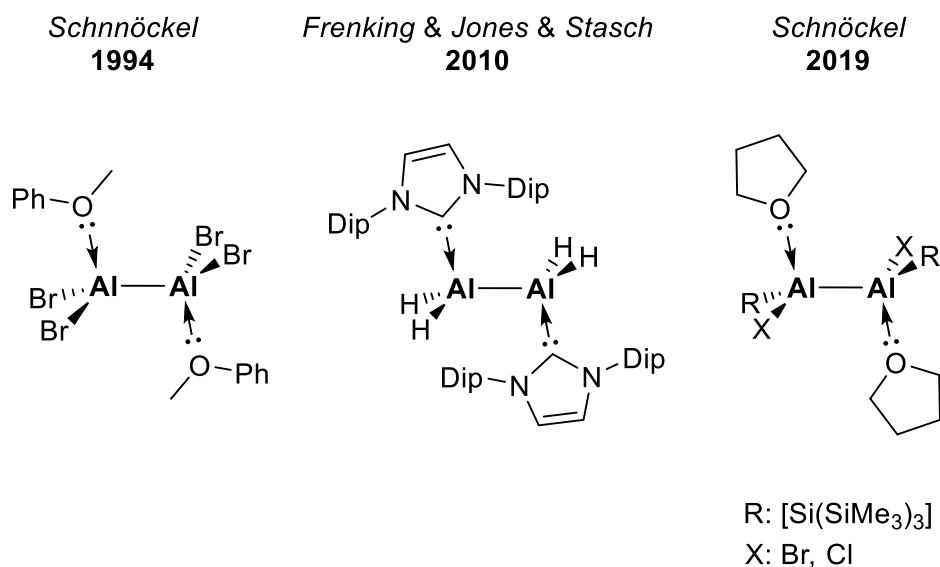
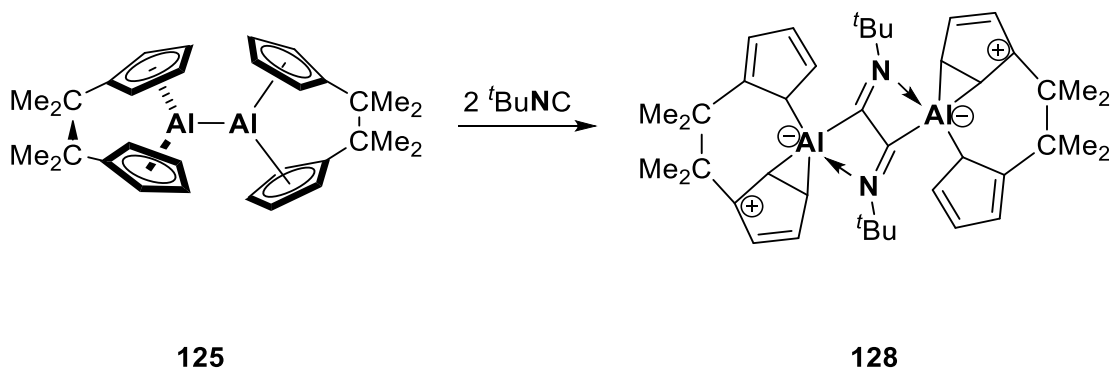


Figure 55: Examples of Lewis acid/base product of dialanes.

However, instead of the coordination of the *tert*-butyl isonitrile (*t*BuNC) to aluminum centers in compound **125**, an oxidative insertion reaction occurred with a reductive C–C coupling and an Al–Al cleavage to yield a heterocyclic compound **128** (Scheme 70). Such insertion reactions are known for related unsaturated main group species,<sup>187,191,359–361</sup> and also for aluminum cyclopentadienyl compounds such as compound **46**.<sup>162</sup>



Scheme 70: Reaction of **125** with two equivalents of *t*BuNC to afford compound **128**.

### 3. Results & Discussion

Compound **128** was isolated as orange-red crystalline solid and was characterized in solution by NMR and in the solid state via X-ray diffraction. Single crystal could be obtained from a saturated solution of toluene at 248 K (Figure 56).

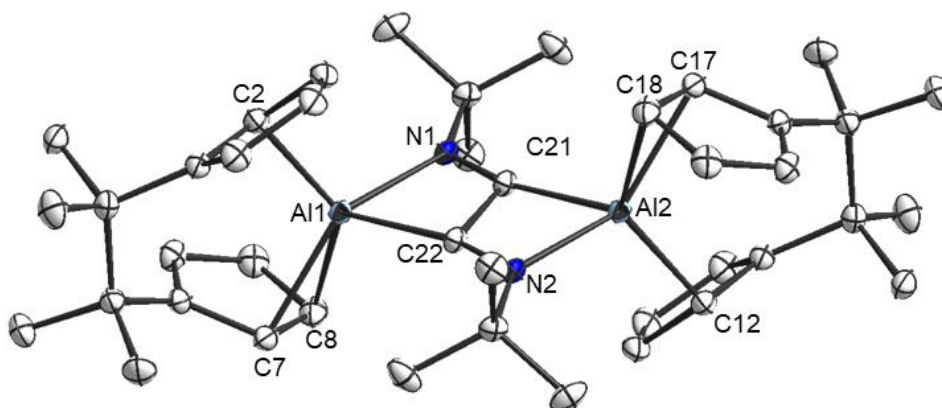


Figure 56: molecular structure of **128** in the crystal, (thermal ellipsoids for 50% probability level, H-atoms were omitted for clarity).

The structure of **128** illustrated in crystal two aluminum atoms building with the diiminoethene-fragment two planar heterocyclic four-membered rings. Both aluminum atoms are bonded to the neighboring cyclopentadienyl rings in  $\eta^1/\eta^2$  coordination mode. Table 3 shows the important bond lengths in compound **128** compared with compound **46**.

The  $\eta^1/\eta^2$  bonding modes between the aluminum centers and the cyclopentadienyl rings lead to variation of the C-C bond lengths within the Cp rings in a range of 136.3-148.2 pm and to localized C=C double bonds and C-C single bonds in the  $\eta^1$  bonded cyclopentadienyl rings. Notably, the double bonds in the cyclopentadienyl rings with an  $\eta^2$  coordination to aluminum atom are localized as well and resemble compounds **24**<sup>143,144</sup> and **29**<sup>157</sup> in this behaviour (Figure 57).

### 3. Results & Discussion

**Table 3: Important bond lengths of compounds 128 and 46.**

Bond	bond length of 128 [pm] <sup>a</sup>	Bond	bond length of 46 [pm] <sup>a</sup>
Al1-N1	201.76(5)	Al1-N1	201.6(10)
Al1-C22	203.45(5)	Al1-C1	202.3(12)
Al1-C7	221.17(6)	-	-
Al1-C8	213.21(6)	-	-
Al1-C2	202.71(5)	Al1-C3	204.6(11)
Al2-N2	201.76(5)	-	-
Al2-C21	203.45(5)	-	-
Al2-C12	202.71(5)	Al1-C4	203.8(12)
Al2-C17	221.17(6)	-	-
Al2-C18	213.21(6)	-	-
C21-C22	150.80(9)	C1-C2	152.6(17)
C22-N2	129.68(6)	N1-C2	129.1(15)
C21-N1	129.68(6)	N2-C1	127.5(16)

<sup>a</sup> The numbering of the atoms corresponds to the labeling of crystal structures in Figures 56 and 57.

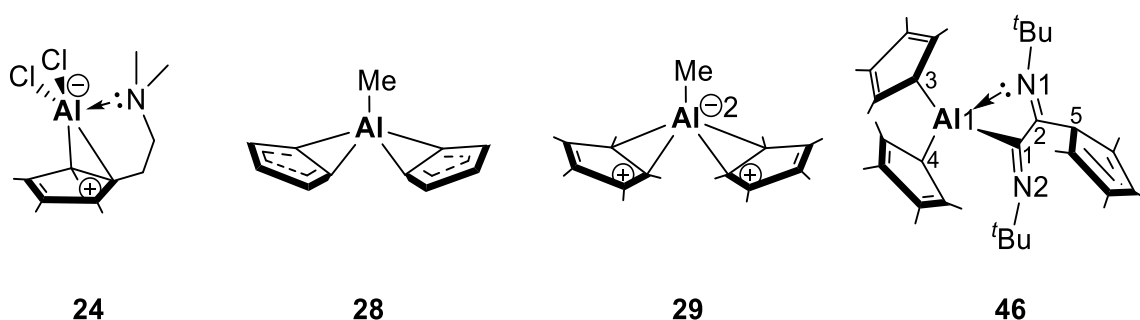


**Figure 57: Representation of compounds 24, 28, 29 and 46.**

It must be pointed out that by an  $\eta^2$  rearrangement of aluminum atom to cyclopentadienyl ligand, the C=C double bond in cyclopentadienyl ligand can be delocalized so that the C-C bond lengths are approximately similar like in compound **28**<sup>110</sup>. Furthermore, the bond lengths of Al-N in the planar heterocyclic ring are in agreement with the Al-N distance in compound **46** of 201.6 pm.<sup>162</sup> On the other hand, C21-C22 bond length of 150.8 pm is 2 pm longer than the C-C bond length in **46**.<sup>162</sup> The C=N double bonds of 129.7 pm are the same in compound **128**, while they differ in compound **46** from 127.5 pm to 129.5 pm.

### 3. Results & Discussion

Regarding the  $^1\text{H}$  NMR spectrum of **128** at ambient temperature (Figure 58), it is obvious that compound **128** possesses a fluxional behaviour in solution because of the sigma tropic rearrangement (Figure 59). Then, only four signals were observed in  $^1\text{H}$  NMR spectrum for the protons of cyclopentadienyl rings.

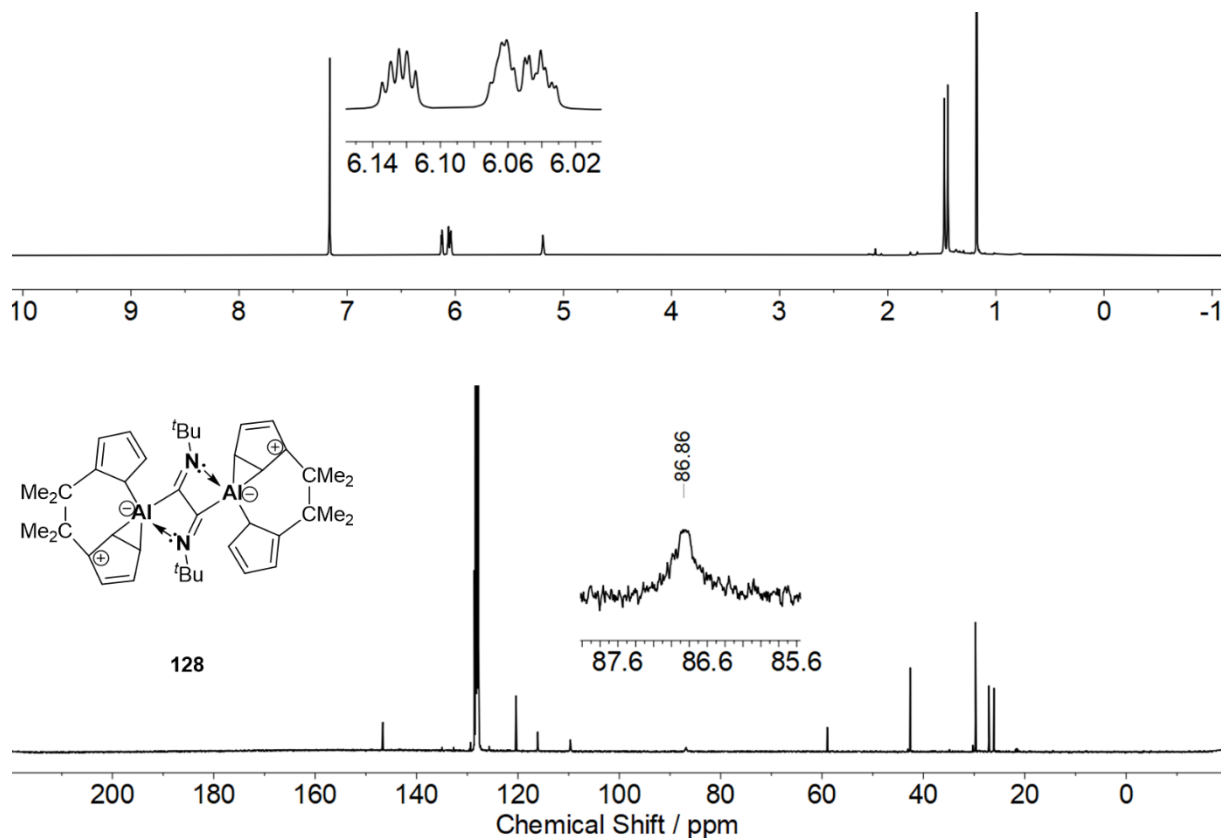


Figure 58:  $^1\text{H}$  NMR spectrum (400.13 MHz,  $\text{C}_6\text{D}_6$ , 298 K) (top) and  $^{13}\text{C}\{^1\text{H}\}$  NMR spectrum (100.62 MHz,  $\text{C}_6\text{D}_6$ , 298 K) (bottom) of **128**.

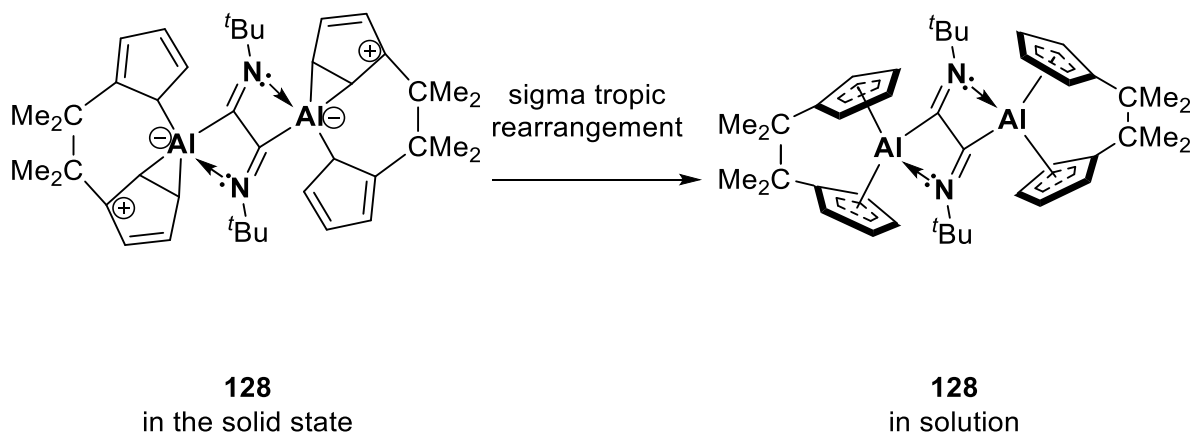


Figure 59: Structure of compound **128** in the solid state and in solution including sigma tropic rearrangement.

### 3. Results & Discussion

The theoretical study and DFT calculations of compound **125** were carried out in cooperation with the group of Dr. *Diego M. Andrada* to investigate the bonding nature in bis(aluminocenophane) **125**. DFT calculations were performed at M06-2X/def2-TZVPP<sup>340</sup> and BP86+D3(BJ)/def2-TZVPP<sup>340</sup> level of theory. The bond lengths of Al-Al and Al-Cp<sub>centroid</sub>, dihedral angle between cyclopentadienyl rings, torsion angle between Cp<sub>centroid</sub>-Al-Al-Cp<sub>centroid</sub>, and the sum of interior angles around aluminum atoms are summarized in Table 4.<sup>347</sup>

**Table 4: Selected theoretical and experimental bond lengths [pm] and angles [°] in compound 125.**

	calc. (BP86+D3(BJ)/BS <sup>a</sup> )	calc. (M06-2X/BS <sup>a</sup> )	experimental
Al-Al	248.1	249.8	250.2
Al-Cp <sub>centroid</sub>	212.4; 231.3; 227.9; 224.3	201.9; 232.8; 220.0; 202.4	204.3; 210.7; 227.3; 234.1
$\alpha^b$	74.4; 77.5	71.0; 69.3	72.3; 73.9
$\tau^c$	92.7; 79.6; 105.1; 82.6	77.2; 91.3; 98.5; 93.0	84.7; 81.0; 95.6; 98.7
$\Sigma\angle\text{Al}^d$	354.9; 359.1	359.7; 358.3	357.1; 360.0

<sup>a</sup> BS = def2-TZVPP; <sup>b</sup> dihedral angle between Cp planes; <sup>c</sup> torsion angle between Cp<sub>centroid</sub>-Al-Al-Cp<sub>centroid</sub>; <sup>d</sup> sum of interior angles around Al

The calculated Al-Al distances of 249.8 pm and 248.2 pm are in good agreement with the experimental Al-Al distance of 250.2 pm (determined via X-ray diffraction). The differences observed in the Al-Cp<sub>centroid</sub> bond distances may be a consequence of the packing effect in the solid lattice, which is common in compounds possessing cyclopentadienyl ligands.<sup>362,363</sup> In order to assess the role of the dispersion interaction, **125** was computed at the BP86/def2-TZVPP<sup>340</sup> level of theory. An Al-Al bond length of 254.5 pm is calculated, when the dispersion correction term was omitted (Figure 60). For a better comparison, NBO analysis was also performed with related dialanes Al<sub>2</sub>H<sub>4</sub> and Al<sub>2</sub>Cl<sub>4</sub> (Figure 61) and the results are summarized in Table 5.

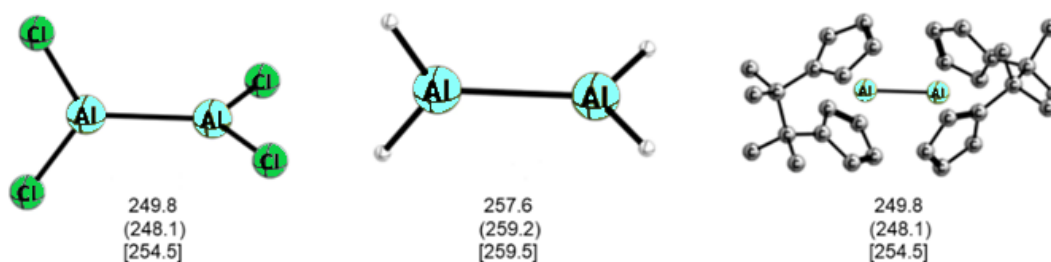


**Figure 60: Optimized structures of Al<sub>2</sub>Cl<sub>4</sub>, Al<sub>2</sub>H<sub>4</sub> and 125 at the M06-2X/def2-TZVPP (BP86+D3(BJ)/def2-TZVPP) [BP86/def2-TZVPP] level of theory (bond lengths in pm, hydrogen atoms of 125 were omitted).**

### 3. Results & Discussion

The calculation of the Kohn-Sham molecular orbitals of **125** at M06-2X/def2-TZVPP indicates that the HOMO-4 corresponds to the Al-Al  $\sigma$ -bond with some participation of cyclopentadienyl orbitals, while the LUMO is related to the Al-Al  $\sigma^*$ -antibonding orbital which also displays interactions with cyclopentadienyl  $\pi$  orbitals (Figure 61).

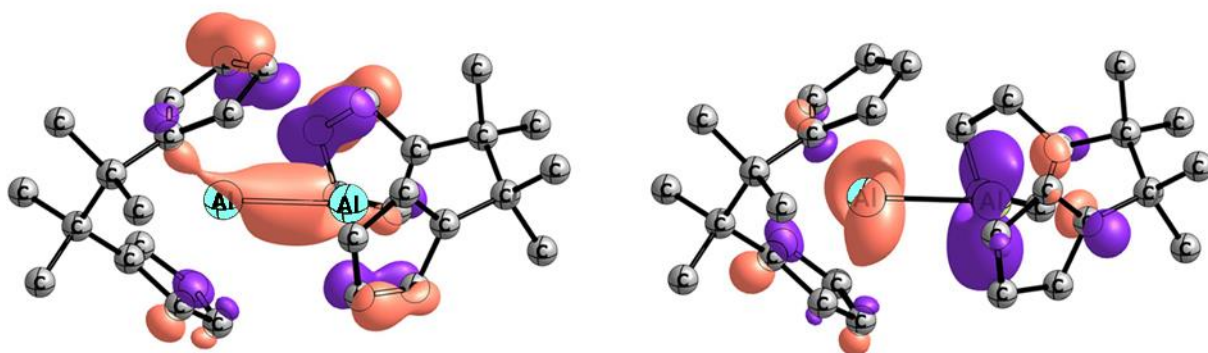


Figure 61: Kohn-Sham molecular orbitals HOMO-4 (left) and LUMO (right) of **125** (isovalue: 0.05) (calculations performed at M06-2X/def2-TZVPP).

The Wiberg bond order exhibits a value of (WBI)  $P = 0.95$  a.u. that is in agreement with an aluminum-aluminum single bond. The  $\sigma$ -bond has a very large  $s$  character of 66.2% pointing to a metallic character of the bond (Figure 62).

Table 5: NBO results at the M06-2X/def2-TZVPP level of theory of compounds  $\text{Al}_2\text{H}_4$ ,  $\text{Al}_2\text{Cl}_4$  and **125**: Wiberg bond order ( $P$ ) and partial charges ( $q$ ).

	$\text{Al}_2\text{H}_4$	$\text{Al}_2\text{Cl}_4$	<b>125</b>
$q(\text{Al})$	+0.76	+1.05	+1.25
$P(\text{Al-Al})$	0.90	0.89	0.93

Table 5 illustrates that the  $\text{Al}_2$  moieties in compounds  $\text{Al}_2\text{H}_4$ ,  $\text{Al}_2\text{Cl}_4$  and **125** are partially charged with +1.52 e, +2.10 e, and +2.10 e, indicating more ionic interaction in **125** than in both compounds  $\text{Al}_2\text{H}_4$ ,  $\text{Al}_2\text{Cl}_4$ , while the WBI values are 0.90 a.u., 0.89 a.u., and 0.93 a.u., respectively. Furthermore, the Al-Al bond in compound **125** shows a more pronounced  $s$  character of 66.2% in contrast to  $\text{Al}_2\text{H}_4$  and  $\text{Al}_2\text{Cl}_4$  with 36.4% and 46.3%.

### 3. Results & Discussion

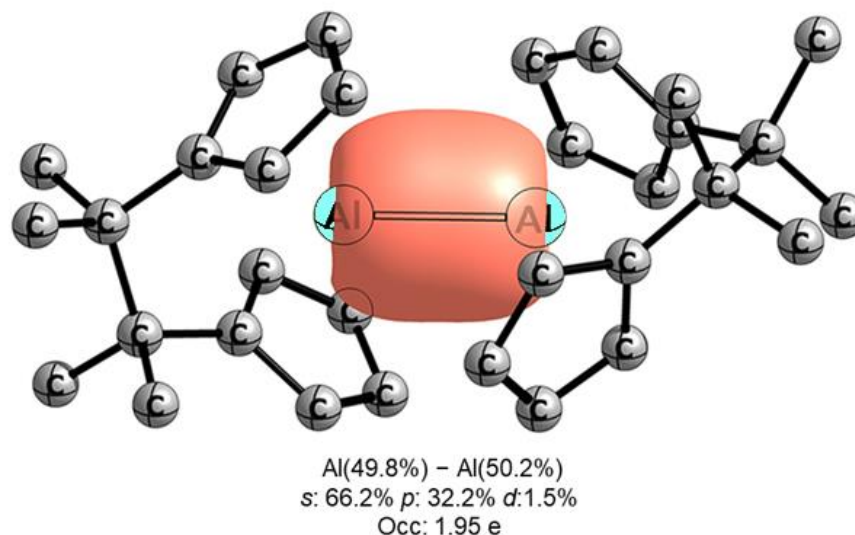


Figure 62: NBO-analysis of Al-Al bond in **125**, hybridization and occupation (calculations carried out at M06-2X/def2-TZVPP).

Moreover, a strong ionic interaction (Figure 63, **125(II)**) between the Al<sub>2</sub> moiety and the cyclopentadienyl rings can be demonstrated in compound **125** via Natural partial charges method.

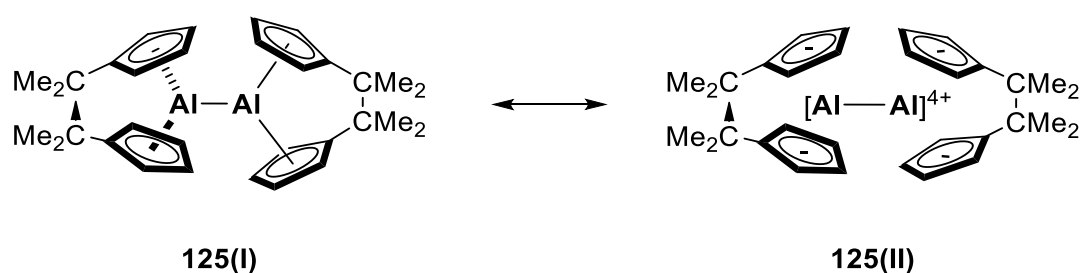


Figure 63: Suggested resonance structures of **125** predicted by on DFT calculations.

In conclusion, the very high *s* character of the Al-Al bond is the main reason for the shortness of the Al-Al bond because the *p*-orbitals of the aluminum atoms are more engaged in the bonding to the cyclopentadienyl substituents than in the Al-Al bond. Also, the shortness of the Al-Al bond can be attributed, as a minor part, to attractive dispersion interactions between the



### 3. Results & Discussion

ligands.<sup>347</sup> A comparison of the Al-Al bond length in compound **125** with the Al-Al bond lengths in compounds **71** and **73** (Figure 64) can confirm this theoretical study.

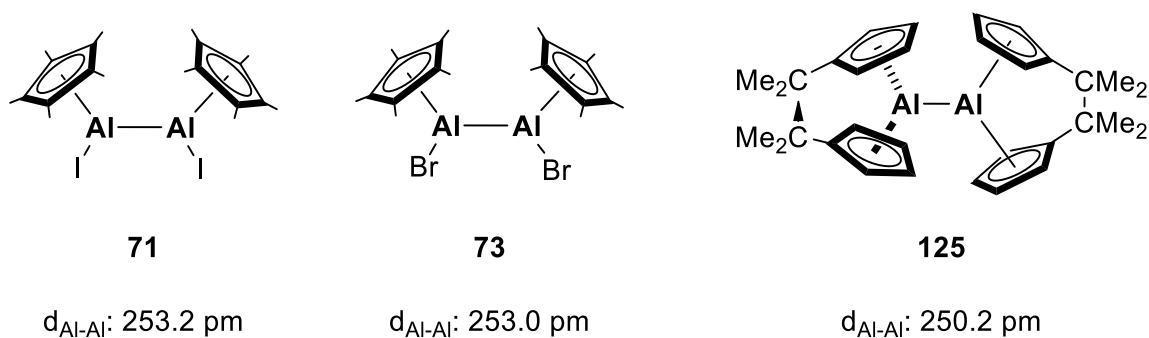


**Figure 64:** Representation of the structures of **71**, **73** and **125** with the Al-Al bond lengths.

A reason for shortness of the Al-Al bond length in compound **125** is that the *s*-orbital of the aluminum atoms is more involved in the Al-Al bond than in **71** and **73** because the *p*-orbitals of the aluminum atoms are engaged in the bonding to both cyclopentadienyl substituents in **125** whereas the *p*-orbitals of the aluminum atoms in compounds **71** and **73** are engaged only with one cyclopentadienyl substituent. Furthermore, compounds **71** and **73** include an Al-I/Br bond which is slightly less ionic than the Al-Cp bond.

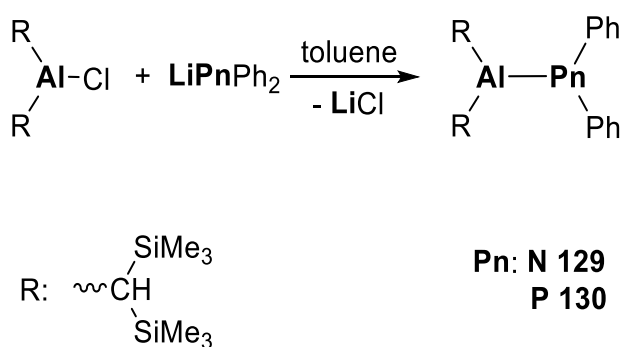
### 3.4. Monomeric and Oligomeric Amino- and Phosphanylalanes

#### 3.4.1. Synthesis and Structures

It has to be mentioned that the trimeric phosphanylalane **99** and the donor stabilized monomeric compounds of it **136-139** as well as the reactivity studies towards CO<sub>2</sub> of these compounds were performed by *Marcus Calvin-Brown* in the course of his bachelor thesis under my supervision. Furthermore, DFT-calculations were carried out in cooperation with the group of Dr. *Diego M. Andrada*.

Aminoalanes and phosphanylalanes with the formular R<sub>2</sub>Al-ER'<sub>2</sub> (E: N, P) have been long investigated (see chapter 1.6.). However, none of the published reports included a direct comparison of the structure and reactivity of monomeric, dimeric, trimeric compounds of aminoalane and phosphanylalane.

The treatment of bis[bis(trimethylsilyl)methyl]chloroalane [(Me<sub>3</sub>Si)<sub>2</sub>CH]<sub>2</sub>AlCl with lithium diphenylamide LiNPh<sub>2</sub> or lithium diphenylphosphide LiPPh<sub>2</sub> in toluene at ambient temperature overnight led to bis[bis(trimethylsilyl)methyl]diphenylaminoalane **129** and bis[bis(trimethylsilyl)methyl]diphenylphosphanylalane **130**, respectively (Scheme 71).



Scheme 71: Synthesis of compounds **129** and **130**.

Both compounds **129** and **130** were isolated as a colorless and air sensitive powders. They are stable at ambient temperature for months and in solution for weeks under argon. Compounds **129** and **130** were characterized by <sup>1</sup>H, <sup>13</sup>C, <sup>29</sup>Si and <sup>31</sup>P (in case of **130**) NMR spectroscopy in solution and in the solid state by X-ray diffraction.

### 3. Results & Discussion

The  $^1\text{H}$  NMR spectra of **129** and **130** exhibited five signals: two signals for the bonded bis[bis(trimethylsilyl)methyl] ligand to aluminum atom in aliphatic field and three signals for the bonded phenyl rings to the pnictogen atom (Figure 65). For compound **130**, the detected signal in  $^1\text{H}$  NMR spectrum, assigned to the proton of the methylene group of the bis[bis(trimethylsilyl)methyl] ligand, splits into a doublet with a coupling constant of  $J = 3.5$  Hz due to coupling with the phosphorous atom (Figure 65b). The  $^{13}\text{C}$  NMR spectrum of compound **130** also exhibited a doublet signal for the methylene carbon atom at  $\delta = 12.0$  ppm indicating a coupling to the phosphorous atom with a coupling constant of  $J = 9.6$  Hz.

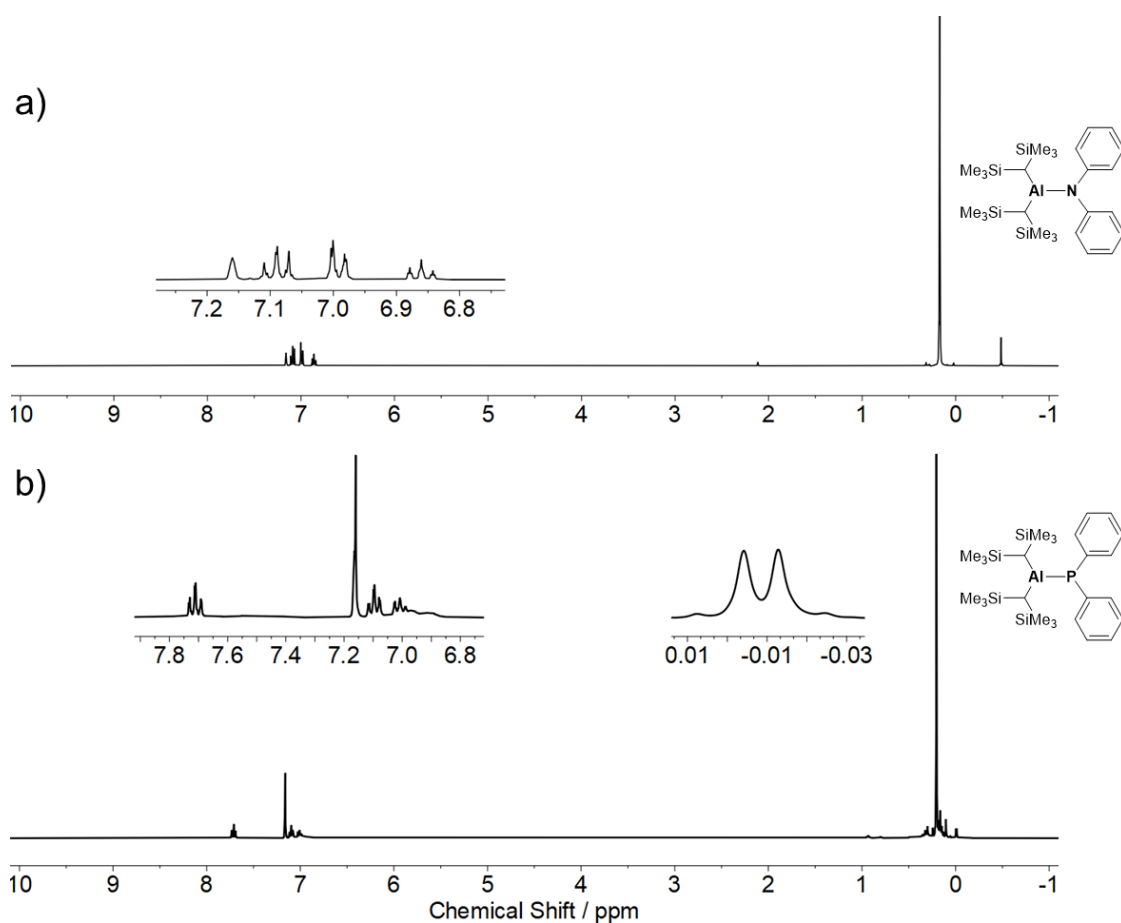


Figure 65:  $^1\text{H}$  NMR spectrum (400.13 MHz,  $\text{C}_6\text{D}_6$ , 298 K) a: **129**; b: **130**.

Furthermore, the signals of the silicon atoms in both compounds **129** and **130** possess approximately similar shift at  $\delta_{\text{Si}} = -2.0$  and  $-3.5$  ppm in  $^{29}\text{Si}$  INEPT NMR spectrum, respectively. Furthermore, a signal at  $\delta_{\text{P}} = -40.2$  ppm was also detected for compound **130** in  $^{31}\text{P}$  NMR spectrum which is very high field shifted compared with many known monomeric phosphanylalanes (Figure 66).<sup>295,302,326</sup>

### 3. Results & Discussion

Monomeric phosphanylalanes			
R: Ad; R': Tip R'': SiPh <sub>3</sub> $\delta^{31}\text{P}$ : -96.7 ppm	R: tmp R': SnMe <sub>3</sub> $\delta^{31}\text{P}$ : -238 ppm	R: tmp R': SiMe <sub>3</sub> $\delta^{31}\text{P}$ : -282 ppm	R: Mes R': <sup>t</sup> Bu $\delta^{31}\text{P}$ : -111 ppm
<b>93</b>	<b>94</b>	<b>95</b>	<b>96</b>

Figure 66: Representation of phosphanylalanes 93-96 highlighting the <sup>31</sup>P NMR shifts.

Compounds **129** and **130** were also characterized in the solid state by X-ray diffraction. Single crystal of both structures could be obtained from a saturated solution of toluene at 248 K (Figure 67).

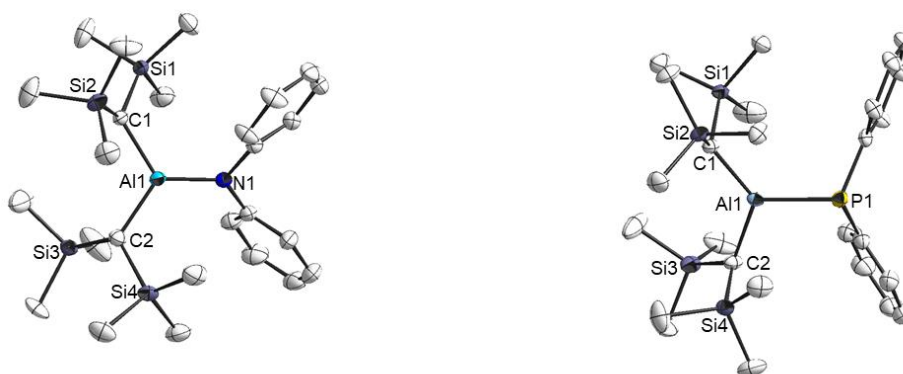


Figure 67: Molecular structure of **129** and **130** in the crystal, (thermal ellipsoids for 50% probability level, H-atoms were omitted for clarity).

The structure **130** in the crystals indicated a disorder in the diphenylphosphanyl fragment so that two Al-P bond lengths are detected. Table 6 highlighted the important parameters and bond lengths.

### 3. Results & Discussion

**Table 6: Bond lengths<sup>a</sup> and parameters of the crystal structures of compounds **129** and **130**.**

	<b>129</b>		<b>130</b>
Al1-N1	182.19(09) pm	Al1-P1	233.66(16) pm
		Al1-P1'	245.40(06) pm
Al1-C1	194.93(11) pm	Al1-C1	195.37(09) pm
Al1-C2	195.70(02) pm	Al1-C2	185.20(10) pm
C1-Si1	187.81(11) pm	C1-Si1	187.84(10) pm
C1-Si2	183.70(07) pm	C1-Si2	184.67(17) pm
C2-Si3	194.90(02) pm	C2-Si4	187.02(11) pm
$\Sigma\angle\text{Al1}$	359.9°	$\Sigma\angle\text{Al1}$	358.3-359.7°
$\Sigma\angle\text{N1}$	360°	$\Sigma\angle\text{P}$	308.1; 318.7°

<sup>a</sup> The numbering of the atoms corresponds to the labeling of crystal structures in Figure 67.

The aluminum centers in both compounds **129** and **130** exhibited a trigonal planar arrangement with a sum of interior angles around aluminum atoms of 359.9° and 358.3-359.7° in the crystal structures, respectively. The pnictogen atoms are bonded to the aluminum centers with different arrangement in the crystal structures so that the nitrogen displays a trigonal planar arrangement with a sum of interior angles around the nitrogen atom of 360.0°, while the phosphorous atom possesses a trigonally pyramidal arrangement with a sum of interior angles around phosphorous atom of 308.1° and 318.7° (two different values due to the disorder of the diphenylphosphanyl fragment in the crystal). While considering the disorder in the crystal of compound **130**, two aluminum-phosphorous bond lengths are detected. The Al1-P1' bond length of 245.4 pm is within the known bond length range of single Al-P bonds in oligomeric structures, while the bond length of 233.7 pm is in line with the reported monomeric phosphanylalanes (see chapter 1.7; Figure 26).

On the other hand, the Al-N bond length of 182.2 pm in compound **129** is in line with bond lengths of the known monomeric compounds (see chapter 1.7; Figure 25) and this Al-N bond length of 182.2 pm is between examples of Al-N single bonds (197.4 pm) and double bonds (173 pm)<sup>311,364</sup> which indicates that the bond between aluminum and nitrogen atoms possesses double bond character due to an interaction between the lone pair of nitrogen atom and the vacant *p*-orbital of the aluminum atom.

### 3. Results & Discussion

DFT calculations were performed at the B3LYP-D3-(BJ)/def2-TZVP<sup>340</sup> level of theory to investigate the electronic structure for both compounds **129** and **130**. (DFT calculations were carried out by the group of Dr. *Diego M. Andrada*). Table 7 illustrates the electronic characteristics of both compounds **129** and **130**.

**Table 7: NBO results for 129 and 130 at B3LYP-D3(BJ)/def2-TZVP level of theory: partial charges (Q, in e) and Wiberg bond order (P, in a.u.)**

Compound	Al-Pn [pm]	Q, Al	Q, Pn	Interaction energy [kJ·mol <sup>-1</sup> ]
<b>129(Al-N)</b>	183.5	2.09	-0.96	46.4
<b>130(Al-P)</b>	236.2	1.82	+0.10	37.2

According to the data in Table 7, the calculated aluminum pnictogen bond lengths are in line with the experimental bond lengths in the crystal structures of **129** and **130**. Furthermore, the aluminum atom in compound **129** bears a more positive charge than in compound **130** and the nitrogen atom is more negatively charged compared to the phosphorous atom in **130** indicating a polar Al-N bond. This is a consequence of the differences in electronegativity (Al:1.61, N: 3.04 and P: 2.19).<sup>365</sup> According to the second order perturbation within the NBO method, the interaction energy, which represents the donation of the lone pair of the pnictogen atom into the vacant  $p_z$ -orbital of aluminum atom, is 46.4 kJ·mol<sup>-1</sup> for aminoalane **129** indicating an Al-N bond with double bond character. This calculated interaction energy between the  $p$ -orbitals of aluminum and nitrogen in **129** is in agreement with the calculated interaction energy between the  $p$ -orbitals of aluminum and nitrogen in the structure model H<sub>2</sub>Al-NH<sub>2</sub> of 45 kJ·mol<sup>-1</sup>.<sup>314</sup> Such an interaction is weaker in case of compound **130** and accounts only for 37.2 kJ·mol<sup>-1</sup> because of the distortion of the phosphorous atom from the planarity.

The bond length of Al-N (182.2 pm) is shorter by *ca* 15.2 pm than the sum of the aluminum and nitrogen covalent radii of Al-N.<sup>311,364</sup> The results of the NBO method show that the reason for this is the combination between a  $\pi$ -bonding via electron-donating of the lone pair on nitrogen atom into the vacant  $p$ -orbital of aluminum atom and electrostatic interactions.

Figures 68 and 69 show the results of the bonding analysis of both compounds and NBO representations of the Al-Pn bonds and the lone pairs at the N/P atoms. Notably, the localization of the  $p$ -orbitals shows an extremely polarized  $\sigma$ -Al-N/P bond with a contribution of 6.1% from the aluminum atom and 93.9% from the nitrogen atom, in compound **129**. While a contribution of 22.4 % on aluminum atom and 77.6% on phosphorous atom is suggested in compound **130**. Furthermore, the pnictogen atoms in both compounds **129** and **130** possess

### 3. Results & Discussion

a lone pair. In case of compound **130**, the lone pair on the phosphorous atom has 50% *s*-character and 50% *p*-character, while in compound **129** the lone pair on nitrogen atom has exclusively *p*-character. The character of the lone pair on the pnictogen atoms N/P is in line with the planarity and pyramidalization of the nitrogen and phosphorous atoms observed in the crystal structures (Figure 67).

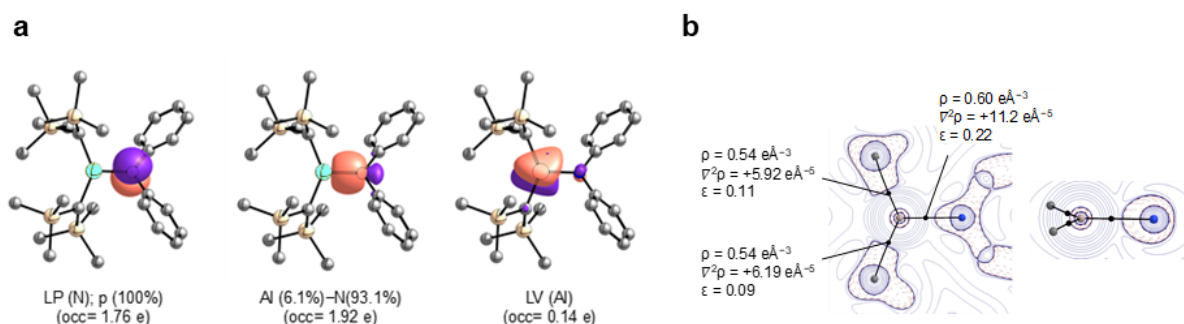


**Figure 68:** a) NBO results of **129** at B3LYP+D3(BJ)/def2-TZVP level of theory representing Al-N bond, lone pair (LP) at N, and lone vacancy (LV) at Al (isovalue = 0.05 pm); b) Laplacian distribution of the electron, contour line diagrams of the Laplacian distribution  $\nabla^2\rho(r)$  on and perpendicular to the C-Al-N plane.

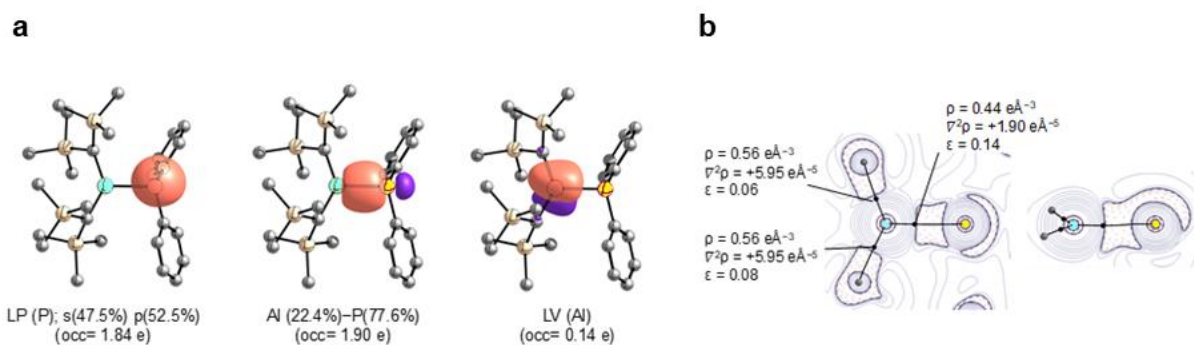


**Figure 69:** a) NBO results of **130** at B3LYP+D3(BJ)/def2-TZVP level of theory representing Al-P bond, lone pair (LP) at P, and lone vacancy (LV) at Al (isovalue = 0.05 pm); b) Laplacian distribution of the electron, contour line diagrams of the Laplacian distribution  $\nabla^2\rho(r)$  on and perpendicular to the C-Al-P plane.

AIM Laplacian plots data of both compounds **129** and **130** show electron density accumulation around the pnictogen element indicating the strong polarization of these bonds. In the case of compound **130**, there is a clear indication of a lone pair on the phosphorous atom. This can be seen by the comparison of ellipticity of the Al-P and Al-N bonds ( $\epsilon_{\text{Al-P}} = 0.14$ ,  $\epsilon_{\text{Al-N}} = 0.22$ ). Moreover, the contour maps of atoms in molecules (AIM) of compound **130** shows an electron concentration at phosphorous atom resulting from the lone pair, while this electron

### 3. Results & Discussion

concentration is absent in compound **129** suggesting that the lone pair on nitrogen atom is involved in the formation of the Al-N bond.

The calculation of the Kohn-Sham Frontier Molecular Orbitals of **129** and **130** (Figure 70) indicates that the HOMO is the lone pair located on the pnictogen atoms, while the LUMO is related to  $\pi$ -orbitals of the phenyl substituents. On the other hand, LUMO+1 is representing the  $p$ -typ orbital localized at the aluminum center. The HOMO-LUMO+1 gaps of **129** and **130** are 5.07 eV and 4.59 eV; respectively, which are lower than the HOMO-LUMO gap of  $\text{H}_2\text{C}=\text{SiH}_2$  (10.9 eV)<sup>366</sup> and higher than the  $\text{H}_2\text{Si}=\text{SiH}_2$  (4.36 eV).<sup>367</sup>

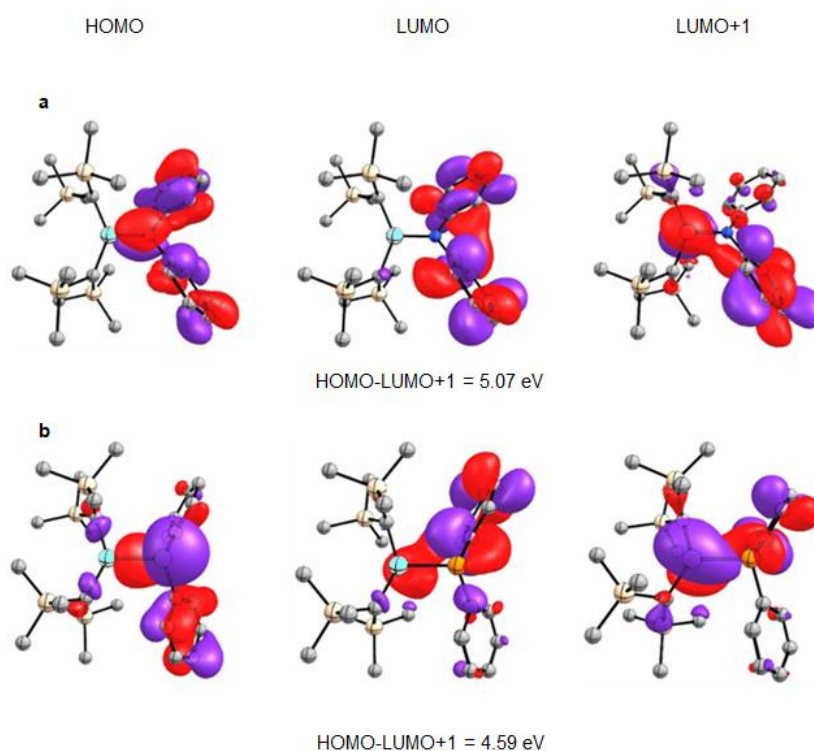
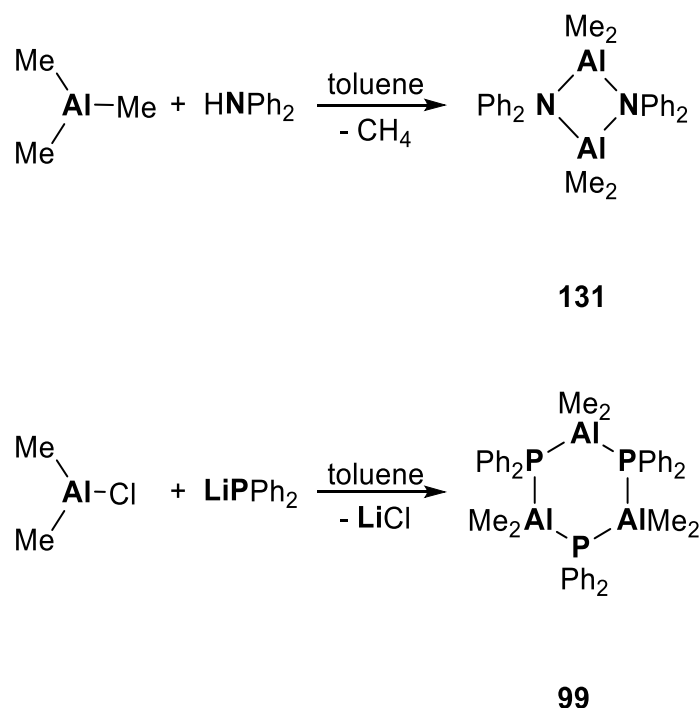


**Figure 70:** KS- Frontier Molecular Orbitals of a) **129** and b) **130** at B3LYP-D3(BJ)/def2-TZVP level of theory (isovalue 0.03). Hydrogen atoms were omitted for clarity.

Diphenylamino dimethylaluminum **131** was synthesis by methane elimination, while trimeric diphenylphosphanyl dimethylaluminum **99** was synthesis by a salt metathesis reaction (Scheme 72). Both complexes were studied before<sup>276,284,296</sup> and compound **99** was even characterized in solution and in the solid state (Figure 26, chapter 1.7.).<sup>296</sup>



### 3. Results & Discussion



Scheme 72: Synthesis of compounds **131** and **99**.

Both compounds **131** and **99** were obtained as oxygen and moisture highly sensitive colorless powders. They are stable at ambient temperature for a month in the solid state and for a week in solution under inert gas. Compound **131** could be characterized in the solid state by X-ray diffraction. Single crystals of the structure could be obtained from a saturated solution of toluene at 248 K (Figure 71). Compound **131** exhibited a dimeric structure in the crystal building a non-planar four membered  $\text{Al}_2\text{N}_2$  ring with Al-N bond lengths in a range of 200.5-202.4 pm which is in accordance with known dimeric structures in the literature (Figure 25; chapter 1.7).<sup>268,284-286</sup> The Al-N bond lengths in the dimeric structure **131** are longer than the Al-N bond in the monomeric structure **129** indicating single bond character.

The non-planar ring of  $\text{Al}_2\text{N}_2$  possesses a N1-Al1-N2 angle of  $86.1^\circ$ , N1-Al2-N2 of  $86.0^\circ$ , Al1-N1-Al2 of  $87.2^\circ$  and Al1-N2-Al2 of  $88.0^\circ$ . Moreover, both aluminum and nitrogen atoms exhibit a distorted tetrahedral arrangement so that every atom of aluminum and nitrogen is bonded to a substituent above the  $\text{Al}_2\text{N}_2$  ring and one substituent below the ring.

### 3. Results & Discussion

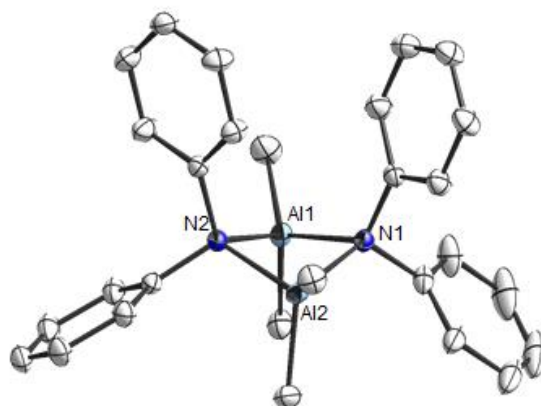
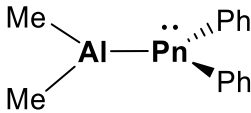
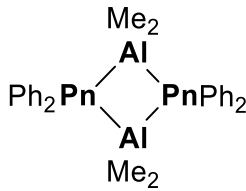
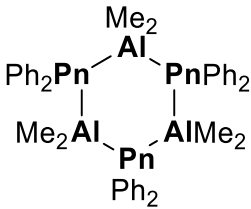


Figure 71: Molecular structure of **131** in the crystal, (thermal ellipsoids for 50% probability level, H-atoms were omitted for clarity).

The four-membered rings of dimeric aminoalanes are either planar or non-planar depending on the steric demand of the substituents on the aluminum and nitrogen atoms.<sup>284</sup> For instance, compound  $[\text{Pr}_2\text{AlNMe}_2]_2$  **89** (Figure 25) possesses a planar  $\text{Al}_2\text{N}_2$  ring,<sup>284</sup> while compound **131** has a non-planar ring with an Al-Al distance of 278.7 pm which is very close to the Al-Al bond length of 275.1 pm in dialane compound of **62** and might be an indication for an Al-Al-interaction.

Compound **131** is a dimer, while compound **99** is a trimer in the solid state. The main factor controlling the oligomerization reaction, which commonly occurs in pnictogenylalanes (see chapter 1.7.) is the steric demand on the aluminum atom. For further understanding of the oligomerization of pnictogenylalane compounds, monomers, dimers and trimers of compounds **131** and **99** were calculated and the relative energies were compared (Figure 72). The calculated energies of compounds **131** and **99** are in line with the isolated structures in the solid state so that the dimeric structure of **131** and the trimeric structure of **99** are global energy minima in the solid state. The dimeric structure of **131** is favored by  $68.4 \text{ kJ}\cdot\text{mol}^{-1}$  over the corresponding monomeric structure **131<sub>M</sub>** and  $103.7 \text{ kJ}\cdot\text{mol}^{-1}$  over the corresponding trimeric structure **131<sub>T</sub>**. On the other hand, the trimeric structure **99** is more favorable than the corresponding monomeric structure **99<sub>M</sub>** by  $296.6 \text{ kJ}\cdot\text{mol}^{-1}$  and the corresponding dimeric structure **99<sub>D</sub>** by  $136.0 \text{ kJ}\cdot\text{mol}^{-1}$ . Furthermore, the oligomerization of phosphanylalane is significantly more pronounced than aminoalane probably because of the better stabilization according to the higher double bond character of the bond Al-N than Al-P.

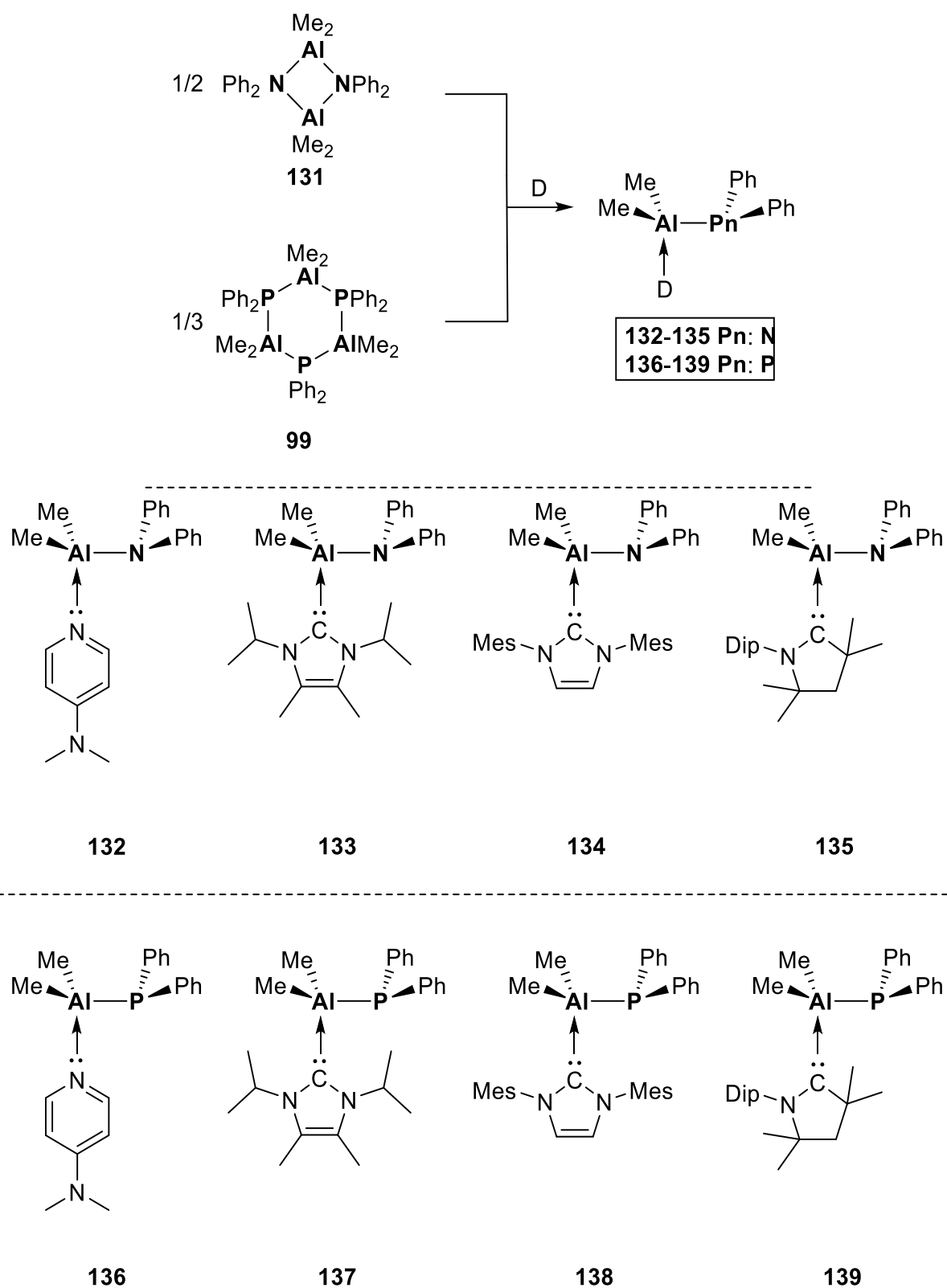
### 3. Results & Discussion

			
<b>Pn: N</b>	<b>131<sub>M</sub></b> : +68.4 kJ mol <sup>-1</sup>	<b>131</b> : 0 kJ mol <sup>-1</sup>	<b>131<sub>T</sub></b> : +103.7 kJ mol <sup>-1</sup>
<b>Pn: P</b>	<b>99<sub>M</sub></b> : +296.6 kJ mol <sup>-1</sup>	<b>99<sub>D</sub></b> : +136.0 kJ mol <sup>-1</sup>	<b>99</b> : 0 kJ mol <sup>-1</sup>

**Figure 72:** Calculated relative Gibbs free energies ( $\Delta G$ , kJ mol<sup>-1</sup>) for monomers, dimers and trimers of (diphenylamino)dimethylalane and (diphenylphosphanyl)dimethylalane at the B3LYP-D3(BJ)/def2-TZVP level of theory.

Increasing the steric demand of the substituent at the aluminum atom or at the pnictogen atom (N or P) is not the only strategy to obtain a monomeric structure of a pnictogenylalane. It can also be obtained by the treatment of oligomeric pnictogenylalanes with  $\sigma$ -donor ligands to afford a monomeric donor stabilized pnictogenylalane. The coordination of  $\sigma$ -donor ligands prevents the self-aggregation process of the oligomeric structures. Following this concept, compounds **131** and **99** were reacted with different  $\sigma$ -donors like 4-dimethylaminopyridine (DMAP), N-heterocyclic carbenes (NHCs) and a cyclic(alkyl)(amino)carbene (CAAC) in toluene to afford compounds **132-139** (Scheme 73).

### 3. Results & Discussion

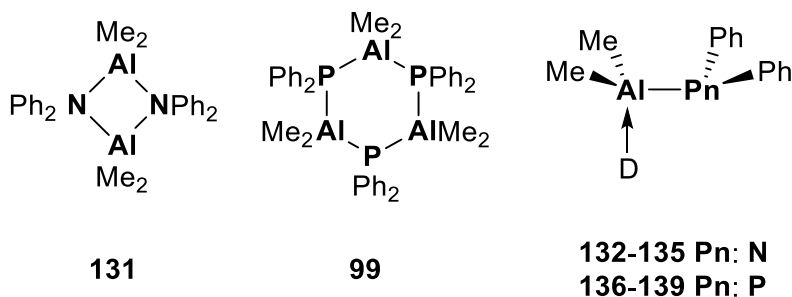


Scheme 73: Synthesis of compounds 132-139.

### 3. Results & Discussion

All compounds **132-139** are isolated as colorless to light yellow highly oxygen and moisture sensitive powders. They are stable for months in the solid state and in solution under inert gas. All complexes were characterized in solution by NMR spectroscopy and in the solid state by X-ray diffraction. The important characteristic shifts are summarized in Table 8 compared with starting compounds **131** and **99**.

Table 8: Characteristic  $^1\text{H}$ - and  $^{31}\text{P}$ -NMR shifts of compounds **99** and **131-139** in  $\text{C}_6\text{D}_6$ .



Compound	Donors	$\delta ^1\text{H (Me-Al)}$ [ppm]	$\delta ^{31}\text{P}$ [ppm]
<b>131</b>	-	-0.25 (s)	-
<b>99</b>	-	0.01 (q)	-60.2
<b>132</b>	DMAP	-0.14 (s)	-
<b>133</b>	$i\text{Pr}_2\text{Me}_2\text{NHC}$	-0.18 (s)	-
<b>134</b>	$\text{Mes}_2\text{H}_2\text{NHC}$	-0.82 (s)	-
<b>135</b>	CAAC	-0.81 (s)	-
<b>136</b>	DMAP	-0.01 (d)	-56.3
<b>137</b>	$i\text{Pr}_2\text{Me}_2\text{NHC}$	-0.03 (d)	-53.5
<b>138</b>	$\text{Mes}_2\text{H}_2\text{NHC}$	-0.92 (s)	-53.7
<b>139</b>	CAAC	-0.74 (d)	-49.3

The  $^{31}\text{P}$  NMR data of compounds **136-139** show that the coordination of a donor molecule to aluminum atom shifts the  $^{31}\text{P}$  signals in the high field by ca 3.9-10.9 ppm in comparison to compound **99** indicating the influence of the coordinated donor molecules. According to the shifts of the bound methyl group to aluminum atom in these compounds, no clear trend is to observe.

Compounds **132-139** were also investigated in the solid state by X-ray diffraction analysis. Single crystals of compounds **132-139** could be obtained from a saturated solution of toluene at 248 K suitable for X-ray diffraction analysis (Figure 73 and 74).

### 3. Results & Discussion

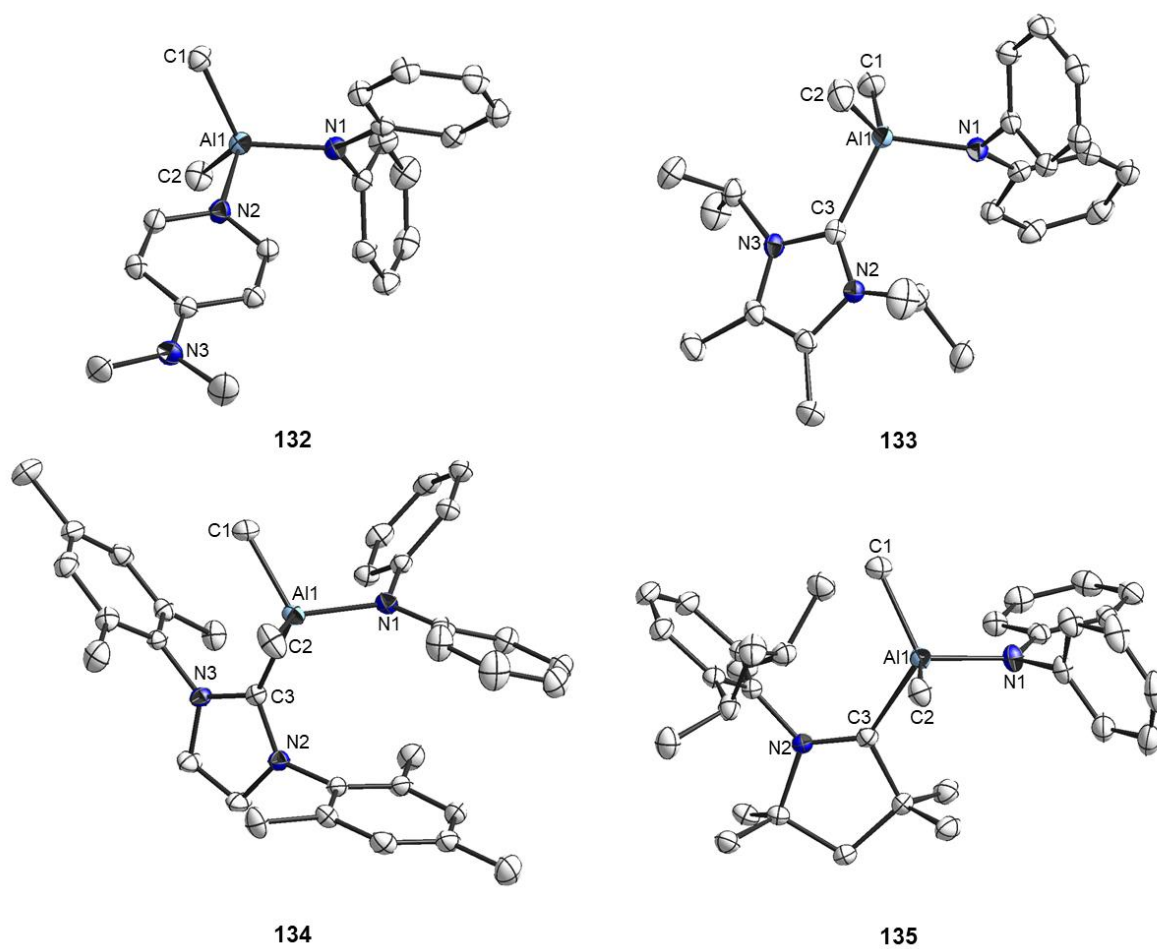


Figure 73: Molecular structure of 132-135 in the crystal, (thermal ellipsoids for 50% probability level, H-atoms were omitted for clarity).

### 3. Results & Discussion

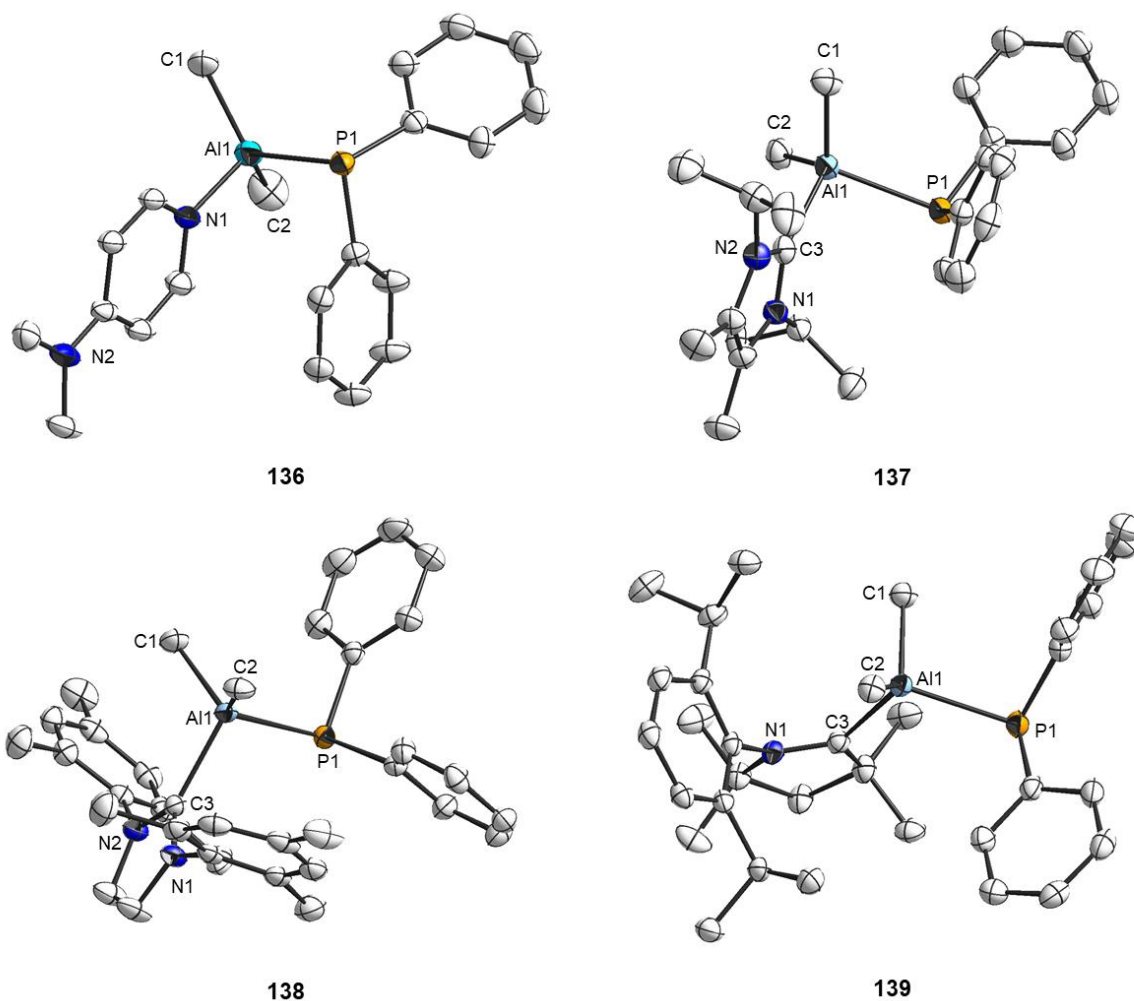


Figure 74: Molecular structure of 136-139 in the crystal, (thermal ellipsoids for 50% probability level, H-atoms were omitted for clarity).

The aluminum atom in all complexes is tetracoordinated in a tetrahedron arrangement with a sum of angles of  $331.3^\circ$  to  $343.8^\circ$  without considering the donor molecules (Table 9). While the phosphorous atom possesses a trigonal pyramidal arrangement with a sum of interior angles of  $304.2^\circ$  to  $317.5^\circ$  in **136-139**, the nitrogen atom indicates a trigonal planar arrangement with a sum of interior angles of  $357.5^\circ$  to  $360.0^\circ$  in **132-135**.

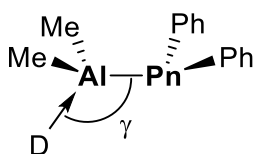
### 3. Results & Discussion

**Table 9: Selected Parameters of the crystal structures of 99 and 132-139 with the calculated bond strength of Al-D.**

Compound	Al-Pn [pm]	$\Sigma\angle\text{Al}^a$ [°]	$\Sigma\angle\text{Pn}$ [°]	D	Al-D [pm]	E(Al-D) <sup>b</sup> [kJ mol <sup>-1</sup> ]
<b>131 (E=N)</b>	200.64(08)			-		
	200.67(08)	-	-		-	-
	201.76(08)					
	202.41(07)					
<b>99 (E=P)</b>	244.35(10)			-		
	244.64(10)	-	-		-	-
	245.32(10)					
	245.44(10)					
	246.53(10)					
247.89(10)						
<b>132 (E=N)</b>	187.90(01)	342.3	360.0	DMAP	197.52(09)	141.7
<b>133 (E=N)</b>	189.46(13)	333.2	357.5	<sup>t</sup> Pr <sub>2</sub> Me <sub>2</sub> NHC	208.96(06)	192.2
			358.5			
<b>134 (E=N)</b>	189.39(01)	333.4	360.0	Mes <sub>2</sub> H <sub>2</sub> NHC	208.72(01)	-
<b>135 (E=N)</b>	190.32(13)	331.9	358.3	CAAC	211.85(14)	176.0
<b>136 (E=P)</b>	241.04(01)	343.8	304.2	DMAP	195.79(00)	163.0
<b>137 (E=P)</b>	241.00(02)	335.7	307.6	<sup>t</sup> Pr <sub>2</sub> Me <sub>2</sub> NHC	206.63(02)	212.5
<b>138 (E=P)</b>	240.62(06)	335.9	317.5	Mes <sub>2</sub> H <sub>2</sub> NHC	208.45(16)	218.5
<b>139 (E=P)</b>	242.52(05)	331.3	308.8	CAAC	210.12(13)	188.8

<sup>a</sup> Sum of angles around Al, N and P atoms are given in case of monomeric compounds and disregarding the donor-molecules in case of **132-139**. <sup>b</sup> The energies are obtained from NBO analysis at the B3LYP(D3-BJ)/def2-TZVP<sup>340</sup> level of theory.

The donor molecules are coordinated to aluminum atoms in different angles ( $\gamma$ ) to the Al-Pn bonds (Pn = N or P) of 97.4° to 109.8° (Figure 75, Table 10).



**132-135 Pn: N**  
**136-139 Pn: P**

**Figure 75: General representation of the structure 132-139 highlighting the angle  $\gamma$ :  $\angle\text{D-Al-Pn}$  between the coordinated donors and the Al-Pn bonds.**



### 3. Results & Discussion

Table 10:  $\gamma$  angle of compounds 132-139.

Compound	Donors	$\gamma$ [°]
132	DMAP	102.4
133	<i>i</i> Pr <sub>2</sub> Me <sub>2</sub> NHC	109.0
134	Mes <sub>2</sub> H <sub>2</sub> NHC	107.9
135	CAAC	109.7
136	DMAP	97.4
137	<i>i</i> Pr <sub>2</sub> Me <sub>2</sub> NHC	97.8
138	Mes <sub>2</sub> H <sub>2</sub> NHC	100.6
139	CAAC	108.9

Furthermore, the coordination of a  $\sigma$ -donor molecule to the aminoalane **131** as well as the phosphanylalane **99** led to shortening the Al-Pn bond length by ca 12 pm and 5 pm, respectively, compared to the starting compounds. This Al-Pn shortening could be interpreted in two different ways: either the aluminum pnictogen bond has more double bond character or the charge separation between aluminum and pnictogen atoms has become stronger so that the ionic character of the Al-Pn bond has increased.

Furthermore, the bond lengths of Al-D are longer in aminoalane compounds **132-135** than in phosphanylalane compounds **136-139** by approximately 2 pm. A reason for this elongation in aminoalane compounds could be the bond nature of the Al-N that has more double bond character than the Al-P bond, which means that the electron density at the aluminum atom is higher in aminoalane compounds than in the phosphanylalane compounds. An exception is the Al-D bond in compounds **134** and **137** including a coordinated Mes<sub>2</sub>H<sub>2</sub>NHC molecule to aluminum; they are approximately similar.

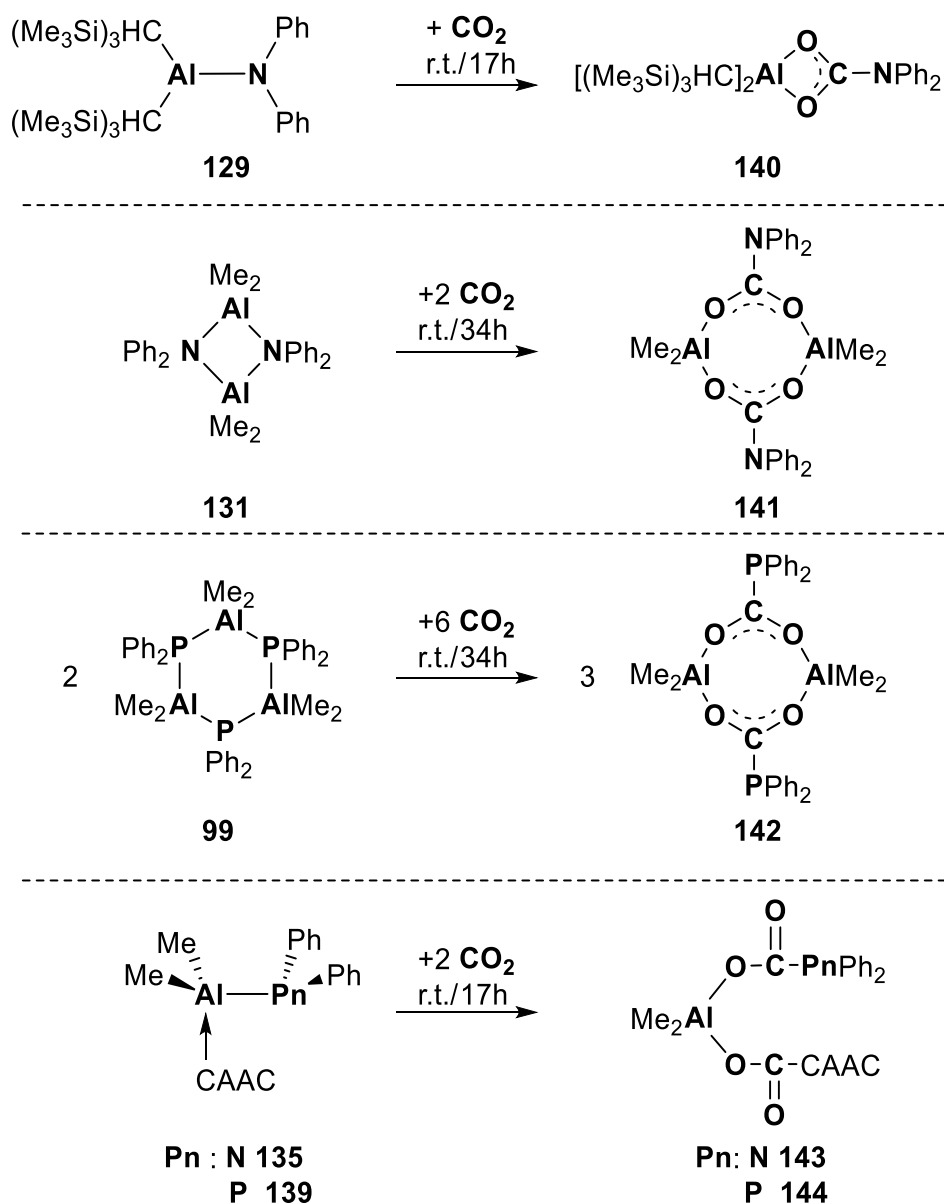
For better understanding of the electronic structures of these compounds and the bond strengths of the Al-D bonds, DFT calculations were carried out at the B3LYP-D3-(BJ)/def2-TZVP<sup>340</sup> level of theory (Table 9). The calculated Al-D and Al-Pn bond lengths are in good agreement with the experimentally determined bond lengths and the calculated geometries are in good agreement with the experimental X-ray analysis. In general, the bond strengths of Al-D in compounds **136-139** (phosphanylalane compounds) are higher than the bond strengths of Al-D in compounds **132-135** which is in accordance with the bond lengths of Al-D in these compounds. In other words, for instance, DMAP is more strongly bound to aluminum atom in compound **136** than in compound **132** by ca 21.3 kJ mol<sup>-1</sup> which is in accordance with the Al-N<sub>DMAP</sub> bond length of 195.8 pm and 197.5 pm, respectively. Besides, CAAC is stronger bonded to aluminum atom in compound **135** than DMAP in compound **132** by ca 34.3 kJ mol<sup>-1</sup> because

### 3. Results & Discussion

of the strong  $\sigma$ -donor property of the CAAC compared with DMAP. Although the CAAC possesses the stronger  $\sigma$ -donor property than the  $i\text{Pr}_2\text{Me}_2\text{NHC}$  and  $\text{Mes}_2\text{H}_2\text{NHC}$ , however, both donors  $i\text{Pr}_2\text{Me}_2\text{NHC}$  and  $\text{Mes}_2\text{H}_2\text{NHC}$  are more strongly bonded to aluminum atom in compounds **137** and **138** than CAAC in compound **139** by  $23.7 \text{ kJ mol}^{-1}$  and  $29.7 \text{ kJ mol}^{-1}$ , respectively. One reason for this behaviour are the attractive dispersion forces which is also observed in donor stabilized [C1]aluminocenophane derivatives **119-124**.<sup>339</sup>

## 3.5.2. Reactivity towards Carbon Dioxide

As mentioned before, the aluminum pnictogen bond is very polar which makes it a good candidate to activate unreactive small molecules such as CO<sub>2</sub>. The reactivity of compounds **129**, **131**, **99**, **136** and **139** towards CO<sub>2</sub> was investigated by the treatment of a solution of these compounds in toluene at ambient temperature in CO<sub>2</sub> atmosphere for 17 hours except compound **99** and **131** for 34 hours (Scheme 74).



Scheme 74: Synthesis of compounds 140-144.

### 3. Results & Discussion

Compounds **142** and **144** were synthesized and characterized by *Marcus Calvin-Brown* in his Bachelor thesis under my supervision.

All compounds **140-144** were isolated as colorless, oxygen and moisture sensitive powders and they are stable in the solid state and in solution for months under inert gas. Compounds **140-144** were characterized in solution by NMR and in the solid state by XRD, IR (Table 11).

**Table 11:**  $^{13}\text{C}\{^1\text{H}\}$  NMR shifts of the carbon atoms of the inserted  $\text{CO}_2$  molecules in solution (100.62 MHz,  $\text{C}_6\text{D}_6$ , 298 K) and the IR shift in solid state.

Compounds	$\delta^{13}\text{C}(\text{CO}_2)$ [ppm]	$\nu(\text{CO}_2)$ [ $\text{cm}^{-1}$ ]
<b>140</b>	165.8 (s)	1494, 1517
<b>141</b>	158.4 (s)	1467, 1491, 1572, 1611
<b>142</b>	193.6 (d, $J=16.7$ Hz)	1388, 1591
<b>143</b>	194.0 (s); 158.4 (s)	1375, 1656, 1699
<b>144</b>	192.7 (s); 179.2 (s)	1259, 1625, 1697

Single crystal could be obtained from a saturated solution of toluene at 248 K suitable for X-ray diffraction analysis (Figures 76 and 77).

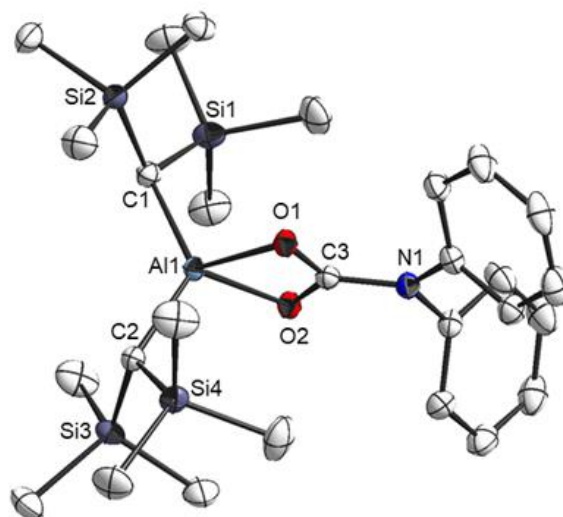


**Figure 76:** Molecular structure of **140** in the crystal, (thermal ellipsoids for 50% probability level, H-atoms were omitted for clarity).

### 3. Results & Discussion

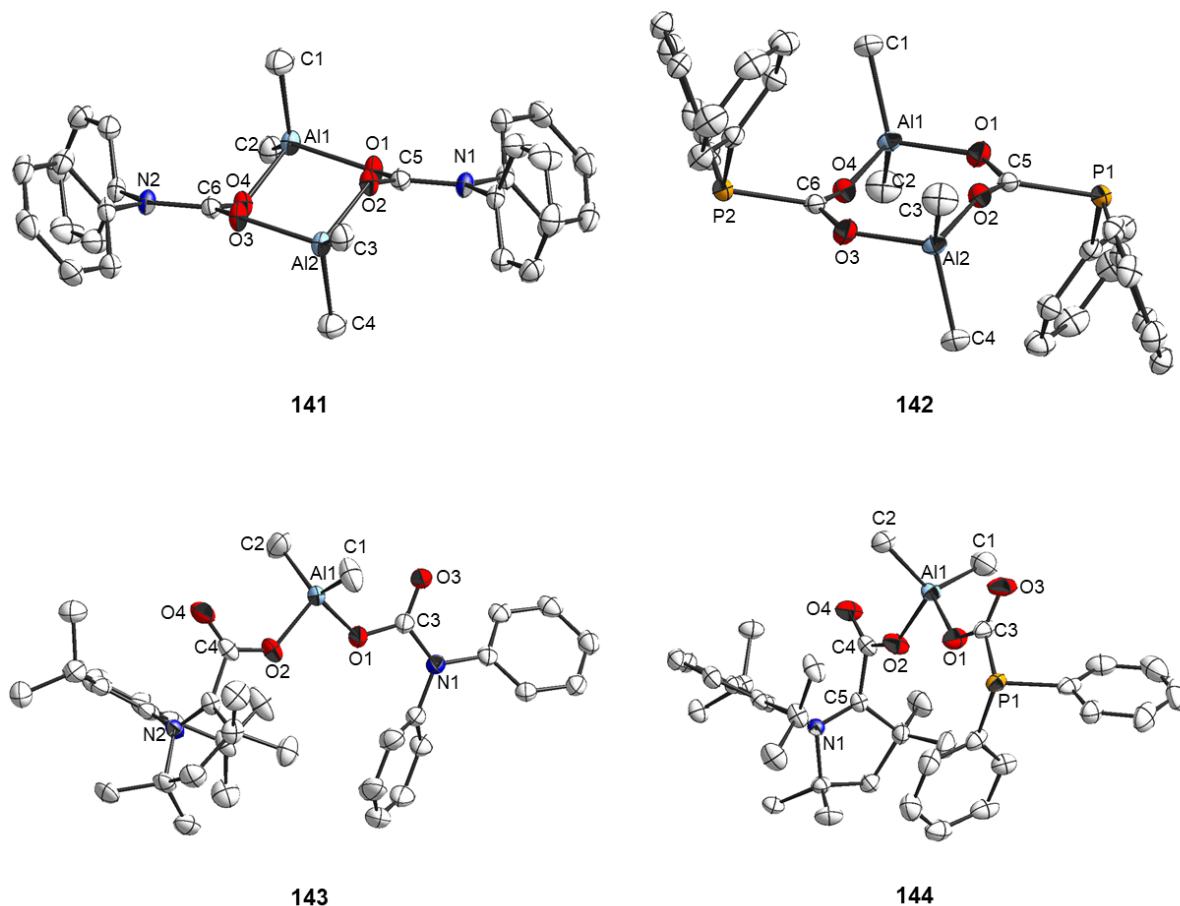


Figure 77: Molecular structure of 141-144 in the crystal, (thermal ellipsoids for 50% probability level, H-atoms were omitted for clarity).

The crystal structures of all compounds **140-144** show that the aluminum atoms adopt a tetrahedron arrangement. While nitrogen atoms indicate a trigonal planar arrangement with a sum of interior angles of  $360.0^\circ$  in compounds **140**, **141** and **143**, the phosphorous atoms possess a trigonal pyramidal arrangement with a sum of interior angles of  $302.0$  and  $307.3^\circ$  in compounds **142** and **144**, respectively. The Al-O bond distances differ between  $180.2 - 190.4$  pm. However, the longest Al-O distance of  $190.4$  pm is detected in the monomeric structure of compound **140** probably due to the steric effect of the bonded substituent to aluminum atom.

Generally, in compounds **129**, **131**, **99**, **135** and **139**, an insertion of  $\text{CO}_2$  molecule into the Al-Pn bonds is observed as well as into the Al-D bond in case of donor-stabilized pnictogenylalane compounds, which is in agreement with previous reports in the literature (see chapter 1.7,



### 3. Results & Discussion

7.9 kJ·mol<sup>-1</sup> to afford stable, exergonic adducts INT4 and INT10 located at -88.7 kJ·mol<sup>-1</sup> and -61.9 kJ·mol<sup>-1</sup>. The high tendency of INT4 to dimerization affords the formation of centrosymmetric structures INT5 and INT11 (-216.3 and -138.9 kJ·mol<sup>-1</sup>) featuring a four-membered planar Al<sub>2</sub>O<sub>2</sub> ring, which isomerizes to 6- and 8-cyclic species that in turn terminates the reaction cascade. The Gibbs free energy profile in Figure 78 indicated that the CO<sub>2</sub> activation is the rate determining step of the reaction of **131<sub>M</sub>** and **99<sub>M</sub>** with CO<sub>2</sub>.

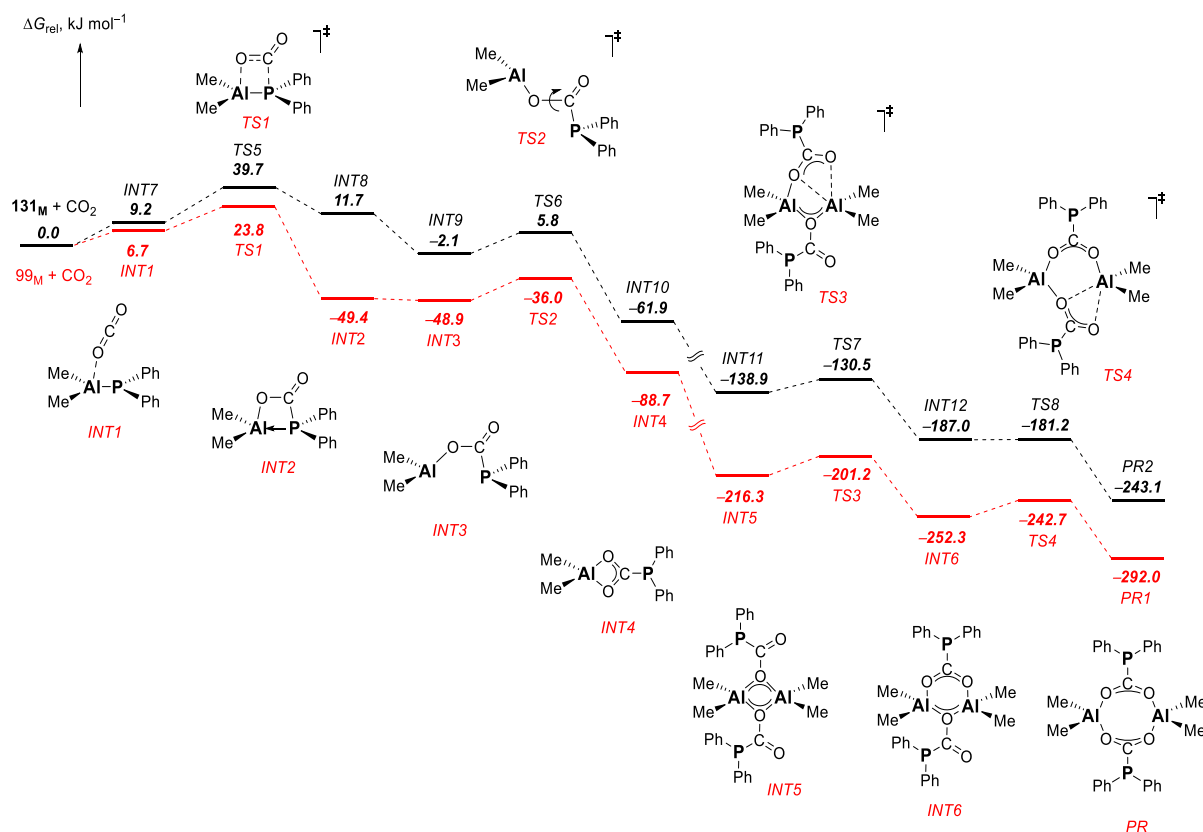
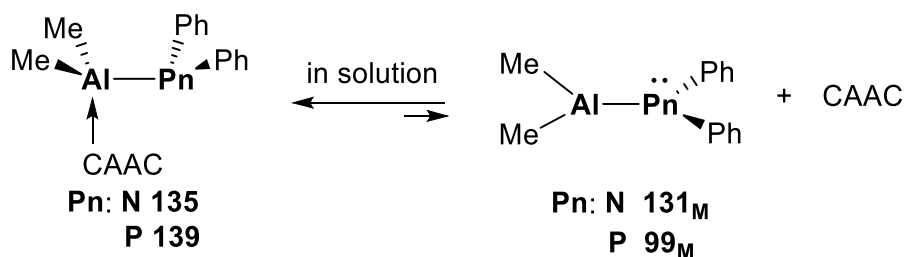


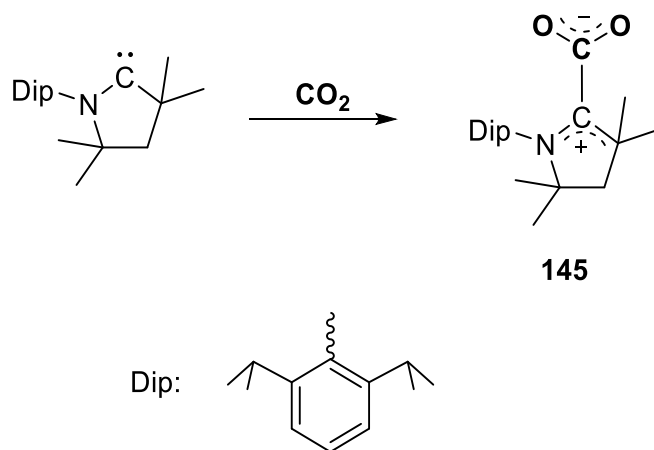
Figure 78: Calculated Gibbs free energy profile for the reaction of a) **131** with CO<sub>2</sub> and b) **99** with CO<sub>2</sub> (calculated at B3LYP+D3(BJ)/def2-TZVP; energies given in kJ·mol<sup>-1</sup>).

In case of donor-stabilized pnictogenylalane compounds, an equilibrium between pnictogenylalane and the donor molecule is also possible in solution (Scheme 76). The reaction of **131<sub>M</sub>** and **99<sub>M</sub>** with CO<sub>2</sub> occurred according the mechanism in Figure 78. On the other hand, it is known that the free CAAC molecule as well as NHC's are able to fix a CO<sub>2</sub> molecule in solution at room temperature as demonstrated by *Bertrand* in 2009 (Scheme 77).<sup>368</sup>

### 3. Results & Discussion



Scheme 76: Suggested behaviour of compounds 135 and 139 in solution.



Scheme 77: Fixation of CO<sub>2</sub> molecule by CAAC in solution at room temperature.

The presence of compound **145** with the insertion products of **131<sub>M</sub>** and **99<sub>M</sub>** with CO<sub>2</sub> (INT4 and INT10 in Figure 78) is able to prevent the dimerization of these species by the coordination of species **145** to aluminum atom leading to the formation of compounds **143** and **144**.

In summary, new monomeric amino- and phosphanylalane compounds were presented depending on the elevated sterically demanding substituents or by using  $\sigma$ -donor ligands, in this chapter, as well as oligomeric structures. The reactivity of these monomeric and oligomeric new structures towards small molecules such as CO<sub>2</sub> have been studied and the mechanism were also demonstrated via DFT calculations.



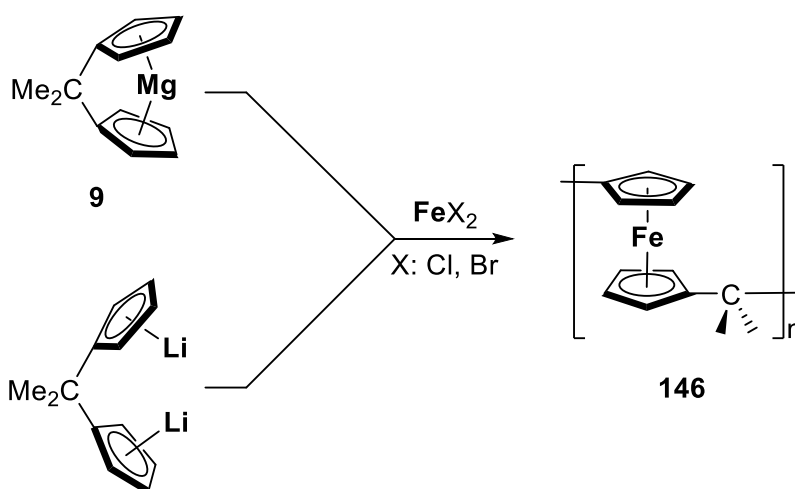
## 3.5. Polyferrocenylmethylene

Polyferrocenylmethylene project was carried out in cooperation with the group of Prof. *M. Gallei* and has been published in *Macromol. Rapid Commun.*, 2021, **42**, 2000738.

Metallocene containing polymers are interesting functional materials and they have attracted much attention because of their diverse applications considering their redox, magnetic and catalytic properties, and applications as etch resistance and self-organized materials.<sup>66–76</sup> One of the most famous class of these polymers are polyferrocenylsilanes which can be synthesized from the sila[1]ferrocenophanes by ring opening polymerizations involving anionic,<sup>81–83</sup> cationic,<sup>84</sup> thermal,<sup>85–88,369</sup> and transition metal catalyzed ring opening polymerizations reactions.<sup>89–91</sup>

Although ring opening polymerization reaction allowed the synthesis of high-molecular-weight polymers, these cannot be utilized for the synthesis of polyferrocenylmethylene simply because a carba[1]ferrocenophane is unknown.<sup>49,58,62,80,370,371</sup> Carba[1]magnesocenophane has been utilized to avoid this problem since magnesocenophanes are very powerful cyclopentadienyl ligand transfer reagents.

The synthesis of polyferrocenylmethylene (PFM) **146** started from either a Me<sub>2</sub>C-magnesocenophane **9** or an dilithiated 2,2-bis(cyclopentadienide)propane with iron(II)chloride and iron(II)bromide (Scheme 78).<sup>372</sup>



Scheme 78: Synthesis of Polyferrocenylmethylene **146**.

### 3. Results & Discussion

The reaction was performed at room temperature to yield PFM **146** after work-up as a yellow and air-stable solid. PFM **146** behaves similarly to polyferrocenylsilane in terms of solubility, so that PFM is soluble in thf and chloroform and insoluble in water.<sup>87</sup>

The investigation of <sup>1</sup>H NMR displays two signals at  $\delta = 1.53$  and 3.94 ppm. The signal at 1.53 ppm corresponds to methyl group bonded to the methylene bridge, while the signal at 3.94 ppm corresponds to the protons attached to cyclopentadienyl rings (Figure 79). Surprisingly, the protons of the cyclopentadienyl rings coincide in one signal in the <sup>1</sup>H NMR spectrum contrary to that in polyferrocenylsilane (PFS) which indicates two signals for cyclopentadienyl protons at 4.25 and 4.10 ppm in C<sub>6</sub>D<sub>6</sub> at room temperature.<sup>87</sup> In the <sup>13</sup>C NMR spectrum (Figure 79), three signals for the Cp carbon atoms at  $\delta = 66.4$ , 67.7 and 101.2 ppm (aromatic) and two signals for carbon atoms of the methylene bridge (aliphatic) at  $\delta = 30.7$  and 33.5 ppm are detected.

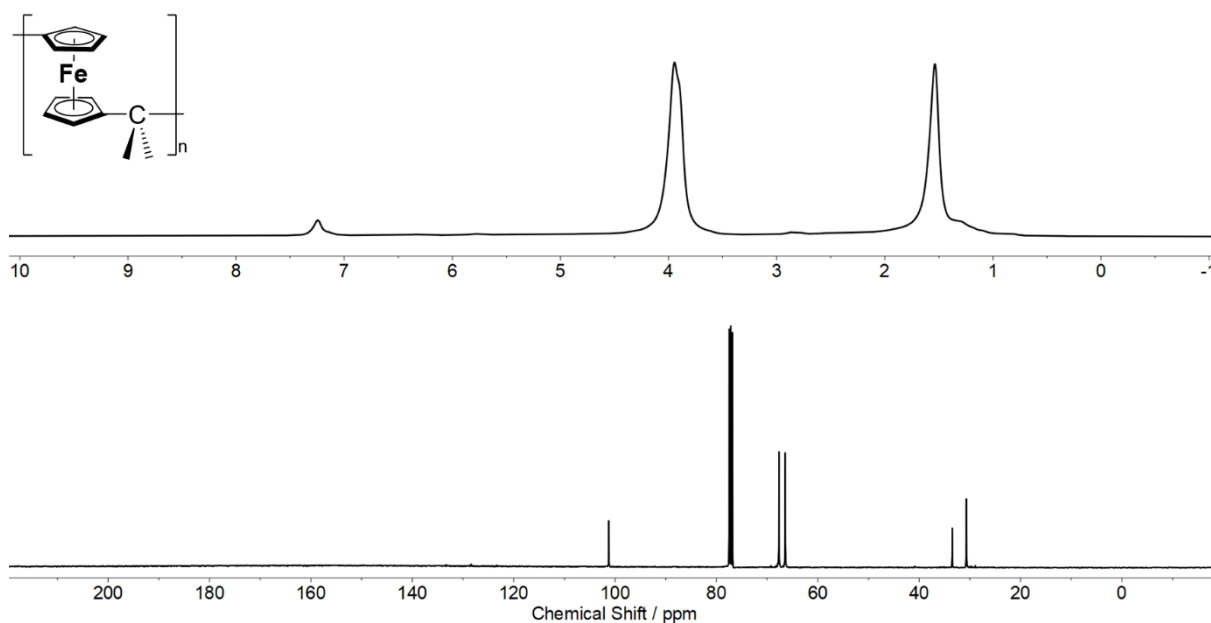


Figure 79: <sup>1</sup>H NMR spectrum (400.13 MHz, CDCl<sub>3</sub>, 298 K) (top) and <sup>13</sup>C {<sup>1</sup>H} NMR spectrum (100.62 MHz, CDCl<sub>3</sub>, 298 K) (bottom) of PFM **146**.

Table 12: Molar masses and dispersity indices of the synthesized polyferrocenylmethylenes using different cyclopentadiene transfer reagents and different iron precursors.

Reaction	FeX <sub>2</sub>	Starting materials	M <sub>w</sub> <sup>a</sup> [g·mol <sup>-1</sup> ]	M <sub>n</sub> <sup>a</sup> [g·mol <sup>-1</sup> ]	Đ
1	FeCl <sub>2</sub>	Me <sub>2</sub> C[1]Cp <sub>2</sub> Li <sub>2</sub>	3000	2200	1.36
2	FeBr <sub>2</sub>	Me <sub>2</sub> C[1]Cp <sub>2</sub> Li <sub>2</sub>	3400	2400	1.37
3	FeCl <sub>2</sub>	Me <sub>2</sub> C[1]Cp <sub>2</sub> Mg	9000	4300	2.09
4	FeBr <sub>2</sub>	Me <sub>2</sub> C[1]Cp <sub>2</sub> Mg	11700	8300	1.40

<sup>a</sup> Determined by size exclusion chromatography in thf vs. polystyrene standards.

### 3. Results & Discussion

Moreover, compound **146** was also investigated by size exclusion chromatography (SEC) in THF vs. Polystyrene (PS) standards (Figure 80) and the data were summarized in Table 12. The SEC data demonstrated that different molar masses depending on the synthesis route were obtained (Table 12).

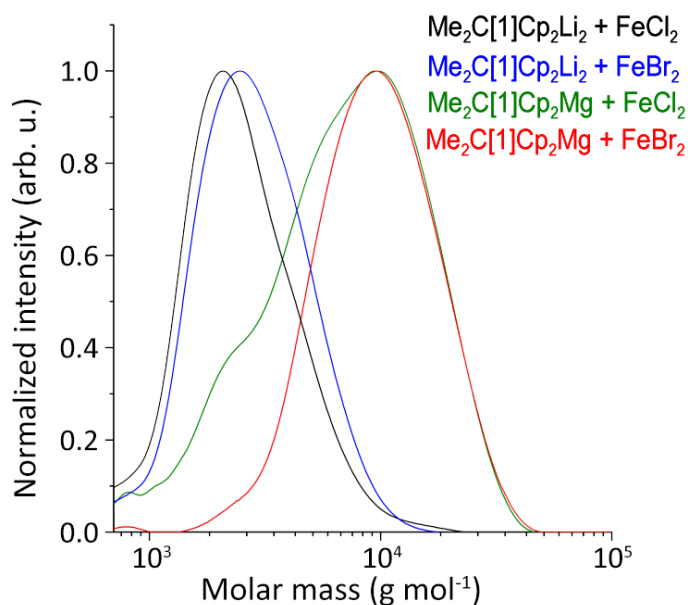


**Figure 80:** Size exclusion chromatography (SEC) spectra of **129** in THF versus PS standards using different precursors:  $\text{Me}_2\text{C}[1]\text{Cp}_2\text{Li}_2 + \text{FeCl}_2$  (black line),  $\text{Me}_2\text{C}[1]\text{Cp}_2\text{Li}_2 + \text{FeBr}_2$  (blue line),  $\text{Me}_2\text{C}[1]\text{Cp}_2\text{Mg} + \text{FeCl}_2$  (green line) and  $\text{Me}_2\text{C}[1]\text{Cp}_2\text{Mg} + \text{FeBr}_2$  (red line).

The molar masses of the investigated polymers in all syntheses vary between  $M_n = 2200$ - $8300 \text{ g}\cdot\text{mol}^{-1}$  and the dispersity were in a range of  $\mathcal{D} = 1.36$ - $2.09$ . The higher molar masses  $M_n$  of PFM around  $4000$ - $8000 \text{ g}\cdot\text{mol}^{-1}$  were observed by utilizing magnesocenophane **9** as precursor. Starting from dilithium 2,2-bis(cyclopentadienide)propane as precursor only led to lower molar masses with  $M_n = 2200 \text{ g}\cdot\text{mol}^{-1}$ . These SEC results indicate that the molecular weight of the PMF polymer could be influenced significantly by utilizing different cyclopentadiene transfer reagents. The usage of different iron precursors also influences the molar mass of the PFM and the dispersity. The reaction between magnesocenophane **9** and iron(II)bromide (Table 12) led to higher molar masses  $M_n = 8300$  and  $M_w = 11700 \text{ g}\cdot\text{mol}^{-1}$  and lower dispersity with  $\mathcal{D} = 1.40$  exhibiting a better control of the reaction so that PFM **146**, synthesized by the usage of iron(II)bromide, has a higher molar masses  $M_n$ .

In method three, where the magnesocenophane **9** and  $\text{FeCl}_2$  have been used as starting materials, the molar mass distribution of the yielded polymer indicates a second lower molar masses shifted band. This band might be matched to cyclic oligomers which might be

### 3. Results & Discussion

promoted by back attacking to produce more cyclic oligomers rather than long chain polymers. It should be mentioned that the apparent molar masses of metallopolymers using relative methods can vary widely from their absolute molecular weights.<sup>373–375</sup> Therefore, the resulting PFM from batch four in Table 12 was further investigated by SEC MALLS to provide insights into the absolute molar mass. Regarding the SEC MALLS investigations, a molar mass of  $M_w = 13144 \text{ g}\cdot\text{mol}^{-1}$  was detected. In conclusion, the hydrodynamic volumes of the samples and the PS standards are mostly similar which promote accordance in the obtained SEC values. In order to obtain more information about the molecular structure of PFM **146**, MALDI-ToF mass spectroscopy was carried out. Two different species of cyclic and non-cyclic oligomers were detected in MALDI-ToF spectrum (Figure 81). Furthermore, a mass difference between the two detected signals is double of the repeat unit of 226 Da (Figure 82).

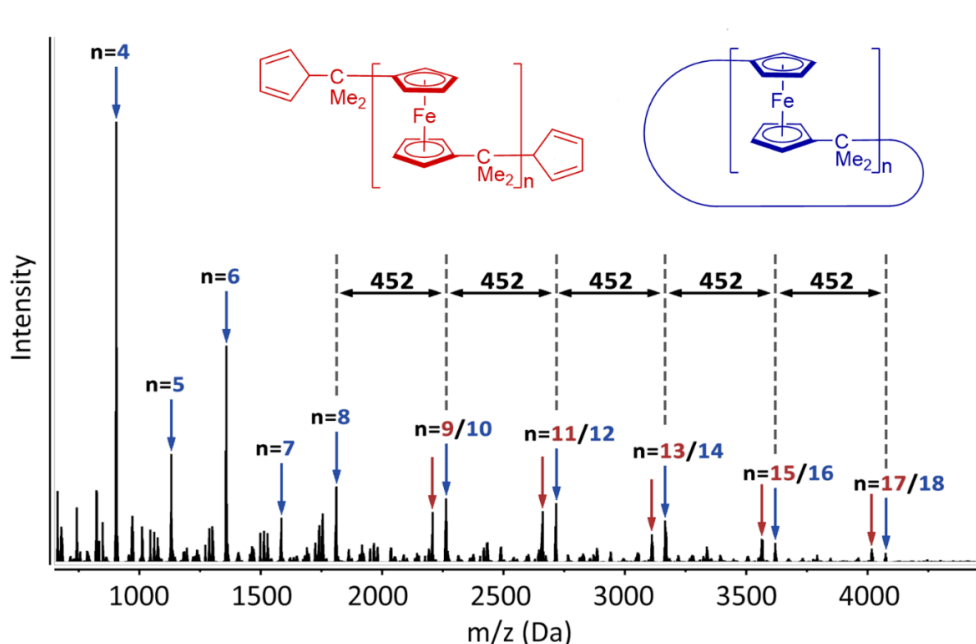
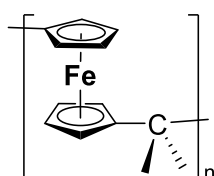


Figure 81: MALDI-ToF mass spectrum of PFM 129 of batch No. 3 Table 12 ( $\text{Me}_2\text{C}[1]\text{Cp}_2\text{Mg} + \text{FeCl}_2$  reaction) (repeat unit: 226 Da).



226 Da

Figure 82: Representation of the repeat unit in MALDI-ToF mass spectroscopy.

### 3. Results & Discussion

The MALDI-ToF investigations clearly demonstrated that not only linear PFM could be obtained but also cyclic compounds. The extraction of the material with hexane led to the isolation of a cyclic hexamer **147**, which could be crystalized and determined by X-ray diffraction analysis (Figure 83).

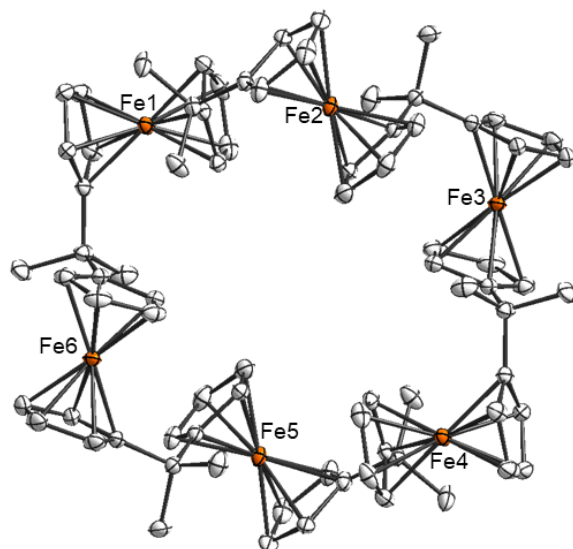


**Figure 83:** Cyclic hexamer of PFM **147** in the crystal (thermal ellipsoids for 50% probability level, H-atoms were omitted for clarity).

The Fe-Cp<sub>centroid</sub> bond lengths of 165.5 pm, the Fe-C<sub>Cp</sub> bond lengths of 204.5-207.2 pm as well as the Cp<sub>centroid</sub>-Fe-Cp<sub>centroid</sub> angle of 178.1° in the ferrocene fragments of the cyclic hexamer structure are similar to unsubstituted ferrocene.<sup>376-378</sup> A similar macro cyclic hexamer has been published before by *Albrecht* and *Long* et al. in 2016. The difference between compound **147** and the macro cyclic hexamer is that the ferrocene fragments in the macro cyclic hexamer are directly linked together, but both hexamers shared similar bonding properties. The Me<sub>2</sub>Si-ferrocenophane also builds such cyclic oligomers with even number of the ferrocene units as well as odd numbers by a polymerization reaction (Figure 84).<sup>379,380</sup>

### 3. Results & Discussion

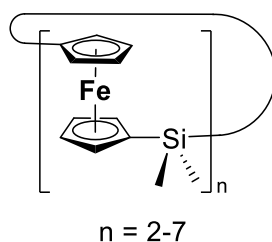


Figure 84: Representation of the oligomeric structures of  $\text{Me}_2\text{Si}$ -ferrocene.

Furthermore, the thermal and ceramic properties enable the metal-containing polymers to be utilized as preceramic materials.<sup>381–383</sup> Therefore, PFM **146** was investigated by thermogravimetric analysis (TGA) (Figure 85) and differential scanning calorimetry (DSC) (Figure 85) to observe these enormously important properties. The DSC thermogram of PFM **146** displayed a glass transition temperature ( $T_g$ ) of 60.5 °C which is twice the size of  $T_g$  of analogous reported polyferrocenylsilanes PFS.<sup>72</sup> The TGA diagram demonstrated two conditional thermal behaviors up to 300°C so that under synthetic air (10%  $\text{O}_2$  and 90%  $\text{N}_2$ ) a mass increase started to be observed at 195°C with a maximum of 250°C and a total increase of the PFM mass of 3 wt%, while in absence of oxygen nothing occurred.

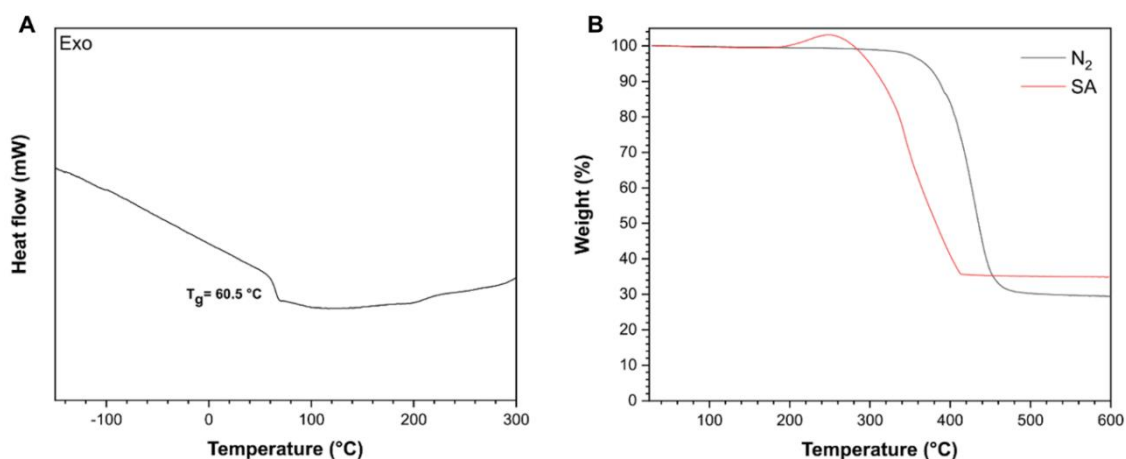


Figure 85: A) DSC thermogram of PFM; B) TGA curves of PFM **146** in an atmosphere of nitrogen ( $\text{N}_2$ , black curve) and synthetic air (SA, red curve) using a heating rate of  $20 \text{ K}\cdot\text{min}^{-1}$ , starting from 303 K to 873 K.

### 3. Results & Discussion

In addition, PFM **146** began to degrade at approximate 285°C under synthetic air and at 340°C under nitrogen atmosphere. The decomposition of PFM revealed a constant value of weight at 410°C under synthetic air and at 480°C under nitrogen. Moreover, the residue, that is obtained at the end of the combustion reaction under both conditions, of approximately 29 wt% under nitrogen and 35 wt% under synthetic air has relatively high ceramic properties in comparison to other linear polyferrocenyls.<sup>382–385</sup> The obtained residue is black in absence of oxygen while under synthetic air it changed from orange to a red brownish powder. The resulting residue under both conditions exhibits a magnetic response, which can be demonstrated by following the obtained powder with a magnet. For more information about the chemical composition of both resulting residues, an X-ray diffraction (XRD) analysis was performed (Figure 86).

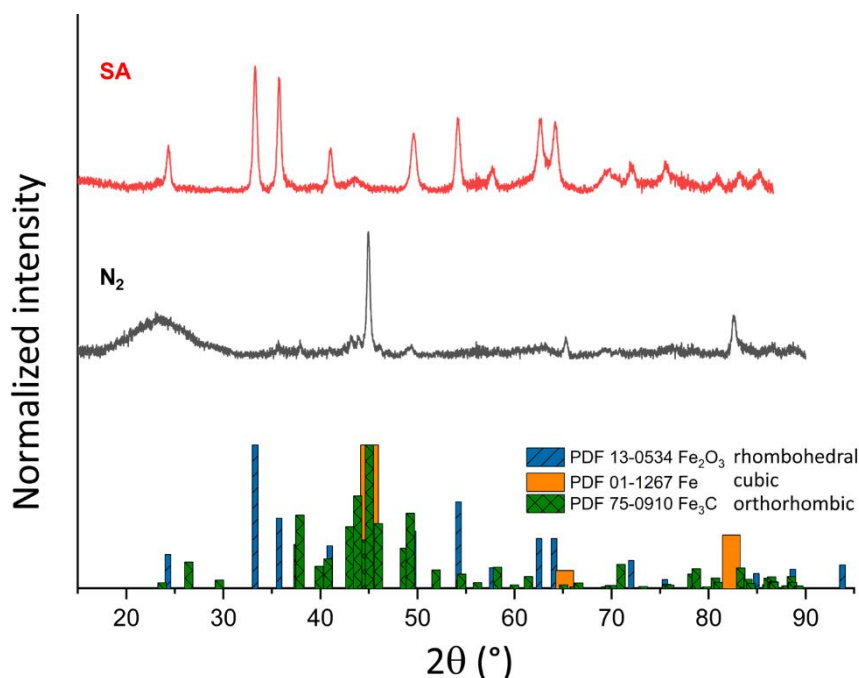
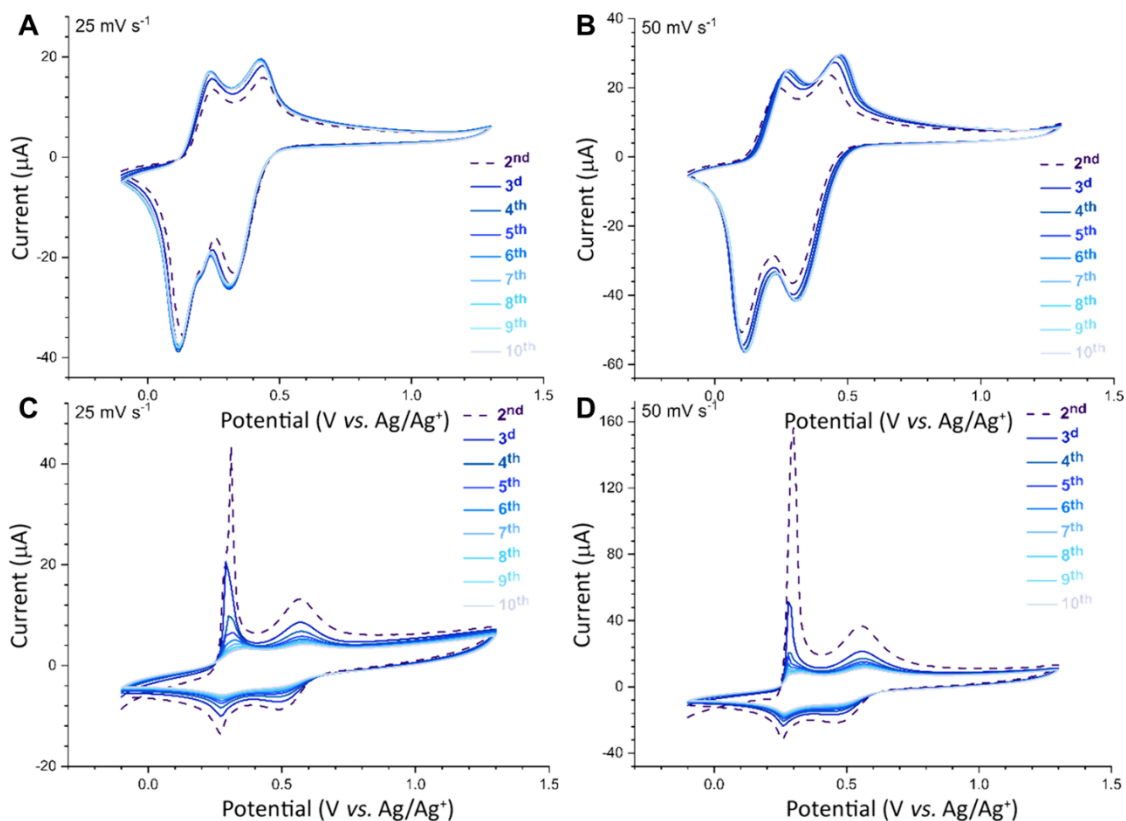


Figure 86: X-ray diffraction pattern of the residues after thermogravimetric analysis and corresponding reference data.

The XRD spectrum demonstrates that the PFM **146** transforms into  $\alpha$ -Fe<sub>2</sub>O<sub>3</sub> (hematite) under synthetic air indicating a trigonal crystal geometry with a  $R\bar{3}c$  space group and cell parameters of  $a = 503 \text{ \AA}$  and  $c = 13.74 \text{ \AA}$ , while the PFM **146** under nitrogen atmosphere resulted in a combination of iron (sharp reflections at  $2\theta$  of 45°, 65°, and 82°) and iron carbide. Considering the iron atoms in PFM structure **146** as metal centers with redox properties including the switching capabilities, this material is extremely interesting in electrochemistry. PFM was investigated by cyclic voltammetry (CV) utilizing 0.1 M solution of tetrabutylammonium hexafluorophosphate as the electrolyte in acetonitrile or tetrahydrofuran in the

### 3. Results & Discussion

potential range of 0.1 V to +1.3 V vs. Ag/Ag<sup>+</sup> were applied for scan rates of 25-50 mV·s<sup>-1</sup> (Figure 87).



**Figure 87: Cyclic voltammogram of PFM 129 in a potential range of -0.1 V to +1.3 V vs. Ag/Ag<sup>+</sup> utilizing tetrabutylammonium hexafluorophosphate in tetrahydrofuran (A, B) and in acetonitrile (C, D). The scan rate is given within the cyclic voltammogram.**

As reported for many main-chain ferrocenes containing polymers as well as cyclic ferrocene containing molecules,<sup>381–386</sup> the cyclic voltammogram demonstrated two quasi reversible oxidation and reduction processes. An explanation for both oxidation processes is based on the configuration of the ferrocenyl fragments and the spacing between them so that an interaction between each other could occur. The oxidation of an iron center has an influence on the neighboring center in PFM so that it requires higher potential to oxidize. Therefore, two oxidation processes were detected in the cyclic voltammogram. The decrease in the intensity of the redox reaction in acetonitrile is an evidence for polymer degradation. Confirming these results, the cyclic voltammetry data in TBAP/THF demonstrated higher reversible redox reaction, which is more uniform under slower scan rate, within ten cycles indicating two oxidation processes at 0.23 V and 0.43 V and two reduction processes at 0.31 V and 0.11 V. Since the separation of the alternating redox peaks demonstrates the electronic interaction



### 3. Results & Discussion

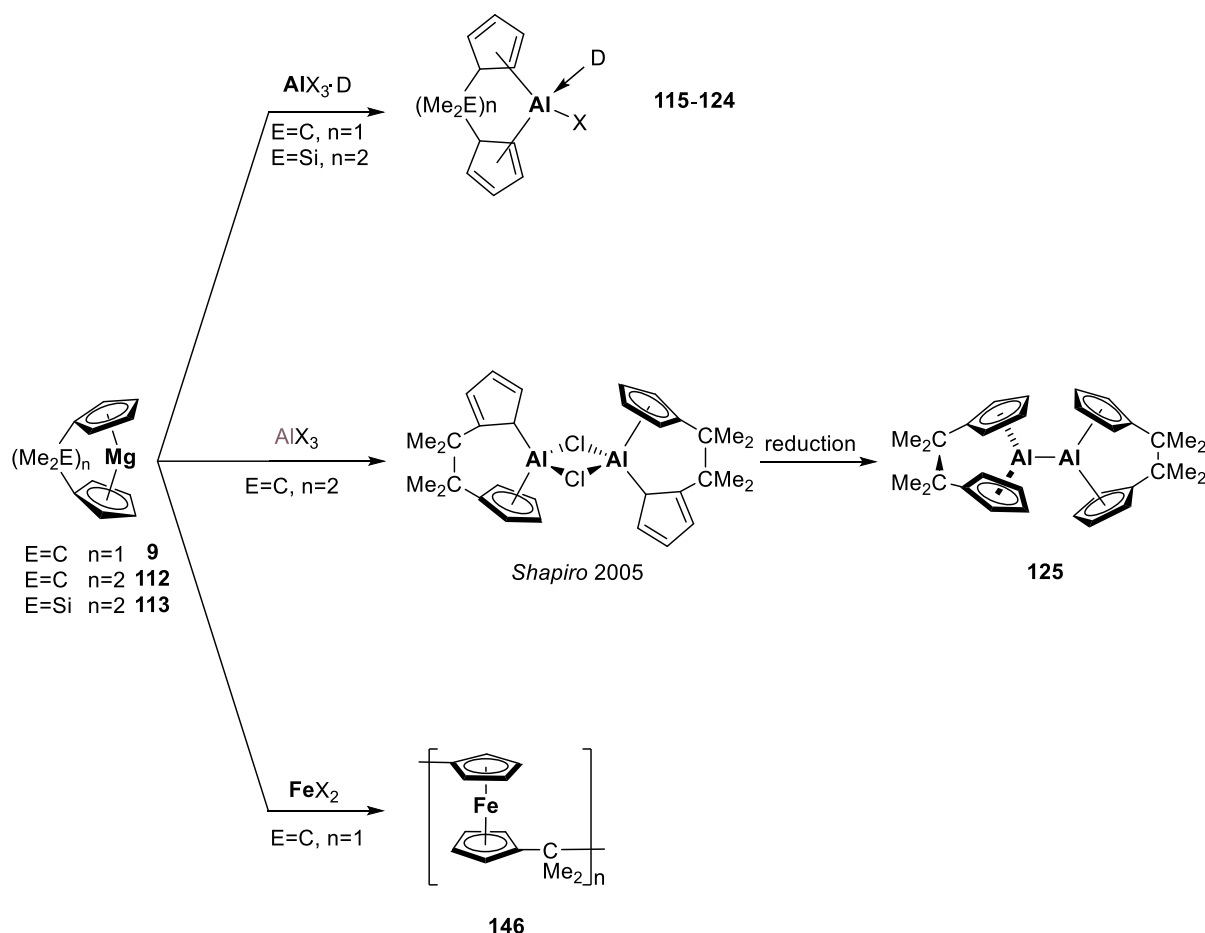
between the iron centers in ferrocene containing polymers, PFM displayed a relatively high interaction between the iron centers with a peak separation of  $\Delta E_{1,2} = 200$  mV, which is in accordance with the peak separation of 200 mV for polyferrocenyldimethylsilane.<sup>387</sup>

In summary, a new synthesis of polyferrocenylmethylene has been presented starting from carba[1]magnesocenophane and iron(II)chloride or iron(II)bromide compared with dilithium 2,2-bis(cyclopentadienide)propane as transmetalation reagent.<sup>372</sup> The yielded materials have been completely characterized via nuclear magnetic resonance NMR, thermogravimetric analysis (TGA), multiangle light scattering (MALS), matrix-assisted laser desorption/ionization time of flight (MALDI-ToF) mass spectrometry, size exclusion chromatography (SEC), differential scanning calorimetry (DSC), and cyclic voltammetry (CV). In addition, it was shown that the polymer synthesis starting from C[1]magnesocenophane led to the higher molar masses of  $M_n = 4000-8000$  g·mol<sup>-1</sup> while the polymerization reaction starting from dilithium 2,2-bis(cyclopentadienide)propane led to molar masses around 2300 g·mol<sup>-1</sup>.

## 4. Summary

In chapter 3.1., three different magnesocenophane compounds **9**, **112** and **113** were presented. Magnesocenophanes supply as powerful cyclopentadienyl transfer reagents in transmetalation reactions (Scheme 79) as well as a catalyst for the dehydrocoupling of amin boranes (Scheme 62).

In the chapter 3.2., the findings on the synthesis and characterization of different donor stabilized aluminocenophane derivatives **115-124** with different Al-Cp-bonding motifs as well as different *ansa*-ligands such as sila[2] and carba[1] are presented. In all cases, the synthesis started from the corresponding magnesocenophanes by the treatment with an aluminum(III)halide precursor in toluene (Scheme 79).<sup>335,339,347</sup>



**Scheme 79:** Representation of the new synthesized compounds starting from different magnesocenophanes.

## 4. Summary

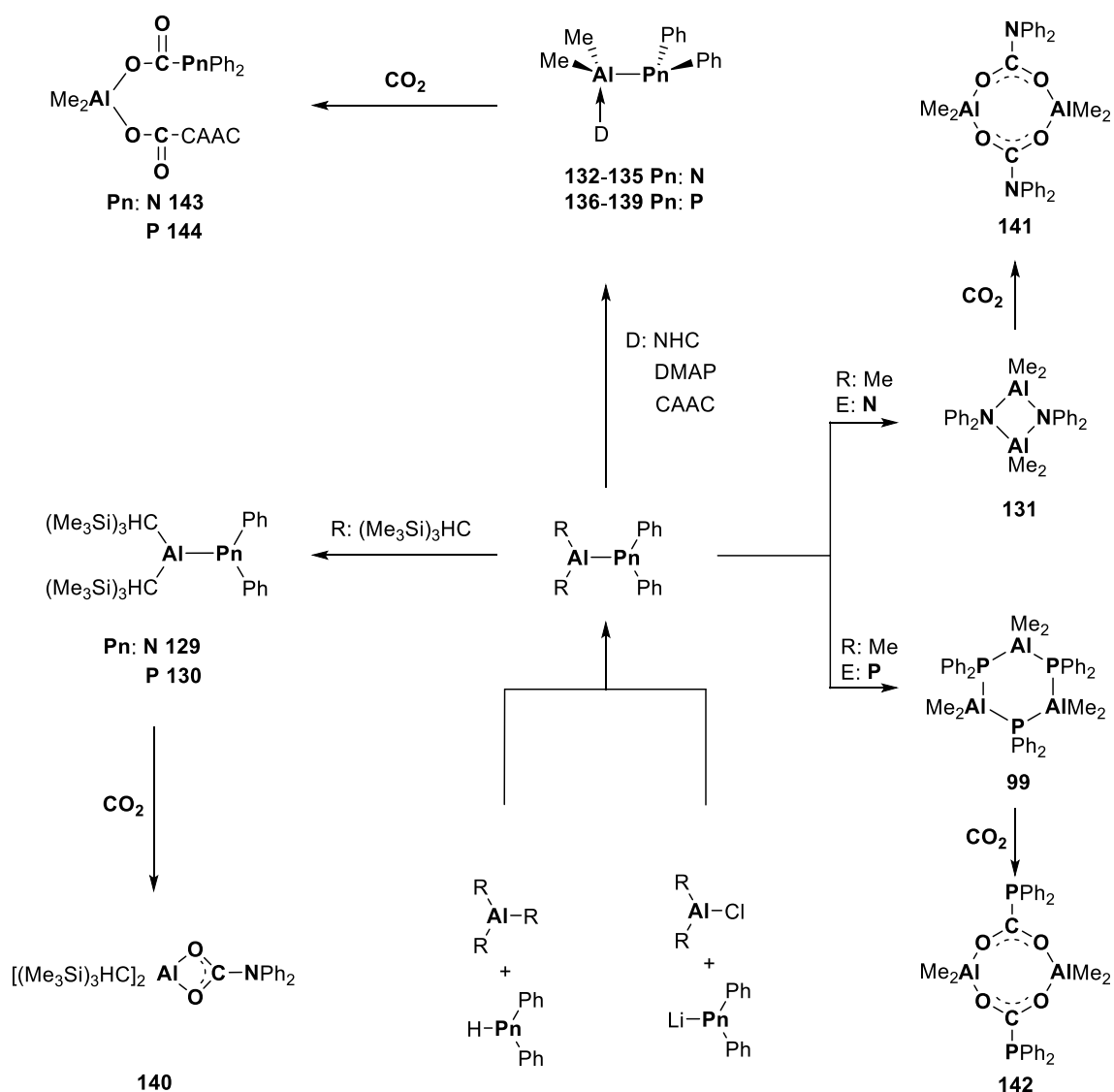
The new aluminum complexes have been characterized in the solid state and in solution demonstrating an indication to a possible static structures of donor stabilized carba[1]aluminocenophane derivatives **119-124** with different NHCs as coordinated donors. On the other hand, donor stabilized sila[2]aluminocenophane derivatives **115-118** undergo a sigma tropic rearrangement in solution. In addition, quantum chemical studies were carried out on these molecules investigating the bond strength of the donors to the aluminum centers.

Furthermore, in chapter 3.3., the first bis(aluminocenophane) **125** has been presented featuring two  $\eta^5$ -bonded cyclopentadienyl rings and the shortest Al-Al single bond of all acyclic dialanes by the reduction of compound **53** with 1,3- $\beta$ -diketimate magnesium(I).<sup>347</sup> Compound **125** contains two aluminocenophane fragments with the aluminum atoms in oxidation state +II. According to the NBO-analysis of Al-Al bond in **125**, the high s character of the Al-Al bond, which is stemming from the ionic nature of **125** with an  $Al_2^{4+}$  fragment, is the main reason for the shortness of the Al-Al bond. Moreover, it could be demonstrated that compound **125** reacts with two equivalents of *tert*-butyl isonitrile ( $tBuNC$ ) to obtain a heterocyclic compound **128** throughout an oxidative insertion reaction with a reductive C-C coupling and an Al-Al bond cleavage.

In chapter 3.5., a new synthesis route for the ferrocene-based polymer polyferrocenylmethylene (PFM) **146** has been presented circumventing the problematic carba[1]ferrocenophane precursor (Scheme 79).<sup>363</sup> The presented synthesis route starts from a carba[1]magnesocenophane **9** and iron(II)chloride or iron(II)bromide. The yielded materials exhibit molar masses of  $M_n = 4000-8000 \text{ g}\cdot\text{mol}^{-1}$  featuring poly dispersities,  $\bar{D}$ , of 136-2.09. Furthermore, a cyclic hexamer has been isolated and its crystal structure could be obtained.

Chapter 3.4. presents the results of the synthesis of different monomeric, dimeric and trimeric aminoalanes as well as phosphanylalanes (Scheme 80). The monomeric structures of aminoalanes and phosphanylalanes have been achieved through elevated sterically demanding substituents and utilizing  $\sigma$ -donor ligands. In the monomeric structures, DFT calculations illuminated that the Al-N bond has more double bond character than the Al-P bond. Besides, the reactivity of the monomeric, dimeric, trimeric and monomeric donor-stabilized amino- and phosphanylalanes towards carbon dioxide has been studied. The finding of these studies showed that monomeric donor-stabilized aminoalane and phosphanylalane fixed two  $CO_2$ -molecules, while dimeric and trimeric as well as monomeric structure of aminoalane fixed only one  $CO_2$ -molecule per Al-N/P unit.

## 4. Summary



**Scheme 80:** Representation of the pnictogenylalane compounds and their reactivity towards  $\text{CO}_2$ .

The  $\text{CO}_2$ -insertion occurs within the Al-N bond and Al-D bond. The crystal structures of the  $\text{CO}_2$ -insertion products **140-144** demonstrated that the elevated steric demanding substituents bound to aluminum atom prevented the dimerization of the product. The insertion mechanism has been illustrated by DFT calculations so that relative energies of transition states and intermediates could be calculated.

## 5. Experimental Details

### 5.1. General Information

All manipulations were carried out under an argon inert gas atmosphere (argon 5.0), using either Schlenk line techniques or a glovebox. Aluminum trichloride, aluminum tribromide lithium aluminum hydride solution (1.0 M in diethyl ether), and *n*-butyl-*sec*-butylmagnesium solution (0.7 M in hexane) were purchased from Sigma Aldrich and used as received. 1,2-dichlorotetramethyldisilane was purchased from ABCR and used as received. Dicyclopentadiene was purchased from ABCR, and cracked and distilled prior to use. All other starting materials HAlX<sub>2</sub>·2thf,<sup>388,389</sup> lithium diphenylphosphide (obtained as a yellow highly air-sensitive solid from the reaction of *n*-butyllithium and diphenylphosphane),<sup>390,391</sup> NHCs and ImS,<sup>392</sup> dilithium 2,2-bis(cyclopentadienide)propane,<sup>336</sup> lithium diphenylamide,<sup>393</sup> CAAC,<sup>362,394–397</sup> Me<sub>2</sub>C-magnesocenophane **9**<sup>46,47,334</sup> and [Me<sub>2</sub>AIPPh<sub>2</sub>]<sub>3</sub> (**99**)<sup>276,301</sup> were synthesized following literature established procedures.

NMR-spectra were recorded on Bruker Avance III 300 and Bruker Avance III 400 spectrometers. The <sup>1</sup>H and <sup>13</sup>C NMR spectra were referenced using the solvent signals ( $\delta^1\text{H}(\text{C}_6\text{HD}_5) = 7.16 \text{ ppm}$ ;  $\delta^{13}\text{C}(\text{C}_6\text{D}_6) = 128.06 \text{ ppm}$ ) <sup>27</sup>Al, <sup>29</sup>Si and <sup>31</sup>P NMR spectra were referenced using external standards ( $\delta^{27}\text{Al}(\text{AlCl}_3 \text{ in } \text{D}_2\text{O}) = 0 \text{ ppm}$ ) ( $\delta^{29}\text{Si}(\text{SiMe}_4) = 0$ ) ( $\delta^{31}\text{P}(\text{H}_3\text{PO}_4 \text{ in } \text{D}_2\text{O}) = 0.0 \text{ ppm}$ ). Elemental analysis was performed on an Elementar vario micro cube. Single crystal X-ray diffraction analysis were carried out at low temperatures on Bruker AXS X8 Apex CCD and Bruker AXS D8 Venture diffractometers operating with graphite monochromated Mo K $\alpha$  radiation. Structure solution and refinement was performed using SHELX.<sup>398</sup> The solvent (hexane, toluene, tetrahydrofuran (thf), 1,2-dimethoxyethane (dme), dichloromethane, diethyl ether) were dried via a MB-SPS-5 system by MBraun. Fourier transformed infrared spectra (FT-IR) were recorded in total reflectance mode with a Bruker Vertex 70 spectrometer from 4500–400 cm<sup>-1</sup> with a 4 nm increment and 16 scans averaged.

Cyclic voltammetry (CV) measurements were carried out on a EmStat3+ potentiostat (Belltec) using PSTrace 5.5 as software to collect the data. All measurements were acquired using an Ag/Ag<sup>+</sup> reference electrode, a platinum counter electrode, and a glassy carbon working electrode with an inner diameter of 5 mm. The scan rate was varied at 10-50 mV s<sup>-1</sup> in a range of -0.1 V to +1.3 V for oxidation and reduction experiments and calibrated versus ferrocene. For CV measurements, a five necked round bottom flask was used with a solution of tetra *n*-butyl ammonium hexafluorophosphate ((*n*-Bu<sub>4</sub>N)PF<sub>6</sub>) (0.1 M) in degassed tetrahydrofuran or acetonitrile as an electrolyte.

## 5. Experimental Details

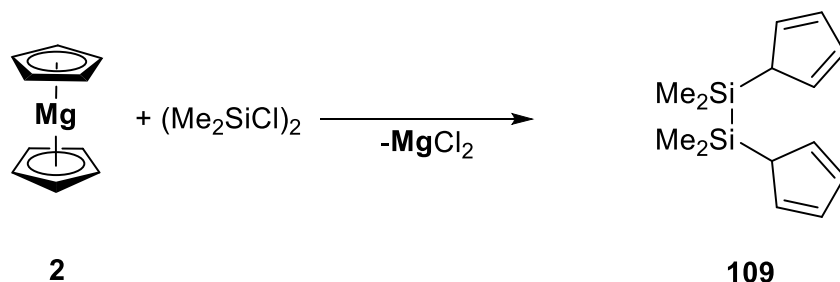
For evaluating the thermal properties, thermogravimetric analysis (TGA) was applied by using a Netzsch TGA 209 F1 Libra with a heating rate of  $20 \text{ K min}^{-1}$  in a range of 30-800 °C in nitrogen or synthetic air atmosphere. Differential scanning calorimetry (DSC) measurements were carried out with a Netzsch Polyma DSC 214 from -160 °C to +300 °C.

Standard size exclusion chromatography (SEC) was performed with a system composed of a 1260 Infinity II (Agilent Technologies), a 1260 VW detector (G7114A) at 260 nm (Agilent Technologies), and a 1260 RI detector (G7162A) at 35 °C (Agilent Technologies), thf as the mobile phase (flow rate  $1 \text{ mL min}^{-1}$ ) on a SDV column set from polymer standard service (PSS) (SDV  $10^3\text{A}$ , SDV  $10^5\text{A}$ , SDV  $10^6\text{A}$ ). Calibration was carried out using PS standards from PSS. X-ray diffraction of the final residues after the thermogravimetric analysis was acquired with a D8 Discover diffractometer (Bruker AXS) using a copper source (Cu- $K_{\alpha}$ , 40 kV, 40 mA), a Göbel mirror, and a 0.5 mm point focus. Data were collected with a two-dimensional VANTEC 500 detector covering an angle range of  $20^{\circ} 2\theta$ . Four frames were recorded at  $2\theta$  of  $20^{\circ}$ ,  $40^{\circ}$ ,  $60^{\circ}$ , and  $80^{\circ}$  using a measurement time of 2500 s for each frame.

## 5.2. Synthesis and Reactivity Studies

5.2.1. Synthesis of **109**:

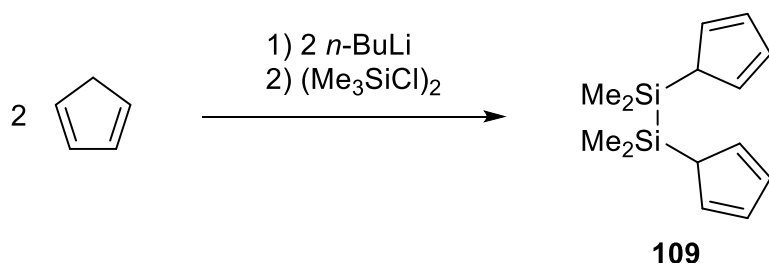
Method A:



Magnesiumocene (10 g, 64.7 mmol) was suspended in 350 mL of hexane. 1,2-dichloro-1,1,2,2-tetramethyldisilane (purity: 90%, 13.5 g, 64.7 mmol) was slowly added. The mixture was stirred at room temperature for 2 h. After filtration, all volatiles were removed under reduced pressure and the residue was distilled in vacuum (0.03 mbar, 67-95°C) to give the product as a colorless to light yellow oil.

Yield: 10.6 g of **109**, 66%.

Method B:



Freshly cracked and distilled cyclopentadiene (19.4 g, 293 mmol) was added slowly to a solution of *n*-butyllithium (2.5 M solution in hexane, 279.5 mmol, 111.8 ml) in 350 ml hexane at -70°C. The mixture warmed to room temperature and stirred for 2 h. Subsequently, 1,2-dichloro-1,1,2,2-tetramethyldisilane (25 g, 119.8 mmol) was added slowly at room temperature and the resulting mixture was stirred overnight. After filtration, all volatiles were removed under vacuum and the residue was distilled in vacuum (0.03 mbar, 67-95°C) to give the product as a colorless to light yellow oil. Yield: 22.0 g, 67%. Purity of the ligand was checked and confirmed by GC-MS and  $^{29}\text{Si}$  NMR spectroscopy. The compound is obtained as a mixture of six isomers, as indicated by nine signals in the  $^{29}\text{Si}$  NMR spectrum (3 symmetrically and 3

## 5. Experimental Details

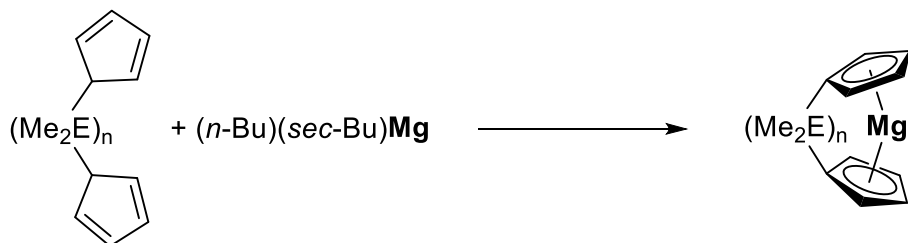
unsymmetrically substituted isomers). It is only marginally stable at room temperature and should therefore be stored at low temperature or used directly for follow-up synthesis.

$^{29}\text{Si}\{^1\text{H}\}$  NMR (60 MHz,  $\text{C}_6\text{D}_6$ , 298 K):  $\delta$ [ppm]= -15.1, -16.1, -16.3, -27.2, -27.5, -28.1, -28.3, -28.5, -28.7.



## 5. Experimental Details

### 5.2.2. Synthesis of 113:



$\text{E}=\text{Si}$   $n=2$  **109**

$\text{E}=\text{Si}$   $n=2$  **113**

A solution of *ansa*- $\text{Me}_4\text{Si}_2(\text{C}_5\text{H}_5)_2$  (16.3 g, 66.0 mmol) in 500 ml hexane was treated with a solution of *n*-butyl-*sec*-butylmagnesium (0.7 M in hexane, 66.0 mmol, 94.2 ml). After stirring for 90 min at room temperature, the mixture was stored at  $-25^\circ\text{C}$  overnight. A colorless precipitate formed and was isolated, washed with small portions of cold hexane and dried in vacuum.

Yield: 9.5 g of **113**, 54%.

$^1\text{H}$  NMR (300 MHz,  $\text{C}_6\text{D}_6$ , 298 K):  $\delta$  [ppm]= 6.10 (s, 8H), 0.51 (s, 12H).

$^{13}\text{C}\{^1\text{H}\}$  NMR (75 MHz,  $\text{C}_6\text{D}_6$ , 298 K):  $\delta$  [ppm]= 117.8, 114.6, 109.6, -3.6.

$^{29}\text{Si}\{^1\text{H}\}$  NMR (60 MHz,  $\text{C}_6\text{D}_6$ , 298 K):  $\delta$  [ppm]= -24.2.

Crystals of sila[2]magnesocenophane·DME, suitable for single crystal X-ray diffraction, were obtained by addition of ~3 eq of dimethoxyethane to a solution of sila[2]magnesocenophane, **113**, in toluene, and subsequent storing of the solution at  $-25^\circ\text{C}$  overnight.

$^1\text{H}$  NMR (300 MHz,  $\text{C}_6\text{D}_6$ , 298 K):  $\delta$  [ppm]= 6.38 – 6.34 (m, 4H), 6.30 – 6.26 (m, 4H), 2.61 (s, 6H), 2.32 (s, 4H), 0.70 (s, 12H).

$^{13}\text{C}\{^1\text{H}\}$  NMR (75 MHz,  $\text{C}_6\text{D}_6$ , 298 K):  $\delta$  [ppm]= 111.6, 111.0, 109.6, 68.3, 58.9, -1.8.

$^{29}\text{Si}\{^1\text{H}\}$  NMR (60 MHz,  $\text{C}_6\text{D}_6$ , 298 K):  $\delta$  [ppm]= -27.2.

Elemental analysis for  $\text{C}_{18}\text{H}_{30}\text{MgO}_2\text{Si}_2$ : found: C: 56.2%, H: 7.46%; calc.: C: 60.24%, H: 8.43% (elemental analysis repeatedly and reproducibly yielded low carbon content, presumably due to the formation of silicon carbide).

## 5. Experimental Details

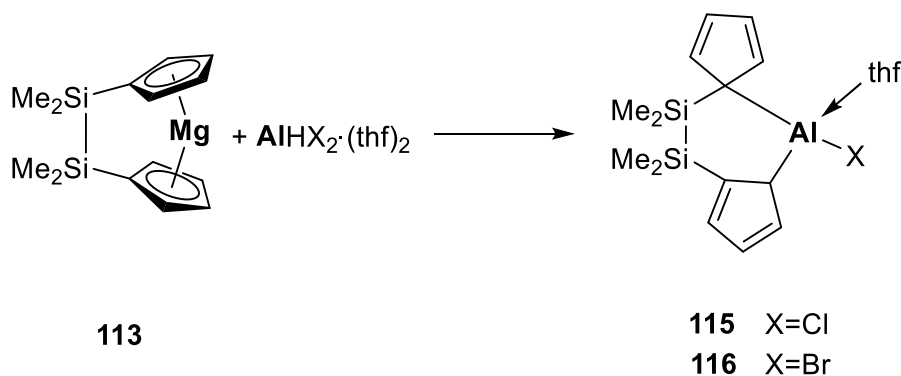
### Crystal structure data of **113-dme**

CCDC code:	1849427	
Empirical formula:	$C_{18}H_{30}Mg_1O_2Si_2$	
Formula weight:	358.91	
Temperature:	142(2) K	
Wavelength:	0.71073 Å	
Crystal system:	monoclinic	
Space group:	P21/n	
Unit cell dimensions:	$a = 11.3620(6)$ Å	$\alpha = 90^\circ$
	$b = 13.9388(7)$ Å	$\beta = 103.8625(19)^\circ$
	$c = 13.4716(6)$ Å	$\gamma = 90^\circ$
Volume:	$2071.39(18)$ Å <sup>3</sup>	
Z:	4	
Density (calculated):	1.151 Mg/m <sup>3</sup>	
Absorption coefficient:	0.208 mm <sup>-1</sup>	
F(000):	776	
Crystal size:	0.270 x 0.176 x 0.092 mm <sup>3</sup>	
Theta range for data collection:	2.111 to 27.886°	
Index ranges:	-14 ≤ h ≤ 14, -18 ≤ k ≤ 17, -17 ≤ l ≤ 11	
Reflections collected:	20320	
Independent reflections:	4945 [R(int) = 0.0370]	
Completeness to theta = 25.242°:	100.0 %	
Absorption correction:	semi-empirical from equivalents	
Max. and min. transmission:	0.7456 and 0.7264	
Refinement method:	full-matrix least-squares on F <sup>2</sup>	
Data / restraints / parameters:	4945 / 0 / 328	
Goodness-of-fit on F <sup>2</sup> :	1.008	
Final R indices [I > 2σ(I)]:	R1 = 0.0344, wR2 = 0.0776	
R indices (all data):	R1 = 0.0502, wR2 = 0.0850	
Extinction coefficient:	n/a	
Largest diff. peak and hole:	0.318 and -0.216 e.Å <sup>-3</sup>	

## 5. Experimental Details

### 5.2.3. Synthesis of **115**, **116**:

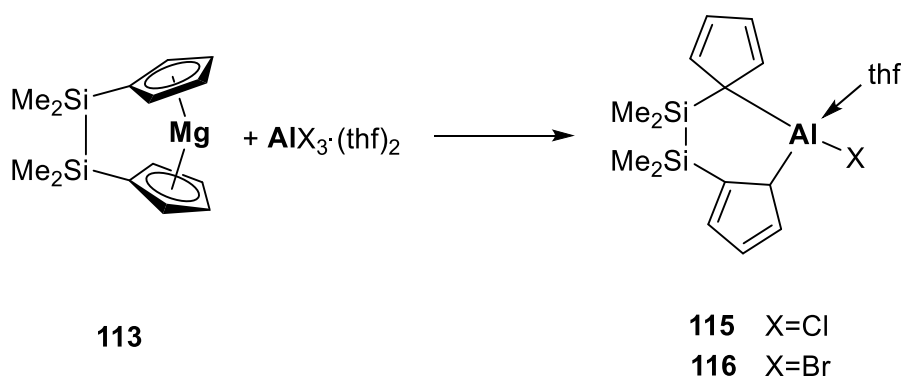
Method A:



Dihaloalane bis(tetrahydrofuran) (0.91 g, 3.72 mmol of  $\text{HAICl}_2 \cdot 2\text{thf}$ ; 1.23 g, 3.72 mmol of  $\text{HAlBr}_2 \cdot 2\text{thf}$  and sila[2]magnesocenophane, **113**, (1.0 g, 3.72 mmol) were charged into a flask. 40 mL of toluene were added and the mixture was stirred overnight at room temperature. After filtration, all volatiles were removed in vacuum and hexane was added. After filtration, the hexane solution was concentrated and stored at  $-20^\circ\text{C}$  overnight, resulting in the crystallization of complexes **115** and **116**. The products were obtained as colorless to light yellow crystalline solids.

Yield: 0.75 g of **115**, 53%; 0.27 g of **115**, 17%.

Method B:



Aluminum trihalide (50 mg, 0.37 mmol of  $\text{AlCl}_3$ ; 99 mg, 0.37 mmol of  $\text{AlBr}_3$ ) and sila[2]magnesocenophane, **113**, (100 g, 0.37 mmol) were charged into a flask. 5 mL of thf were

## 5. Experimental Details

added and the mixture was stirred at room temperature overnight. Workup was identical to that described in method A.

Compound **115**:

$^1\text{H}$  NMR (300 MHz,  $\text{C}_6\text{D}_6$ , 298 K):  $\delta$  [ppm]= 7.08 (dt,  $J = 3.3$  Hz,  $J = 1.3$  Hz, 2H), 6.98 (td,  $J = 3.4$  Hz,  $J = 0.7$  Hz, 2H), 6.83 – 6.79 (m, 2H), 5.92 (d,  $J = 2.8$  Hz, 2H), 3.26 (ddd,  $J = 6.8$  Hz,  $J = 4.4$  Hz,  $J = 2.7$  Hz, 4H), 0.93 – 0.86 (m, 4H), 0.66 (s, 6H), 0.21 (s, 6H).

$^{13}\text{C}\{^1\text{H}\}$  NMR (75 MHz,  $\text{C}_6\text{D}_6$ , 298 K):  $\delta$  [ppm]= 133.6, 128.8, 127.3, 105.8, 96.7, 74.4, 24.5, -3.0, -3.2.

$^{29}\text{Si}\{^1\text{H}\}$  NMR (60 MHz,  $\text{C}_6\text{D}_6$ , 298 K)  $\delta$  [ppm]= -23.4.

Elemental analysis for  $\text{C}_{18}\text{H}_{28}\text{AlClOSi}_2$ : found: C: 56.2%, H: 7.46%; calc.: C: 57.0%, H: 7.45%.

Crystal structure data of **115**

CCDC code:	1849424
Empirical formula:	$\text{C}_{18}\text{H}_{28}\text{AlClOSi}_2$
Formula weight:	379.01
Temperature:	152(2) K
Wavelength:	0.71073 Å
Crystal system:	triclinic
Space group:	P-1
Unit cell dimensions:	$a = 9.1113(2)$ Å $\alpha = 71.9090(10)^\circ$ $b = 10.3235(2)$ Å $\beta = 85.5720(10)^\circ$ $c = 11.3696(2)$ Å $\gamma = 84.1350(10)^\circ$
Volume:	1010.07(4) Å <sup>3</sup>
Z:	2
Density (calculated):	1.246 Mg/m <sup>3</sup>
Absorption coefficient:	0.353 mm <sup>-1</sup>
F(000):	404
Crystal size:	0.450 x 0.371 x 0.340 mm <sup>3</sup>
Theta range for data collection:	1.886 to 33.260°
Index ranges:	-14 ≤ h ≤ 14, -15 ≤ k ≤ 15, -17 ≤ l ≤ 17
Reflections collected:	28872
Independent reflections:	7554 [R(int) = 0.0202]
Completeness to theta = 25.242°:	100.0 %
Absorption correction:	semi-empirical from equivalents

## 5. Experimental Details

Max. and min. transmission:	0.7465 and 0.7228
Refinement method:	full-matrix least-squares on $F^2$
Data / restraints / parameters:	7554 / 51 / 307
Goodness-of-fit on $F^2$ :	1.042
Final R indices [ $I > 2\sigma(I)$ ]:	R1 = 0.0307, wR2 = 0.0883
R indices (all data):	R1 = 0.0364, wR2 = 0.0921
Extinction coefficient:	n/a
Largest diff. peak and hole:	0.479 and -0.537 e.Å <sup>-3</sup>

### Compound **116**:

<sup>1</sup>H NMR (400 MHz, C<sub>6</sub>D<sub>6</sub>, 298 K):  $\delta$ [ppm]= 7.18 – 7.03 (m, 2H), 7.06 – 6.91 (m, 2H), 6.81 (td,  $J$  = 3.1 Hz, 1.2 Hz, 2H), 5.93 (d,  $J$  = 2.5 Hz, 2H), 3.25 (s, 4H), 0.86 (s, 4H), 0.69 (s, 6H), 0.20 (s, 6H).

<sup>13</sup>C{<sup>1</sup>H} NMR (101 MHz, C<sub>6</sub>D<sub>6</sub>, 298 K):  $\delta$ [ppm]= 134.1, 129.1, 127.6, 106.8, 74.6, 24.5, -2.5, -3.2.

<sup>29</sup>Si{<sup>1</sup>H} NMR (79 MHz, C<sub>6</sub>D<sub>6</sub>, 298 K):  $\delta$ [ppm]= -23.3.

Elemental analysis for C<sub>18</sub>H<sub>28</sub>AlBrOSi<sub>2</sub>: found: C: 50.96%, H: 6.86%; calc.: C: 51.05%, H: 6.66%.

### Crystal structure data of **116**

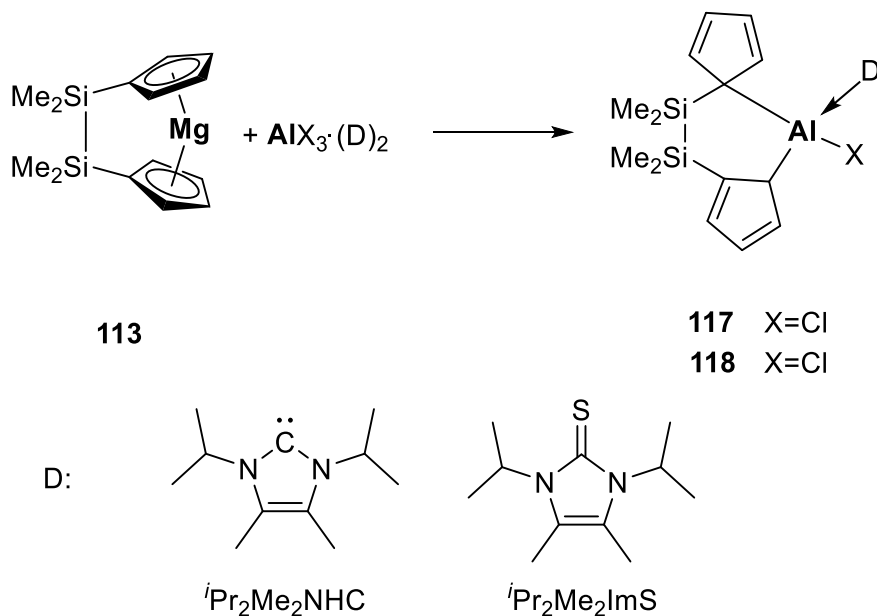
CCDC code:	1849423
Empirical formula:	C <sub>18</sub> H <sub>28</sub> AlBrOSi <sub>2</sub>
Formula weight:	423.47
Temperature:	152(2) K
Wavelength:	0.71073 Å
Crystal system:	monoclinic
Space group:	P21/c
Unit cell dimensions:	$a = 9.3142(4)$ Å $\alpha = 90^\circ$ $b = 16.0816(7)$ Å $\beta = 95.313(2)^\circ$ $c = 14.3879(6)$ Å $\gamma = 90^\circ$
Volume:	2145.86(16) Å <sup>3</sup>
Z:	4
Density (calculated):	1.311 Mg/m <sup>3</sup>
Absorption coefficient:	2.070 mm <sup>-1</sup>
F(000):	880
Crystal size:	0.241 x 0.202 x 0.054 mm <sup>3</sup>

## 5. Experimental Details

Theta range for data collection:	1.904 to 29.720°
Index ranges:	-12<=h<=8, -22<=k<=22, -19<=l<=19
Reflections collected:	22822
Independent reflections:	6007 [R(int) = 0.0504]
Completeness to theta = 25.242°:	99.6 %
Absorption correction:	semi-empirical from equivalents
Max. and min. transmission:	0.7459 and 0.6385
Refinement method:	full-matrix least-squares on F <sup>2</sup>
Data / restraints / parameters:	6007 / 81 / 245
Goodness-of-fit on F <sup>2</sup> :	1.012
Final R indices [I>2sigma(I)]:	R1 = 0.0453, wR2 = 0.0971
R indices (all data):	R1 = 0.0885, wR2 = 0.1099
Extinction coefficient:	n/a
Largest diff. peak and hole:	0.555 and -0.435 e.Å <sup>-3</sup>

## 5. Experimental Details

### 5.2.4. Synthesis of **117**, **118**:



The aluminum trichloride Lewis base complexes used in the synthesis of **117** and **118** were generated *in situ*.

Aluminum trichloride (1.0 g, 7.5 mmol) and carbene or thione (1.35 g, 7.5 mmol of  $i\text{Pr}_2\text{Me}_2\text{NHC}$ ; 1.17 g, 7.5 mmol of  $i\text{Pr}_2\text{Me}_2\text{ImS}$ ) were suspended in 10 ml of toluene and stirred for 15-20 min until all components were completely dissolved. The solution was then used directly in the synthesis of **117** and **118**.

To a suspension of sila[2]magnesocenophane, **113**, in 150 mL of toluene, a toluene solution of the corresponding aluminum trichloride·(Lewis base) complex was slowly added and the mixture was stirred at room temperature overnight. All volatiles were removed under reduced pressure and hexane was added. After filtration, the filtrate was concentrated and stored at -20°C overnight. The colorless crystalline precipitate was collected, washed with small portions of cold hexane and dried in vacuum.

Yield: 1,57 g of **117**, 43%; 0.66 g of **118**, 17%.

$\text{AlCl}_3 \cdot (i\text{Pr}_2\text{Me}_2\text{NHC})$ :

$^1\text{H}$  NMR (400 MHz,  $\text{C}_6\text{D}_6$ , 298 K):  $\delta$  [ppm]= 5.72 (s, 2H), 1.69 (s, 6H), 1.14 (d,  $J = 7.0$  Hz, 12H).

## 5. Experimental Details

$^{27}\text{Al}\{^1\text{H}\}$  NMR (104 MHz,  $\text{C}_6\text{D}_6$ , 298 K):  $\delta$  [ppm]= 106, 104 ( $^{27}\text{Al}$  NMR indicates an equilibrium in solution between  $\text{AlCl}_3 \cdot i\text{-Pr}_2\text{Me}_2\text{NHC}$  and  $[\text{AlCl}_2 \cdot (i\text{-Pr}_2\text{Me}_2\text{NHC})_2][\text{AlCl}_4]$  for this compound).

$\text{AlCl}_3 \cdot (i\text{-Pr}_2\text{Me}_2\text{ImS})$ :

$^1\text{H}$  NMR (400 MHz,  $\text{C}_6\text{D}_6$ , 298 K):  $\delta$  [ppm]= 5.38 (s, 2H), 1.62 (s, 6H), 1.15 (d,  $J = 7.1$  Hz, 12H).

$^{27}\text{Al}\{^1\text{H}\}$  NMR (104 MHz,  $\text{C}_6\text{D}_6$ , 298 K):  $\delta$  [ppm]= 110, 104 ( $^{27}\text{Al}$  NMR indicates an equilibrium in solution between  $\text{AlCl}_3 \cdot i\text{-Pr}_2\text{Me}_2\text{ImS}$  and  $[\text{AlCl}_2 \cdot (i\text{-Pr}_2\text{Me}_2\text{ImS})_2][\text{AlCl}_4]$  for this compound).

Compound **117**:

$^1\text{H}$  NMR (400 MHz,  $\text{C}_6\text{D}_6$ , 298 K):  $\delta$  [ppm]= 7.32 – 7.24 (m, 2H), 7.02 – 6.90 (m, 2H), 6.83 (d,  $J = 1.2$  Hz, 2H), 6.26 (s, 2H), 4.87 (sept,  $J = 7.0$  Hz, 2H), 1.41 (s, 6H), 1.09 (d,  $J = 7.0$  Hz, 12H), 0.87 (s, 6H), 0.33 (s, 6H).

$^{13}\text{C}$  NMR (101 MHz,  $\text{C}_6\text{D}_6$ , 298 K):  $\delta$  [ppm]= 164.0, 134.4, 132.2, 128.6, 126.9, 126.4, 52.0, 21.9, 10.0, -2.0.

$^{27}\text{Al}$  NMR (104 MHz,  $\text{C}_6\text{D}_6$ , 298 K):  $\delta$  [ppm]= 124.

$^{29}\text{Si}$  NMR (79 MHz,  $\text{C}_6\text{D}_6$ , 298 K):  $\delta$  [ppm]= -21.8.

Elemental analysis for  $\text{C}_{25}\text{H}_{40}\text{AlClN}_2\text{Si}_2$ : found: C: 58.06%, H: 8.73%; calc.: C: 61.63%, H: 8.28% (elemental analysis repeatedly and reproducibly yielded low carbon content, presumably due to the formation of silicon carbide).

Crystal structure data of **117**

CCDC code:	1849425	
Empirical formula:	$\text{C}_{25}\text{H}_{40}\text{AlClN}_2\text{Si}_2$	
Formula weight:	487.20	
Temperature:	102(2) K	
Wavelength:	0.71073 Å	
Crystal system:	monoclinic	
Space group:	P21/c	
Unit cell dimensions:	$a = 9.7469(17)$ Å	$\alpha = 90^\circ$
	$b = 20.074(4)$ Å	$\beta = 97.939(6)^\circ$
	$c = 14.418(3)$ Å	$\gamma = 90^\circ$
Volume:	$2794.0(9)$ Å <sup>3</sup>	
Z:	4	
Density (calculated):	1.158 Mg/m <sup>3</sup>	
Absorption coefficient:	0.269 mm <sup>-1</sup>	



## 5. Experimental Details

F(000):	1048
Crystal size:	0.587 x 0.086 x 0.039 mm <sup>3</sup>
Theta range for data collection:	1.750 to 26.777°
Index ranges:	-12<=h<=12, -25<=k<=24, -18<=l<=18
Reflections collected:	23827
Independent reflections:	5967 [R(int) = 0.0821]
Completeness to theta = 25.242°:	100.0 %
Absorption correction:	semi-empirical from equivalents
Max. and min. transmission:	0.7454 and 0.6532
Refinement method:	full-matrix least-squares on F <sup>2</sup>
Data / restraints / parameters:	5967 / 0 / 293
Goodness-of-fit on F <sup>2</sup> :	1.032
Final R indices [I>2sigma(I)]:	R1 = 0.0585, wR2 = 0.1261
R indices (all data):	R1 = 0.1077, wR2 = 0.1451
Extinction coefficient:	n/a
Largest diff. peak and hole:	0.559 and -0.349 e.Å <sup>-3</sup>

### Compound **118**:

<sup>1</sup>H NMR (400 MHz, C<sub>6</sub>D<sub>6</sub>, 298 K):  $\delta$ [ppm]= 7.18 – 7.12 (m, 2H), 7.01 (dt,  $J$  = 3.1 Hz, 1.5 Hz, 2H), 6.72 (dt,  $J$  = 3.1 Hz, 1.4 Hz, 2H), 5.46 (sept.,  $J$  = 7.2 Hz, 2H), 1.34 (s, 6H), 1.07 (d,  $J$  = 7.1 Hz, 12H), 0.72 (s, 6H), 0.40 (s, 6H).

<sup>13</sup>C NMR (101 MHz, C<sub>6</sub>D<sub>6</sub>, 298 K):  $\delta$ [ppm]= 146.27, 129.27, 128.60, 127.35, 125.39, 118.60, 51.18, 20.62, 9.65, -2.29, -2.34.

<sup>29</sup>Si NMR (79 MHz, C<sub>6</sub>D<sub>6</sub>, 298 K):  $\delta$ [ppm]= -22.17.

No signal was detected in the <sup>27</sup>Al NMR spectrum in a range of -200 ppm to +200 ppm.

Elemental analysis for C<sub>25</sub>H<sub>40</sub>AlClN<sub>2</sub>SSi<sub>2</sub>: found: C: 56.19%, H: 8.50%; calc.: C: 57.83%, H: 7.76% (elemental analysis repeatedly and reproducibly yielded low carbon content, presumably due to the formation of silicon carbide).

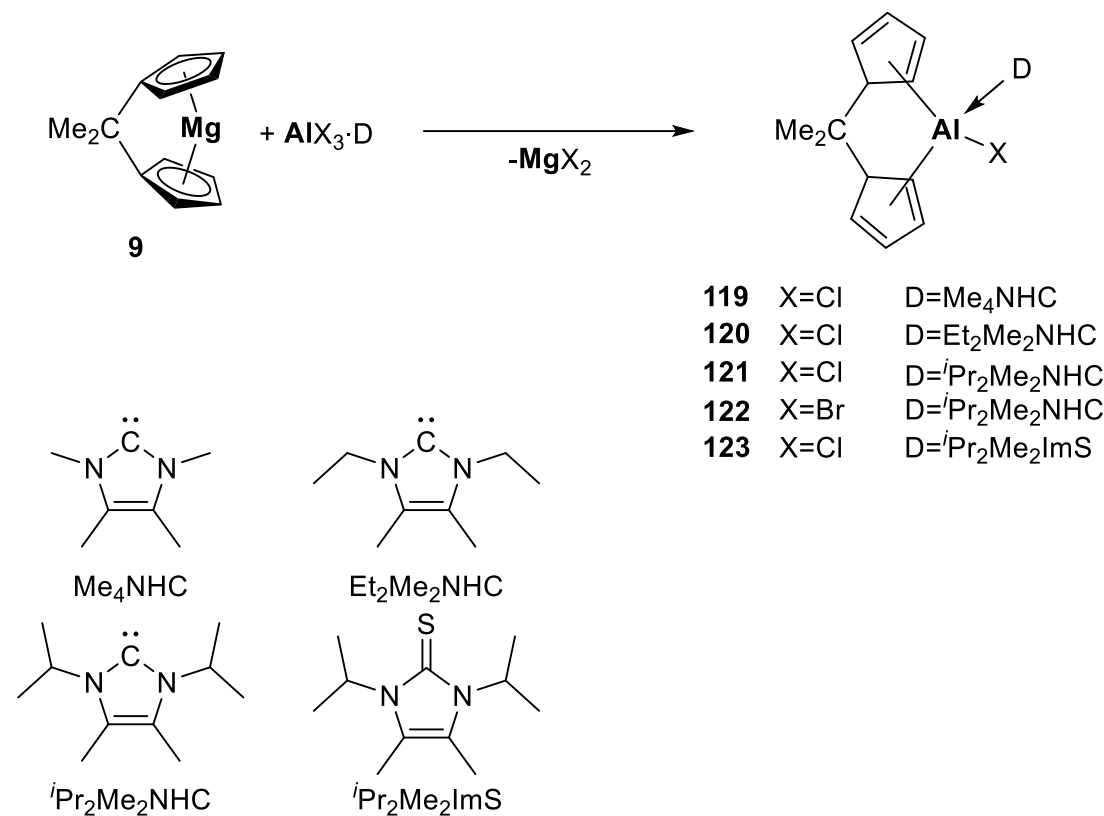
### Crystal structure data of **118**

CCDC code:	1849426
Empirical formula:	C <sub>25</sub> H <sub>40</sub> Al <sub>1</sub> Cl <sub>1</sub> N <sub>2</sub> S <sub>1</sub> Si <sub>2</sub>
Formula weight:	519.26
Temperature:	102(2) K

## 5. Experimental Details

Wavelength:	0.71073 Å
Crystal system:	orthorhombic
Space group:	Pnma
Unit cell dimensions:	a = 11.6832(5) Å $\alpha = 90^\circ$ b = 17.3962(10) Å $\beta = 90^\circ$ c = 13.8225(8) Å $\gamma = 90^\circ$
Volume:	2809.3(3) Å <sup>3</sup>
Z:	4
Density (calculated):	1.228 Mg/m <sup>3</sup>
Absorption coefficient:	0.343 mm <sup>-1</sup>
F(000):	1112
Crystal size:	-
Theta range for data collection:	1.882 to 31.422°
Index ranges:	-14 ≤ h ≤ 17, -21 ≤ k ≤ 25, -20 ≤ l ≤ 20
Reflections collected:	20489
Independent reflections:	4770 [R(int) = 0.0378]
Completeness to theta = 25.242°:	99.9 %
Absorption correction:	semi-empirical from equivalents
Max. and min. transmission:	0.7462 and 0.6940
Refinement method:	full-matrix least-squares on F <sup>2</sup>
Data / restraints / parameters:	4770 / 0 / 231
Goodness-of-fit on F <sup>2</sup> :	1.028
Final R indices [I > 2σ(I)]:	R1 = 0.0333, wR2 = 0.0770
R indices (all data):	R1 = 0.0477, wR2 = 0.0840
Extinction coefficient:	n/a
Largest diff. peak and hole:	0.436 and -0.255 e.Å <sup>-3</sup>

## 5.2.5. Syntheses of 119-123:



General method:

The aluminum trichloride-NHC complexes used in the synthesis of **119-123** were generated *in situ*.

The corresponding aluminum halide (**119**: 0.69 g, 5.13 mmol of AlCl<sub>3</sub>; **120**: 0.69 g, 5.13 mmol of AlCl<sub>3</sub>; **121**: 2.06 g, 15.4 mmol of AlCl<sub>3</sub>; **122**: 3.0 g, 11.2 mmol of AlBr<sub>3</sub>; **123**: 2.06 g, 15.4 mmol of AlCl<sub>3</sub>) and the corresponding NHC or thione (**119**: 0.64 g, 5.13 mmol of Me<sub>4</sub>NHC; **120**: 0.78 g, 5.13 mmol of Et<sub>2</sub>Me<sub>2</sub>NHC; **121**: 2.78 g, 15.4 mmol of *i*Pr<sub>2</sub>Me<sub>2</sub>NHC; **122**: 2.03 g, 11.2 mmol of *i*Pr<sub>2</sub>Me<sub>2</sub>NHC; **123**: 3.27 g, 15.4 mmol of *i*Pr<sub>2</sub>Me<sub>2</sub>ImS) were suspended in 10 ml of toluene and stirred for 15-20 min until all components were completely dissolved. The solution was then used directly in the synthesis of **119-123**.

To a suspension of carba[1]magnesocenophane **9** (**119** and **120**: 1.0 g, 5.13 mmol; **121**: 3.0 g, 15.4 mmol; **122**: 2.18 g, 11.2 mmol; **123**: 3.0 g, 15.4 mmol) in 50 ml of toluene, a toluene solution of the corresponding aluminum halide-NHC complex was slowly added and the

## 5. Experimental Details

mixture was stirred at room temperature overnight. After filtration, the filtrate was concentrated to approximately 20 ml and stored at 253 K overnight. The colorless crystalline precipitate was collected, washed with small portions of cold toluene and dried in vacuum.

Yield: 0.73 g of **119**, 41%; 0.39 g of **120**, 20%; 4.45 g of **121**, 70%; 2.87 g of **122**, 56%; 2.64 g of **123**, 39%.

### Compound **119**

$^1\text{H}$  NMR (400 MHz,  $\text{C}_6\text{D}_6$ , 298 K):  $\delta$ [ppm]= 6.91 (d,  $J = 4.4$  Hz, 2H), 6.31 (dd,  $J = 2.5$  Hz, 1.5 Hz, 2H), 6.23 (dd,  $J = 4.5$  Hz, 2.4 Hz, 2H), 4.91 (s, 2H), 2.69 (s, 6H), 1.90 (s, 3H), 1.76 (s, 3H), 0.98 (s, 6H).

$^{13}\text{C}\{^1\text{H}\}$  NMR (101 MHz,  $\text{C}_6\text{D}_6$ , 298 K):  $\delta$ [ppm]= 157.56, 127.52, 125.88, 121.89, 115.30, 65.65, 39.08, 34.01, 33.96, 27.47, 7.82.

$^{27}\text{Al}\{^1\text{H}\}$  NMR (104 MHz,  $\text{C}_6\text{D}_6$ , 298 K):  $\delta$ [ppm]= 125.

Elemental analysis for  $\text{C}_{20}\text{H}_{26}\text{AlClN}_2$ : calc.: 67.31% C, 7.34% H; 7.85% N; found: 66.64% C, 7.14% H; 7.83% N.

### Crystallographic data for **119**

CCDC code:	2009459
Empirical formula	$\text{C}_{20}\text{H}_{26}\text{AlClN}_2$
Formula weight	356.86
Temperature	132(2) K
Wavelength	0.71073 Å
Crystal system	monoclinic
Space group	P21/n
Unit cell dimensions	$a = 13.7688(3)$ Å $\alpha = 90^\circ$ $b = 8.4561(2)$ Å $\beta = 93.733(2)^\circ$ $c = 16.3214(4)$ Å $\gamma = 90^\circ$
Volume	1896.27(8) Å <sup>3</sup>
Z	4
Density (calculated)	1.250 Mg/m <sup>3</sup>
Absorption coefficient	0.252 mm <sup>-1</sup>
F(000)	760
Crystal size	0.402 x 0.310 x 0.106 mm <sup>3</sup>
Theta range for data collection	1.876 to 32.696°.

## 5. Experimental Details

Index ranges	-19<=h<=20, -12<=k<=12, -24<=l<=24
Reflections collected	20826
Independent reflections	6914 [R(int) = 0.0347]
Completeness to theta = 25.242°	99.9 %
Absorption correction	semi-empirical from equivalents
Max. and min. transmission	0.7464 and 0.7132
Refinement method	full-matrix least-squares on F <sup>2</sup>
Data / restraints / parameters	6914 / 0 / 321
Goodness-of-fit on F <sup>2</sup>	1.019
Final R indices [I>2sigma(I)]	R1 = 0.0418, wR2 = 0.0947
R indices (all data)	R1 = 0.0672, wR2 = 0.1072
Extinction coefficient	n/a
Largest diff. peak and hole	0.379 and -0.229 e.Å <sup>-3</sup>

### Compound **120**

<sup>1</sup>H NMR (400 MHz, C<sub>6</sub>D<sub>6</sub>, 298 K): δ [ppm]= 6.90 (d, *J* = 4.6 Hz, 2H), 6.32 (dd, *J* = 4.6 Hz, 2.3 Hz, 2H), 6.17 (dd, *J* = 2.3 Hz, 1.3 Hz, 2H), 5.04 (s, 2H), 3.20 (q, *J* = 7.2 Hz, 4H), 1.91 (s, 3H), 1.78 (s, 3H), 1.12 (s, 6H), 0.87 (t, *J* = 7.1 Hz, 6H).

<sup>13</sup>C{<sup>1</sup>H} NMR (101 MHz, C<sub>6</sub>D<sub>6</sub>, 298 K): δ [ppm]= 158.58, 129.34, 126.05, 122.39, 111.60, 68.88, 42.82, 39.20, 33.97, 27.99, 16.45, 7.98.

<sup>27</sup>Al{<sup>1</sup>H} NMR (104 MHz, C<sub>6</sub>D<sub>6</sub>, 298 K): δ [ppm]= 126.

Elemental analysis for C<sub>22</sub>H<sub>30</sub>AlClN<sub>2</sub>: calc.: 68.65% C, 7.86% H; 7.28% N; found: 68.22% C, 7.85% H; 6.87% N.

### Crystallographic data for **120**

CCDC code:	2009460
Empirical formula	C <sub>22</sub> H <sub>30</sub> AlClN <sub>2</sub>
Formula weight	384.91
Temperature	123(2) K
Wavelength	0.71073 Å
Crystal system	monoclinic
Space group	P21/c
Unit cell dimensions	a = 12.3073(6) Å      α = 90° b = 12.1350(5) Å      β = 104.3982(17)°

## 5. Experimental Details

	$c = 14.4827(6) \text{ \AA}$	$\gamma = 90^\circ$
Volume	2095.04(16) $\text{\AA}^3$	
Z	4	
Density (calculated)	1.220 $\text{Mg/m}^3$	
Absorption coefficient	0.233 $\text{mm}^{-1}$	
F(000)	824	
Crystal size	0.330 x 0.211 x 0.054 $\text{mm}^3$	
Theta range for data collection	2.219 to 29.576°.	
Index ranges	-15 ≤ h ≤ 17, -16 ≤ k ≤ 16, -20 ≤ l ≤ 20	
Reflections collected	21991	
Independent reflections	5842 [R(int) = 0.0328]	
Completeness to theta = 25.242°	99.9 %	
Absorption correction	semi-empirical from equivalents	
Max. and min. transmission	0.7459 and 0.7237	
Refinement method	full-matrix least-squares on F <sup>2</sup>	
Data / restraints / parameters	5842 / 0 / 355	
Goodness-of-fit on F <sup>2</sup>	1.050	
Final R indices [I > 2σ(I)]	R1 = 0.0390, wR2 = 0.0904	
R indices (all data)	R1 = 0.0491, wR2 = 0.0962	
Extinction coefficient	n/a	
Largest diff. peak and hole	0.389 and -0.196 $\text{e.\AA}^{-3}$	

### Compound **121**

<sup>1</sup>H NMR (400 MHz, C<sub>6</sub>D<sub>6</sub>, 298 K):  $\delta$  [ppm] = 6.88 (d,  $J = 4.5$  Hz, 2H), 6.37 (dd,  $J = 2.4$  Hz, 1.5 Hz, 2H), 6.26 (dd,  $J = 4.5$  Hz, 2.4 Hz, 2H), 4.86 (s, 2H), 3.67 (p,  $J = 6.9$  Hz, 2H), 1.89 (s, 3H), 1.72 (s, 3H), 1.36 (s, 6H), 1.03 (d,  $J = 6.9$  Hz, 12H).

<sup>13</sup>C{<sup>1</sup>H} NMR (101 MHz, C<sub>6</sub>D<sub>6</sub>, 298 K):  $\delta$  [ppm] = 158.61, 128.52, 126.93, 122.22, 116.52, 63.96, 52.61, 39.11, 22.25, 10.05.

<sup>27</sup>Al{<sup>1</sup>H} NMR (104 MHz, C<sub>6</sub>D<sub>6</sub>, 298 K):  $\delta$  [ppm] = 127.

Elemental analysis for C<sub>24</sub>H<sub>34</sub>AlClN<sub>2</sub>: calc.: 69.80% C, 8.30% H; 6.53% N; found: 69.37% C, 8.28% H; 7.28% N.

### Crystallographic data for **121**

CCDC code:	2009461
Empirical formula	C <sub>24</sub> H <sub>34</sub> AlClN <sub>2</sub>

## 5. Experimental Details

Formula weight	412.96
Temperature	122(2) K
Wavelength	0.71073 Å
Crystal system	monoclinic
Space group	Cc
Unit cell dimensions	$a = 9.9159(13) \text{ \AA}$ $\alpha = 90^\circ$ $b = 14.9657(13) \text{ \AA}$ $\beta = 104.022(3)^\circ$ $c = 15.8200(15) \text{ \AA}$ $\gamma = 90^\circ$
Volume	2277.7(4) Å <sup>3</sup>
Z	4
Density (calculated)	1.204 Mg/m <sup>3</sup>
Absorption coefficient	0.218 mm <sup>-1</sup>
F(000)	888
Crystal size	0.400 x 0.225 x 0.212 mm <sup>3</sup>
Theta range for data collection	2.517 to 36.510°.
Index ranges	-16<=h<=16, -24<=k<=24, -26<=l<=26
Reflections collected	37582
Independent reflections	10604 [R(int) = 0.0308]
Completeness to theta = 25.242°	100.0 %
Absorption correction	semi-empirical from equivalents
Max. and min. transmission	0.7471 and 0.7233
Refinement method	full-matrix least-squares on F <sup>2</sup>
Data / restraints / parameters	10604 / 2 / 389
Goodness-of-fit on F <sup>2</sup>	1.021
Final R indices [I>2sigma(I)]	R1 = 0.0305, wR2 = 0.0719
R indices (all data)	R1 = 0.0371, wR2 = 0.0755
Absolute structure parameter	0.003(13)
Extinction coefficient	n/a
Largest diff. peak and hole	0.444 and -0.194 e.Å <sup>-3</sup>

### Compound 122

<sup>1</sup>H NMR (400 MHz, C<sub>6</sub>D<sub>6</sub>, 298 K):  $\delta$ [ppm]= 6.90 (dt,  $J = 4.5$  Hz, 1.5 Hz, 2H), 6.38 (dd,  $J = 2.5$  Hz, 1.5 Hz, 2H), 6.26 (dd,  $J = 4.5$  Hz, 2.4 Hz, 2H), 4.89 (s, 2H), 3.67 (hept,  $J = 6.9$  Hz, 2H), 1.87 (s, 3H), 1.70 (s, 3H), 1.34 (s, 6H), 1.02 (d,  $J = 6.9$  Hz, 12H).

<sup>13</sup>C{<sup>1</sup>H} NMR (101 MHz, C<sub>6</sub>D<sub>6</sub>, 298 K):  $\delta$ [ppm]= 158.63, 128.81, 127.05, 122.38, 116.96, 64.24, 52.66, 39.13, 35.06, 27.09, 22.32, 10.03.

## 5. Experimental Details

$^{27}\text{Al}\{^1\text{H}\}$  NMR (104 MHz,  $\text{C}_6\text{D}_6$ , 298 K):  $\delta$  [ppm] = 124.

Elemental analysis for  $\text{C}_{24}\text{H}_{34}\text{AlBrN}_2$ : calc.: 63.02% C, 7.49% H; 6.12% N; found: 63.15% C, 7.59% H; 6.42% N.

### Crystallographic data for **122**

CCDC code:	2009462
Empirical formula	$\text{C}_{24}\text{H}_{34}\text{Al}_1\text{Br}_1\text{N}_2$
Formula weight	457.42
Temperature	122(2) K
Wavelength	0.71073 Å
Crystal system	monoclinic
Space group	Cc
Unit cell dimensions	$a = 9.9087(4)$ Å $\alpha = 90^\circ$ $b = 14.9364(4)$ Å $\beta = 104.533(3)^\circ$ $c = 16.0534(6)$ Å $\gamma = 90^\circ$
Volume	$2299.89(14)$ Å <sup>3</sup>
Z	4
Density (calculated)	1.321 Mg/m <sup>3</sup>
Absorption coefficient	1.838 mm <sup>-1</sup>
F(000)	960
Crystal size	0.452 x 0.270 x 0.194 mm <sup>3</sup>
Theta range for data collection	2.524 to 32.726°.
Index ranges	-15 ≤ h ≤ 15, -22 ≤ k ≤ 22, -24 ≤ l ≤ 24
Reflections collected	58838
Independent reflections	8462 [R(int) = 0.0280]
Completeness to theta = 25.242°	100.0 %
Absorption correction	semi-empirical from equivalents
Max. and min. transmission	0.7464 and 0.6217
Refinement method	full-matrix least-squares on F <sup>2</sup>
Data / restraints / parameters	8462 / 2 / 381
Goodness-of-fit on F <sup>2</sup>	1.013
Final R indices [I > 2σ(I)]	R1 = 0.0199, wR2 = 0.0471
R indices (all data)	R1 = 0.0220, wR2 = 0.0479
Absolute structure parameter	-0.0028(18)
Extinction coefficient	n/a
Largest diff. peak and hole	0.395 and -0.225 e.Å <sup>-3</sup>



## 5. Experimental Details

### Compound **123**

$^1\text{H}$  NMR (400 MHz,  $\text{C}_6\text{D}_6$ , 298 K):  $\delta$ [ppm]= 6.90 (dt,  $J$  = 3.3 Hz, 1.6 Hz, 2H), 6.72 (t,  $J$  = 2.1 Hz, 2H), 6.62 (dd,  $J$  = 4.5 Hz, 2.5 Hz, 2H), 5.47 (p,  $J$  = 7.2 Hz, 2H), 4.84 (s, 2H), 2.01 (s, 3H), 1.76 (s, 3H), 1.32 (s, 6H), 1.03 (d,  $J$  = 7.1 Hz, 12H).

$^{13}\text{C}\{^1\text{H}\}$  NMR (101 MHz,  $\text{C}_6\text{D}_6$ , 298 K):  $\delta$ [ppm]= 155.8, 146.4, 126.8, 125.5, 122.2, 117.3, 64.0, 51.3, 39.2, 33.2, 27.2, 20.5, 9.6.

$^{27}\text{Al}\{^1\text{H}\}$  NMR (104 MHz,  $\text{C}_6\text{D}_6$ , 298 K):  $\delta$ [ppm]= 134.

Elemental analysis for  $\text{C}_{24}\text{H}_{34}\text{AlClSN}_2$ : calc.: 64.77%, 7.70% H; 6.29% N; found: 64.52% C, 7.67% H; 5.92% N.

### Crystallographic data for **123**

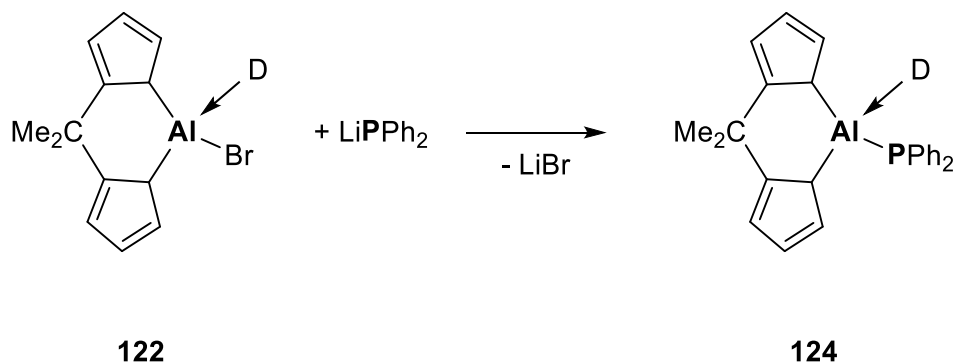
CCDC code:	2009464
Empirical formula	$\text{C}_{24}\text{H}_{34}\text{AlClN}_2\text{S}$
Formula weight	537.151
Temperature	140(2) K
Wavelength	0.71073 Å
Crystal system	monoclinic
Space group	P21/m
Unit cell dimensions	$a = 6.6604(2)$ Å $\alpha = 90^\circ$ $b = 19.5542(6)$ Å $\beta = 92.3940(10)^\circ$ $c = 11.6546(4)$ Å $\gamma = 90^\circ$
Volume	1516.56(8) Å <sup>3</sup>
Z	2
Density (calculated)	1.176 Mg/m <sup>3</sup>
Absorption coefficient	0.245 mm <sup>-1</sup>
F(000)	576
Crystal size	0.242 x 0.143 x 0.026 mm <sup>3</sup>
Theta range for data collection	2.036 to 35.003°.
Index ranges	-10 ≤ h ≤ 10, -20 ≤ k ≤ 31, -18 ≤ l ≤ 18
Reflections collected	63953
Independent reflections	6821 [R(int) = 0.0437]
Completeness to theta = 25.242°	99.6 %
Absorption correction	semi-empirical from equivalents
Max. and min. transmission	0.7469 and 0.7171
Refinement method	full-matrix least-squares on F <sup>2</sup>

## 5. Experimental Details

Data / restraints / parameters	6821 / 122 / 215
Goodness-of-fit on $F^2$	1.072
Final R indices [ $I > 2\sigma(I)$ ]	R1 = 0.0469, wR2 = 0.1318
R indices (all data)	R1 = 0.0626, wR2 = 0.1442
Extinction coefficient	n/a
Largest diff. peak and hole	1.336 and -0.434 e.Å <sup>-3</sup>

## 5. Experimental Details

### 5.2.6. Synthesis of **124**:



Compound **122** (500 mg, 1.09 mmol) and Lithium diphenylphosphide (209 mg, 1.09 mmol) were charged into a Schlenk flask. 20 mL of toluene were added and the mixture was stirred overnight at room temperature. After filtration, the solution was concentrated to approximately 20 ml and stored at 253 K overnight, resulting in the crystallization of **124**. Isolation of the precipitate and drying *in vacuo* yielded the product as a colorless crystalline solid.

Yield: 0.40 g of **124**, 65%.

$^1\text{H}$  NMR (400 MHz,  $\text{C}_6\text{D}_6$ , 298 K):  $\delta$ [ppm]= 7.82 – 7.75 (m, 4H), 7.16 – 7.08 (m, 4H), 7.03 – 6.97 (m, 2H), 6.78 (dt,  $J = 4.4$  Hz, 1.3 Hz, 2H), 6.39 (dd,  $J = 2.3$  Hz, 1.5 Hz, 2H), 6.31 (dd,  $J = 4.5$  Hz, 2.4 Hz, 2H), 4.61 (s, 2H), 3.98 (d,  $J = 6.4$  Hz, 2H), 1.87 (s, 3H), 1.47 (s, 3H), 1.30 (s, 6H), 1.12 (d,  $J = 6.9$  Hz, 12H).

$^{13}\text{C}\{^1\text{H}\}$  NMR (101 MHz,  $\text{C}_6\text{D}_6$ , 298 K):  $\delta$ [ppm]= 160.28, 142.07 (d,  $J = 22.6$  Hz), 134.05 (d,  $J = 15.7$  Hz), 128.95, 128.69 (d,  $J = 5.9$  Hz), 128.59, 127.12, 126.16, 121.88, 116.29, 59.24, 52.53 (d,  $J = 12.3$  Hz), 38.94, 35.03, 27.05, 22.73, 10.16.

$^{27}\text{Al}\{^1\text{H}\}$  NMR (104 MHz,  $\text{C}_6\text{D}_6$ , 298 K):  $\delta$ [ppm]= 138.

$^{31}\text{P}$  NMR (162 MHz,  $\text{C}_6\text{D}_6$ , 298 K):  $\delta$ [ppm]= -51.10;

Elemental analysis for  $\text{C}_{36}\text{H}_{44}\text{AlPN}_2$ : calc.: 76.84% C, 7.88% H; 4.98% N; found: 75.57% C, 7.99% H; 4.85% N.

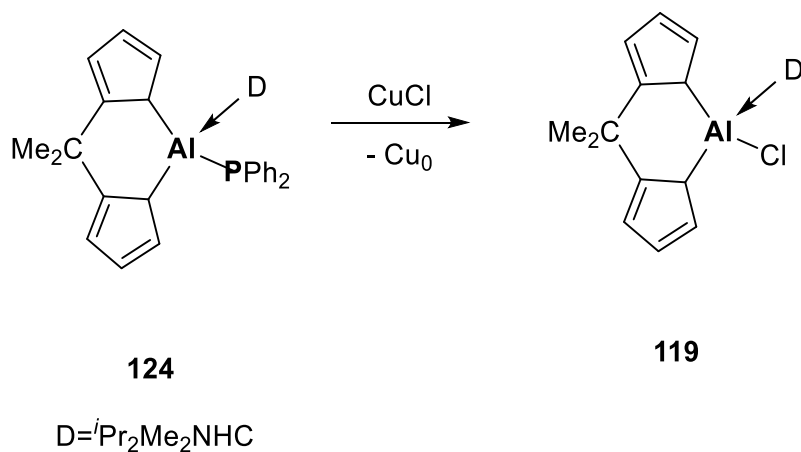
## 5. Experimental Details

### Crystallographic data for **124**

CCDC code:	2009463
Empirical formula	$C_{36}H_{44}Al_1N_2P_1$
Formula weight	562.68
Temperature	133(2) K
Wavelength	1.54178 Å
Crystal system	monoclinic
Space group	P21/c
Unit cell dimensions	$a = 17.5311(6)$ Å $\alpha = 90^\circ$ $b = 10.4341(4)$ Å $\beta = 107.9422(10)^\circ$ $c = 18.3127(6)$ Å $\gamma = 90^\circ$
Volume	3186.87(19) Å <sup>3</sup>
Z	4
Density (calculated)	1.173 Mg/m <sup>3</sup>
Absorption coefficient	1.219 mm <sup>-1</sup>
F(000)	1208
Crystal size	0.453 x 0.090 x 0.063 mm <sup>3</sup>
Theta range for data collection	2.649 to 79.958°.
Index ranges	-22 ≤ h ≤ 21, 0 ≤ k ≤ 13, 0 ≤ l ≤ 23
Reflections collected	6672
Independent reflections	6672 [R(int) = ?]
Completeness to theta = 67.679°	99.0 %
Absorption correction	semi-empirical from equivalents
Max. and min. transmission	0.7543 and 0.6151
Refinement method	full-matrix least-squares on F <sup>2</sup>
Data / restraints / parameters	6672 / 0 / 376
Goodness-of-fit on F <sup>2</sup>	1.047
Final R indices [I > 2σ(I)]	R1 = 0.0304, wR2 = 0.0838
R indices (all data)	R1 = 0.0312, wR2 = 0.0851
Extinction coefficient	n/a
Largest diff. peak and hole	0.303 and -0.271 e.Å <sup>-3</sup>

## 5. Experimental Details

### 5.2.7. The reaction between **124** and CuCl:



Compound **124** (300 mg, 0.319 mmol) and CuCl (32 mg, 0.319 mmol) were dissolved in thf (5 ml). The mixture was stirred overnight at room temperature. A bronze particle was filtrated and all volatiles was removed under vacuum to colorless powder. After drying for two hours the powder was identified during NMR.

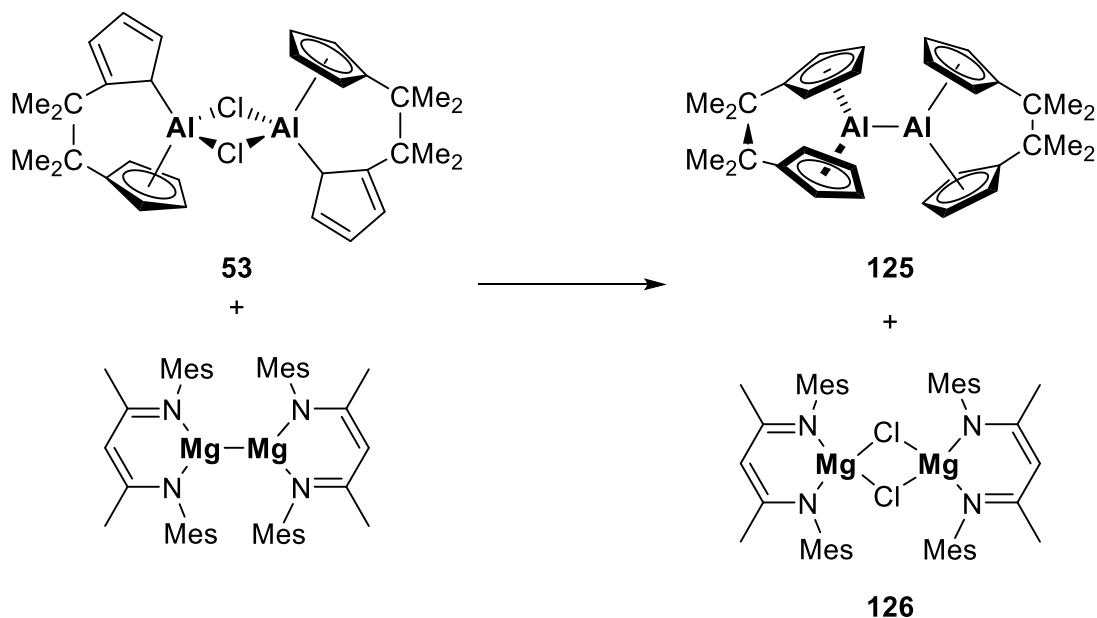
<sup>1</sup>H NMR (400 MHz, C<sub>6</sub>D<sub>6</sub>, 298 K):  $\delta$ [ppm]= 6.88 (d,  $J$  = 4.5 Hz, 2H), 6.37 (dd,  $J$  = 2.4 Hz, 1.5 Hz, 2H), 6.26 (dd,  $J$  = 4.5 Hz, 2.4 Hz, 2H), 4.86 (s, 2H), 3.67 (p,  $J$  = 6.9 Hz, 2H), 1.89 (s, 3H), 1.72 (s, 3H), 1.36 (s, 6H), 1.03 (d,  $J$  = 6.9 Hz, 12H).

<sup>13</sup>C{<sup>1</sup>H} NMR (101 MHz, C<sub>6</sub>D<sub>6</sub>, 298 K):  $\delta$ [ppm]= 158.61, 128.52, 126.93, 122.22, 116.52, 63.96, 52.61, 39.11, 22.25, 10.05.

<sup>27</sup>Al{<sup>1</sup>H} NMR (104 MHz, C<sub>6</sub>D<sub>6</sub>, 298 K):  $\delta$ [ppm]= 124.

## 5. Experimental Details

### 5.2.8. Synthesis of **125**:



Compound **53** (236 mg, 0.43 mmol) and 1,3- $\beta$ -diketiminato magnesium(I) dimer ( $\{^{\text{Mes}}\text{NacNacMg}\}_2$ ) (307 mg, 0.43 mmol) were charged into a Schlenk flask. 20 mL of toluene were added and the mixture was stirred overnight at room temperature. After filtration, the solution was concentrated and stored at 253 K overnight, resulting in the crystallization of bis(aluminocenophane) **125**. Isolation of the precipitate and drying *in vacuo* yielded the product as a colorless crystalline solid, which can be stored at 248 K under an inert gas atmosphere for at least several weeks.

Yield: 0.18 g of **125**, 80%

$^1\text{H}$  NMR (400 MHz,  $\text{C}_6\text{D}_6$ , 298 K):  $\delta$ [ppm]= 6.08 (t,  $J$  = 2.5 Hz, 8H), 5.67 (t,  $J$  = 2.5 Hz, 8H), 1.30 (s, 24H).

$^{13}\text{C}\{^1\text{H}\}$  NMR (101 MHz,  $\text{C}_6\text{D}_6$ , 298 K):  $\delta$ [ppm]= 125.7, 119.7, 106.2, 42.7, 27.6.

No signal was observed in the  $^{27}\text{Al}$  NMR spectrum of a  $\text{C}_6\text{D}_6$  solution in the range of +200 ppm to -200 ppm.

Elemental analysis for  $\text{C}_{32}\text{H}_{40}\text{Al}_2$ : calc.: 80.30% C, 8.42% H; found: 78.18% C, 8.50% H (carbon values were repeatedly reproducibly low even upon analysis of crystalline material, presumably due to the formation of aluminum carbide).

## 5. Experimental Details

### Crystallographic data for **125**

CCDC code:	1936579
Empirical formula	C <sub>32</sub> H <sub>40</sub> Al <sub>2</sub>
Formula weight	478.60
Temperature	122(2) K
Wavelength	0.71073 Å
Crystal system	orthorhombic
Space group	P212121
Unit cell dimensions	a = 8.9879(3) Å      α = 90° b = 10.9776(3) Å      β = 90° c = 26.2559(7) Å      γ = 90°
Volume	2590.55(13) Å <sup>3</sup>
Z	4
Density (calculated)	1.227 Mg/m <sup>3</sup>
Absorption coefficient	0.131 mm <sup>-1</sup>
F(000)	1032
Crystal size	0.438 x 0.322 x 0.228 mm <sup>3</sup>
Theta range for data collection	1.551 to 32.766°
Index ranges	-13 ≤ h ≤ 13, -16 ≤ k ≤ 16, -39 ≤ l ≤ 39
Reflections collected	46884
Independent reflections	9536 [R(int) = 0.0232]
Completeness to theta = 25.242°	100.0%
Absorption correction	semi-empirical from equivalents
Max. and min. transmission	0.7464 and 0.7238
Refinement method	full-matrix least-squares on F <sup>3</sup>
Data / restraints / parameters	9536 / 0 / 467
Goodness-of-fit on F <sup>2</sup>	1.052
Final R indices [I > 2σ(I)]	R1 = 0.0286, wR2 = 0.0717
R indices (all data)	R1 = 0.0316, wR2 = 0.0733
Absolute structure parameter	0.02(2)
Extinction coefficient	n/a
Largest diff. peak and hole	0.301 and -0.200 e.Å <sup>-3</sup>

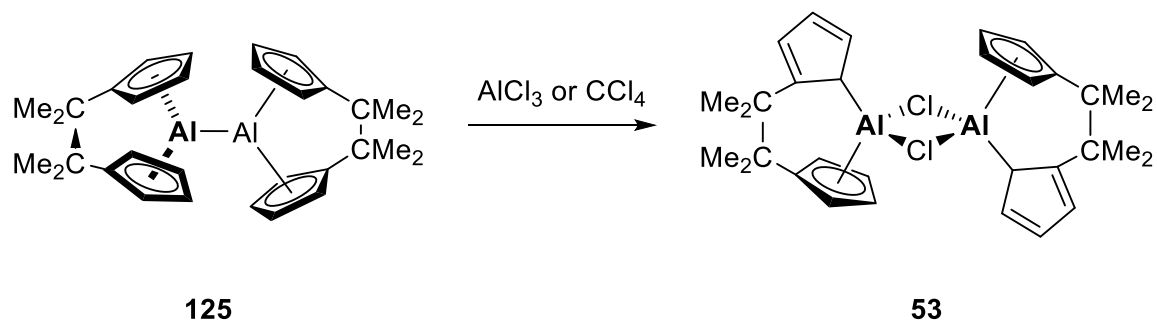
### Crystallographic data for **126**

Identification code	sh4172
Empirical formula	C <sub>46</sub> H <sub>58</sub> Cl <sub>2</sub> Mg <sub>2</sub> N <sub>4</sub>
Formula weight	786.48

## 5. Experimental Details

Temperature	133(2) K
Wavelength	0.71073 Å
Crystal system	Triclinic
Space group	P-1
Unit cell dimensions	a = 8.5047(3) Å $\alpha = 69.6013(11)^\circ$ . b = 10.3556(3) Å $\beta = 83.5599(12)^\circ$ . c = 13.5729(4) Å $\gamma = 81.3923(12)^\circ$ .
Volume	1105.48(6) Å <sup>3</sup>
Z	1
Density (calculated)	1.181 Mg/m <sup>3</sup>
Absorption coefficient	0.211 mm <sup>-1</sup>
F(000)	420
Crystal size	0.265 x 0.202 x 0.188 mm <sup>3</sup>
Theta range for data collection	2.427 to 29.575°.
Index ranges	-11 ≤ h ≤ 11, -14 ≤ k ≤ 13, -18 ≤ l ≤ 18
Reflections collected	24440
Independent reflections	6190 [R(int) = 0.0202]
Completeness to theta = 25.242°	99.9 %
Absorption correction	Semi-empirical from equivalents
Max. and min. transmission	0.7459 and 0.7183
Refinement method	Full-matrix least-squares on F <sup>2</sup>
Data / restraints / parameters	6190 / 0 / 360
Goodness-of-fit on F <sup>2</sup>	1.037
Final R indices [I > 2σ(I)]	R1 = 0.0339, wR2 = 0.0938
R indices (all data)	R1 = 0.0387, wR2 = 0.0986
Extinction coefficient	n/a
Largest diff. peak and hole	0.406 and -0.195 e.Å <sup>-3</sup>

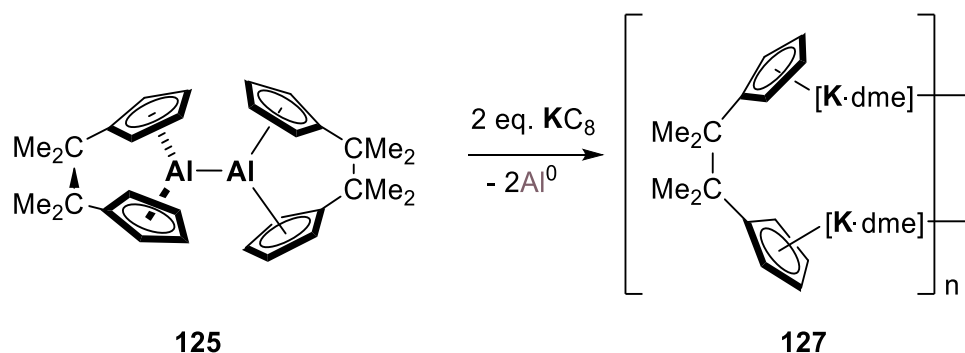


5.2.9. Reaction of **125** with element chlorides:

Bis(aluminocenophane) **125** (20 mg / 0.04 mmol) and the corresponding element chloride ( $\text{CCl}_4$ : 8,2  $\mu\text{L}$ , 0.08 mmol;  $\text{AlCl}_3$ : 6 mg, 0.04 mmol) were dissolved in 1 mL of deuterated benzene and the solution was stirred for 1 h. Subsequently, insoluble components were filtered off and the mixtures were analyzed by  $^1\text{H}$  and  $^{13}\text{C}$  NMR-spectroscopic, which revealed formation of **53**, in case of the reaction with  $\text{CCl}_4$  along with some unidentified by-products.

$^1\text{H}$  NMR (400 MHz,  $\text{C}_6\text{D}_6$ , 293 K):  $\delta$  [ppm]= 6.26 (t,  $J$  = 1.9 Hz, 8H), 5.21 (s, 8H), 1.05 (s, 24H).

$^{13}\text{C}\{^1\text{H}\}$  NMR (101 MHz,  $\text{C}_6\text{D}_6$ , 293 K):  $\delta$  [ppm]= 146.8, 128.6, 117.6, 41.6, 24.1.

5.2.10. Synthesis of **127**:

Bis(aluminocenophane) **125** (50 mg, 0.1 mmol) and potassium graphite (29 mg, 0.2 mmol) were dissolved in 5 mL of dme and the solution was stirred overnight. Insoluble black components were filtered off and the mixtures were analyzed by  $^1\text{H}$  NMR-spectroscopy in solution and by X-ray diffraction analysis in the solid state, which revealed formation of **127**. Single crystal was obtained from a saturated solution of dme at 248 K suitable for X-ray diffraction analysis.

Yield: 25 mg of **127**, 86%

$^1\text{H}$  NMR (400 MHz,  $\text{C}_6\text{D}_6$ , 293 K):  $\delta$  [ppm]= 5.71 – 5.55 (t,  $J$  = 2.7 Hz, 4H), 5.46 – 5.23 (t,  $J$  = 2.7 Hz, 4H), 0.11 (s, 12H).

Crystal data and structure refinement for **127**.

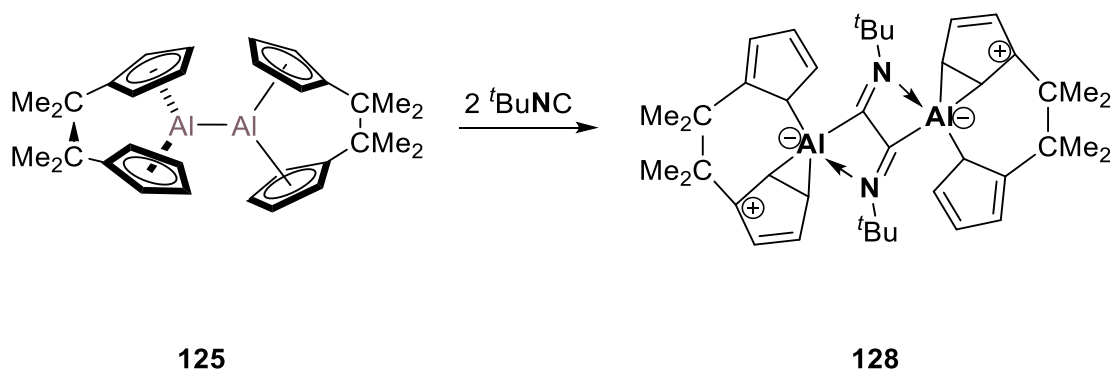
Identification code	sh4138	
Empirical formula	$\text{C}_{12} \text{H}_{20} \text{K}_1 \text{O}_2$	
Formula weight	235.38	
Temperature	152(2) K	
Wavelength	0.71073 Å	
Crystal system	Monoclinic	
Space group	$\text{P}2_1/\text{n}$	
Unit cell dimensions	$a = 10.9758(11)$ Å	$\alpha = 90^\circ$ .
	$b = 10.2862(12)$ Å	$\beta = 102.297(4)^\circ$ .
	$c = 11.8990(12)$ Å	$\gamma = 90^\circ$ .
Volume	$1312.6(2)$ Å <sup>3</sup>	

## 5. Experimental Details

Z	4
Density (calculated)	1.191 Mg/m <sup>3</sup>
Absorption coefficient	0.386 mm <sup>-1</sup>
F(000)	508
Crystal size	0.296 x 0.243 x 0.140 mm <sup>3</sup>
Theta range for data collection	2.293 to 32.095°.
Index ranges	-16<=h<=16, -15<=k<=15, -17<=l<=17
Reflections collected	34940
Independent reflections	4599 [R(int) = 0.0389]
Completeness to theta = 25.242°	100.0 %
Absorption correction	Semi-empirical from equivalents
Max. and min. transmission	0.7463 and 0.7150
Refinement method	Full-matrix least-squares on F <sup>2</sup>
Data / restraints / parameters	4599 / 0 / 216
Goodness-of-fit on F <sup>2</sup>	1.028
Final R indices [I>2sigma(I)]	R1 = 0.0313, wR2 = 0.0774
R indices (all data)	R1 = 0.0425, wR2 = 0.0836
Extinction coefficient	n/a
Largest diff. peak and hole	0.416 and -0.212 e.Å <sup>-3</sup>

## 5. Experimental Details

### 5.2.11. Synthesis of **128**:



Bis(aluminocenophane) **125** (20 mg, 0.042 mmol) and *tert*-butyl isocyanide (12 mg, 0.14 mmol) were mixed and dissolved in toluene and the solution was stirred for 16 h at ambient temperature and subsequently cooled down to 248 K overnight, resulting in the precipitation of **128** in form of orange needles. The crystals were separated from the mother liquor and dried in *in vacuo*.

Yield: 0.12 g of **128**, 45%.

$^1\text{H}$  NMR (300 MHz,  $\text{C}_6\text{D}_6$ , 293 K):  $\delta$ [ppm]= 6.13 – 6.11 (m, 4H), 6.07 – 6.03 (m, 8H), 5.19 (br s, 4H), 1.48 (s, 12H), 1.45 (s, 12H), 1.18 (s, 18H).

$^{13}\text{C}\{^1\text{H}\}$  NMR (75 MHz,  $\text{C}_6\text{D}_6$ , 296 K):  $\delta$ [ppm]= 146.6, 128.6, 120.4, 116.1, 109.6, 86.8 (br), 59.0, 42.6, 29.7, 27.1, 26.1.

No signal was observed in the  $^{27}\text{Al}$  NMR spectrum of a  $\text{C}_6\text{D}_6$  solution in the range of +200 ppm to -200 ppm.

Elemental analysis for  $\text{C}_{42}\text{H}_{58}\text{Al}_2\text{N}_2$ : calc.: 78.22% C, 9.07% H, 4.34% N; found: 77.22% C, 9.24% H, 4.19% N (carbon value was repeatedly reproducibly low even upon analysis of crystalline material, presumably due to the formation of aluminum carbide).

#### Crystallographic data for **128**

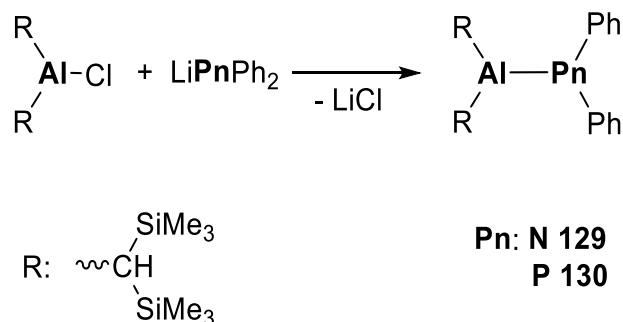
CCDC code:	1936580
Empirical formula	$\text{C}_{42}\text{H}_{58}\text{Al}_2\text{N}_2$
Formula weight	644.86

## 5. Experimental Details

Temperature	133(2) K
Wavelength	0.71073 Å
Crystal system	triclinic
Space group	P-1
Unit cell dimensions	$a = 11.2373(4)$ Å $\alpha = 63.7160(13)^\circ$ $b = 13.3899(4)$ Å $\beta = 70.0821(13)^\circ$ $c = 14.1649(5)$ Å $\gamma = 80.4239(13)^\circ$
Volume	1796.37(11) Å <sup>3</sup>
Z	2
Density (calculated)	1.192 Mg/m <sup>3</sup>
Absorption coefficient	0.113 mm <sup>-1</sup>
F(000)	700
Crystal size	0.535 x 0.179 x 0.110 mm <sup>3</sup>
Theta range for data collection	2.844 to 47.880°
Index ranges	-23 ≤ h ≤ 23, -27 ≤ k ≤ 27, -29 ≤ l ≤ 29
Reflections collected	227033
Independent reflections	34041 [R(int) = 0.0545]
Completeness to theta = 25.242°	99.1%
Absorption correction	semi-empirical from equivalents
Max. and min. transmission	0.7494 and 0.6929
Refinement method	full-matrix least-squares on F <sup>2</sup>
Data / restraints / parameters	34041 / 167 / 546
Goodness-of-fit on F <sup>2</sup>	1.036
Final R indices [I > 2σ(I)]	R1 = 0.0435, wR2 = 0.1142
R indices (all data)	R1 = 0.0752, wR2 = 0.1357
Extinction coefficient	n/a
Largest diff. peak and hole	0.552 and -0.468 e.Å <sup>-3</sup>

## 5. Experimental Details

### 5.2.12. Synthesis of **129** and **130**:



[(Me<sub>3</sub>Si)<sub>2</sub>CH]<sub>2</sub>AlCl (1.0 g, 2.62 mmol) and Ph<sub>2</sub>NLi (0.46 g, 2.62 mmol) or Ph<sub>2</sub>PLi (0.51 g, 2.62 mmol) were suspended in 10 ml of toluene. The reaction mixture was stirred at room temperature overnight. After filtration over celite, the solution was concentrated to approximately half its volume and stored at 253 K overnight. The precipitated crystals were collected and dried *in vacuo* at 323 K for three hours, affording the products as a colorless solid.

Yield: 0.40 g of **129**, 0.78 mmol, 30%; Yield: 0.35 g of **130**, 0.78 mmol, 30%.

#### Compound **129**

<sup>1</sup>H NMR (400 MHz, C<sub>6</sub>D<sub>6</sub>, 298 K): δ [ppm]= 7.12 – 7.06 (m, 4H), 7.02 – 6.96 (m, 4H), 6.89 – 6.83 (m, 2H), 0.17 (s, 36H), -0.49 (s, 2H).

<sup>13</sup>C{<sup>1</sup>H} NMR (101 MHz, C<sub>6</sub>D<sub>6</sub>, 298 K): δ [ppm]= 151.1, 129.8, 125.81, 123.0, 7.0, 4.2.

<sup>29</sup>Si{<sup>1</sup>H} NMR (79 MHz, C<sub>6</sub>D<sub>6</sub>, 298 K): δ [ppm]= -2.0.

No signal was detected in the <sup>27</sup>Al NMR spectrum between +200 ppm and -200 ppm.

Elemental analysis for C<sub>26</sub>H<sub>48</sub>Al<sub>1</sub>N<sub>1</sub>Si<sub>4</sub>: calc.: 60.76% C, 9.41% H; 2.73% N; found: 60.41% C, 8.66% H; 2.48% N.

#### Crystallographic data for **129**

CCDC code:	2026461
Empirical formula	C <sub>26</sub> H <sub>48</sub> Al <sub>1</sub> N <sub>1</sub> Si <sub>4</sub>
Formula weight	513.99
Temperature	140(2) K

## 5. Experimental Details

Wavelength	0.71073 Å
Crystal system	monoclinic
Space group	P21/c
Unit cell dimensions	$a = 10.4015(2)$ Å $\alpha = 90^\circ$ $b = 11.9113(3)$ Å $\beta = 96.1430(10)^\circ$ $c = 25.8749(6)$ Å $\gamma = 90^\circ$
Volume	3187.37(13) Å <sup>3</sup>
Z	4
Density (calculated)	1.071 mg / m <sup>3</sup>
Absorption coefficient	0.228 mm <sup>-1</sup>
F(000)	1120
Crystal size	0.346 x 0.228 x 0.220 mm <sup>3</sup>
Theta range for data collection	1.884 to 30.528°
Index ranges	-14 ≤ h ≤ 14, -17 ≤ k ≤ 17, -36 ≤ l ≤ 36
Reflections collected	62383
Independent reflections	9693 [R(int) = 0.0324]
Completeness to theta = 25.242°	99.3 %
Absorption correction	semi-empirical from equivalents
Max. and min. transmission	0.7461 and 0.7235
Refinement method	full-matrix least-squares on F <sup>2</sup>
Data / restraints / parameters	9693 / 249 / 390
Goodness-of-fit on F <sup>2</sup>	1.035
Final R indices [I > 2σ(I)]	R1 = 0.0328, wR2 = 0.0857
R indices (all data)	R1 = 0.0419, wR2 = 0.0921
Extinction coefficient	n/a
Largest diff. peak and hole	0.502 and -0.266 e.Å <sup>-3</sup>

### Compound **130**

<sup>1</sup>H NMR (400 MHz, C<sub>6</sub>D<sub>6</sub>, 298 K):  $\delta$  [ppm] = 7.71 (m, 4H), 7.10 (m, 4H), 7.04–6.98 (m, 2H), 0.20 (s, 36H), -0.01 (d,  $J$  = 3.5 Hz, 2H).

<sup>13</sup>C{<sup>1</sup>H} NMR (101 MHz, C<sub>6</sub>D<sub>6</sub>, 298 K):  $\delta$  [ppm] = 136.0 (d,  $J$  = 17.9 Hz), 128.9 (d,  $J$  = 8.0 Hz), 128.6, 127.6, 12.0 (d,  $J$  = 9.6 Hz), 4.5.

<sup>29</sup>Si{<sup>1</sup>H} NMR (79 MHz, C<sub>6</sub>D<sub>6</sub>, 298 K):  $\delta$  [ppm] = -3.5.

<sup>31</sup>P{<sup>1</sup>H} NMR (162 MHz, C<sub>6</sub>D<sub>6</sub>, 298 K):  $\delta$  [ppm] = -40.2.

No signal was detected in the <sup>27</sup>Al NMR spectrum between +200 ppm and -200 ppm.

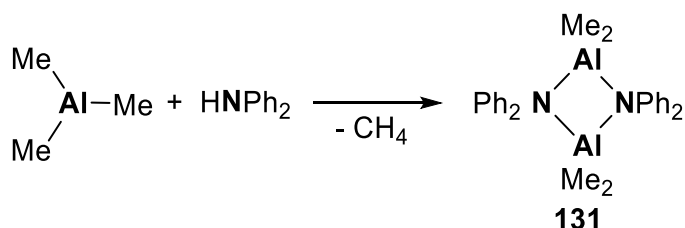
## 5. Experimental Details

Elemental analysis for  $C_{26}H_{48}Al_1P_1Si_4$ : calc.: 58.41% C, 9.11% H; found: 58.21% C, 9.01% H.

### Crystallographic data for **130**

CCDC code:	2026463
Empirical formula	$C_{26}H_{48}Al_1P_1Si_4$
Formula weight	530.95
Temperature	132(2) K
Wavelength	0.71073 Å
Crystal system	triclinic
Space group	P-1
Unit cell dimensions	$a = 9.0099(6)$ Å $\alpha = 93.0184(19)^\circ$ $b = 9.5284(7)$ Å $\beta = 90.8156(17)^\circ$ $c = 20.6827(14)$ Å $\gamma = 114.0061(16)^\circ$
Volume	$1618.5(2)$ Å <sup>3</sup>
Z	2
Density (calculated)	1.089 mg / m <sup>3</sup>
Absorption coefficient	$0.273$ mm <sup>-1</sup>
F(000)	576
Crystal size	$0.398 \times 0.333 \times 0.321$ mm <sup>3</sup>
Theta range for data collection	$1.974$ to $40.271^\circ$
Index ranges	$-16 \leq h \leq 16$ , $-17 \leq k \leq 17$ , $-37 \leq l \leq 37$
Reflections collected	89122
Independent reflections	20377 [R(int) = 0.0342]
Completeness to theta = $25.242^\circ$	99.9 %
Absorption correction	semi-empirical from equivalents
Max. and min. transmission	0.7479 and 0.6936
Refinement method	full-matrix least-squares on F <sup>2</sup>
Data / restraints / parameters	20377 / 72 / 432
Goodness-of-fit on F <sup>2</sup>	1.053
Final R indices [I > 2sigma(I)]	R1 = 0.0510, wR2 = 0.1162
R indices (all data)	R1 = 0.0842, wR2 = 0.1306
Extinction coefficient	n/a
Largest diff. peak and hole	0.768 and -0.474 e.Å <sup>-3</sup>



5.2.13. Synthesis of **131**:

Trimethylaluminium (15 ml, 1.0 M, heptane solution) was added to diphenylamine (2.53 g, 15 mmol) dissolved in 50 mL of toluene and stirred at 343 K for 3 h. Subsequently, the solution was concentrated to approximately half its volume and stored at 253 K overnight. The precipitated crystals were collected and dried *in vacuo* at 323 K for three hours, affording the product as a colorless solid.

Yield: 3.04 g of **131**, 13.5 mmol, 90%.

$^1\text{H}$  NMR (400 MHz,  $\text{C}_6\text{D}_6$ , 298 K):  $\delta$  [ppm]= 7.28 – 7.21 (m, 4H), 6.94 – 6.88 (m, 4H), 6.84–6.76 (m, 2H), -0.25 (s, 6H).

$^{13}\text{C}\{^1\text{H}\}$  NMR (101 MHz,  $\text{C}_6\text{D}_6$ , 298 K):  $\delta$  [ppm]= 151.2, 129.1, 128.4, 125.3, -3.3.

No signal was detected in the  $^{27}\text{Al}$  NMR spectrum between +200 ppm and -200 ppm.

Elemental analysis for  $\text{C}_{14}\text{H}_{16}\text{Al}_1\text{N}_1$ : calc.: 74.65% C, 7.16% H; 6.22% N; found: 73.93% C, 7.12% H; 6.00% N.

Crystal data of **131**

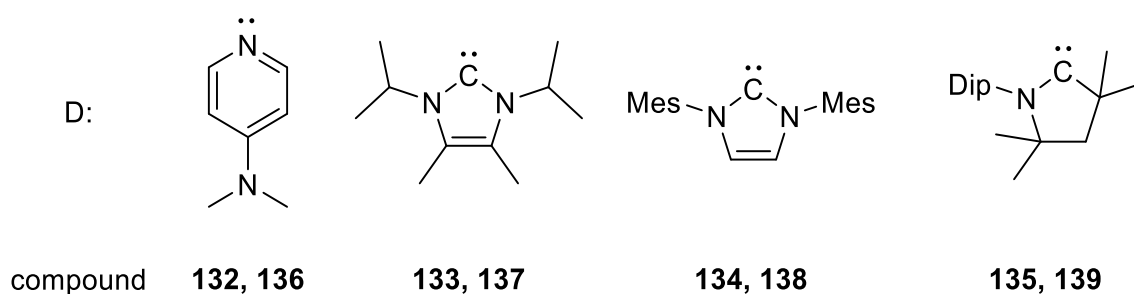
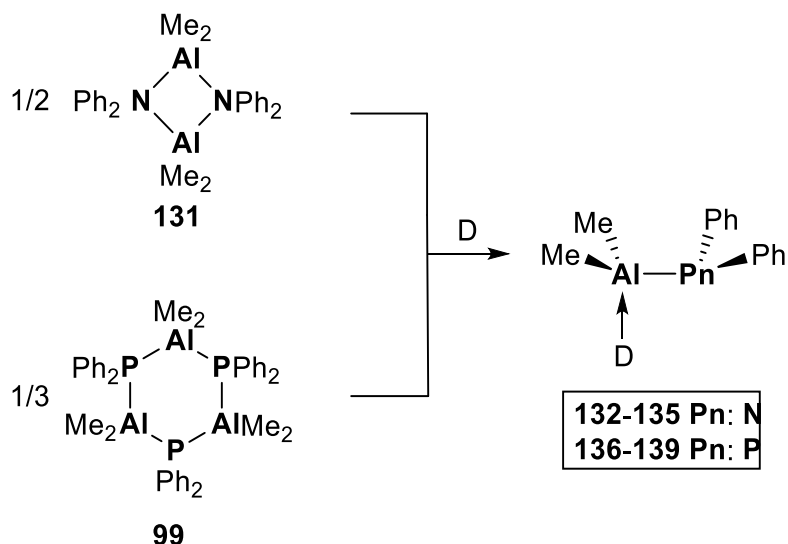
CCDC code:	2026462	
Empirical formula	$\text{C}_{28}\text{H}_{32}\text{Al}_2\text{N}_2$	
Formula weight	450.51	
Temperature	130(2) K	
Wavelength	0.71073 Å	
Crystal system	monoclinic	
Space group	P21/n	
Unit cell dimensions	$a = 11.6461(3)$ Å	$\alpha = 90^\circ$
	$b = 13.4938(4)$ Å	$\beta = 107.4853(10)^\circ$

## 5. Experimental Details

	$c = 16.6600(4) \text{ \AA}$	$\gamma = 90^\circ$
Volume	2497.15(12) $\text{\AA}^3$	
Z	4	
Density (calculated)	1.198 mg / m <sup>3</sup>	
Absorption coefficient	0.134 mm <sup>-1</sup>	
F(000)	960	
Crystal size	0.231 x 0.226 x 0.200 mm <sup>3</sup>	
Theta range for data collection	1.980 to 31.525°.	
Index ranges	-17<=h<=17, -19<=k<=19, -22<=l<=24	
Reflections collected	89427	
Independent reflections	8326 [R(int) = 0.0259]	
Completeness to theta = 25.242°	100.0 %	
Absorption correction	semi-empirical from equivalents	
Max. and min. transmission	0.7462 and 0.7043	
Refinement method	full-matrix least-squares on F <sup>2</sup>	
Data / restraints / parameters	8326 / 0 / 401	
Goodness-of-fit on F <sup>2</sup>	1.053	
Final R indices [I>2sigma(I)]	R1 = 0.0321, wR2 = 0.0924	
R indices (all data)	R1 = 0.0349, wR2 = 0.0950	
Extinction coefficient	n/a	
Largest diff. peak and hole	0.400 and -0.263 e. $\text{\AA}^{-3}$	

## 5. Experimental Details

### 5.2.14. Synthesis of 132-139:



The oligomeric aminoalane **131** or phosphanylalane **99** and the corresponding donor ligand

**132:131:** 0.50 g, 2.22 mmol; DMAP: 0.27 g, 2.22 mmol;

**133: 131:** 0.50 g, 2.22 mmol;  $i\text{Pr}_2\text{Me}_2\text{NHC}$ : 0.40 g, 2.22 mmol;

**134: 131:** 0.20 g, 0.89 mmol;  $\text{Mes}_2\text{H}_2\text{NHC}$ : 0.27 g, 0.89 mmol;

**135: 131:** 0.20 g, 0.89 mmol; CAAC: 0.25 g, 0.89 mmol;

**136: 99:** 0.50 g, 2.06 mmol; DMAP: 0.25 g, 2.06 mmol;

**137: 99:** 1.00 g, 4.13 mmol;  $i\text{Pr}_2\text{Me}_2\text{NHC}$ : 0.75 g, 4.13 mmol;

**138: 99:** 0.30 g, 1.24 mmol;  $\text{Mes}_2\text{H}_2\text{NHC}$ : 0.38 g, 1.24 mmol;

**139: 99:** 0.20 g, 0.83 mmol; CAAC: 0.23 g, 0.83 mmol; were dissolved in toluene. The solution was stirred at room temperature for 2 h and subsequently stored at 253 K

## 5. Experimental Details

overnight. The precipitated crystals were collected and dried *in vacuo* at room temperature for 2 h.

Yield: **132**: 0.60 g, 78%; **133**: 0.29 g, 32%;  
**134**: 0.42 g, 90%. **135**: 0.18 g, 39%;  
**136**: 0.34 g, 46%; **137**: 1.33 g, 76%;  
**138**: 0.37 g, 46%. **139**: 0.21 g, 42%;

### Compound **132**

$^1\text{H}$  NMR (400 MHz,  $\text{C}_6\text{D}_6$ , 298 K):  $\delta$ [ppm]= 8.08–7.83 (m, 2H), 7.25 (d,  $J$  = 5.4 Hz, 8H), 6.98–6.78 (m, 2H), 5.73–5.35 (m, 2H), 1.92 (s, 6H), -0.14 (s, 6H).

$^{13}\text{C}\{^1\text{H}\}$  NMR (101 MHz,  $\text{C}_6\text{D}_6$ , 298 K):  $\delta$ [ppm]= 155.17, 154.17, 146.17, 129.46, 123.96, 119.59, 106.74, -7.46.

No signal was detected in the  $^{27}\text{Al}$  NMR spectrum between +200 ppm and -200 ppm.

Elemental analysis for  $\text{C}_{21}\text{H}_{26}\text{Al}_1\text{N}_3$ : calc.: 72.60% C, 7.54% H, 12.09% N; found: 72.26% C, 7.73% H, 12.06% N.

### Crystal data of **132**

CCDC code:	2026464	
Empirical formula	$\text{C}_{21}\text{H}_{26}\text{Al}_1\text{N}_3$	
Formula weight	347.43	
Temperature	140(2) K	
Wavelength	0.71073 Å	
Crystal system	triclinic	
Space group	P-1	
Unit cell dimensions	$a = 9.8093(3)$ Å	$\alpha = 92.0190(10)^\circ$
	$b = 9.9054(3)$ Å	$\beta = 111.8790(10)^\circ$
	$c = 11.0653(3)$ Å	$\gamma = 93.1950(10)^\circ$
Volume	994.35(5) Å <sup>3</sup>	
Z	2	
Density (calculated)	1.160 mg / m <sup>3</sup>	
Absorption coefficient	0.110 mm <sup>-1</sup>	
F(000)	372	
Crystal size	0.246 x 0.155 x 0.064 mm <sup>3</sup>	

## 5. Experimental Details

Theta range for data collection	1.987 to 31.538°
Index ranges	-14<=h<=14, -14<=k<=14, -16<=l<=13
Reflections collected	29983
Independent reflections	6650 [R(int) = 0.0286]
Completeness to theta = 25.242°	100.0 %
Absorption correction	semi-empirical from equivalents
Max. and min. transmission	0.7462 and 0.7149
Refinement method	full-matrix least-squares on F <sup>2</sup>
Data / restraints / parameters	6650 / 0 / 230
Goodness-of-fit on F <sup>2</sup>	1.016
Final R indices [I>2sigma(I)]	R1 = 0.0389, wR2 = 0.1027
R indices (all data)	R1 = 0.0458, wR2 = 0.1086
Extinction coefficient	n/a
Largest diff. peak and hole	0.354 and -0.265 e.Å <sup>-3</sup>

### Compound **133**

<sup>1</sup>H NMR (300 MHz, C<sub>6</sub>D<sub>6</sub>, 298 K): δ [ppm]= 7.28 – 7.20 (m, 8H), 6.92 – 6.81 (m, 2H), 5.58 (hept, J = 7.0 Hz, 2H), 1.47 (s, 6H), 1.04 (d, J = 7.1 Hz, 12H), -0.18 (s, 6H).

<sup>13</sup>C{<sup>1</sup>H} NMR (75 MHz, C<sub>6</sub>D<sub>6</sub>, 298 K): δ [ppm]= 154.31, 129.27, 125.90, 123.66, 119.26, 51.37, 21.76, 10.00, -5.17 (d, J = 21.2 Hz).

No signal was detected in the <sup>27</sup>Al NMR spectrum between +200 ppm and -200 ppm.

Elemental analysis for C<sub>25</sub>H<sub>36</sub>Al<sub>1</sub>N<sub>3</sub>: calc.: 74.04% C, 8.95% H, 10.36% N; found: 73.41% C, 8.26% H, 9.65% N.

### Crystal data of **133**

CCDC code:	2026466
Empirical formula	C <sub>25</sub> H <sub>36</sub> Al <sub>1</sub> N <sub>3</sub>
Formula weight	405.55
Temperature	140(2) K
Wavelength	0.71073 Å
Crystal system	monoclinic
Space group	P21/c
Unit cell dimensions	a = 21.2090(7) Å      α = 90° b = 13.5587(5) Å      β = 116.1070(10)° c = 19.0138(6) Å      γ = 90°

## 5. Experimental Details

Volume	4909.9(3) Å <sup>3</sup>
Z	8
Density (calculated)	1.097 mg / m <sup>3</sup>
Absorption coefficient	0.097 mm <sup>-1</sup>
F(000)	1760
Crystal size	0.395 x 0.390 x 0.176 mm <sup>3</sup>
Theta range for data collection	2.139 to 27.000°
Index ranges	-27<=h<=27, -17<=k<=16, -23<=l<=24
Reflections collected	58798
Independent reflections	10710 [R(int) = 0.0376]
Completeness to theta = 25.242°	99.9 %
Absorption correction	semi-empirical from equivalents
Max. and min. transmission	0.7456 and 0.6937
Refinement method	full-matrix least-squares on F <sup>2</sup>
Data / restraints / parameters	10710 / 0 / 539
Goodness-of-fit on F <sup>2</sup>	1.018
Final R indices [I>2sigma(I)]	R1 = 0.0378, wR2 = 0.0946
R indices (all data)	R1 = 0.0489, wR2 = 0.1026
Extinction coefficient	n/a
Largest diff. peak and hole	0.262 and -0.276 e.Å <sup>-3</sup>

### Compound **134**

<sup>1</sup>H NMR (300 MHz, C<sub>6</sub>D<sub>6</sub>, 298 K): δ [ppm]= 7.15 – 7.07 (m, 4H), 6.85 – 6.78 (m, 2H), 6.72 (s, 4H), 6.66 (dd, J = 8.6 Hz, 1.2 Hz, 4H), 5.91 (s, 2H), 2.14 (s, 6H), 1.93 (s, 12H), -0.82 (s, 6H).

<sup>13</sup>C{<sup>1</sup>H} NMR (75 MHz, C<sub>6</sub>D<sub>6</sub>, 298 K): δ [ppm]= 174.80, 154.46, 139.70, 135.55, 135.32, 129.60, 128.76, 123.61, 123.44, 118.51, 21.03, 17.68, -6.66.

No signal was detected in the <sup>27</sup>Al NMR spectrum between +200 ppm and -200 ppm.

Elemental analysis for C<sub>35</sub>H<sub>40</sub>Al<sub>1</sub>N<sub>3</sub>: calc.: 79.36% C, 7.61% H, 7.93% N; found: 79.37% C, 7.11% H, 7.55% N.

### Crystal data of **134**

CCDC code:	2026467
Empirical formula	C <sub>35</sub> H <sub>40</sub> Al <sub>1</sub> N <sub>3</sub>
Formula weight	529.68
Temperature	132(2) K

## 5. Experimental Details

Wavelength	0.71073 Å
Crystal system	orthorhombic
Space group	Pbca
Unit cell dimensions	a = 15.0291(7) Å $\alpha = 90^\circ$ b = 15.4656(6) Å $\beta = 90^\circ$ c = 25.8775(11) Å $\gamma = 90^\circ$
Volume	6014.8(4) Å <sup>3</sup>
Z	8
Density (calculated)	1.170 mg / m <sup>3</sup>
Absorption coefficient	0.095 mm <sup>-1</sup>
F(000)	2272
Crystal size	0.382 x 0.316 x 0.112 mm <sup>3</sup>
Theta range for data collection	2.047 to 29.579°
Index ranges	-20 ≤ h ≤ 20, -21 ≤ k ≤ 21, -21 ≤ l ≤ 35
Reflections collected	46769
Independent reflections	8417 [R(int) = 0.0615]
Completeness to theta = 25.242°	100.0 %
Absorption correction	semi-empirical from equivalents
Max. and min. transmission	0.7459 and 0.6940
Refinement method	full-matrix least-squares on F <sup>2</sup>
Data / restraints / parameters	8417 / 0 / 360
Goodness-of-fit on F <sup>2</sup>	1.024
Final R indices [I > 2σ(I)]	R1 = 0.0489, wR2 = 0.1214
R indices (all data)	R1 = 0.0860, wR2 = 0.1421
Extinction coefficient	n/a
Largest diff. peak and hole	0.345 and -0.253 e.Å <sup>-3</sup>

### Compound 135

<sup>1</sup>H NMR (400 MHz, C<sub>6</sub>D<sub>6</sub>, 298 K):  $\delta$ [ppm]= 7.28 (m, 4H), 7.12 – 7.06 (m, 5H), 7.02–6.98 (m, 2H), 6.95 – 6.87 (m, 2H), 2.86 – 2.74 (m, 2H), 1.51 (s, 6H), 1.40 (d,  $J = 6.6$  Hz, 6H), 1.29 (s, 2H), 1.10 (d,  $J = 6.5$  Hz, 6H), 0.81 (s, 2H), -0.81 (s, 6H).

<sup>13</sup>C{<sup>1</sup>H} NMR (101 MHz, C<sub>6</sub>D<sub>6</sub>, 298 K):  $\delta$ [ppm]= 252.4, 154.4, 145.6, 134.3, 129.9, 129.2, 125.8, 124.4, 119.2, 82.2, 57.2, 51.2, 29.6, 29.3, 29.0, 27.6, 25.2, -5.0.

No signal was detected in the <sup>27</sup>Al NMR spectrum between +200 ppm and -200 ppm.

## 5. Experimental Details

Elemental analysis for  $C_{34}H_{47}Al_1N_2$ : calc.: 79.96% C, 9.28% H, 5.48% N; found: 80.37% C, 9.43% H, 5.07% N.

### Crystal data of **135**

CCDC code:	2026465
Empirical formula	$C_{34}H_{47}Al_1N_2$
Formula weight	510.71
Temperature	140(2) K
Wavelength	0.71073 Å
Crystal system	monoclinic
Space group	P21/n
Unit cell dimensions	$a = 10.6632(2)$ Å $\alpha = 90^\circ$ $b = 13.3867(3)$ Å $\beta = 90.1850(10)^\circ$ $c = 20.8815(4)$ Å $\gamma = 90^\circ$
Volume	$2980.72(10)$ Å <sup>3</sup>
Z	4
Density (calculated)	1.138 mg / m <sup>3</sup>
Absorption coefficient	0.092 mm <sup>-1</sup>
F(000)	1112
Crystal size	0.200 x 0.198 x 0.076 mm <sup>3</sup>
Theta range for data collection	2.142 to 29.592°
Index ranges	-13<=h<=14, -18<=k<=16, -29<=l<=29
Reflections collected	43546
Independent reflections	8371 [R(int) = 0.0656]
Completeness to theta = 25.242°	99.7 %
Absorption correction	semi-empirical from equivalents
Max. and min. transmission	0.7459 and 0.6990
Refinement method	full-matrix least-squares on F <sup>2</sup>
Data / restraints / parameters	8371 / 0 / 344
Goodness-of-fit on F <sup>2</sup>	1.051
Final R indices [I>2sigma(I)]	R1 = 0.0485, wR2 = 0.1117
R indices (all data)	R1 = 0.0755, wR2 = 0.1271
Extinction coefficient	n/a
Largest diff. peak and hole	0.299 and -0.319 e.Å <sup>-3</sup>



## 5. Experimental Details

### Compound **136**

$^1\text{H}$  NMR (400 MHz,  $\text{C}_6\text{D}_6$ , 298 K):  $\delta$  [ppm]= 7.87 – 7.86 (m; 4-H; 2H), 7.84 – 7.80 (m, 4H), 7.17 – 7.13 (m, 4H), 7.04 – 7.00 (m, 2H), 5.51 – 5.50 (m, 2H), 1.87 (s, 6H), -0.01 (d,  $J$  = 2.3 Hz; 6H).

$^{13}\text{C}\{^1\text{H}\}$  NMR (101 MHz,  $\text{C}_6\text{D}_6$ , 298 K):  $\delta$  [ppm]= 155.1, 146.5, 143.4 (d,  $J$  = 23.0 Hz), 133.8 (d,  $J$  = 15.6 Hz), 128.9 (d,  $J$  = 6.2 Hz), 125.1, 106.5, 38.2, -8.8 (d,  $J$  = 16.0 Hz).

$^{31}\text{P}\{^1\text{H}\}$  NMR (162 MHz, 298 K):  $\delta$  [ppm]= -56.3.

No signal was detected in the  $^{27}\text{Al}$  spectrum NMR between +200 ppm and -200 ppm.

Elemental analysis for  $\text{C}_{21}\text{H}_{26}\text{Al}_1\text{N}_2\text{P}_1$ : calc.: 69.22% C, 7.19% H; 7.69% N; found: 68.00% C, 7.02% H; 6.87% N.

### Crystal data of **136**

CCDC code:	2026468	
Empirical formula	$\text{C}_{21}\text{H}_{26}\text{Al}_1\text{N}_2\text{P}_1$	
Formula weight	364.39	
Temperature	123(2) K	
Wavelength	0.71073 Å	
Crystal system	triclinic	
Space group	P-1	
Unit cell dimensions	$a = 9.9589(2)$ Å	$\alpha = 94.0502(8)^\circ$
	$b = 10.2221(2)$ Å	$\beta = 108.6943(7)^\circ$
	$c = 12.6901(3)$ Å	$\gamma = 118.8144(7)^\circ$
Volume	1032.00(4) Å <sup>3</sup>	
Z	2	
Density (calculated)	1.173 mg / m <sup>3</sup>	
Absorption coefficient	0.181 mm <sup>-1</sup>	
F(000)	388	
Crystal size	0.241 x 0.198 x 0.152 mm <sup>3</sup>	
Theta range for data collection	2.363 to 30.526°	
Index ranges	-14 ≤ h ≤ 14, -14 ≤ k ≤ 14, -18 ≤ l ≤ 18	
Reflections collected	30856	
Independent reflections	6306 [R(int) = 0.0211]	
Completeness to theta = 25.242°	99.9 %	
Absorption correction	semi-empirical from equivalents	

## 5. Experimental Details

Max. and min. transmission	0.7461 and 0.7196
Refinement method	full-matrix least-squares on $F^2$
Data / restraints / parameters	6306 / 0 / 308
Goodness-of-fit on $F^2$	1.048
Final R indices [ $I > 2\sigma(I)$ ]	R1 = 0.0385, wR2 = 0.1074
R indices (all data)	R1 = 0.0425, wR2 = 0.1113
Extinction coefficient	n/a
Largest diff. peak and hole	0.654 and -0.588 e.Å <sup>-3</sup>

### Compound **137**

<sup>1</sup>H NMR (400 MHz, C<sub>6</sub>D<sub>6</sub>, 298 K):  $\delta$ [ppm]= 7.86 – 6.99 (m; 10H), 5.41 (d sep;  $J = 7.1$  Hz,  $J = 3.0$  Hz, 2H), 1.44 (s; 6H), 1.01 (d;  $J = 7.1$  Hz, 12H), -0.03 (d;  $J = 2.4$  Hz, 6H).

<sup>13</sup>C{<sup>1</sup>H} NMR (101 MHz, C<sub>6</sub>D<sub>6</sub>, 298 K):  $\delta$ [ppm]= 169.2 (d,  $J = 20.0$  Hz), 144.4 (d,  $J = 23.9$  Hz), 134.0 (d,  $J = 15.5$  Hz), 128.8 (d,  $J = 6.2$  Hz), 126.1, 125.0, 52.0 (d,  $J = 6.6$  Hz), 21.8, 10.0, -7.0.

<sup>31</sup>P{<sup>1</sup>H} NMR (162 MHz, C<sub>6</sub>D<sub>6</sub>, 298 K): -53.5.

No signal was detected in the <sup>27</sup>Al NMR spectrum between 200 ppm and -200 ppm.

Elemental analysis for C<sub>25</sub>H<sub>36</sub>Al<sub>1</sub>N<sub>2</sub>P<sub>1</sub>: calc.: 71.07% C, 8.59% H; 6.63% N; found: 70.12% C, 8.54% H; 6.34% N.

### Crystal data of **137**

CCDC code:	2026470
Empirical formula	C <sub>25</sub> H <sub>36</sub> Al <sub>1</sub> N <sub>2</sub> P <sub>1</sub>
Formula weight	422.51
Temperature	130(2) K
Wavelength	0.71073 Å
Crystal system	monoclinic
Space group	P21/n
Unit cell dimensions	a = 8.9520(8) Å $\alpha = 90^\circ$ b = 27.693(3) Å $\beta = 95.255(3)^\circ$ c = 10.0602(8) Å $\gamma = 90^\circ$
Volume	2483.5(4) Å <sup>3</sup>
Z	4
Density (calculated)	1.130 mg / m <sup>3</sup>

## 5. Experimental Details

Absorption coefficient	0.159 mm <sup>-1</sup>
F(000)	912
Crystal size	0.160 x 0.065 x 0.042 mm <sup>3</sup>
Theta range for data collection	2.162 to 26.444°
Index ranges	-11<=h<=11, -34<=k<=34, -12<=l<=12
Reflections collected	57265
Independent reflections	5115 [R(int) = 0.1349]
Completeness to theta = 25.242°	99.9 %
Absorption correction	semi-empirical from equivalents
Max. and min. transmission	0.7454 and 0.6383
Refinement method	full-matrix least-squares on F <sup>2</sup>
Data / restraints / parameters	5115 / 0 / 406
Goodness-of-fit on F <sup>2</sup>	1.078
Final R indices [I>2sigma(I)]	R1 = 0.0690, wR2 = 0.1791
R indices (all data)	R1 = 0.0946, wR2 = 0.1982
Extinction coefficient	n/a
Largest diff. peak and hole	0.697 and -0.370 e.Å <sup>-3</sup>

### Compound **138**

<sup>1</sup>H NMR (400 MHz, C<sub>6</sub>D<sub>6</sub>, 298 K): δ [ppm]= 7.56 (t, *J* = 6.9 Hz, 4H), 7.08 (d, *J* = 7.3 Hz, 4H), 7.00 (d, *J* = 7.2 Hz, 2H), 6.70 (s, 3H), 5.89 (s, 2H), 2.08 (s, 6H), 2.03 (s, 12H), -0.92 (s, 6H).

<sup>13</sup>C{<sup>1</sup>H} NMR (101 MHz, C<sub>6</sub>D<sub>6</sub>, 298 K): δ [ppm]= 174.4 (d, *J* = 28.4 Hz), 144.2 (d, *J* = 23.0 Hz), 139.8, 135.4, 135.0 (d, *J* = 16.1 Hz), 134.3 (d, *J* = 17.0 Hz), 129.6, 127.6 (d, *J* = 6.0 Hz), 124.8, 123.3, 21.1, 18.06 (d, *J* = 5.2 Hz), -8.9 (br. s).

<sup>31</sup>P{<sup>1</sup>H} NMR (162 MHz, C<sub>6</sub>D<sub>6</sub>, 298 K): δ [ppm]= -53.7.

No signal was detected in the <sup>27</sup>Al NMR spectrum between +200 ppm and -200 ppm.

Elemental analysis for C<sub>35</sub>H<sub>40</sub>Al<sub>1</sub>N<sub>2</sub>P<sub>1</sub>: calc.: 76.90% C, 7.38% H; 5.12% N; found: 76.46% C, 6.93% H; 4.84% N.

### Crystal data of **138**

CCDC code:	2026471
Empirical formula	C <sub>35</sub> H <sub>40</sub> Al <sub>1</sub> N <sub>2</sub> P <sub>1</sub>
Formula weight	546.64
Temperature	132(2) K

## 5. Experimental Details

Wavelength	0.71073 Å
Crystal system	orthorhombic
Space group	Pbca
Unit cell dimensions	a = 16.0908(3) Å $\alpha = 90^\circ$ b = 18.9918(3) Å $\beta = 90^\circ$ c = 20.8423(3) Å $\gamma = 90^\circ$
Volume	6369.27(18) Å <sup>3</sup>
Z	8
Density (calculated)	1.140 mg / m <sup>3</sup>
Absorption coefficient	0.139 mm <sup>-1</sup>
F(000)	2336
Crystal size	0.511 x 0.321 x 0.094 mm <sup>3</sup>
Theta range for data collection	1.925 to 30.084°
Index ranges	-22 ≤ h ≤ 21, -26 ≤ k ≤ 26, -29 ≤ l ≤ 29
Reflections collected	45867
Independent reflections	9346 [R(int) = 0.0678]
Completeness to theta = 25.242°	100.0 %
Absorption correction	semi-empirical from equivalents
Max. and min. transmission	0.7460 and 0.6613
Refinement method	full-matrix least-squares on F <sup>2</sup>
Data / restraints / parameters	9346 / 0 / 501
Goodness-of-fit on F <sup>2</sup>	1.004
Final R indices [I > 2σ(I)]	R1 = 0.0462, wR2 = 0.0981
R indices (all data)	R1 = 0.0951, wR2 = 0.1181
Extinction coefficient	n/a
Largest diff. peak and hole	0.270 and -0.285 e.Å <sup>-3</sup>

### Compound 139

<sup>1</sup>H NMR (400 MHz, C<sub>6</sub>D<sub>6</sub>, 298 K):  $\delta$ [ppm] = 7.93 (t,  $J$  = 6.6 Hz, 4H), 7.19 – 7.17 (m, 1H), 7.15 – 7.10 (m, 2H), 7.07 – 6.99 (m, 4H), 6.94 (d,  $J$  = 7.8 Hz, 2H), 2.59 (sep,  $J$  = 6.6 Hz; 2H), 1.64 (s, 6H), 1.33 (s, 2H), 1.15 (d,  $J$  = 6.6 Hz, 6H), 1.02 (d,  $J$  = 6.6 Hz, 6H), 0.79 (s, 6H), -0.74 (d,  $J$  = 2.4 Hz; 6H).

<sup>13</sup>C{<sup>1</sup>H} NMR (101 MHz, C<sub>6</sub>D<sub>6</sub>, 298 K):  $\delta$ [ppm] = 249.9 (d,  $J$  = 18.6 Hz), 145.3, 143.7 (d,  $J$  = 22.8 Hz), 135.8 (d,  $J$  = 16.0 Hz), 135.0, 134.2, 130.2, 127.9 (d,  $J$  = 6.3 Hz), 125.5 (d,  $J$  = 15.8 Hz), 81.7, 56.9 (d,  $J$  = 1.8 Hz), 51.0 (d,  $J$  = 2.3 Hz), 29.2 (d,  $J$  = 12.1 Hz), 29.0 (d,  $J$  = 11.9 Hz), 26.5, 24.6, -6.5 (br. s).

## 5. Experimental Details

$^{31}\text{P}\{^1\text{H}\}$  NMR (162 MHz,  $\text{C}_6\text{D}_6$ , 298 K):  $\delta$  [ppm] = -49.3.

No signal was detected in the  $^{27}\text{Al}$  NMR spectrum between +200 ppm and -200 ppm.

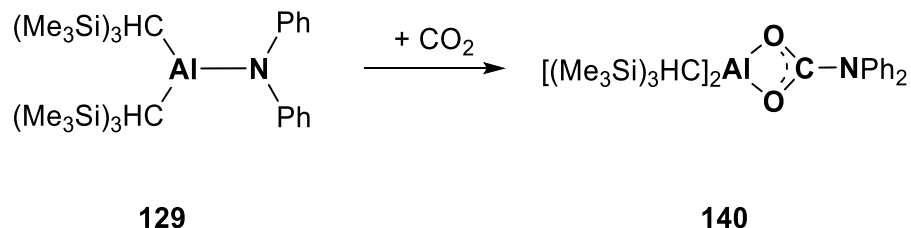
Elemental analysis for  $\text{C}_{41}\text{H}_{55}\text{Al}_1\text{N}_1\text{P}_1$  (+ 1eq toluene): calc.: 79.45% C, 8.94% H; 2.26% N; found: 79.32% C, 9.40% H; 2.01% N.

### Crystal data of **139**

CCDC code:	2026469
Empirical formula	$\text{C}_{34}\text{H}_{37}\text{Al}_1\text{N}_1\text{P}_1, 0.5(\text{C}_7\text{H}_8)$
Formula weight	573.74
Temperature	122(2) K
Wavelength	0.71073 Å
Crystal system	monoclinic
Space group	P21/c
Unit cell dimensions	$a = 10.9000(2)$ Å $\alpha = 90^\circ$ $b = 23.3528(6)$ Å $\beta = 107.0948(8)^\circ$ $c = 13.9995(4)$ Å $\gamma = 90^\circ$
Volume	3406.07(15) Å <sup>3</sup>
Z	4
Density (calculated)	1.119 mg / m <sup>3</sup>
Absorption coefficient	0.132 mm <sup>-1</sup>
F(000)	1244
Crystal size	0.462 x 0.370 x 0.106 mm <sup>3</sup>
Theta range for data collection	1.955 to 30.532°
Index ranges	-15 ≤ h ≤ 15, -26 ≤ k ≤ 33, -17 ≤ l ≤ 19
Reflections collected	40633
Independent reflections	10381 [R(int) = 0.0310]
Completeness to theta = 25.242°	100.0 %
Absorption correction	semi-empirical from equivalents
Max. and min. transmission	0.7461 and 0.6895
Refinement method	full-matrix least-squares on F <sup>2</sup>
Data / restraints / parameters	10381 / 48 / 382
Goodness-of-fit on F <sup>2</sup>	1.025
Final R indices [I > 2σ(I)]	R1 = 0.0493, wR2 = 0.1308
R indices (all data)	R1 = 0.0618, wR2 = 0.1399
Extinction coefficient	n/a
Largest diff. peak and hole	0.900 and -0.427 e.Å <sup>-3</sup>

## 5. Experimental Details

### 5.2.15. Synthesis of **140**:



The aminoalane **129** used in the synthesis of **142** was generated *in situ*.

$[(\text{Me}_3\text{Si})_2\text{CH}]_2\text{AlCl}$  (0.47 g, 1.23 mmol) and  $\text{Ph}_2\text{NLi}$  (0.22 g, 1.23 mmol) were suspended in 10 ml of toluene. The reaction mixture was stirred at room temperature overnight. After filtration over celite, the solution was stirred at room temperature in  $\text{CO}_2$ -atmosphere for 17 h. After concentration of the solution to the half in vacuum, subsequently stored at 253 K overnight to precipitate colorless crystals **140**, which were collected and washed with hexane und dried under vacuum.

Yield: 98 mg of **140**, 0.18 mmol, 14%.

$^1\text{H}$  NMR (300 MHz,  $\text{C}_6\text{D}_6$ , 298 K):  $\delta$ [ppm]= 7.36 (dd,  $J = 8.6$  Hz, 1.3 Hz, 4H), 7.03 – 6.96 (m, 4H), 6.87 – 6.79 (m, 2H), 0.31 (s, 38H), -0.84 (s, 2H).

$^{13}\text{C}\{^1\text{H}\}$  NMR (75 MHz,  $\text{C}_6\text{D}_6$ , 298 K):  $\delta$ [ppm]= 165.82, 140.92, 129.51, 127.62, 126.72, 4.18, 1.46.

$^{29}\text{Si}\{^1\text{H}\}$  NMR (60 MHz,  $\text{C}_6\text{D}_6$ , 298 K):  $\delta$ [ppm]= -1.6.

IR [ $\text{cm}^{-1}$ ]: 2948, 1517, 1494, 1072, 623.

No signal was detected in the  $^{27}\text{Al}$  NMR spectrum between +200 ppm and -200 ppm.

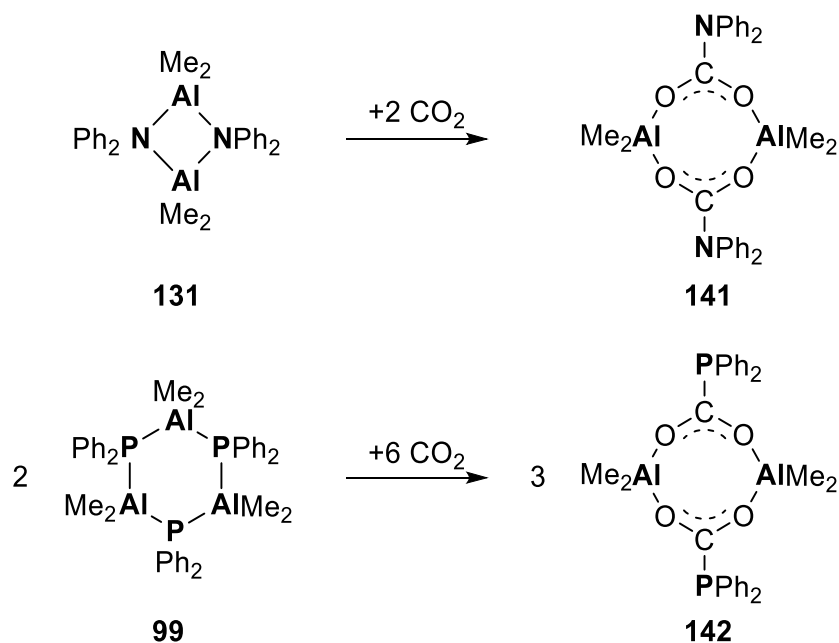
Elemental analysis for  $\text{C}_{27}\text{H}_{49}\text{Al}_1\text{N}_1\text{O}_2\text{Si}_4$ : calc.: 58.01% C, 8.84% H; 2.51% N; found: 58.24% C, 8.41% H; 2.35% N.

#### Crystal data of **140**

CCDC code	2026472
Empirical formula	$\text{C}_{27}\text{H}_{48}\text{Al}_1\text{N}_1\text{O}_2\text{Si}_4$
Formula weight	558.00

## 5. Experimental Details

Temperature	133(2) K
Wavelength	0.71073 Å
Crystal system	monoclinic
Space group	P21/c
Unit cell dimensions	$a = 11.7758(3) \text{ \AA}$ $\alpha = 90^\circ$ $b = 23.7354(5) \text{ \AA}$ $\beta = 114.9370(10)^\circ$ $c = 13.0842(3) \text{ \AA}$ $\gamma = 90^\circ$
Volume	3316.13(14) Å <sup>3</sup>
Z	4
Density (calculated)	1.118 mg / m <sup>3</sup>
Absorption coefficient	0.228 mm <sup>-1</sup>
F(000)	1208
Crystal size	0.318 x 0.272 x 0.183 mm <sup>3</sup>
Theta range for data collection	1.919 to 31.533°
Index ranges	-17 ≤ h ≤ 16, -34 ≤ k ≤ 34, -19 ≤ l ≤ 19
Reflections collected	69021
Independent reflections	11059 [R(int) = 0.0299]
Completeness to theta = 25.242°	100.0 %
Absorption correction	semi-empirical from equivalents
Max. and min. transmission	0.7462 and 0.6903
Refinement method	full-matrix least-squares on F <sup>2</sup>
Data / restraints / parameters	11059 / 0 / 328
Goodness-of-fit on F <sup>2</sup>	1.033
Final R indices [I > 2σ(I)]	R1 = 0.0305, wR2 = 0.0814
R indices (all data)	R1 = 0.0385, wR2 = 0.0869
Extinction coefficient	n/a
Largest diff. peak and hole	0.354 and -0.229 e. Å <sup>-3</sup>

5.2.16. Synthesis of **141** and **142**:

**131** (0.50 g, 1.11 mmol) or **99** (1.0 g, 1.38 mmol) were dissolved in toluene. The solution was stirred at room temperature in CO<sub>2</sub>-atmosphere for 17 h. After concentration of the solution to the half in vacuum, subsequently stored at 253 K overnight to precipitate a colorless crystal, which were collected and washed with hexane und dried under vacuum.

Yield: 0.42 g of **141**, 0.78 mmol, 70%; 0.28 g of **142**, 0.49 mmol, 37%.

Compound **141**

<sup>1</sup>H NMR (400 MHz, C<sub>6</sub>D<sub>6</sub>, 298 K): δ [ppm]= 7.10 – 7.05 (m, 4H), 6.99 – 6.90 (m, 4H), 6.90 – 6.82 (m, 2H), -0.49 (s, 6H).

<sup>13</sup>C{<sup>1</sup>H} NMR (101 MHz, C<sub>6</sub>D<sub>6</sub>, 298 K): δ [ppm]= 158.4, 141.8, 129.3, 127.4, 127.3, -11.0.

IR [cm<sup>-1</sup>]: 3048, 2937, 2362, 1611, 1572, 1491, 1467, 1431, 683.

No signal was detected in the <sup>27</sup>Al NMR spectrum between +200 ppm and -200 ppm.

Elemental analysis for C<sub>30</sub>H<sub>32</sub>Al<sub>2</sub>N<sub>2</sub>O<sub>4</sub>: calc.: 66.91% C, 5.99% H; 5.20% N; found: 66.13% C, 5.75% H; 5.04% N.



## 5. Experimental Details

### Crystal data of **141**

CCDC code:	2026473
Empirical formula	$C_{30}H_{32}Al_2N_2O_4 \cdot 2(C_7H_8)$
Formula weight	722.80
Temperature	132(2) K
Wavelength	0.71073 Å
Crystal system	triclinic
Space group	P-1
Unit cell dimensions	$a = 9.7368(7)$ Å $\alpha = 69.808(2)^\circ$ $b = 9.7451(7)$ Å $\beta = 89.030(2)^\circ$ $c = 12.1320(8)$ Å $\gamma = 71.680(2)^\circ$
Volume	1020.22(12) Å <sup>3</sup>
Z	1
Density (calculated)	1.176 mg / m <sup>3</sup>
Absorption coefficient	0.114 mm <sup>-1</sup>
F(000)	384
Crystal size	0.331 x 0.207 x 0.056 mm <sup>3</sup>
Theta range for data collection	1.798 to 28.744°
Index ranges	-12 ≤ h ≤ 13, -13 ≤ k ≤ 13, -16 ≤ l ≤ 16
Reflections collected	15293
Independent reflections	5279 [R(int) = 0.0373]
Completeness to theta = 25.242°	100.0 %
Absorption correction	semi-empirical from equivalents
Max. and min. transmission	0.7458 and 0.7019
Refinement method	full-matrix least-squares on F <sup>2</sup>
Data / restraints / parameters	5279 / 0 / 315
Goodness-of-fit on F <sup>2</sup>	1.045
Final R indices [I > 2σ(I)]	R1 = 0.0453, wR2 = 0.0955
R indices (all data)	R1 = 0.0848, wR2 = 0.1089
Extinction coefficient	n/a
Largest diff. peak and hole	0.336 and -0.246 e.Å <sup>-3</sup>

### Compound **142**

<sup>1</sup>H NMR (400 MHz, C<sub>6</sub>D<sub>6</sub>, 298 K):  $\delta$  [ppm] = 7.47 – 7.39 (m, 4H), 7.02 (m, 6H), -0.60 (s, 6H).

<sup>13</sup>C{<sup>1</sup>H} NMR (101 MHz, C<sub>6</sub>D<sub>6</sub>, 298 K):  $\delta$  [ppm] = 193.6 (d,  $J$  = 16.7 Hz), 134.9 (d,  $J$  = 20.0 Hz), 131.1 (d,  $J$  = 3.0 Hz), 130.3, 129.1 (d,  $J$  = 8.3 Hz), -11.2.

## 5. Experimental Details

$^{31}\text{P}\{^1\text{H}\}$  NMR (162 MHz,  $\text{C}_6\text{D}_6$ , 298 K):  $\delta$  [ppm] = 5.2.

IR [ $\text{cm}^{-1}$ ]: 3052, 2937, 1591, 1388, 686.

No signal was detected in the  $^{27}\text{Al}$  NMR spectrum between +200 ppm and -200 ppm.

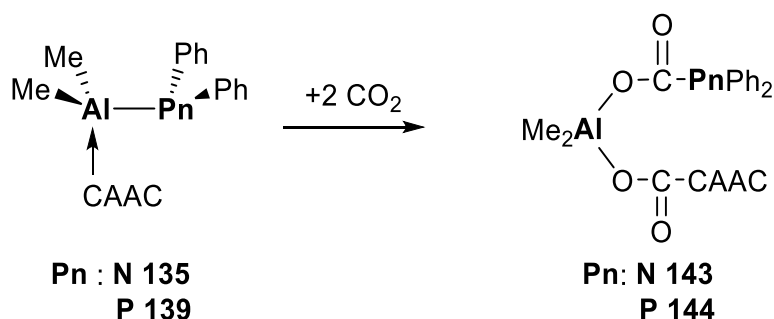
Elemental analysis for  $\text{C}_{30}\text{H}_{32}\text{Al}_2\text{P}_2\text{O}_2$ : calc.: 62.94% C, 5.63% H; found: 62.13% C, 5.78% H.

### Crystal data of **142**

CCDC code:	2026474
Empirical formula	$\text{C}_{30}\text{H}_{32}\text{Al}_2\text{O}_4\text{P}_2$
Formula weight	572.45
Temperature	133(2) K
Wavelength	0.71073 Å
Crystal system	monoclinic
Space group	P21/n
Unit cell dimensions	$a = 6.0725(2)$ Å $\alpha = 90^\circ$ $b = 11.9669(5)$ Å $\beta = 97.291(2)^\circ$ $c = 20.9811(8)$ Å $\gamma = 90^\circ$
Volume	1512.35(10) Å <sup>3</sup>
Z	2
Density (calculated)	1.257 mg / m <sup>3</sup>
Absorption coefficient	0.234 mm <sup>-1</sup>
F(000)	600
Crystal size	0.415 x 0.175 x 0.038 mm <sup>3</sup>
Theta range for data collection	1.963 to 34.992°
Index ranges	-9 ≤ h ≤ 9, -19 ≤ k ≤ 19, -33 ≤ l ≤ 33
Reflections collected	36944
Independent reflections	6641 [R(int) = 0.0395]
Completeness to theta = 25.242°	100.0 %
Absorption correction	semi-empirical from equivalents
Max. and min. transmission	0.7469 and 0.6575
Refinement method	full-matrix least-squares on F <sup>2</sup>
Data / restraints / parameters	6641 / 0 / 174
Goodness-of-fit on F <sup>2</sup>	1.068
Final R indices [I > 2σ(I)]	R1 = 0.0458, wR2 = 0.1172
R indices (all data)	R1 = 0.0623, wR2 = 0.1270
Extinction coefficient	n/a
Largest diff. peak and hole	0.778 and -0.337 e.Å <sup>-3</sup>

## 5. Experimental Details

### 5.2.17. Synthesis of 143 and 144:



**135** (0.30 g, 0.59 mmol) or **139** (1.03 g, 1.41 mmol) were dissolved in toluene. The solution was stirred at room temperature in CO<sub>2</sub>-atmosphere for 17 h. After concentration of the solution to the half in vacuum, subsequently stored at 253 K overnight to precipitate a colorless crystal, which were collected and washed with hexane und dried under vacuum.

Yield: 0.28 g of **143**, 0.47 mmol, 79%; 0.31 g of **144**; 0.50 mmol, 77%.

#### Compound **143**

<sup>1</sup>H NMR (400 MHz, C<sub>6</sub>D<sub>6</sub>, 298 K):  $\delta$ [ppm]= 7.87 (td,  $J = 7.9$  Hz, 1.4 Hz, 4H), 7.19 – 6.98 (m, 8H), 6.89 (d,  $J = 7.8$  Hz Hz, 2H), 2.42 (q,  $J = 6.6$  Hz Hz, 2H), 1.55 (s, 2H), 1.39 (s, 6H), 1.34 (d,  $J = 6.5$  Hz, 6H), 1.02 (d,  $J = 6.6$  Hz, 6H), 0.82 (s, 6H), -0.29 (s, 6H).

<sup>13</sup>C{<sup>1</sup>H} NMR (101 MHz, C<sub>6</sub>D<sub>6</sub>, 298 K):  $\delta$ [ppm]= 194.0, 158.35, 157.63, 156.43, 146.30, 141.79, 129.34, 129.28, 127.41, 127.28, 125.77, 49.42, 30.23, 29.92, 28.84, 28.18, 26.75, 24.34, -8.98, -11.00.

IR [cm<sup>-1</sup>]: 3060, 2973, 1699, 1656, 1375, 759, 676.

No signal was detected in the <sup>27</sup>Al NMR spectrum between +200 ppm and -200 ppm.

Elemental analysis for C<sub>36</sub>H<sub>47</sub>Al<sub>1</sub>N<sub>1</sub>O<sub>4</sub>P<sub>1</sub>: calc.: 70.22% C, 7.69% H; 2.27% N; found: 70.24% C, 7.68% H; 1.89 % N.

#### Crystal data of **143**

CCDC code	2026475
Empirical formula	C <sub>36</sub> H <sub>47</sub> Al <sub>1</sub> N <sub>2</sub> O <sub>4</sub>
Formula weight	598.73

## 5. Experimental Details

Temperature	140(2) K
Wavelength	0.71073 Å
Crystal system	monoclinic
Space group	P21/n
Unit cell dimensions	$a = 11.2204(3) \text{ \AA}$ $\alpha = 90^\circ$ $b = 15.1846(3) \text{ \AA}$ $\beta = 94.3880(10)^\circ$ $c = 20.2678(5) \text{ \AA}$ $\gamma = 90^\circ$
Volume	3443.05(14) Å <sup>3</sup>
Z	4
Density (calculated)	1.155 mg / m <sup>3</sup>
Absorption coefficient	0.098 mm <sup>-1</sup>
F(000)	1288
Crystal size	0.632 x 0.270 x 0.267 mm <sup>3</sup>
Theta range for data collection	2.261 to 27.935°
Index ranges	-14 ≤ h ≤ 14, -19 ≤ k ≤ 18, -26 ≤ l ≤ 26
Reflections collected	42871
Independent reflections	8216 [R(int) = 0.0361]
Completeness to theta = 25.242°	99.6 %
Absorption correction	semi-empirical from equivalents
Max. and min. transmission	0.7456 and 0.7027
Refinement method	full-matrix least-squares on F <sup>2</sup>
Data / restraints / parameters	8216 / 0 / 398
Goodness-of-fit on F <sup>2</sup>	1.045
Final R indices [I > 2σ(I)]	R1 = 0.0413, wR2 = 0.1030
R indices (all data)	R1 = 0.0558, wR2 = 0.1121
Extinction coefficient	n/a
Largest diff. peak and hole	0.248 and -0.257 e.Å <sup>-3</sup>

### Compound 144

<sup>1</sup>H NMR (400 MHz, C<sub>6</sub>D<sub>6</sub>, 298 K): δ [ppm] = 7.87 (td, *J* = 7.9 Hz, 1.4 Hz, 4H), 7.19 – 6.98 (m, 8H), 6.89 (d, *J* = 7.8 Hz, 2H), 2.42 (q, *J* = 6.6 Hz, 2H), 1.55 (s, 2H), 1.39 (s, 6H), 1.34 (d, *J* = 6.5 Hz, 6H), 1.03 (d, 6H), 0.82 (s, *J* = 6.6 Hz, 6H), -0.29 (s, 6H).

<sup>13</sup>C{<sup>1</sup>H} NMR (101 MHz, C<sub>6</sub>D<sub>6</sub>, 298 K): δ [ppm] = 192.7, 179.6, 157.3, 145.5, 137.7 (d, *J* = 8.4 Hz), 135.2 (d, *J* = 18.2 Hz), 131.6, 129.34, 125.9, 125.7, 81.4, 49.2, 30.2, 29.8, 28.1, 28.0, 26.5, 24.3, -9.1 (signals of carbene-C and carbonyl-C were detected in <sup>1</sup>H-<sup>13</sup>C-HMBC).

## 5. Experimental Details

$^{31}\text{P}\{^1\text{H}\}$  NMR (162 MHz,  $\text{C}_6\text{D}_6$ , 298 K):  $\delta$  [ppm] = -3.2.

IR [ $\text{cm}^{-1}$ ]: 3066, 2972, 1697, 1625, 1259, 696, 665.

No signal was detected in the  $^{27}\text{Al}$  NMR spectrum between +200 ppm and -200 ppm.

Elemental analysis for  $\text{C}_{30}\text{H}_{32}\text{Al}_2\text{N}_2\text{O}_4$ : calc.: 66.91% C, 5.99% H; 5.20% N; found: 66.13% C, 5.75% H; 5.04% N.

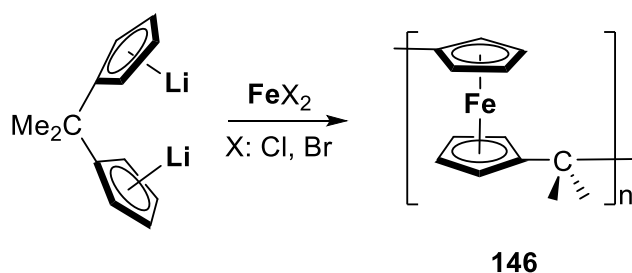
Crystal data of **144**

CCDC code	2026476
Empirical formula	$\text{C}_{36}\text{H}_{47}\text{Al}_1\text{N}_1\text{O}_4\text{P}_1$
Formula weight	615.69
Temperature	130(2) K
Wavelength	0.71073 Å
Crystal system	monoclinic
Space group	P21/n
Unit cell dimensions	$a = 13.0443(2)$ Å $\alpha = 90^\circ$ $b = 15.1370(3)$ Å $\beta = 90.8661(7)^\circ$ $c = 17.6587(3)$ Å $\gamma = 90^\circ$
Volume	3486.34(11) Å <sup>3</sup>
Z	4
Density (calculated)	1.173 mg / m <sup>3</sup>
Absorption coefficient	0.141 mm <sup>-1</sup>
F(000)	1320
Crystal size	0.291 x 0.278 x 0.094 mm <sup>3</sup>
Theta range for data collection	2.061 to 28.729°
Index ranges	-17 ≤ h ≤ 17, -20 ≤ k ≤ 20, -23 ≤ l ≤ 23
Reflections collected	104035
Independent reflections	9027 [R(int) = 0.0329]
Completeness to theta = 25.242°	100.0 %
Absorption correction	semi-empirical from equivalents
Max. and min. transmission	0.7458 and 0.7253
Refinement method	full-matrix least-squares on F <sup>2</sup>
Data / restraints / parameters	9027 / 63 / 426
Goodness-of-fit on F <sup>2</sup>	1.054
Final R indices [I > 2σ(I)]	R1 = 0.0399, wR2 = 0.1069
R indices (all data)	R1 = 0.0455, wR2 = 0.1119
Extinction coefficient	n/a
Largest diff. peak and hole	0.360 and -0.340 e.Å <sup>-3</sup>

## 5. Experimental Details

### 5.2.18. Synthesis of 146:

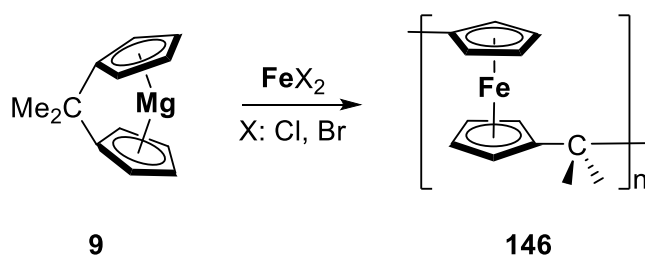
Method A:



Dilithium 2,2-bis(cyclopentadienide)propane (1.0 g, 5.43 mmol) and iron(II)-chloride (0.7 g, 5.43 mmol) or iron(II)-bromide (1.2 g, 5.43 mmol) were mixed and dissolved in 100 ml of dry thf. After the mixture was stirred overnight (during the stirring, the mixture turned from yellow to red/brown) under an inert gas atmosphere at ambient temperature, the reaction mixture was poured into 200 ml of an ice-cold hexane/methanol/water mixture (10:9:1 by volume). The product was then precipitated and collected by filtration, washed several times with water, and dried *in vacuo*. The material was diluted with thf to separate all insoluble components by filtration. The addition of cold hexane again led to precipitate the product that afforded after drying *in vacuo* at 353 K for 3 h as a pale-yellow powder

Yield: from FeCl<sub>2</sub>: 12 mg; from FeBr<sub>2</sub>: 115 mg of **145**.

Method B:



C[1]Magnesocenophane **9** (1.5 g, 7.88 mmol, 0.9 g, 4.63 mmol) and iron(II)-chloride (1.0 g, 7.88 mmol) or iron(II)-bromide (1.0 g, 4.63 mmol) were mixed and dissolved in 100 ml of dry thf. After the mixture was stirred overnight (during the stirring, the mixture turned from yellow to red/brown) under an inert gas atmosphere at ambient temperature, the reaction mixture was

## 5. Experimental Details

poured into 200 ml of an ice-cold hexane/methanol/water mixture (10:9:1 by volume). The product was then precipitated and collected by filtration, washed several times with water, and dried *in vacuo*. The material was diluted with thf to separate all insoluble components by filtration. The addition of cold hexane again led to precipitate the product that afforded after drying *in vacuo* at 353 K for 3 h as a pale-yellow powder

Yield: from FeCl<sub>2</sub>: 100 mg; from FeBr<sub>2</sub>: 396 mg of **146**.

<sup>1</sup>H NMR (400 MHz, C<sub>6</sub>D<sub>6</sub>, 298 K):  $\delta$  [ppm]= 3.94 (br. s), 1.53, (br. s).

<sup>13</sup>C{<sup>1</sup>H} NMR (75 MHz, C<sub>6</sub>D<sub>6</sub>, 298 K):  $\delta$  [ppm]= 101.2, 67.7, 66.4, 33.5, 30.7.

Elemental analysis for C<sub>13</sub>H<sub>14</sub>Fe: calc.: 69.06 at% C, 6.24 at% H; found: 66.18 at% C 6.09 at% H (Note: low-carbon values were repeatedly and reproducibly observed upon analysis of different samples and have been described before in case of polyferrocenylsilanes).<sup>87,399</sup>

### Crystallographic data for **147**

CCDC code:	2049104
Empirical formula	C <sub>93</sub> H <sub>120</sub> Fe <sub>6</sub>
Formula weight	1572.98
Temperature	152(2) K
Wavelength	0.71073 Å
Crystal system	trigonal
Space group	R-3
Unit cell dimensions	a = 22.7410(10) Å $\alpha = 90^\circ$ b = 22.7410(10) Å $\beta = 90^\circ$ c = 12.4656(6) Å $\gamma = 120^\circ$
Volume	5582.9(6) Å <sup>3</sup>
Z	3
Density (calculated)	1.404 mg m <sup>-3</sup>
Absorption coefficient	1.187 mm <sup>-1</sup>
F(000)	2502
Crystal size	0.552 x 0.405 x 0.220 mm <sup>3</sup>
Theta range for data collection	1.791 to 36.163°
Index ranges	-35 ≤ h ≤ 37, -37 ≤ k ≤ 37, -20 ≤ l ≤ 20
Reflections collected	58994
Independent reflections	5931 [R(int) = 0.0240]
Completeness to theta = 25.242°	100.0 %

## 5. Experimental Details

Absorption correction	semi-empirical from equivalents
Max. and min. transmission	0.7471 and 0.6826
Refinement method	full-matrix least-squares on $F^2$
Data / restraints / parameters	5931 / 13 / 203
Goodness-of-fit on $F^2$	1.070
Final R indices [ $I > 2\sigma(I)$ ]	R1 = 0.0321, wR2 = 0.0959
R indices (all data)	R1 = 0.0380, wR2 = 0.1006
Extinction coefficient	n/a
Largest diff. peak and hole	0.793 and -0.834 e. $\text{\AA}^{-3}$



### 5.3. Computational Details

All calculations were performed using the Gaussian 09, Revision D.01 package of programs.<sup>400</sup> All geometry optimizations have been carried out at the B3LYP-D3<sup>401</sup>/def2-TZVP<sup>402</sup> level of theory, starting from the corresponding crystal structures. Every optimized structure was confirmed to be a minimum on the potential energy surface by a subsequent frequency analysis (all positive eigenvalues).

## 5. Experimental Details

### Optimized Geometry of 115

Al	-0.21939900	0.07244600	-0.50241900	H	-2.63905900	-2.35785600	-1.61526500
Cl	-0.46297300	-0.76012300	-2.49060200	H	0.84741400	-0.81000300	3.79840700
C	1.84539900	0.18572000	-0.17193300	H	1.37582000	-3.06694500	2.45618700
C	-0.95201200	-1.14000000	0.96627100	H	-3.57072900	1.90688300	-2.78073200
C	-1.18431800	1.88784200	-0.43542500	H	-1.34524300	3.18360600	-3.51931700
N	2.77358000	-0.74118900	-0.51556200	H	6.16199200	-0.46350900	-0.16708600
N	2.54294700	1.17448600	0.44185900	H	5.38051000	-1.49728700	-1.34843600
Si	-2.81882400	-1.43655100	0.70410200	H	5.37916600	-1.95328700	0.35206700
C	-0.58244500	-0.40766600	2.18816800	H	2.39356900	-0.98087700	-3.17772700
C	-0.12699100	-2.35018500	1.03177600	H	2.49870000	-2.73621300	-3.27082800
C	-2.56664400	1.56724400	-0.86797400	H	3.93608800	-1.80160600	-2.85434700
H	-1.06377300	2.22278000	0.59602200	H	4.04087400	-3.40761800	-0.77125900
C	-0.61671200	2.69788000	-1.51974000	H	2.44297100	-4.09978700	-0.99501800
C	4.04346400	-0.33635200	-0.12551200	H	2.80078600	-3.21253000	0.48535000
C	2.44865200	-1.98037900	-1.26269900	H	4.68420600	2.13974400	2.03777600
C	3.89798600	0.87227500	0.48455000	H	5.19942900	2.58508500	0.41410000
C	1.90084200	2.37773900	1.01276900	H	5.87449300	1.16317600	1.20205800
Si	-3.81775100	0.62871100	0.13970000	H	1.76350300	4.48582600	0.64602000
C	-3.52343100	-2.15613800	2.30337700	H	2.54824500	3.60078700	-0.66275500
C	-3.07388900	-2.69725500	-0.67524900	H	3.42437200	3.93941700	0.83831200
H	-1.02527800	0.52740300	2.50268800	H	2.90070800	2.51498000	2.95544100
C	0.38112800	-1.10697400	2.86874400	H	1.50687500	1.42057600	2.90919000
C	0.66245300	-2.31323300	2.15227200	H	1.27022400	3.17350600	2.90314900
H	-0.16136500	-3.14560000	0.30132700	H	-6.14859600	-0.15496100	-0.29494300
C	-2.70255700	2.04374400	-2.15016100	H	-5.19678500	-0.16944300	-1.78266800
H	0.36828400	3.14119800	-1.52178900	H	-5.82347600	1.35680800	-1.14920700
C	-1.51064200	2.73339100	-2.55055000	H	-3.32963500	1.78203000	2.30810600
C	5.30203000	-1.10872300	-0.33477700	H	-4.92659200	1.03627600	2.34972700
H	1.36736000	-2.03375600	-1.22921400	H	-4.67942700	2.55647300	1.47446700
C	2.85431100	-1.85906600	-2.72865000				
C	2.98065000	-3.24252600	-0.58783600				
C	4.96279400	1.74086800	1.06474600				
H	0.87056400	2.29392300	0.69469700				
C	2.45475600	3.67305100	0.42098900				
C	1.90495900	2.36356000	2.53977400				
C	-5.39540600	0.39136300	-0.86739900				
C	-4.22868800	1.59099000	1.71780200				
H	-2.97366400	-3.05566500	2.59141600				
H	-4.57557000	-2.42582900	2.17992800				
H	-3.44980600	-1.44192000	3.12514900				
H	-4.14219500	-2.86547500	-0.83298300				
H	-2.62002800	-3.65635800	-0.41364800				

## 5. Experimental Details

### Optimized Geometry of 116

Si	2.88691900	-0.08799900	-0.82277700	C	-1.34556700	3.01262400	-0.93066100
C	0.02069300	1.50811400	0.19461700	H	0.17057400	1.89226600	-2.03771800
C	2.54814600	3.26355200	0.35747200	C	-1.69273500	3.05138600	0.45981800
C	2.14464600	1.01859200	2.40656000	H	-0.89595900	1.98769400	2.20218900
C	1.66047400	-1.48705600	-0.96783900	C	-0.25245200	-2.75600600	-1.46901200
C	3.22162800	0.65442400	-2.52992100	H	0.07627500	-0.75548600	-2.35803400
C	4.49660100	-0.74815600	-0.09605700	C	0.66781500	-3.56730500	-0.86550800
Al	-0.58288300	-0.40714300	0.04665200	H	2.70546400	-3.17874900	-0.05168200
C	-0.32698600	2.11309700	-1.10346200	C	-2.87864400	-0.19533400	-1.85687100
C	-0.88287900	2.17883700	1.13903600	C	-3.52236900	-0.01902600	0.46878200
H	3.59410400	3.33151300	0.66719800	H	-1.80638100	3.60687900	-1.70812000
H	1.97074700	3.97530400	0.95258500	H	-2.46272100	3.67352100	0.89547800
H	2.48166800	3.56905200	-0.68784900	H	-1.23050100	-3.05455100	-1.81967900
H	1.62623900	1.70729500	3.07794200	H	0.53440600	-4.61349500	-0.63034800
H	3.20905500	1.04942700	2.65210200	H	-2.55574700	-1.09248500	-2.37964800
H	1.77818100	0.01200800	2.60926200	H	-2.39748400	0.68406900	-2.28148300
C	0.27454500	-1.39329300	-1.49531100	C	-4.38686200	-0.03995900	-1.74774700
C	1.83037500	-2.79230000	-0.55609000	C	-4.55899400	0.66591200	-0.39787400
H	3.67867800	-0.08843600	-3.18848300	H	-3.11737000	0.60039700	1.26264800
H	3.89476500	1.51249100	-2.46341800	H	-3.85759100	-0.97462100	0.87106400
H	2.29768500	0.99481200	-3.00266600	H	-4.87363700	-1.01700600	-1.73361300
H	5.24019100	0.04676600	-0.00395200	H	-4.79025300	0.53072300	-2.58304500
H	4.33378800	-1.17092400	0.89724300	H	-4.32167500	1.72706900	-0.48667600
H	4.91743800	-1.53057800	-0.73241600	H	-5.56258500	0.56236600	0.01247300
Br	-0.76187900	-1.51445100	2.06109100	Si	1.88860600	1.51278400	0.60583100
O	-2.41950900	-0.30553600	-0.46479900				

## 5. Experimental Details

### Optimized Geometry of 117

Al	-0.21939900	0.07244600	-0.50241900	C	-4.22868800	1.59099000	1.71780200
Cl	-0.46297300	-0.76012300	-2.49060200	H	-2.97366400	-3.05566500	2.59141600
C	1.84539900	0.18572000	-0.17193300	H	-4.57557000	-2.42582900	2.17992800
C	-0.95201200	-1.14000000	0.96627100	H	-3.44980600	-1.44192000	3.12514900
C	-1.18431800	1.88784200	-0.43542500	H	-4.14219500	-2.86547500	-0.83298300
N	2.77358000	-0.74118900	-0.51556200	H	-2.62002800	-3.65635800	-0.41364800
N	2.54294700	1.17448600	0.44185900	H	-2.63905900	-2.35785600	-1.61526500
Si	-2.81882400	-1.43655100	0.70410200	H	0.84741400	-0.81000300	3.79840700
C	-0.58244500	-0.40766600	2.18816800	H	1.37582000	-3.06694500	2.45618700
C	-0.12699100	-2.35018500	1.03177600	H	-3.57072900	1.90688300	-2.78073200
C	-2.56664400	1.56724400	-0.86797400	H	-1.34524300	3.18360600	-3.51931700
H	-1.06377300	2.22278000	0.59602200	H	6.16199200	-0.46350900	-0.16708600
C	-0.61671200	2.69788000	-1.51974000	H	5.38051000	-1.49728700	-1.34843600
C	4.04346400	-0.33635200	-0.12551200	H	5.37916600	-1.95328700	0.35206700
C	2.44865200	-1.98037900	-1.26269900	H	2.39356900	-0.98087700	-3.17772700
C	3.89798600	0.87227500	0.48455000	H	2.49870000	-2.73621300	-3.27082800
C	1.90084200	2.37773900	1.01276900	H	3.93608800	-1.80160600	-2.85434700
Si	-3.81775100	0.62871100	0.13970000	H	4.04087400	-3.40761800	-0.77125900
C	-3.52343100	-2.15613800	2.30337700	H	2.44297100	-4.09978700	-0.99501800
C	-3.07388900	-2.69725500	-0.67524900	H	2.80078600	-3.21253000	0.48535000
H	-1.02527800	0.52740300	2.50268800	H	4.68420600	2.13974400	2.03777600
C	0.38112800	-1.10697400	2.86874400	H	5.19942900	2.58508500	0.41410000
C	0.66245300	-2.31323300	2.15227200	H	5.87449300	1.16317600	1.20205800
H	-0.16136500	-3.14560000	0.30132700	H	1.76350300	4.48582600	0.64602000
C	-2.70255700	2.04374400	-2.15016100	H	2.54824500	3.60078700	-0.66275500
H	0.36828400	3.14119800	-1.52178900	H	3.42437200	3.93941700	0.83831200
C	-1.51064200	2.73339100	-2.55055000	H	2.90070800	2.51498000	2.95544100
C	5.30203000	-1.10872300	-0.33477700	H	1.50687500	1.42057600	2.90919000
H	1.36736000	-2.03375600	-1.22921400	H	1.27022400	3.17350600	2.90314900
C	2.85431100	-1.85906600	-2.72865000	H	-6.14859600	-0.15496100	-0.29494300
C	2.98065000	-3.24252600	-0.58783600	H	-5.19678500	-0.16944300	-1.78266800
C	4.96279400	1.74086800	1.06474600	H	-5.82347600	1.35680800	-1.14920700
H	0.87056400	2.29392300	0.69469700	H	-3.32963500	1.78203000	2.30810600
C	2.45475600	3.67305100	0.42098900	H	-4.92659200	1.03627600	2.34972700
C	1.90495900	2.36356000	2.53977400	H	-4.67942700	2.55647300	1.47446700
C	-5.39540600	0.39136300	-0.86739900				

## 5. Experimental Details

### Optimized Geometry of 118

Si	3.43594400	-1.18934200	0.65662300	H	0.23408400	-4.46316400	-1.17516600
Si	3.43573000	1.18950800	0.65690300	H	1.34895100	-3.24708900	-3.29305400
C	1.90438600	-1.65291200	-0.38094500	H	0.23390500	4.46316800	-1.17512300
C	4.98337800	-1.96633900	-0.09102000	H	1.34911500	3.24722400	-3.29290400
C	3.19819700	-1.83159800	2.41432100	N	-2.98449600	-1.08962600	-0.09473500
C	1.90422100	1.65296000	-0.38078000	N	-2.98455700	1.08955800	-0.09481600
C	4.98312000	1.96697000	-0.09034300	C	-4.04970000	-0.68137200	0.69967400
C	3.19763200	1.83129000	2.41472700	C	-2.53636600	-2.47379900	-0.37822200
Al	0.75046400	-0.00004200	-0.15294600	C	-4.04974100	0.68130600	0.69961900
C	1.11249600	-2.82991800	-0.01209200	C	-2.53650100	2.47373100	-0.37841600
C	2.07399700	-1.78781200	-1.83679900	C	-4.97353800	-1.60037500	1.42188700
H	4.85784500	-3.04838600	-0.17685400	C	-2.29925500	-3.27476000	0.89769600
H	5.18215100	-1.57262400	-1.08907600	C	-3.46051900	-3.15709600	-1.38059600
H	5.85992800	-1.77011900	0.53168200	H	-1.56837200	-2.34058300	-0.85519800
H	3.16951300	-2.92358900	2.42758600	C	-4.97364800	1.60031200	1.42173900
H	4.01808300	-1.50501400	3.05842800	C	-2.29956600	3.27486400	0.89742800
H	2.26577000	-1.45855200	2.84126200	C	-3.46061800	3.15685200	-1.38094200
C	1.11222400	2.82991200	-0.01199000	H	-1.56845500	2.34052400	-0.85528900
C	2.07402000	1.78791800	-1.83660600	H	-5.27606700	-2.44512500	0.80558900
H	4.85743300	3.04902300	-0.17587900	H	-4.51948000	-1.99530600	2.33246700
H	5.18205700	1.57356800	-1.08848900	H	-5.87537600	-1.06343600	1.71020800
H	5.85963100	1.77070300	0.53239900	H	-1.72984300	-2.68559000	1.61616200
H	3.16866800	2.92327000	2.42826300	H	-3.22278400	-3.61718600	1.36189300
H	4.01753900	1.50475300	3.05883100	H	-1.70776100	-4.15381600	0.64261800
H	2.26526100	1.45789700	2.84147900	H	-3.54414700	-2.56361900	-2.29165200
Cl	-0.18194300	-0.00015400	1.83187800	H	-3.04155900	-4.12859500	-1.64633000
S	-1.00708100	-0.00003100	-1.67653500	H	-4.46127700	-3.32230500	-0.97929400
C	0.82042400	-3.55458600	-1.13797300	H	-5.27619900	2.44500700	0.80537500
H	0.80487000	-3.05977800	0.99685800	H	-4.51964700	1.99532800	2.33231100
C	1.41518300	-2.90743400	-2.26903300	H	-5.87547200	1.06334800	1.71006300
H	2.64004000	-1.11334400	-2.46160700	H	-1.73024500	2.68580500	1.61605800
C	0.82027500	3.55461100	-1.13788300	H	-3.22316000	3.61734800	1.36145500
H	0.80445300	3.05971200	0.99692900	H	-1.70804700	4.15389000	0.64230700
C	1.41521900	2.90752900	-2.26888700	H	-3.54412900	2.56327100	-2.29194100
H	2.64018100	1.11349800	-2.46136100	H	-3.04171000	4.12835400	-1.64674700
C	-2.34766900	-0.00003400	-0.57891600	H	-4.46142100	3.32202600	-0.97973600

## 5. Experimental Details

### Optimized Geometry of thf donor

O	-0.00012100	-1.24931000	-0.00031700
C	1.16588700	-0.42761700	0.13272200
C	-1.16609400	-0.42734200	-0.13232000
H	1.94672700	-0.81927700	-0.52271600
H	1.52746800	-0.47794200	1.16728300
C	0.73126900	0.99261200	-0.22855100
C	-0.73092500	0.99291300	0.22836900
H	-1.94646200	-0.81867500	0.52389000
H	-1.52858700	-0.47783500	-1.16653400
H	0.79037500	1.14578900	-1.30882300
H	1.33914600	1.75607600	0.25724200
H	-0.78993900	1.14658200	1.30857500
H	-1.33858400	1.75637200	-0.25769900

### Optimized Geometry of *i*Pr<sub>2</sub>Me<sub>2</sub>NHC donor

C	-0.00000200	-1.23877600	0.24138800
H	2.25027000	-2.00032000	0.41725400
H	-2.25031900	-2.00022600	0.41771800
N	1.06597600	-0.40382000	0.12031600
N	-1.06598500	-0.40381200	0.12042900
C	2.42588500	-0.95940600	0.14633900
C	-2.42589100	-0.95940500	0.14641300
C	0.68042600	0.92507700	-0.08369300
C	-0.68044900	0.92507800	-0.08363100
C	3.30854100	-0.33164100	1.22485800
C	3.07632100	-0.93746300	-1.23727900
C	-3.07602200	-0.93795800	-1.23735300
C	-3.30877100	-0.33127900	1.22453800
C	1.60666300	2.08712900	-0.21321000
C	-1.60670600	2.08713000	-0.21300800
H	3.60805300	0.68616600	0.97538700
H	4.21891600	-0.92306300	1.33818200
H	2.78993600	-0.31576200	2.18437300
H	3.28187100	0.07829500	-1.57759800
H	2.42575700	-1.41972600	-1.96752200
H	4.02532000	-1.47675500	-1.21079000
H	-3.28132100	0.07768500	-1.57817200
H	-4.02511200	-1.47709100	-1.21085300
H	-2.42535200	-1.42063700	-1.96722700
H	-3.60835200	0.68639300	0.97461400
H	-2.79031600	-0.31495800	2.18412800
H	-4.21910100	-0.92274900	1.33796700
H	2.41535500	1.89490100	-0.91862900
H	2.06324000	2.35699400	0.74253200
H	1.06361200	2.96073600	-0.57167700
H	-1.06381200	2.96061600	-0.57201200
H	-2.06278900	2.35727800	0.74289300
H	-2.41576800	1.89472900	-0.91795600

## 5. Experimental Details

### Optimized Geometry of ${}^i\text{Pr}_2\text{Me}_2\text{ImS}$ donor

S	-0.00007700	-2.53719400	-0.00018300	C	-3.32633700	-0.01217900	-1.17658200
N	1.09231000	-0.02298900	0.04840900	H	4.07906900	-0.89520900	-1.35153900
N	-1.09231400	-0.02294000	-0.04847300	H	-4.22294800	-0.62812600	-1.26216600
C	-0.00002100	-0.85325800	-0.00008700	C	3.32619000	-0.01302900	1.17677500
C	0.67777800	1.31132200	0.02497000	C	-3.11060200	-0.39235800	1.33908200
C	-0.67772900	1.31135400	-0.02480300	H	4.22275000	-0.62909100	1.26207100
C	1.60177900	2.48011500	0.06672600	H	-4.07898400	-0.89585800	1.35119500
C	-1.60168400	2.48019000	-0.06632600	H	3.65066700	1.01406400	1.01344800
H	2.39853600	2.39861600	-0.67287700	H	-3.27582900	0.65464500	1.59767200
H	-2.39858600	2.39843300	0.67308800	H	2.78999500	-0.06477500	2.12523700
H	2.07141200	2.59833100	1.04554000	H	-2.48148800	-0.84556400	2.10559200
H	-1.05208900	3.39415400	0.14985600	H	1.05216400	3.39417000	-0.14902100
C	2.46518200	-0.55224700	0.03617600	H	-2.07112900	2.59876800	-1.04518600
C	-2.46519900	-0.55217300	-0.03643100	H	2.48168900	-0.84401400	-2.10609800
H	2.31527800	-1.61824700	0.20747900	H	3.27625500	0.65563700	-1.59690800
H	-2.31535200	-1.61807000	-0.20842600	H	-3.65072000	1.01483200	-1.01255800
C	3.11078500	-0.39152800	-1.33914700	H	-2.79028000	-0.06334000	-2.12515300

### Optimized Geometry of donor-free structures $(\text{Me}_2\text{SiCp})_2\text{AlCl}$

Si	-1.76321100	1.17294300	-0.14738900	H	-1.93192800	1.03035300	-2.63906700
C	-0.00465900	-1.71108800	-0.11258000	H	-3.74759700	1.81928800	1.21070500
C	-3.00717900	-2.13150300	-0.69211500	H	-2.27488000	1.93353900	2.17280400
C	-2.01415200	-1.44388000	2.15229900	H	-2.65659600	3.19714700	0.99735800
C	0.04499500	1.71513300	-0.10306400	Cl	3.03783100	-0.13200900	1.03111500
C	-2.46762800	1.56581100	-1.85209700	C	1.73256200	-2.49175600	-1.46128900
C	-2.69817500	2.12184200	1.18425700	H	0.23546500	-1.07600800	-2.28423900
Al	1.27417800	-0.00395300	-0.11223400	C	1.77056300	-3.18594800	-0.24814800
C	0.66828900	-1.56564300	-1.42107800	H	0.56526700	-3.01692400	1.58933500
C	0.74074900	-2.71510300	0.56713200	C	2.02028900	2.65664500	-0.90934400
H	-4.02738600	-1.82453300	-0.44827000	H	0.71663800	1.48250100	-2.26363800
H	-2.91513500	-3.20031200	-0.48513800	C	1.82643300	3.10170600	0.40284500
H	-2.85954500	-1.98287600	-1.76373000	H	0.27215400	2.65581400	1.90016900
H	-1.93699800	-2.50617700	2.39530800	H	2.42298600	-2.60930700	-2.28339100
H	-3.00458100	-1.10079600	2.45881700	H	2.51978400	-3.90818000	0.03876900
H	-1.27460300	-0.90749100	2.75074100	H	2.86219100	2.89424400	-1.54245300
C	0.96333100	1.79366200	-1.25793500	H	2.50999600	3.72011500	0.96441700
C	0.65284000	2.53332900	0.89667200	Si	-1.74673300	-1.14973000	0.30933600
H	-2.39386700	2.63486600	-2.06490200				
H	-3.51912400	1.27604900	-1.91411000				

## 5. Experimental Details

### Optimized Geometry of donor-free structures (Me<sub>2</sub>SiCp)<sub>2</sub>AlBr

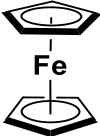
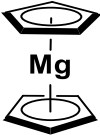
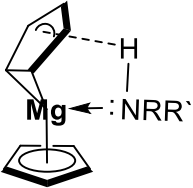
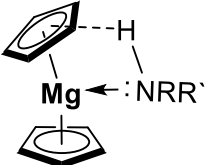
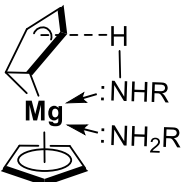
Si	2.15767600	1.08872200	0.08863000	H	3.99307200	0.97565000	1.76787000
C	0.30055100	-1.70502000	0.20054300	H	2.43073100	0.78421400	2.55764700
C	3.33648300	-2.27105100	0.28759000	H	4.11546700	1.72715300	-1.31001400
C	1.94735700	-1.42377500	-2.33941300	H	2.61400400	1.95386700	-2.20673400
C	0.37831400	1.71823100	0.17353900	H	3.09218900	3.13400100	-0.98116200
C	2.96124100	1.33445100	1.77741500	Br	-2.94378300	-0.03968400	-0.67670400
C	3.08132900	2.06983100	-1.22691700	C	-1.26771900	-2.39278700	1.78742900
Al	-0.91594800	0.05817400	0.33670900	H	0.36737500	-1.00792100	2.36503500
C	-0.19253400	-1.49990700	1.57961200	C	-1.48154900	-3.11839800	0.61277500
C	-0.55384100	-2.70176500	-0.34408700	H	-0.52389300	-3.03562300	-1.37091700
H	4.32202700	-1.97411100	-0.07991400	C	-1.47165000	2.78711200	1.10666000
H	3.18273800	-3.32314400	0.03640500	H	-0.11888100	1.58701500	2.38841000
H	3.34359300	-2.18333500	1.37582200	C	-1.36835700	3.17925400	-0.23273300
H	1.76939200	-2.46873100	-2.60451200	H	0.02833200	2.60419600	-1.83772200
H	2.89833300	-1.12319800	-2.78422900	H	-1.84856500	-2.46532200	2.69500600
H	1.15781900	-0.82392800	-2.79724300	H	-2.28176400	-3.82372600	0.44716900
C	-0.43342800	1.88190600	1.39681800	H	-2.24475100	3.08762700	1.79798500
C	-0.27171600	2.53361500	-0.80230000	H	-2.06535800	3.81478500	-0.75736700
H	2.96757300	2.39047700	2.05690000	Si	1.98185300	-1.19925400	-0.46810100

The optimized geometries of the remaining compounds can be found in the supporting information of the publications.

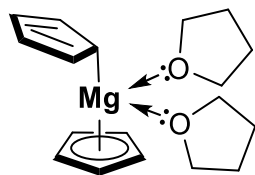


## 6. Appendix

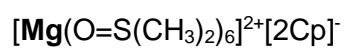
## 6.1. List of Compounds:

Structures	Compound Number
	1
	2
	3 R = H R' = C <sub>6</sub> H <sub>11</sub>
	4 R = CH(CH <sub>3</sub> ) <sub>2</sub> R' = CH <sub>2</sub> C <sub>6</sub> H <sub>5</sub>
	5 R = CH <sub>2</sub> C <sub>6</sub> H <sub>5</sub>

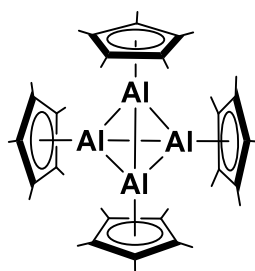
6. Appendix



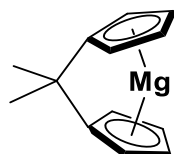
6



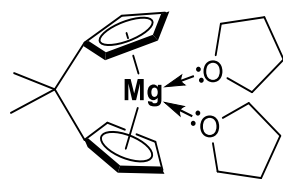
7



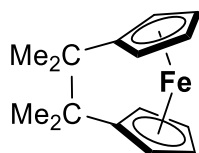
8



9

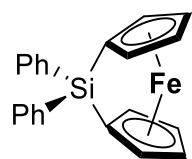


9a

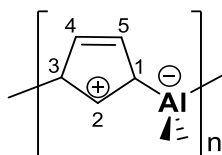


10

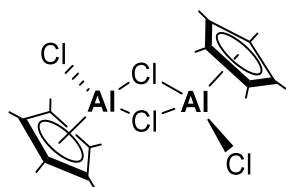
## 6. Appendix



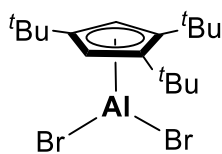
11



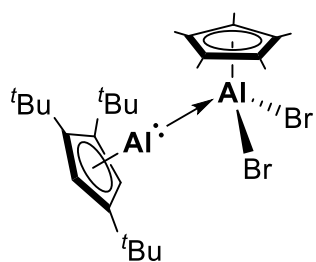
12



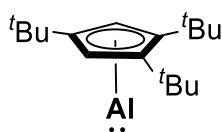
13



14

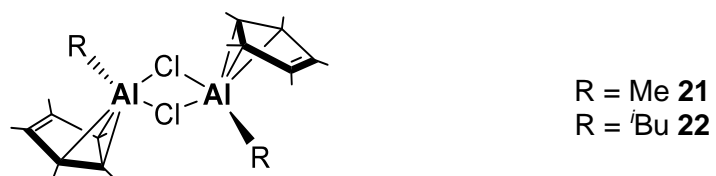
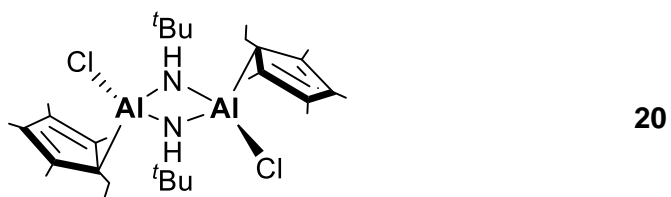
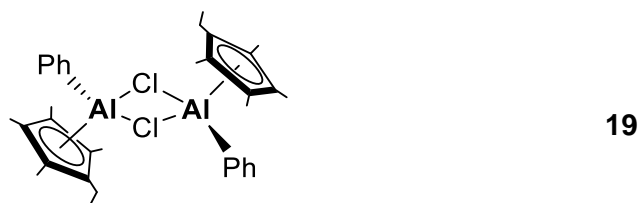
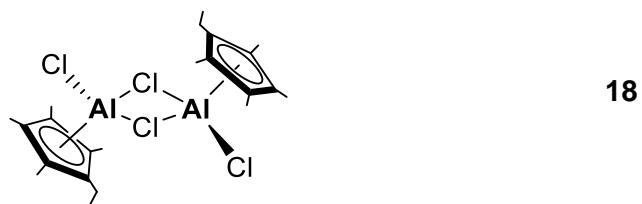
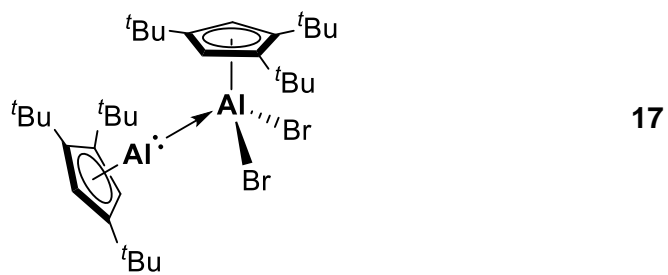


15

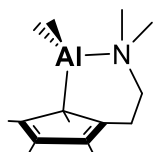


16

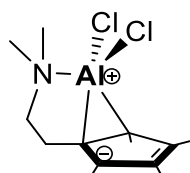
6. Appendix



## 6. Appendix



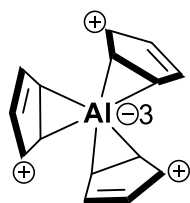
23



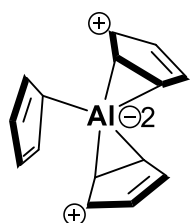
24

AlCp<sub>3</sub>

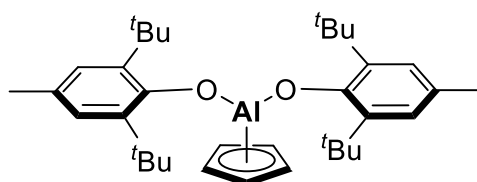
25



25a

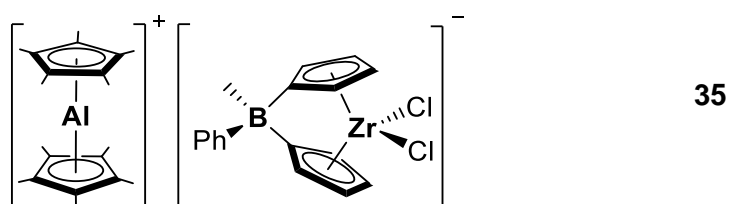
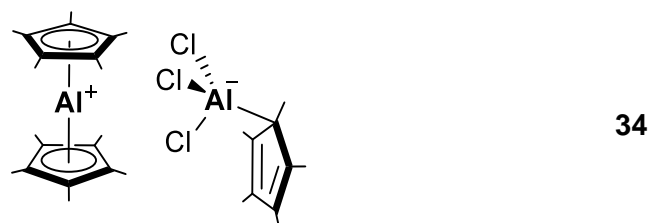
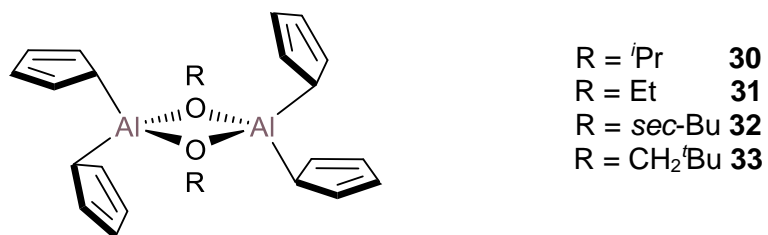
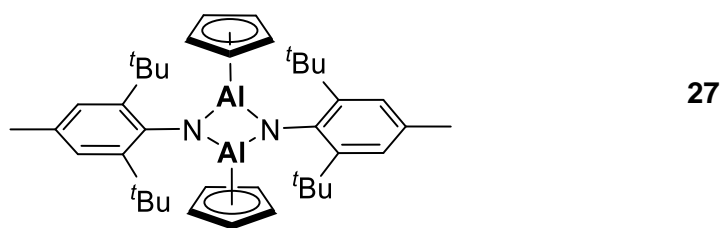


25b

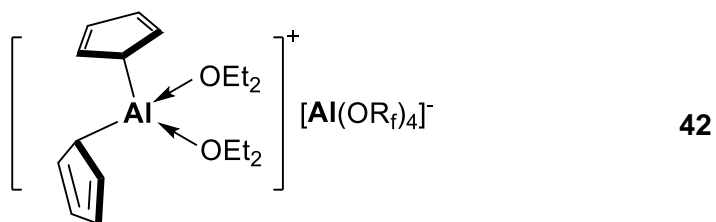
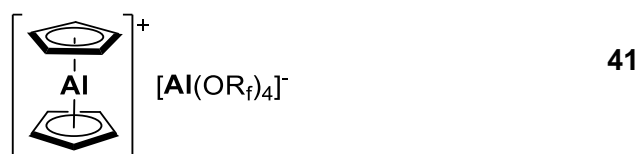
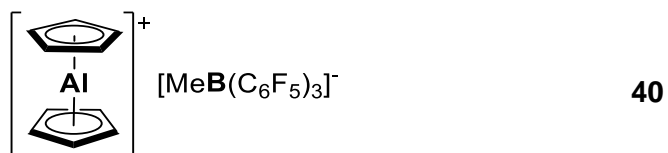
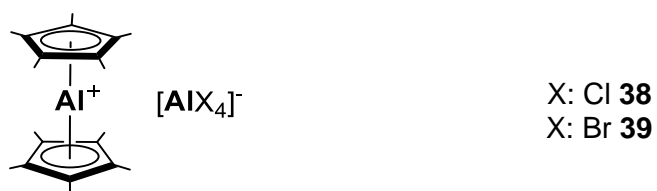
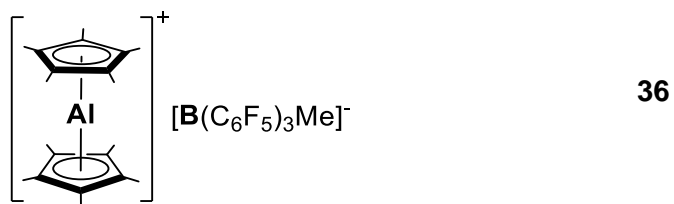


26

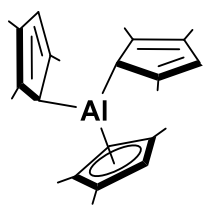
## 6. Appendix



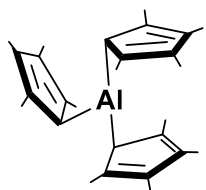
## 6. Appendix



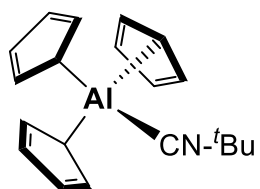
## 6. Appendix



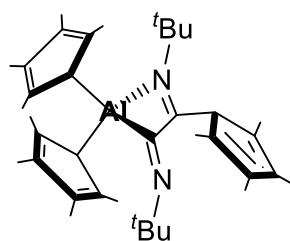
43



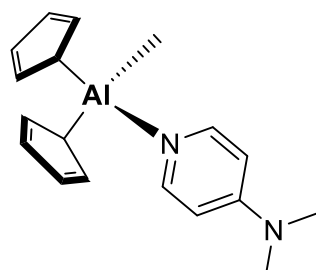
44



45



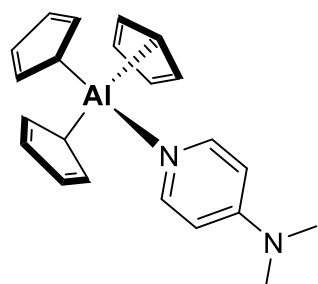
46



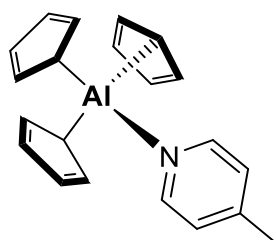
47



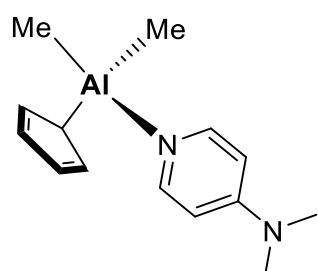
6. Appendix



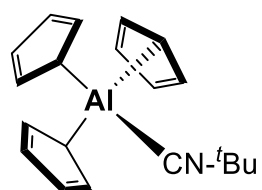
48



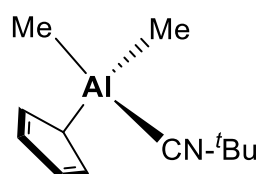
49



50

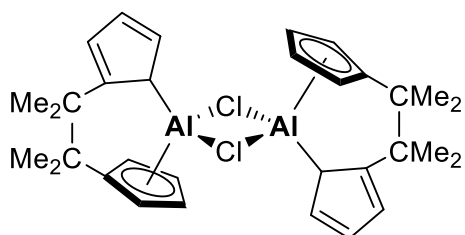


51

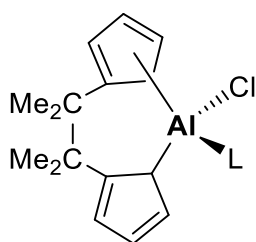


52

## 6. Appendix

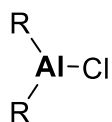


**53**



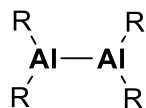
L = thf **54**

L = CN<sup>t</sup>Bu **55**



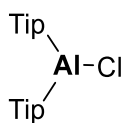
**56**

R = (Me<sub>3</sub>Si)<sub>2</sub>CH



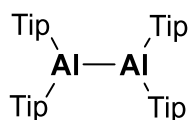
**57**

R = (Me<sub>3</sub>Si)<sub>2</sub>CH



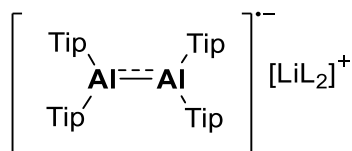
**58**

Tip = 2,4,6-<sup>i</sup>Pr<sub>3</sub>C<sub>6</sub>H<sub>2</sub>



**59**

Tip = 2,4,6-<sup>i</sup>Pr<sub>3</sub>C<sub>6</sub>H<sub>2</sub>

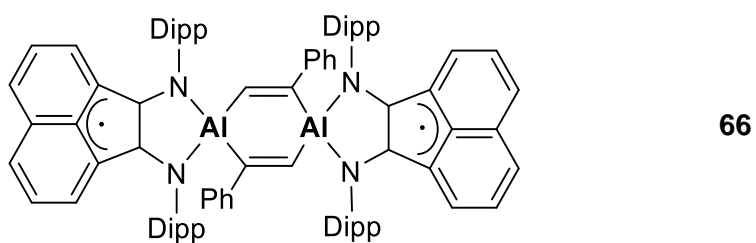
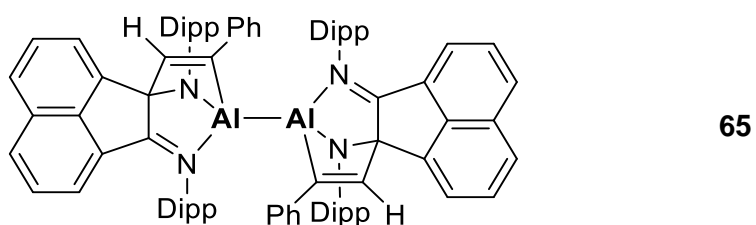
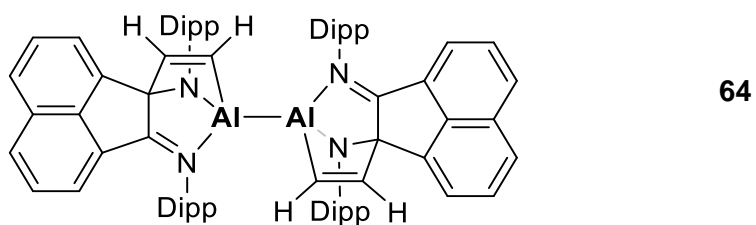
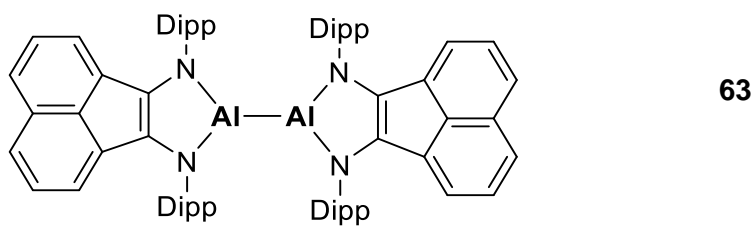
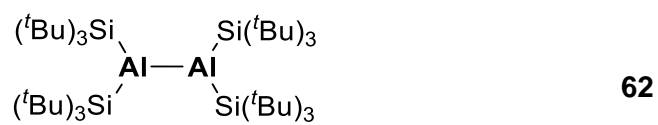


L = TMEDA **60**

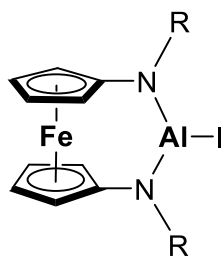
L = 12-crown-4 **61**

Tip = 2,4,6-<sup>i</sup>Pr<sub>3</sub>C<sub>6</sub>H<sub>2</sub>

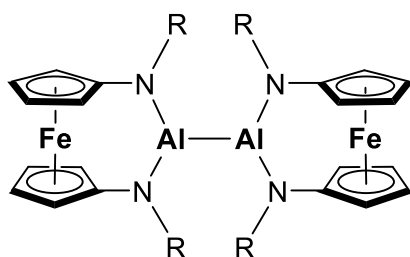
## 6. Appendix



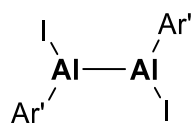
## 6. Appendix



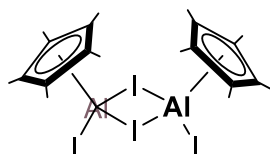
**67**  
R = SiMe<sub>2</sub><sup>t</sup>Bu



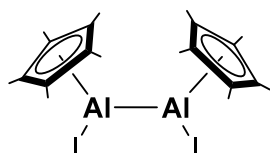
**68**  
R = SiMe<sub>2</sub><sup>t</sup>Bu



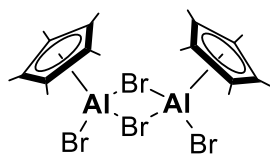
**69**  
Ar' = 2,6-(Dip)<sub>2</sub>C<sub>6</sub>H<sub>3</sub>  
Dip = 2,6-<sup>i</sup>PrC<sub>6</sub>H<sub>3</sub>



**70**

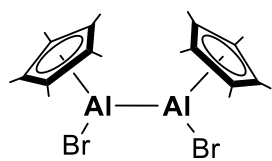


**71**

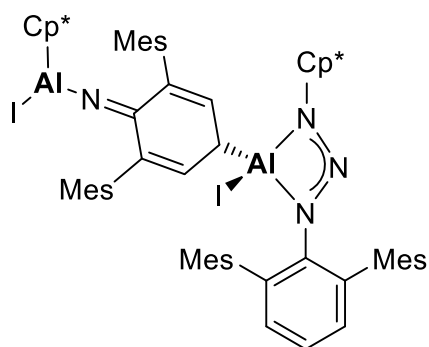


**72**

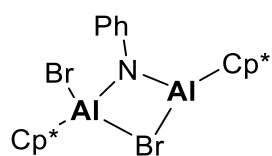
## 6. Appendix



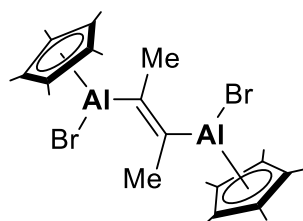
73



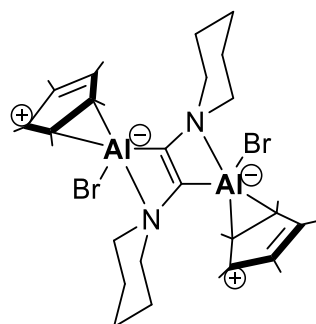
74



75

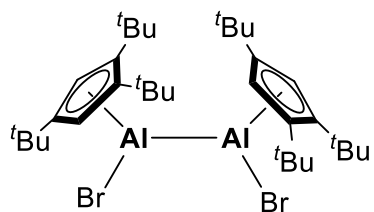


76

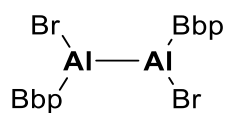


77

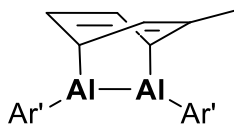
## 6. Appendix



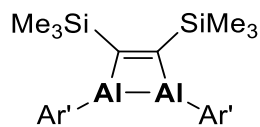
**78**



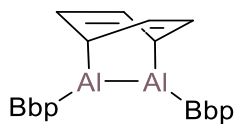
**79**  
Bbp = 2,6-[(Me<sub>3</sub>Si)<sub>2</sub>CH]<sub>2</sub>-C<sub>6</sub>H<sub>3</sub>



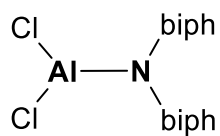
**80**  
Ar' = 2,6-(Dip)<sub>2</sub>C<sub>6</sub>H<sub>3</sub>  
Dip = 2,6-<sup>i</sup>PrC<sub>6</sub>H<sub>3</sub>



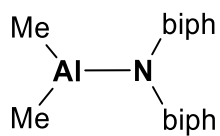
**81**  
Ar' = 2,6-(Dip)<sub>2</sub>C<sub>6</sub>H<sub>3</sub>  
Dip = 2,6-<sup>i</sup>PrC<sub>6</sub>H<sub>3</sub>



**82**  
Bbp = 2,6-[(Me<sub>3</sub>Si)<sub>2</sub>CH]<sub>2</sub>-C<sub>6</sub>H<sub>3</sub>

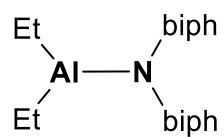


**83**

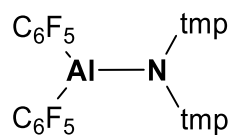


**84**

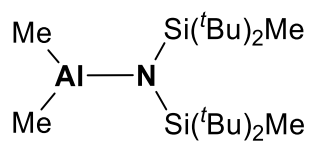
## 6. Appendix



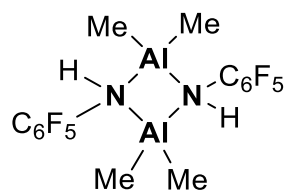
85



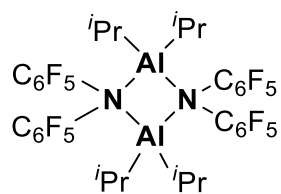
86  
tmp: *tetra*-methylpiperidin



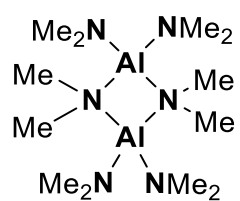
87



88

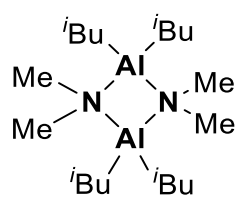


89

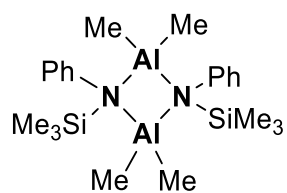


90

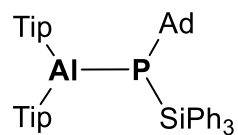
## 6. Appendix



91

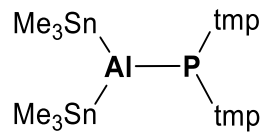


92

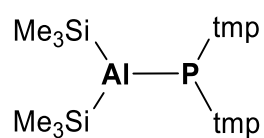


93

Tip = 2,4,6-*i*Pr<sub>3</sub>C<sub>6</sub>H<sub>2</sub>  
Ad = 1-Adamantyl

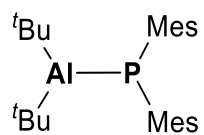


94

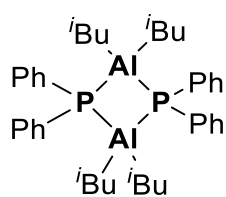


95

tmp: *tetra*-methylpiperidin



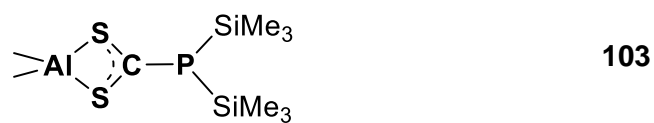
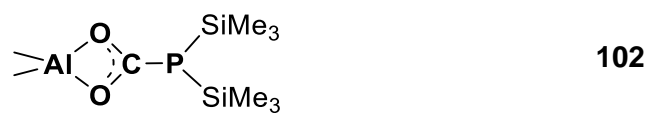
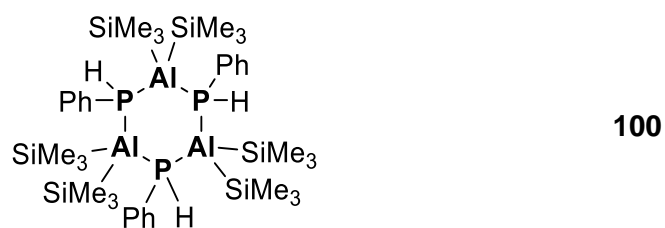
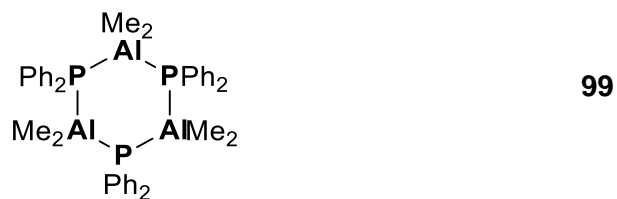
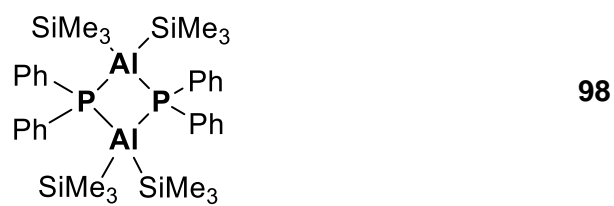
96



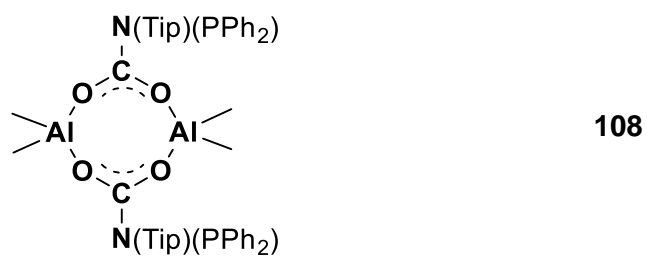
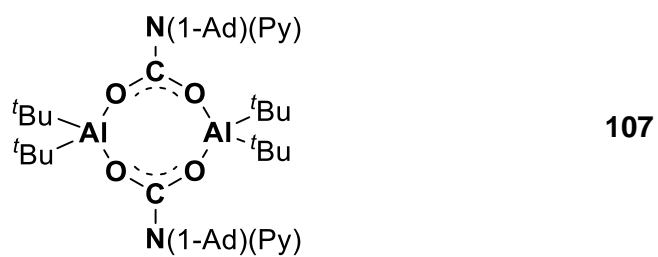
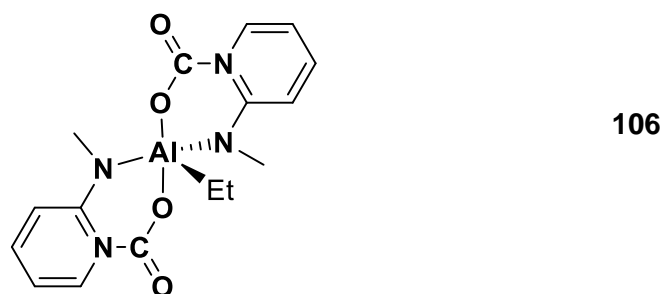
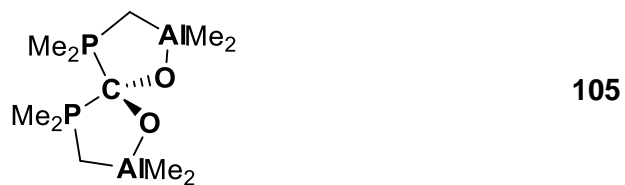
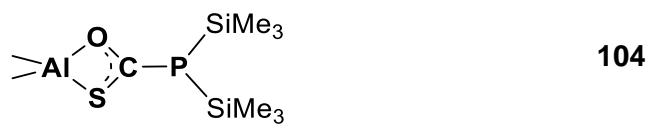
97



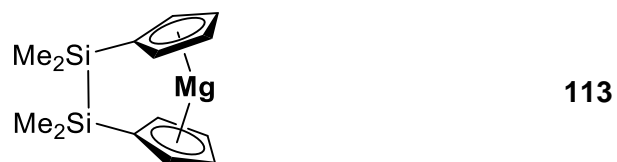
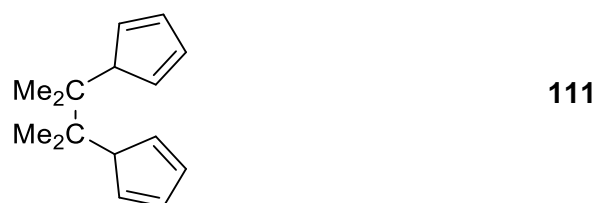
## 6. Appendix



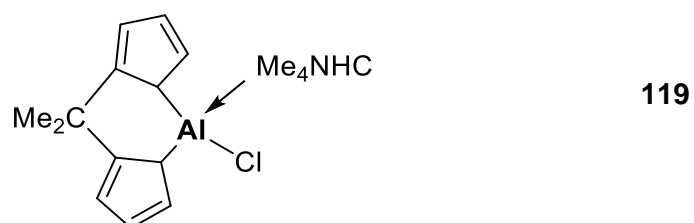
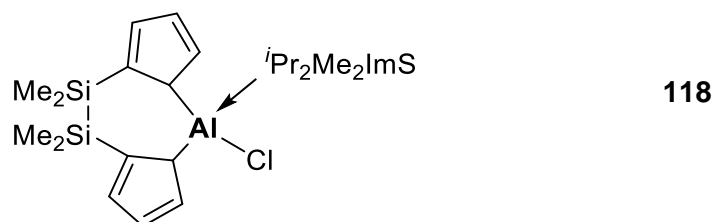
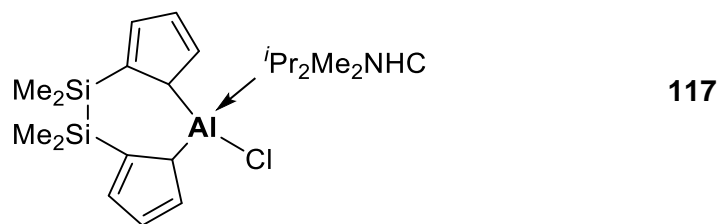
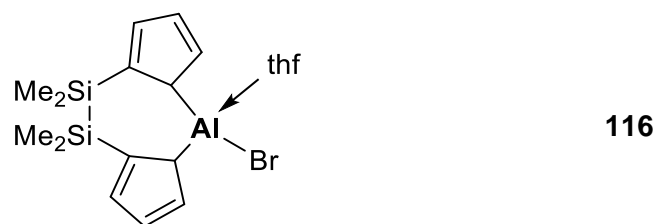
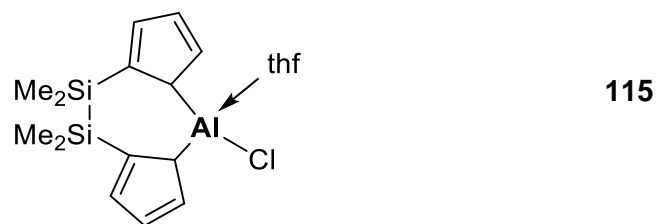
## 6. Appendix



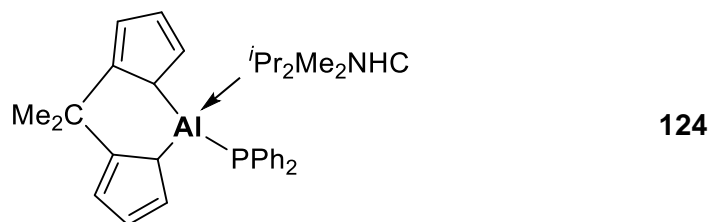
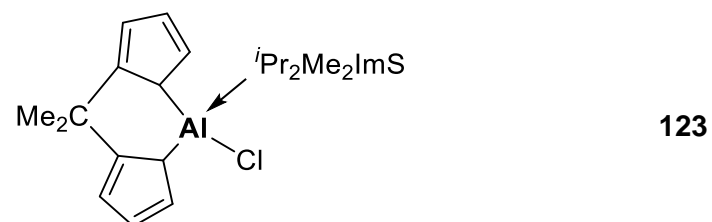
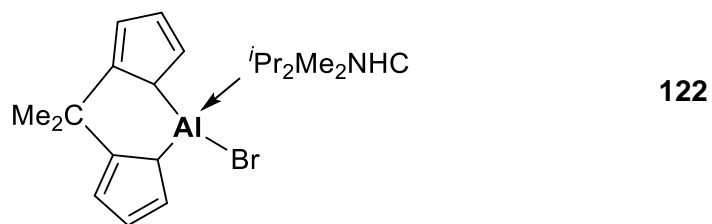
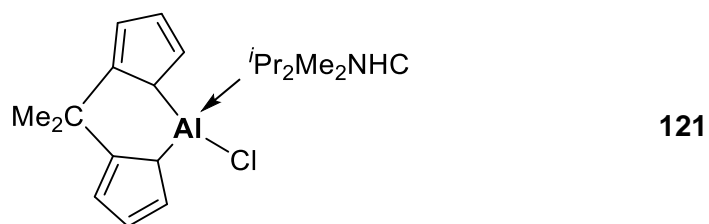
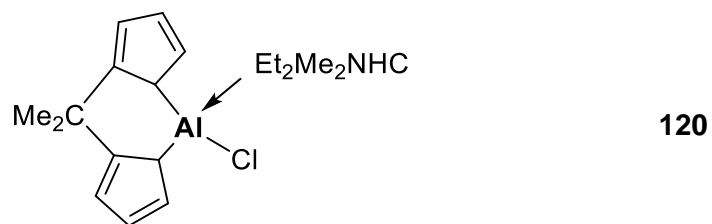
## 6. Appendix



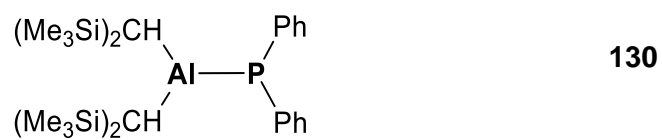
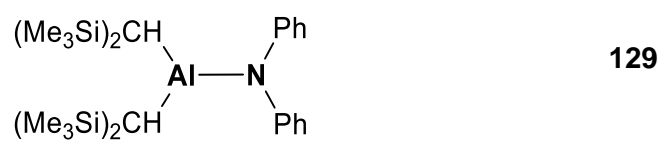
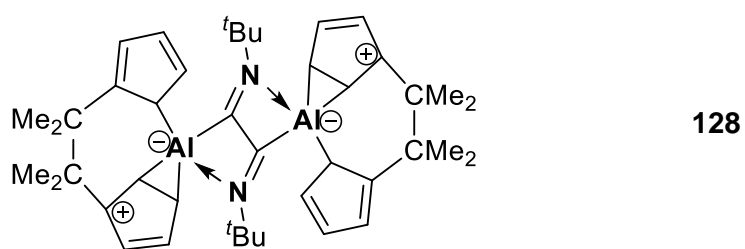
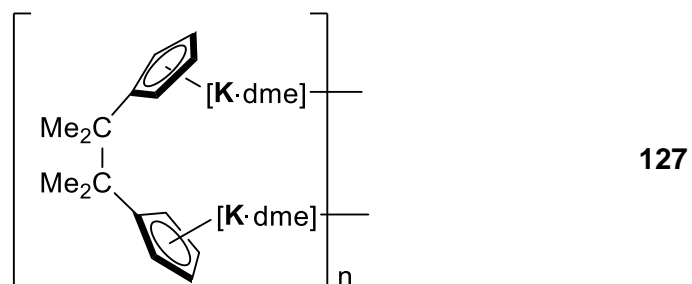
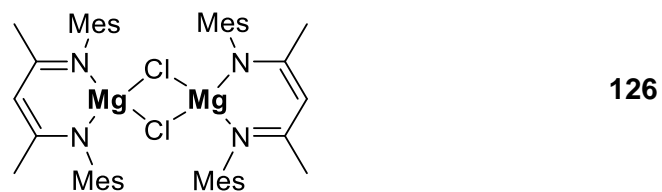
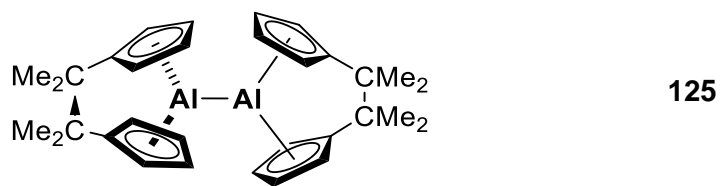
## 6. Appendix



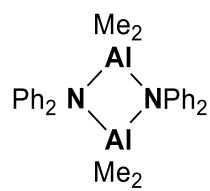
## 6. Appendix



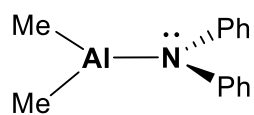
## 6. Appendix



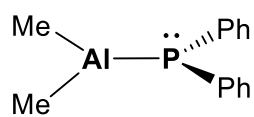
## 6. Appendix



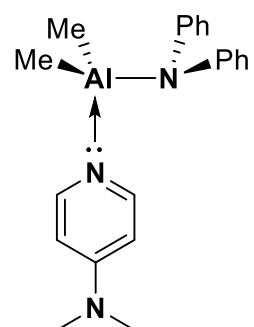
131



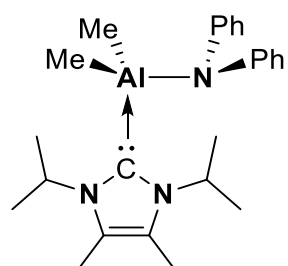
131<sub>M</sub>



99<sub>M</sub>

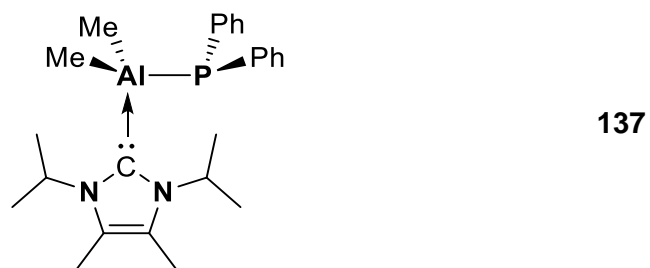
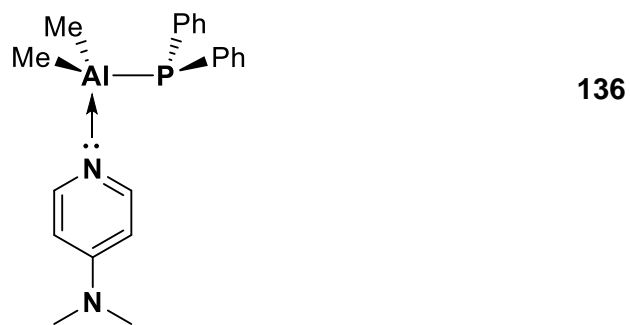
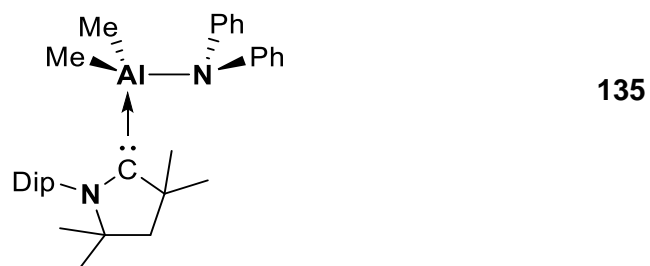
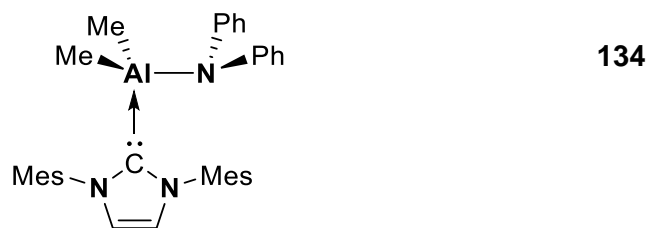


132



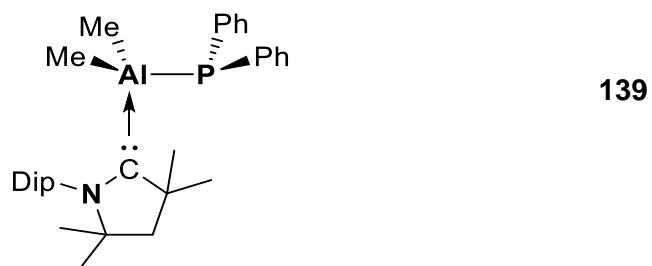
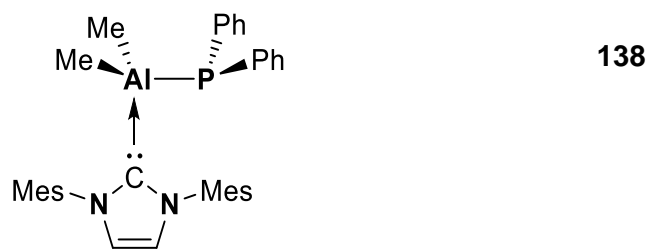
133

## 6. Appendix

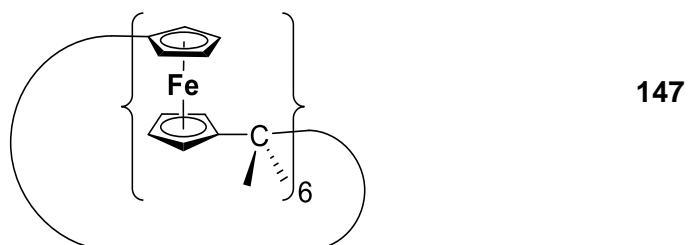
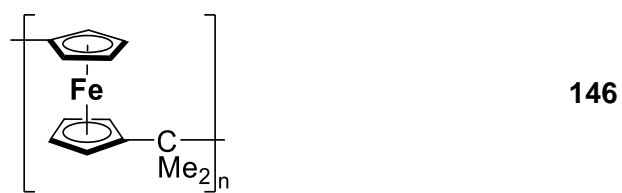
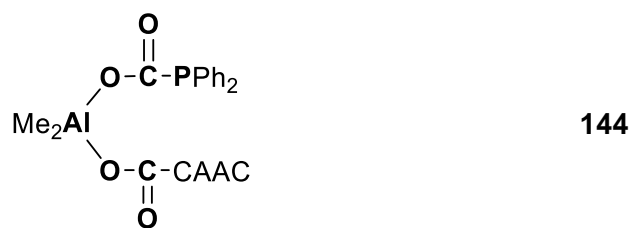
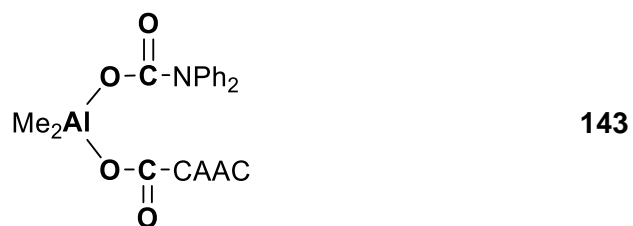




## 6. Appendix



6. Appendix



## 6. Appendix

### 6.2. List of Schemes:

<b>Scheme 1:</b> Synthesis of magnesocene <b>2</b> in different routes.	<b>5</b>
<b>Scheme 2:</b> Reactions of magnesocene <b>2</b> and different amines to give <b>3</b> and <b>4</b> .	<b>6</b>
<b>Scheme 3:</b> Synthesis of <b>5</b> .	<b>7</b>
<b>Scheme 4:</b> Synthesis of <b>6</b> .	<b>7</b>
<b>Scheme 5:</b> Reaction of magnesocene with dmsol to give <b>7</b> .	<b>8</b>
<b>Scheme 6:</b> General reaction of the metathesis with magnesocene <b>2</b> as transmetalation reagent.	<b>9</b>
<b>Scheme 7:</b> Synthesis of <b>8</b> by transmetalation reaction.	<b>9</b>
<b>Scheme 8:</b> Reaction of the C[1]magnesocenophane <b>9</b> with thf to give <b>9a</b> .	<b>10</b>
<b>Scheme 9:</b> General synthesis of magnesocenophanes.	<b>10</b>
<b>Scheme 10:</b> Synthesis of the first ferrocenophane <b>10</b> .	<b>11</b>
<b>Scheme 11:</b> Synthesis of ferrocenophane <b>11</b> .	<b>11</b>
<b>Scheme 12:</b> General ring opening polymerization reaction starting from a strained ferrocenophane.	<b>13</b>
<b>Scheme 13:</b> Synthesis of ferrocenylphosphine polymer by polycondensation reaction.	<b>14</b>
<b>Scheme 14:</b> Synthesis of compounds R <sub>2</sub> AlMeCp (R: Me, Et, <sup>t</sup> Bu).	<b>18</b>
<b>Scheme 15:</b> Synthesis of compounds <b>8</b> and <b>13</b> .	<b>22</b>
<b>Scheme 16:</b> Synthesis of compound <b>16</b> .	<b>22</b>
<b>Scheme 17:</b> Representation of the Lewis basicity of <b>16</b> .	<b>23</b>
<b>Scheme 18:</b> Synthesis of compound <b>18</b> by Me <sub>3</sub> SiCl elimination.	<b>23</b>
<b>Scheme 19:</b> Synthesis of compounds <b>15</b> and <b>16</b> .	<b>24</b>
<b>Scheme 20:</b> Synthesis of compounds <b>21</b> and <b>22</b> .	<b>24</b>
<b>Scheme 21:</b> Synthesis of compound <b>26</b> by alcoholysis of <b>25</b> .	<b>26</b>
<b>Scheme 22:</b> Synthesis of <b>27</b> .	<b>26</b>
<b>Scheme 23:</b> Synthesis of compound <b>28</b> .	<b>27</b>
<b>Scheme 24:</b> Synthesis of compound <b>29</b> .	<b>27</b>
<b>Scheme 25:</b> Synthesis of compounds <b>30-33</b> .	<b>28</b>

## 6. Appendix

<b>Scheme 26:</b> Synthesis of complex <b>34</b> .	<b>29</b>
<b>Scheme 27:</b> Synthesis of <b>34</b> and <b>35</b> .	<b>30</b>
<b>Scheme 28:</b> Synthesis of compound <b>40</b> .	<b>31</b>
<b>Scheme 29:</b> Synthesis of <b>41</b> .	<b>31</b>
<b>Scheme 30:</b> Synthesis of compound <b>25</b> , <b>43</b> and <b>44</b> .	<b>33</b>
<b>Scheme 31:</b> Reaction of compounds <b>25</b> and <b>44</b> with <i>tert</i> -butyl isocyanide to afford compounds <b>45</b> and <b>46</b> .	<b>35</b>
<b>Scheme 32:</b> Synthesis of compounds <b>47-49</b> .	<b>36</b>
<b>Scheme 33:</b> Equilibrium of compound <b>47</b> in solution.	<b>37</b>
<b>Scheme 34:</b> Equilibrium of compound <b>28</b> in the presence of Lewis base like <i>tert</i> -butyl isocyanide.	<b>37</b>
<b>Scheme 35:</b> Synthesis of compound <b>53</b> .	<b>38</b>
<b>Scheme 36:</b> Monomer-dimer equilibrium of compound <b>53</b> .	<b>39</b>
<b>Scheme 37:</b> Synthesis of compounds <b>54</b> and <b>55</b> .	<b>40</b>
<b>Scheme 38:</b> Synthesis of <b>57</b> .	<b>42</b>
<b>Scheme 39:</b> Synthesis of <b>59</b> .	<b>43</b>
<b>Scheme 40:</b> Synthesis of compounds <b>60</b> and <b>61</b> .	<b>43</b>
<b>Scheme 41:</b> Synthesis of compound <b>62</b> .	<b>44</b>
<b>Scheme 42:</b> Reactions of <b>62</b> with different substrates.	<b>44</b>
<b>Scheme 43:</b> Synthesis of compound <b>63</b> .	<b>45</b>
<b>Scheme 44:</b> Synthesis of compounds <b>64</b> and <b>65</b> .	<b>45</b>
<b>Scheme 45:</b> Rearrangement of compound <b>65</b> into compound <b>66</b> .	<b>46</b>
<b>Scheme 46:</b> Synthesis of compound <b>68</b> .	<b>46</b>
<b>Scheme 47:</b> Synthesis of compound <b>69</b> .	<b>47</b>
<b>Scheme 48:</b> Synthesis of complex <b>71</b> .	<b>47</b>
<b>Scheme 49:</b> Synthesis of complex <b>73</b> .	<b>48</b>
<b>Scheme 50:</b> Reaction of different azide substrates with compounds <b>71</b> and <b>73</b> .	<b>48</b>
<b>Scheme 51:</b> Reaction of compound <b>73</b> with unsaturated substrates via insertion reaction into the Al-Al bond.	<b>49</b>

## 6. Appendix

<b>Scheme 52:</b> Isomerization of <b>17</b> to dialane <b>78</b> .	<b>49</b>
<b>Scheme 53:</b> Synthesis of compound <b>79</b> .	<b>50</b>
<b>Scheme 54:</b> General representation of the synthesis of cyclic dialanes.	<b>53</b>
<b>Scheme 55:</b> Representation of the synthesis routes of aminoalane and phosphanylalane.	<b>55</b>
<b>Scheme 56:</b> Reaction of aminoalane and phosphanylalane compounds with small molecules.	<b>60</b>
<b>Scheme 57:</b> Reactivity of ambiphilic molecule $(R_2PCH_2AlMe_2)_2$ with $CO_2$ .	<b>62</b>
<b>Scheme 58:</b> Synthesis of compounds <b>106</b> and <b>107</b> .	<b>62</b>
<b>Scheme 59:</b> General mechanism of the $CO_2$ insertion into the Al-Pn bond.	<b>63</b>
<b>Scheme 60:</b> Synthesis of the different ansa-ligands <b>109-111</b> .	<b>66</b>
<b>Scheme 61:</b> Synthesis of magnesocenophanes <b>9,112</b> and <b>113</b> .	<b>68</b>
<b>Scheme 62:</b> Magnesocenophans catalyzed dehydrocoupling reaction of the dimethylamine borane.	<b>70</b>
<b>Scheme 63:</b> Synthesis of compounds <b>115-123</b> .	<b>71</b>
<b>Scheme 64:</b> Synthesis of compounds <b>115</b> and <b>116</b> by reacting <b>113</b> and dihalogenoalane·2thf.	<b>72</b>
<b>Scheme 65:</b> Synthesis of compound <b>124</b> .	<b>73</b>
<b>Scheme 66:</b> The reaction of compound <b>124</b> with CuCl and AuCl·tht.	<b>85</b>
<b>Scheme 67:</b> Synthesis of compound <b>125</b> .	<b>87</b>
<b>Scheme 68:</b> Reaction of compound <b>125</b> with element chloride to yield compound <b>53</b> .	<b>90</b>
<b>Scheme 69:</b> Reduction of <b>125</b> with potassium graphite.	<b>91</b>
<b>Scheme 70:</b> Reaction of <b>125</b> with two equivalents of $tBuNC$ to afford compound <b>128</b> .	<b>92</b>
<b>Scheme 71:</b> Synthesis of compounds <b>129</b> and <b>130</b> .	<b>100</b>
<b>Scheme 72:</b> Synthesis of compounds <b>131</b> and <b>99</b> .	<b>107</b>
<b>Scheme 73:</b> Synthesis of compounds <b>132-139</b> .	<b>110</b>
<b>Scheme 74:</b> Synthesis of compounds <b>140-144</b> .	<b>117</b>
<b>Scheme 75:</b> Suggested behaviour of compounds <b>131</b> and <b>99</b> in solution.	<b>120</b>

## 6. Appendix

<b>Scheme 76:</b> Suggested behaviour of compounds <b>135</b> and <b>139</b> in solution.	<b>122</b>
<b>Scheme 77:</b> Fixation of CO <sub>2</sub> molecule by CAAC in solution at room temperature.	<b>122</b>
<b>Scheme 78:</b> Synthesis of Polyferrocenylmethylene <b>146</b> .	<b>123</b>
<b>Scheme 79:</b> Representation of the new synthesized compounds starting from different magnesocenophanes.	<b>132</b>
<b>Scheme 80:</b> Representation of the pnictogenylalane compounds and their reactivity towards CO <sub>2</sub> .	<b>134</b>

## 6.3. List of Figures:

<b>Figure 1:</b> Structures of ferrocene <b>1</b> and magnesocene <b>2</b> .	<b>6</b>
<b>Figure 2:</b> Dissociation of magnesocene <b>2</b> in ethereal solution.	<b>8</b>
<b>Figure 3:</b> General illustration of a metallocenophane with a definition of the related angles.	<b>12</b>
<b>Figure 4:</b> Color in solution (hexane) of ferrocene and different [1]ferrocenophanes with the corresponding $\lambda_{\text{max}}$ and $\alpha$ -angle.	<b>12</b>
<b>Figure 5:</b> Various examples of different ferrocenophanes that undergo ROP.	<b>14</b>
<b>Figure 6:</b> General presentation of the bonding mode between aluminum and cyclopentadienyl ligand.	<b>15</b>
<b>Figure 7:</b> Structures of the metallocenium cations of boron, aluminum and gallium.	<b>15</b>
<b>Figure 8:</b> The dynamic sigmatropic rearrangement process in $\text{C}_5\text{H}_5\text{E}$ compounds.	<b>16</b>
<b>Figure 9:</b> Representation of energy of the sigmatropic rearrangement in $\text{C}_5\text{H}_5\text{E}$ compounds.	<b>17</b>
<b>Figure 10:</b> Presentation of the dimeric structure of $\text{Et}_2\text{AlCp}$ as suggested by <i>Giannini &amp; Cesca</i> .	<b>18</b>
<b>Figure 11:</b> A static structure of $\text{R}_2\text{Al}^{\text{Me}}\text{Cp}$ ( $\text{R} = \text{Me}, \text{Et}$ ) analogous to the suggestion of <i>Fritz</i> for stannane and plumbane based on VT- $^1\text{H}$ -NMR.	<b>19</b>
<b>Figure 12:</b> Suggested structures of $\text{Me}_2\text{AlCp}$ as monomer and polymer by <i>Haaland and Weidlein</i> .	<b>20</b>
<b>Figure 13:</b> Structure of $[(\mu\text{-Cp})\text{AlMe}_2]_n$ <b>12</b> in the solid state as cyclopentadienyl bridged polymeric.	<b>20</b>
<b>Figure 14:</b> Representation of the equilibrium between <b>8</b> and <b>8a</b> .	<b>21</b>
<b>Figure 15:</b> Representation of structures <b>19</b> , <b>20</b> .	<b>25</b>
<b>Figure 16:</b> Representation of compounds <b>35</b> and <b>36</b> .	<b>30</b>
<b>Figure 17:</b> Projection of Compound <b>42</b> .	<b>32</b>
<b>Figure 18:</b> A dynamic and temperature dependent equilibrium between the cations in compounds <b>41</b> and <b>42</b> .	<b>32</b>

## 6. Appendix

**Figure 19:** Representation of the two coordination isomers of compound **25** in the crystal.

**34**

**Figure 20:** Representation of the two possible depictions of *ansa*-ligand in compound **53**.

**40**

**Figure 21:** Representation of examples for acyclic symmetrically and dialanes. **51**

**Figure 22:** Representation of examples for acyclic asymmetrically and dialanes. **52**

**Figure 23:** Representation of examples for cyclic dialanes with corresponding Al-Al bond lengths. **54**

**Figure 24:** Representation of the lone pair donation of nitrogen into the vacant *p*-orbital in the boron. **55**

**Figure 25:** Presentation of instances of monomeric and oligomeric aminoalane structures with Al-N bond lengths (biph: biphenyl, tmp: *tetra*-methylpyridin, <sup>t</sup>Bu: *tert*-butyl, <sup>i</sup>Bu: *iso*-butyl).

**56**

**Figure 26:** Presentation of instances of monomeric and oligomeric phosphanylalane structures with Al-P bond lengths (Ad: 1-adamantyl, tmp: *tetra*-methylpyridin, <sup>t</sup>Bu: *tert*-butyl, <sup>i</sup>Bu: *iso*-butyl, Tip: 2,4,6-*tri-isopropylphenyl*). **57**

**Figure 27:** Orientation of the lone pair in R<sub>2</sub>Al-ER'<sub>2</sub> (E: pnictogen) compared with aminoalane and phosphanylalane compounds. **58**

**Figure 28:** Geometry of phosphorous in R<sub>2</sub>Al-PR'<sub>2</sub> a) planar and b) pyramidal. **58**

**Figure 29:** Qualitative energy diagram of the *p* orbitals of the aluminum, nitrogen and phosphorous fragments. **59**

**Figure 30:** Depiction of the amphoteric nature of amino- and phosphanylalane and the possible types of stabilization. **60**

**Figure 31:** Representation of aminoalane and phosphanylalane compounds with CO<sub>2</sub>-, CS<sub>2</sub>- and COS-insertion. **61**

**Figure 32:** Representation of the only instances of aluminocenophane derivatives until 2018. **64**

**Figure 33:** Representation of the scope of this doctoral thesis. **65**



## 6. Appendix

- Figure 34:** Representation of the isomers from the *ansa*-ligands **109-111** (**109**; E = Si, n = 2; **110**: E = C, n = 1; **111**: E = C, n = 2). **67**
- Figure 35:** Molecular structure of **113·dme** in the crystal (thermal ellipsoids for 50% probability level, H-atoms were omitted for clarity). **68**
- Figure 36:** <sup>1</sup>H NMR spectra of **113** and **113·dme** in C<sub>6</sub>D<sub>6</sub> by (398 K, 400 MHz)(•=C<sub>6</sub>HD<sub>5</sub> signal). **69**
- Figure 37:** Disproportionation of MgHCl. **72**
- Figure 38:** Molecular structure of compounds **115-118** in the crystals (thermal ellipsoids for 50% probability level, H-atoms were omitted for clarity). **74**
- Figure 39:** Molecular structure of compounds **119-124** in the crystals (thermal ellipsoids for 50% probability level, H-atoms were omitted for clarity). **75**
- Figure 40:** General representation of carba[1]- and sila[2]bis(cyclopentadienyl)aluminum with numbering on the cyclopentadienyl ligands. **76**
- Figure 41:** Molecular structure of **115** and **119** in the crystals, highlighting their six membered ring chair conformation (H-atoms were omitted for clarity). **76**
- Figure 42:** Molecular structure of **118** in the crystal, highlighting its five-membered ring envelope conformation (H-atoms were omitted for clarity). **77**
- Figure 43:** Molecular structure of **117** in the crystals, highlighting the symmetry of the molecules. **78**
- Figure 44:** <sup>1</sup>H NMR spectrum (400.13 MHz, C<sub>6</sub>D<sub>6</sub>, 298 K) (top) and <sup>13</sup>C{<sup>1</sup>H} NMR spectrum (100.62 MHz, C<sub>6</sub>D<sub>6</sub>, 298 K) (bottom) of **117** (• = C<sub>6</sub>HD<sub>5</sub> signal). **79**
- Figure 45:** Structure of compound **117** in solid state and in solution containing [1,5] Al sigma tropic rearrangement. **80**
- Figure 46:** Molecular structure of **118** and **121** in the crystals, highlighting the symmetry of the molecules in the solid state. **80**
- Figure 47:** <sup>1</sup>H NMR spectrum (400.13 MHz, C<sub>6</sub>D<sub>6</sub>, 298 K) (top) and <sup>13</sup>C{<sup>1</sup>H} NMR spectrum (100.62 MHz, C<sub>6</sub>D<sub>6</sub>, 298 K) (bottom) of **121** in solution (• = C<sub>6</sub>HD<sub>5</sub> signal). **81**
- Figure 48:** <sup>1</sup>H NMR spectrum (400.13 MHz, C<sub>6</sub>D<sub>6</sub>, 298 K) (top) and <sup>13</sup>C{<sup>1</sup>H} NMR spectrum (100.62 MHz, C<sub>6</sub>D<sub>6</sub>, 298 K) (bottom) of **118** in solution (• = C<sub>6</sub>HD<sub>5</sub> signal). **82**
- Figure 49:** Structures of compounds **115-124**. **83**
- Figure 50:** Molecular structure of **53**·[AlCl<sub>3</sub>·OEt<sub>2</sub>] in the crystal, (thermal ellipsoids for 50% probability level, H-atoms were omitted for clarity). **86**

## 6. Appendix

- Figure 51:** a) Molecular structure of **125** in the crystal; b) Molecular structure of **125** in crystal highlighting the trigonal planar geometry of aluminum centers, (thermal ellipsoids for 50% probability level, H-atoms were omitted for clarity). **88**
- Figure 52:** Molecular structure of **126** in the crystal, (thermal ellipsoids for 50% probability level, H-atoms were omitted for clarity). **88**
- Figure 53:** Representation of compounds **8**, **34** and **53**. **90**
- Figure 54:** Polymeric Molecular structure of **127** in the crystal, (thermal ellipsoids for 50% probability level, H-atoms were omitted for clarity). **91**
- Figure 55:** Examples of Lewis acid/base product of dialanes. **92**
- Figure 56:** Molecular structure of **128** in the crystal, highlighting the C<sub>2</sub>-rotation axis (H-atoms were omitted for clarity). **93**
- Figure 57:** Representation of compounds **24**, **28**, **29** and **46**. **94**
- Figure 58:** <sup>1</sup>H NMR spectrum (400.13 MHz, C<sub>6</sub>D<sub>6</sub>, 298 K) (top) and <sup>13</sup>C{<sup>1</sup>H} NMR spectrum (100.62 MHz, C<sub>6</sub>D<sub>6</sub>, 298 K) (bottom) of **128**. **95**
- Figure 59:** Structure of compound **128** in the solid state and in solution including sigma tropic rearrangement. **95**
- Figure 60:** Optimized structures of Al<sub>2</sub>Cl<sub>4</sub>, Al<sub>2</sub>H<sub>4</sub> and **125** at the M06-2X/def2-TZVPP (BP86+D3(BJ)/def2-TZVPP) [BP86/def2-TZVPP] level of theory (bond lengths in pm, hydrogen atoms of **125** were omitted). **96**
- Figure 61:** Kohn-Sham molecular orbitals HOMO-4 (left) and LUMO (right) of **125** (isovalue: 0.05) (calculations performed at M06-2X/def2-TZVPP). **97**
- Figure 62:** NBO-analysis of Al–Al bond in **125**, hybridization and occupation. (calculations carried out at M06-2X/def2-TZVPP). **98**
- Figure 63:** Suggested resonance structures of **125** predicted by on DFT calculations. **98**
- Figure 64:** Representation of the structures of **71**, **73** and **125** with the Al-Al bond lengths. **99**
- Figure 65:** <sup>1</sup>H NMR spectrum (400.13 MHz, C<sub>6</sub>D<sub>6</sub>, 298 K) a: **131**; b:**132**. **101**
- Figure 66:** Representation of phosphanylalanes **93-96** highlighting the <sup>31</sup>P NMR shifts. **102**
- Figure 67:** Molecular structure of **129** and **130** in the crystal, (thermal ellipsoids for 50% probability level, H-atoms were omitted for clarity). **102**

## 6. Appendix

- Figure 68:** a) NBO results of **129** at B3LYP+D3(BJ)/def2-TZVP level of theory representing Al-N bond, lone pair (LP) at N, and lone vacancy (LV) at Al (isovalue = 0.05 pm); b) Laplacian distribution of the electron, contour line diagrams of the Laplacian distribution  $\nabla^2\rho(r)$  on and perpendicular to the C-Al-N plane. **105**
- Figure 69:** a) NBO results of **130** at B3LYP+D3(BJ)/def2-TZVP level of theory representing Al-P bond, lone pair (LP) at P, and lone vacancy (LV) at Al (isovalue = 0.05 pm); b) Laplacian distribution of the electron, contour line diagrams of the Laplacian distribution  $\nabla^2\rho(r)$  on and perpendicular to the C-Al-P plane. **105**
- Figure 70:** KS- Frontier Molecular Orbitals of a) **129** and b) **130** at B3LYP-D3(BJ)/def2-TZVP level of theory (isovalue 0.03). Hydrogen atoms were omitted for clarity. **106**
- Figure 71:** Molecular structure of **131** in the crystal, (thermal ellipsoids for 50% probability level, H-atoms were omitted for clarity). **108**
- Figure 72:** Calculated relative Gibbs free energies ( $\Delta G$ , kJ mol<sup>-1</sup>) for monomers, dimers and trimers of (diphenylamino)dimethylalane and (diphenylphosphanyl)dimethylalane at the B3LYP-D3(BJ)/def2-TZVP level of theory. **109**
- Figure 73:** Molecular structure of **132-135** in the crystal, (thermal ellipsoids for 50% probability level, H-atoms were omitted for clarity). **112**
- Figure 74:** Molecular structure of **136-139** in the crystal, (thermal ellipsoids for 50% probability level, H-atoms were omitted for clarity). **113**
- Figure 75:** General representation of the structure **132-139** highlighting the angle  $\gamma$ :  $\angle D-Al-P_n$  between the coordinated donors and the Al-P<sub>n</sub> bonds. **114**
- Figure 76:** Molecular structure of **140** in the crystal, (thermal ellipsoids for 50% probability level, H-atoms were omitted for clarity). **118**
- Figure 77:** Molecular structure of **141-144** in the crystal, (thermal ellipsoids for 50% probability level, H-atoms were omitted for clarity). **119**
- Figure 78:** Calculated Gibbs free energy profile for the reaction of a) **131** with CO<sub>2</sub> and b) **99** with CO<sub>2</sub> (calculated at B3LYP+D3(BJ)/def2-TZVP; energies given in kJ·mol<sup>-1</sup>). **121**
- Figure 79:** <sup>1</sup>H NMR spectrum (400.13 MHz, CDCl<sub>3</sub>, 298 K) (top) and <sup>13</sup>C {<sup>1</sup>H} NMR spectrum (100.62 MHz, CDCl<sub>3</sub>, 298 K) (bottom) of PFM **146**. **124**
- Figure 80:** Size exclusion chromatography (SEC) spectra of **129** in thf versus PS standards using different precursors: Me<sub>2</sub>C[1]Cp<sub>2</sub>Li<sub>2</sub> + FeCl<sub>2</sub> (black line), Me<sub>2</sub>C[1]Cp<sub>2</sub>Li<sub>2</sub> + FeBr<sub>2</sub> (blue line), Me<sub>2</sub>C[1]Cp<sub>2</sub>Mg + FeCl<sub>2</sub> (green line) and Me<sub>2</sub>C[1]Cp<sub>2</sub>Mg + FeBr<sub>2</sub> (red line). **125**

## 6. Appendix

- Figure 81:** MALDI-ToF mass spectrum of PFM **129** of batch No. 3 Table 12 (Me<sub>2</sub>C[1]Cp<sub>2</sub>Mg + FeCl<sub>2</sub> reaction) (repeat unit: 226 Da). **126**
- Figure 82:** Representation of the repeat unit in MALDI-ToF mass spectroscopy. **126**
- Figure 83:** Cyclic hexamer of PFM **147** in the crystal (thermal ellipsoids for 50% probability level, H-atoms were omitted for clarity). **127**
- Figure 84:** Representation of the oligomeric structures of Me<sub>2</sub>Si-ferrocene. **128**
- Figure 85:** A) DSC thermogram of PFM; B) TGA curves of PFM **146** in an atmosphere of nitrogen (N<sub>2</sub>, black curve) and synthetic air (SA, red curve) using a heating rate of 20 K·min<sup>-1</sup>, starting from 303 K to 873 K. **128**
- Figure 86:** X-ray diffraction pattern of the residues after thermogravimetric analysis and corresponding reference data. **129**
- Figure 87:** Cyclic voltammetry diagram of PFM **146** in a potential range of -0.1 V to +1.3 V vs. Ag/Ag<sup>+</sup> utilizing tetrabutylammonium hexafluorophosphate in tetrahydrofuran (A, B) and in acetonitrile (C, D). The scan rate is given within the cyclic voltammogram. **130**

## 6.3. List of Tables:

<b>Table 1:</b> Bond lengths of $\sigma$ -bonds Al-Cp, Al-Cp', Al-D and Al-X in compounds <b>115-124</b> .	<b>78</b>
<b>Table 2:</b> Calculated bond strengths of complexes <b>115-124</b> .	<b>83</b>
<b>Table 3:</b> Bond lengths of compound <b>128</b> and <b>46</b> .	<b>94</b>
<b>Table 4:</b> Selected theoretical and experimental bond lengths [pm] and angles [°] in compound <b>125</b> .	<b>96</b>
<b>Table 5:</b> NBO results at the M06-2X/def2-TZVPP level of theory of compounds Al <sub>2</sub> H <sub>4</sub> , Al <sub>2</sub> Cl <sub>4</sub> and <b>125</b> : Wiberg bond order (P) and partial charges (q).	<b>97</b>
<b>Table 6:</b> Bond lengths and parameters of the crystal structures of compounds <b>129</b> and <b>130</b> .	<b>103</b>
<b>Table 7:</b> NBO results for <b>129</b> and <b>130</b> at B3LYP-D3(BJ)/def2-TZVP level of theory: partial charges (Q, in e) and Wiberg bond order (P, in a.u.)	<b>104</b>
<b>Table 8:</b> Characteristic <sup>1</sup> H- and <sup>31</sup> P-NMR shifts of compounds <b>99</b> and <b>131-139</b> in C <sub>6</sub> D <sub>6</sub> .	<b>111</b>
<b>Table 9:</b> Selected Parameters of the crystal structures of <b>99</b> and <b>132-139</b> with the calculated bond strength of Al-D.	<b>114</b>
<b>Table 10:</b> $\gamma$ angle of compounds <b>132-139</b> .	<b>115</b>
<b>Table 11:</b> <sup>13</sup> C{ <sup>1</sup> H} NMR shifts of the carbon atoms of the inserted CO <sub>2</sub> molecules in solution (100.62 MHz, C <sub>6</sub> D <sub>6</sub> , 298 K) and the IR shift in solid state.	<b>118</b>
<b>Table 12:</b> Molar masses and dispersity indices of the synthesized polyferrocenylmethylenes using different cyclopentadiene transfer reagents and different iron precursors.	<b>124</b>

## 7. References

### 7. References

- 1 W. F. McDonough and S.-S. Sun, *Chem. Geol.*, 1995, **120**, 223–253.
- 2 K. Lodders, *Astrophys. J.*, 2003, **591**, 1220–1247.
- 3 R. Benn and W. Hermann, *Angew. Chem. Int. Ed. Engl.*, 1991, **30**, 426–428.
- 4 R. Köster and P. Binger, in *Advances in Inorganic Chemistry and Radiochemistry*, eds. H. J. Emeléus and A. G. Sharpe, Academic Press, 1965, vol. 7, pp. 263–348.
- 5 M. R. Mason, J. M. Smith, S. G. Bott and A. R. Barron, *J. Am. Chem. Soc.*, 1993, **115**, 4971–4984.
- 6 A. P. Shreve, R. Mulhaupt, W. Fultz, J. Calabrese, W. Robbins and S. D. Ittel, *Organometallics*, 1988, **7**, 409–416.
- 7 K. J. Wynne and R. W. Rice, *Annu. Rev. Mater. Sci.*, 1984, **14**, 297–334.
- 8 P. Martin, R. Netterfield, T. Kinder and A. Bendavid, *Appl. Opt.*, 1992, **31**, 6734–6740.
- 9 R. Bensalem, A. Abid and B. J. Sealy, *Thin Solid Films*, 1986, **143**, 141–153.
- 10 V. M. Orera and R. I. Merino, *Bol. Soc. Esp. Cerámica Vidr.*, 2015, **54**, 1–10.
- 11 A. S. Wagh, in *Chemically Bonded Phosphate Ceramics (Second Edition)*, ed. A. S. Wagh, Elsevier, 2016, pp. 233–254.
- 12 C. C. Tin, Y. Song, T. Isaacs-Smith, V. Madangakli and T. S. Sudarshan, *J. Electron. Mater.*, 1997, **26**, 212–216.
- 13 A. N. Cleland, M. Pophristic and I. Ferguson, *Appl. Phys. Lett.*, 2001, **79**, 2070–2072.
- 14 V. Nesterov, D. Reiter, P. Bag, P. Frisch, R. Holzner, A. Porzelt and S. Inoue, *Chem. Rev.*, 2018, **118**, 9678–9842.
- 15 A. Doddi, M. Peters and M. Tamm, *Chem. Rev.*, 2019, **119**, 6994–7112.
- 16 P. Andrews, C. M. Latham, M. Magre, D. Willcox and S. Woodward, *Chem. Commun.*, 2013, **49**, 1488–1490.
- 17 G. Schnee, A. Bolley, F. Hild, D. Specklin and S. Dagorne, *Catal. Today*, 2017, **289**, 204–210.
- 18 R. J. Haines and G. J. Leigh, *Chem. Soc. Rev.*, 1975, **4**, 155–188.
- 19 I. C. Watson, Y. Zhou, M. J. Ferguson, M. Kränzlein, B. Rieger and E. Rivard, *Z. Anorg. All. Chem.*, 2020, **646**, 547–551.
- 20 A. T. S. Wee, A. J. Murrell, N. K. Singh, D. O'Hare and J. S. Foord, *J. Chem. Soc. Chem. Commun.*, 1990, 11–13.
- 21 W. L. Gladfelter, D. C. Boyd and K. F. Jensen, *Chem. Mater.*, 1989, **1**, 339–343.
- 22 T. J. Kealy and P. L. Pauson, *Nature*, 1951, **168**, 1039–1040.
- 23 E. O. Fischer and W. Hafner, *Z. Naturforsch. B*, 1954, **9**, 503–504.
- 24 G. Wilkinson, F. A. Cotton and J. M. Birmingham, *J. Inorg. Nucl. Chem.*, 1956, **2**, 95–113.
- 25 E. Weiss and E. O. Fischer, *Z. Anorg. All. Chem.*, 1955, **278**, 219–224.
- 26 F. A. Cotton and L. T. Reynolds, *J. Am. Chem. Soc.*, 1958, **80**, 269–273.
- 27 W. A. Barber, *J. Inorg. Nucl. Chem.*, 1957, **4**, 373–374.
- 28 E. R. Lippincott, J. Xavier and D. Steele, *J. Am. Chem. Soc.*, 1961, **83**, 2262–2266.
- 29 A. Haaland, J. Luszytk, D. P. Novak, J. Brunvoll and K. B. Starowieyski, *J. Chem. Soc. Chem. Commun.*, 1974, 54–55.
- 30 W. Bünder and E. Weiss, *J. Organomet. Chem.*, 1975, **92**, 1–6.
- 31 V. T. Aleksanyan, I. A. Garbuzova, V. V. Gavrilenko and L. I. Zakharkin, *J. Organomet. Chem.*, 1977, **129**, 139–143.
- 32 T. Saito, *J. Chem. Soc. Chem. Commun.*, 1971, 1422–1422.

## 7. References

- 33 J. J. Eisch and R. Sanchez, *J. Organomet. Chem.*, 1985, **296**, c27–c31.
- 34 J. D. Dunitz and L. E. Orgel, *J. Chem. Phys.*, 1955, **23**, 954–958.
- 35 A. Xia, J. E. Knox, M. J. Heeg, H. B. Schlegel and C. H. Winter, *Organometallics*, 2003, **22**, 4060–4069.
- 36 A. Jaenschke, J. Paap and U. Behrens, *Organometallics*, 2003, **22**, 1167–1169.
- 37 R. Schwarz, M. Pejic, P. Fischer, M. Marinaro, L. Jörisen and M. Wachtler, *Angew. Chem. Int. Ed.*, 2016, **55**, 14958–14962.
- 38 M. Rask, G. Landgren, S. G. Andersson and Å. Lundberg, *J. Electron. Mater.*, 1988, **17**, 311–314.
- 39 M. Kondo, C. Anayama, H. Sekiguchi and T. Tanahashi, *J. Cryst. Growth*, 1994, **141**, 1–10.
- 40 H. S. Hull, A. F. Reid and A. G. Turnbull, *Inorg. Chem.*, 1967, **6**, 805–807.
- 41 C. Dohmeier, C. Robl, M. Tacke and H. Schnöckel, *Angew. Chem. Int. Ed. Engl.*, 1991, **30**, 564–565.
- 42 C. Dohmeier, C. Robl, M. Tacke and H. Schnöckel, *Angew. Chem.*, 1991, **103**, 594–595.
- 43 C. Dohmeier, D. Loos and H. Schnöckel, *Angew. Chem. Int. Ed. Engl.*, 1996, **35**, 129–149.
- 44 C. Dohmeier, D. Loos and H. Schnöckel, *Angew. Chem.*, 1996, **108**, 141–161.
- 45 K. L. Rinehart and R. J. Curby, *J. Am. Chem. Soc.*, 1957, **79**, 3290–3291.
- 46 C. Cremer, H. Jacobsen and P. Burger, *Chimia*, 1997, **51**, 650–653.
- 47 C. Cremer, H. Jacobsen and P. Burger, *Chimia*, 1997, **51**, 968.
- 48 C. L. Lund, J. A. Schachner, J. W. Quail and J. Müller, *Organometallics*, 2006, **25**, 5817–5823.
- 49 V. Bellas and M. Rehahn, *Angew. Chem. Int. Ed.*, 2007, **46**, 5082–5104.
- 50 P. Perrotin, P. J. Shapiro, M. Williams and B. Twamley, *Organometallics*, 2007, **26**, 1823–1826.
- 51 H.-R. H. Damrau, A. Geyer, M.-H. Prosenc, A. Weeber, F. Schaper and H.-H. Brintzinger, *J. Organomet. Chem.*, 1998, **553**, 331–343.
- 52 M. Schultz, C. D. Sofield, M. D. Walter and R. A. Andersen, *New J. Chem.*, 2005, **29**, 919–927.
- 53 P. J. Shapiro, S.-J. Lee, P. Perrotin, T. Cantrell, A. Blumenfeld and B. Twamley, *Polyhedron*, 2005, **24**, 1366–1381.
- 54 M. Westerhausen, N. Makropoulos, B. Wieneke, K. Karaghiosoff, H. Nöth, H. Schwenk-Kircher, J. Knizek and T. Seifert, *Eur. J. Inorg. Chem.*, 1998, **1998**, 965–971.
- 55 A. Antiñolo, R. Fernández-Galán, N. Molina, A. Otero, I. Rivilla and A. M. Rodríguez, *J. Organomet. Chem.*, 2009, **694**, 1959–1970.
- 56 K. L. Rinehart, A. K. Frerichs, P. A. Kittle, L. F. Westman, D. H. Gustafson, R. L. Pruett and J. E. McMahon, *J. Am. Chem. Soc.*, 1960, **82**, 4111–4112.
- 57 A. G. Osborne and R. H. Whiteley, *J. Organomet. Chem.*, 1975, **101**, C27–C28.
- 58 D. E. Herbert, U. F. J. Mayer and I. Manners, *Angew. Chem. Int. Ed.*, 2007, **46**, 5060–5081.
- 59 R. M. Shaltout, J. Y. Corey and N. P. Rath, *J. Organomet. Chem.*, 1995, **503**, 205–212.
- 60 T. K. Woo, L. Fan and T. Ziegler, *Organometallics*, 1994, **13**, 2252–2261.
- 61 R. Rulkens, D. P. Gates, D. Balaishtis, J. K. Pudelski, D. F. McIntosh, A. J. Lough and I. Manners, *J. Am. Chem. Soc.*, 1997, **119**, 10976–10986.
- 62 H. H. Brintzinger and D. Fischer, in *Polyolefins: 50 years after Ziegler and Natta II: Polyolefins by Metallocenes and Other Single-Site Catalysts*, ed. W. Kaminsky, Springer, Berlin, Heidelberg, 2013, pp. 29–42.
- 63 R. A. Musgrave, A. D. Russell and I. Manners, *Organometallics*, 2013, **32**, 5654–5667.
- 64 E. W. Neuse and H. Rosenberg, *J. Macromol. Sci. Part C*, 1970, **4**, 1–145.
- 65 D. A. Foucher, B. Z. Tang and I. Manners, *J. Am. Chem. Soc.*, 1992, **114**, 6246–6248.
- 66 H. Wang, W. Lin, K. P. Fritz, G. D. Scholes, M. A. Winnik and I. Manners, *J. Am. Chem. Soc.*, 2007, **129**, 12924–12925.
- 67 D. P. Puzzo, A. C. Arsenault, I. Manners and G. A. Ozin, *Angew. Chem. Int. Ed.*, 2009, **48**, 943–947.

## 7. References

- 68 F. Wurm, S. Hilf and H. Frey, *Chem. Eur. J.*, 2009, **15**, 9068–9077.
- 69 A. Natalello, A. Alkan, A. Friedel, I. Lieberwirth, H. Frey and F. R. Wurm, *ACS Macro Lett.*, 2013, **2**, 313–316.
- 70 B. V. K. J. Schmidt, J. Elbert, D. Scheid, C. J. Hawker, D. Klinger and M. Gallei, *ACS Macro Lett.*, 2015, **4**, 731–735.
- 71 F. Fleischhaker, A. C. Arsenault, V. Kitaev, F. C. Peiris, G. von Freymann, I. Manners, R. Zentel and G. A. Ozin, *J. Am. Chem. Soc.*, 2005, **127**, 9318–9319.
- 72 R. L. N. Hailes, A. M. Oliver, J. Gwyther, G. R. Whittell and I. Manners, *Chem. Soc. Rev.*, 2016, **45**, 5358–5407.
- 73 J. Song and G. J. Vancso, *Langmuir*, 2011, **27**, 6822–6829.
- 74 I. Korczagin, M. A. Hempenius, R. G. Fokink, M. A. Cohen Stuart, M. Al-Hussein, P. H. H. Bomans, P. M. Frederik and G. J. Vancso, *Macromolecules*, 2006, **39**, 2306–2315.
- 75 M. J. MacLachlan, M. Ginzburg, N. Coombs, N. P. Raju, J. E. Greedan, G. A. Ozin and I. Manners, *J. Am. Chem. Soc.*, 2000, **122**, 3878–3891.
- 76 J. Song, M. A. Hempenius, H. J. Chung and G. J. Vancso, *Nanoscale*, 2015, **7**, 9970–9974.
- 77 A. S. Abd-El-Aziz and I. Manners, *J. Am. Chem. Soc.*, 2007, **129**, 6962–6963.
- 78 E. W. Neuse, *J. Macromol. Sci. Part - Chem.*, 1981, **16**, 3–72.
- 79 R. Knapp, U. Velten and M. Rehahn, *Polymer*, 1998, **39**, 5827–5838.
- 80 I. Manners, *Synthetic Metal-Containing Polymers*, John Wiley & Sons, 2006.
- 81 D. A. Rider, K. A. Cavicchi, K. N. Power-Billard, T. P. Russell and I. Manners, *Macromolecules*, 2005, **38**, 6931–6938.
- 82 R. Rulkens, A. J. Lough, I. Manners, S. R. Lovelace, C. Grant and W. E. Geiger, *J. Am. Chem. Soc.*, 1996, **118**, 12683–12695.
- 83 R. Rulkens, Y. Ni and I. Manners, *J. Am. Chem. Soc.*, 1994, **116**, 12121–12122.
- 84 Y. Hatanaka, S. Okada, T. Minami, M. Goto and K. Shimada, *Organometallics*, 2005, **24**, 1053–1055.
- 85 K. H. Pannell, V. V. Dementiev, H. Li, F. Cervantes-Lee, M. T. Nguyen and A. F. Diaz, *Organometallics*, 1994, **13**, 3644–3650.
- 86 D. Foucher, R. Ziembinski, R. Petersen, J. Pudelski, M. Edwards, Y. Ni, J. Massey, C. R. Jaeger, G. J. Vancso and I. Manners, *Macromolecules*, 1994, **27**, 3992–3999.
- 87 D. A. Foucher, R. Ziembinski, B. Z. Tang, P. M. Macdonald, J. Massey, C. R. Jaeger, G. J. Vancso and I. Manners, *Macromolecules*, 1993, **26**, 2878–2884.
- 88 E. Khozeimeh Sarbisheh, J. Esteban Flores, B. J. Anderson, J. Zhu and J. Müller, *Organometallics*, 2017, **36**, 2182–2189.
- 89 N. Prabhakar Reddy, H. Yamashita and M. Tanaka, *J. Chem. Soc. Chem. Commun.*, 1995, **0**, 2263–2264.
- 90 K. Temple, F. Jäkle, J. B. Sheridan and I. Manners, *J. Am. Chem. Soc.*, 2001, **123**, 1355–1364.
- 91 Y. Ni, R. Rulkens, J. K. Pudelski and I. Manners, *Macromol. Rapid Commun.*, 1995, **16**, 637–641.
- 92 H. P. Withers, D. Seyferth, J. D. Fellmann, P. E. Garrou and S. Martin, *Organometallics*, 1982, **1**, 1283–1288.
- 93 N. Giannini and S. Cesca, *Gazz Chem Ital*, 1961, **91**, 597–599.
- 94 P. J. Shapiro, in *Group 13 Chemistry*, American Chemical Society, 2002, vol. 822, pp. 31–48.
- 95 P. H. M. Budzelaar, J. J. Engelberts and J. H. van Lenthe, *Organometallics*, 2003, **22**, 1562–1576.
- 96 S. A. Miller, J. A. Tebboth and J. F. Tremaine, *J. Chem. Soc. Resumed*, 1952, 632–635.
- 97 K. R. Flower and P. B. Hitchcock, *J. Organomet. Chem.*, 1996, **507**, 275–277.
- 98 E. O. Fischer and W. Pfab, *Z. Naturforsch. B*, 1952, **7**, 377–379.
- 99 H. Werner and A. Salzer, *Synth. React. Inorg. Met.-Org. Chem.*, 1972, **2**, 239–248.



## 7. References

- 100 P. J. Chirik, *Organometallics*, 2010, **29**, 1500–1517.
- 101 L. Y. Kuo, M. G. Kanatzidis, M. Sabat, A. L. Tipton and T. J. Marks, *J. Am. Chem. Soc.*, 1991, **113**, 9027–9045.
- 102 R. B. King and M. B. Bisnette, *J. Organomet. Chem.*, 1967, **8**, 287–297.
- 103 G. Wilkinson, M. Rosenblum, M. C. Whiting and R. B. Woodward, *J. Am. Chem. Soc.*, 1952, **74**, 2125–2126.
- 104 C. L. B. Macdonald, J. D. Gordon, A. Voigt and A. H. Cowley, *J. Am. Chem. Soc.*, 2000, **122**, 11725–11726.
- 105 C. Dohmeier, H. Schnöckel, U. Schneider, R. Ahlrichs and C. Robl, *Angew. Chem. Int. Ed. Engl.*, 1993, **32**, 1655–1657.
- 106 C. Dohmeier, H. Schnöckel, C. Robl, U. Schneider and R. Ahlrichs, *Angew. Chem.*, 1993, **105**, 1714–1716.
- 107 C. Dohmeier, H. Schnöckel, C. Robl, U. Schneider and R. Ahlrichs, *ChemInform*, 1994, **25**, 1.
- 108 C. T. Burns, D. S. Stelck, P. J. Shapiro, A. Vij, K. Kunz, G. Kehr, T. Concolino and A. L. Rheingold, *Organometallics*, 1999, **18**, 5432–5434.
- 109 M. Bochmann and D. M. Dawson, *Angew. Chem. Int. Ed. Engl.*, 1996, **35**, 2226–2228.
- 110 M. Bochmann and D. M. Dawson, *Angew. Chem.*, 1996, **108**, 2371–2373.
- 111 T. S. Piper and G. Wilkinson, *J. Inorg. Nucl. Chem.*, 1956, **3**, 104–124.
- 112 G. Wilkinson and T. S. Piper, *J. Inorg. Nucl. Chem.*, 1956, **2**, 32–37.
- 113 N. M. Sergeyev, *Prog. Nucl. Magn. Reson. Spectrosc.*, 1973, **9**, 71–144.
- 114 E. W. Abel, M. O. Dunster and A. Waters, *J. Organomet. Chem.*, 1973, **49**, 287–321.
- 115 R. B. Larrabee, *J. Organomet. Chem.*, 1974, **74**, 313–364.
- 116 F. Cotton A\_ and L. M. Jackman, *J. Mol. Struct.*, 1977, **36**, 170.
- 117 C. W. Spangler, *Chem. Rev.*, 1976, **76**, 187–217.
- 118 P. Jutzi, *Chem. Rev.*, 1986, **86**, 983–996.
- 119 J. W. Faller, H. H. Murray and M. Saunders, *J. Am. Chem. Soc.*, 1980, **102**, 2306–2309.
- 120 A. Haaland and J. Weidlein, *J. Organomet. Chem.*, 1972, **40**, 35–41.
- 121 Berhan. Tecele, P. W. R. Corfield and J. P. Oliver, *Inorg. Chem.*, 1982, **21**, 458–461.
- 122 H. D. Johnson, T. W. Hartford and C. W. Spangler, *J. Chem. Soc. Chem. Commun.*, 1978, 242a–242a.
- 123 A. J. Ashe, *J. Am. Chem. Soc.*, 1970, **92**, 1233–1235.
- 124 K. W. Egger and T. Li. James, *J. Organomet. Chem.*, 1971, **26**, 335–343.
- 125 E. W. Abel and M. O. Dunster, *J. Organomet. Chem.*, 1971, **33**, 161–167.
- 126 K. Mertz, F. Zettler, H. D. Hausen and J. Weidlein, *J. Organomet. Chem.*, 1976, **122**, 159–170.
- 127 C. Gaffney and P. G. Harrison, *J. Chem. Soc. Dalton Trans.*, 1982, **0**, 1055–1060.
- 128 W. R. Kroll and W. Naegele, *J. Chem. Soc. Chem. Commun.*, 1969, 246–247.
- 129 W. R. Kroll, J. R. McDivitt and W. Naegele, *Inorg. Nucl. Chem. Lett.*, 1969, **5**, 973–976.
- 130 H. P. Fritz and C. G. Kreiter, *J. Organomet. Chem.*, 1965, **4**, 313–319.
- 131 H. P. Fritz and K.-E. Schwarzahns, *Chem. Ber.*, 1964, **97**, 1390–1397.
- 132 C. Panattoni, G. Bombieri and U. Croatto, *Acta Crystallogr.*, 1966, **21**, 823–826.
- 133 E. Frasson, F. Menegus and C. Panattoni, *Nature*, 1963, **199**, 1087–1089.
- 134 D. A. Drew, A. Haaland, S. B. Christensen, L. Brehm and W. Nimmich, *Acta Chem. Scand.*, 1973, **27**, 3735–3745.
- 135 J. P. Oliver, *Adv. Organomet. Chem.*, 1977, **15**, 235–271.
- 136 W. Klemm, E. Voss and K. Geiersberger, *Z. Anorg. Allg. Chem.*, 1948, **256**, 15–24.

## 7. References

- 137 H.-J. Koch, S. Schulz, H. W. Roesky, M. Noltemeyer, H.-G. Schmidt, A. Heine, R. Herbst-Irmer, D. Stalke and G. M. Sheldrick, *Chem. Ber.*, 1992, **125**, 1107–1109.
- 138 S. Schulz, H. W. Roesky, H. J. Koch, G. M. Sheldrick, D. Stalke and A. Kuhn, *Angew. Chem. Int. Ed. Engl.*, 1993, **32**, 1729–1731.
- 139 A. Hofmann, T. Tröster, T. Kupfer and H. Braunschweig, *Chem. Sci.*, 2019, **10**, 3421–3428.
- 140 S. Schulz, H. W. Roesky, M. Noltemeyer and H.-G. Schmidt, *J. Organomet. Chem.*, 1995, **493**, 69–75.
- 141 P. R. Schonberg, R. T. Paine and C. F. Campana, *J. Am. Chem. Soc.*, 1979, **101**, 7726–7728.
- 142 P. R. Schonberg, R. T. Paine, C. F. Campana and E. N. Duesler, *Organometallics*, 1982, **1**, 799–807.
- 143 P. Jutzi, J. Dahlhaus, B. Neumann and H.-G. Stammler, *Organometallics*, 1996, **15**, 747–752.
- 144 P. Jutzi, J. Dahlhaus and M. Bangel, *J. Organomet. Chem.*, 1993, **460**, C13–C15.
- 145 J. D. Fisher, P. J. Shapiro, P. M. H. Budzelaar and R. J. Staples, *Inorg. Chem.*, 1998, **37**, 1295–1298.
- 146 J. D. Fisher, P. J. Shapiro, G. P. A. Yap and A. L. Rheingold, *Inorg. Chem.*, 1996, **35**, 271–272.
- 147 J. D. Fisher, M.-Y. Wei, R. Willett and P. J. Shapiro, *Organometallics*, 1994, **13**, 3324–3329.
- 148 J. D. Fisher, M.-Y. Wei, R. Willett and P. J. Shapiro, *Organometallics*, 1995, **14**, 4030–4030.
- 149 C. T. Burns, P. J. Shapiro, P. H. M. Budzelaar, R. Willett and A. Vij, *Organometallics*, 2000, **19**, 3361–3367.
- 150 S. Szumacher, I. Madura, J. Zachara, A. R. Kunicki, A. Cebulski and L. Jerzykiewicz, *J. Organomet. Chem.*, 2003, **669**, 64–71.
- 151 A. Kunicki, R. Sadowski and J. Zachara, *J. Organomet. Chem.*, 1996, **508**, 249–253.
- 152 J. D. Fisher, P. J. Shapiro, P. M. H. Budzelaar and R. J. Staples, *Inorg. Chem.*, 1998, **37**, 1295–1298.
- 153 D. P. Freyberg, J. L. Robbins, K. N. Raymond and J. C. Smart, *J. Am. Chem. Soc.*, 1979, **101**, 892–897.
- 154 J. Vollet, E. Baum and H. Schnöckel, *Organometallics*, 2003, **22**, 2525–2527.
- 155 P. Jutzi, D. Kanne and C. Krüger, *Angew. Chem. Int. Ed. Engl.*, 1986, **25**, 164–164.
- 156 P. Jutzi, D. Kanne and C. Krüger, *Angew. Chem.*, 1986, **98**, 163–164.
- 157 C. T. Burns, P. J. Shapiro, P. H. M. Budzelaar, R. Willett and A. Vij, *Organometallics*, 2000, **19**, 3361–3367.
- 158 U. Holtmann, P. Jutzi, T. Kühler, B. Neumann and H.-G. Stammler, *Organometallics*, 1999, **18**, 5531–5538.
- 159 M. Huber, A. Kurek, I. Krossing, R. Mülhaupt and H. Schnöckel, *Z. Anorg. Allg. Chem.*, 2009, **635**, 1787–1793.
- 160 J. D. Fisher, M.-Y. Wei, R. Willett and P. J. Shapiro, *Organometallics*, 1994, **13**, 3324–3329.
- 161 J. D. Fisher, P. H. M. Budzelaar, P. J. Shapiro, R. J. Staples, G. P. A. Yap and A. L. Rheingold, *Organometallics*, 1997, **16**, 871–879.
- 162 P. J. Shapiro, A. Vij, G. P. A. Yap and A. L. Rheingold, *Polyhedron*, 1995, **14**, 203–209.
- 163 P. J. Shapiro, *Coord. Chem. Rev.*, 1999, **189**, 1–17.
- 164 J. D. Fisher, M.-Y. Wei, R. Willett and P. J. Shapiro, *Organometallics*, 1994, **13**, 3324–3329.
- 165 K. Leszczyńska, I. Madura, A. R. Kunicki and J. Zachara, *J. Organomet. Chem.*, 2006, **691**, 5970–5979.
- 166 H. Lee, P. J. Desrosiers, I. Guzei, A. L. Rheingold and G. Parkin, *J. Am. Chem. Soc.*, 1998, **120**, 3255–3256.
- 167 D. Churchill, J. H. Shin, T. Hascall, J. M. Hahn, B. M. Bridgewater and G. Parkin, *Organometallics*, 1999, **18**, 2403–2406.
- 168 J. H. Shin and G. Parkin, *Chem. Commun.*, 1999, 887–888.
- 169 D. G. Churchill, B. M. Bridgewater and G. Parkin, *J. Am. Chem. Soc.*, 2000, **122**, 178–179.
- 170 W. Uhl, *Angew. Chem. Int. Ed. Engl.*, 1993, **32**, 1386–1397.
- 171 C. Dohmeier, D. Loos and H. Schnöckel, *Angew. Chem. Int. Ed. Engl.*, 1996, **35**, 129–149.

## 7. References

- 172 C. Dohmeier, D. Loos and H. Schnöckel, *Angew. Chem.*, 1996, **108**, 141–161.
- 173 N. Wiberg, K. Amelunxen, H. Nöth, M. Schmidt and H. Schwenk, *Angew. Chem. Int. Ed. Engl.*, 1996, **35**, 65–67.
- 174 N. Wiberg, K. Amelunxen, H. Nöth, M. Schmidt and H. Schwenk, *Angew. Chem.*, 1996, **108**, 110–112.
- 175 W. Uhl, *Z. Naturforsch. B*, 1988, **43**, 1113–1118.
- 176 R. J. Wehmschulte, K. Ruhlandt-Senge, M. M. Olmstead, H. Hope, B. E. Sturgeon and P. P. Power, *Inorg. Chem.*, 1993, **32**, 2983–2984.
- 177 M. A. Petrie, P. P. Power, H. V. R. Dias, K. Ruhlandt-Senge, K. M. Waggoner and R. J. Wehmschulte, *Organometallics*, 1993, **12**, 1086–1093.
- 178 X. He, R. A. Bartlett, M. M. Olmstead, K. Ruhlandt-Senge, B. E. Sturgeon and P. P. Power, *Angew. Chem. Int. Ed. Engl.*, 1993, **32**, 717–719.
- 179 X. He, R. A. Bartlett, M. M. Olmstead, K. Ruhlandt-Senge, B. E. Sturgeon and P. P. Power, *Angew. Chem.*, 1993, **105**, 761–762.
- 180 C. Pluta, K.-R. Pörschke, C. Krüger and K. Hildenbrand, *Angew. Chem. Int. Ed. Engl.*, 1993, **32**, 388–390.
- 181 C. Pluta, K.-R. Pörschke, C. Krüger and K. Hildenbrand, *Angew. Chem.*, 1993, **105**, 451–453.
- 182 W. Uhl, A. Vester, W. Kaim and J. Poppe, *J. Organomet. Chem.*, 1993, **454**, 9–13.
- 183 N. Wiberg, K. Amelunxen, T. Blank, H. Nöth and J. Knizek, *Organometallics*, 1998, **17**, 5431–5433.
- 184 N. Wiberg, H. Schuster, A. Simon and K. Peters, *Angew. Chem. Int. Ed. Engl.*, 1986, **25**, 79–80.
- 185 N. Wiberg, H. Schuster, A. Simon and K. Peters, *Angew. Chem.*, 1986, **98**, 100–101.
- 186 N. Wiberg, *Coord. Chem. Rev.*, 1997, **163**, 217–252.
- 187 I. L. Fedushkin, M. V. Moskalev, A. N. Lukoyanov, A. N. Tishkina, E. V. Baranov and G. A. Abakumov, *Chem. Eur. J.*, 2012, **18**, 11264–11276.
- 188 B. A. C. Bicho, C. Bruhn, R. Guthardt, N. Weyer and U. Siemeling, *Z. Anorg. Allg. Chem.*, 2018, **644**, 1329–1336.
- 189 R. J. Wright, A. D. Phillips and P. P. Power, *J. Am. Chem. Soc.*, 2003, **125**, 10784–10785.
- 190 S. G. Minasian and J. Arnold, *Chem. Commun.*, 2008, 4043–4045.
- 191 A. Hofmann, A. Lamprecht, O. F. González-Belman, R. D. Dewhurst, J. O. C. Jiménez-Halla, S. Kachel and H. Braunschweig, *Chem. Commun.*, 2018, **54**, 1639–1642.
- 192 T. Agou, K. Nagata, H. Sakai, Y. Furukawa and N. Tokitoh, *Organometallics*, 2012, **31**, 3806–3809.
- 193 T. Agou, K. Nagata and N. Tokitoh, *Angew. Chem. Int. Ed.*, 2013, **52**, 10818–10821.
- 194 T. Agou, K. Nagata and N. Tokitoh, *Angew. Chem.*, 2013, **125**, 11018–11021.
- 195 C. Cui, X. Li, C. Wang, J. Zhang, J. Cheng and X. Zhu, *Angew. Chem.*, 2006, **118**, 2303–2305.
- 196 C. Cui, X. Li, C. Wang, J. Zhang, J. Cheng and X. Zhu, *Angew. Chem. Int. Ed.*, 2006, **45**, 2245–2247.
- 197 P. Bag, A. Porzelt, P. J. Altmann and S. Inoue, *J. Am. Chem. Soc.*, 2017, **139**, 14384–14387.
- 198 C. C. Wang, M. Zaheeruddin and L. H. Spinar, *J. Inorg. Nucl. Chem.*, 1963, **25**, 326–327.
- 199 G. Fritz and G. Trenczek, *Z. Anorg. Allg. Chem.*, 1964, **331**, 206–215.
- 200 W. Cherry, N. Epiotis and W. T. Borden, *Acc. Chem. Res.*, 1977, **10**, 167–173.
- 201 P. Koelle and H. Noeth, *Chem. Rev.*, 1985, **85**, 399–418.
- 202 R. A. Bartlett, Hong. Chen, H. V. Rasika. Dias, M. M. Olmstead and P. P. Power, *J. Am. Chem. Soc.*, 1988, **110**, 446–449.
- 203 P. B. Hitchcock, H. A. Jasim, M. F. Lappert and H. D. Williams, *Polyhedron*, 1990, **9**, 245–251.
- 204 P. P. Power, *Angew. Chem. Int. Ed. Engl.*, 1990, **29**, 449–460.
- 205 A. Meller, *B Boron Compounds: 4th Supplement, Boron and Nitrogen*, Springer-Verlag, Berlin Heidelberg, 8th edn., 1991.

## 7. References

- 206 S. M. Stuczynski, R. L. Opila, P. Marsh, J. G. Brennan and M. L. Steigerwald, *Chem. Mater.*, 1991, **3**, 379–381.
- 207 B. Lee, W. T. Pennington and G. H. Robinson, *Inorganica Chim. Acta*, 1991, **190**, 173–178.
- 208 R. L. Wells, *Coord. Chem. Rev.*, 1992, **112**, 273–291.
- 209 R. T. Paine and H. Noeth, *Chem. Rev.*, 1995, **95**, 343–379.
- 210 P. J. Brothers and P. P. Power, in *Advances in Organometallic Chemistry*, eds. F. Gordon, A. Stone and R. West, Academic Press, 1996, vol. 39, pp. 1–69.
- 211 L. K. Krannich, C. L. Watkins, S. J. Schauer and C. H. Lake, *Organometallics*, 1996, **15**, 3980–3984.
- 212 R. L. Wells, R. A. Baldwin, P. S. White, W. T. Pennington, A. L. Rheingold and G. P. A. Yap, *Organometallics*, 1996, **15**, 91–97.
- 213 W. Uhl, J. Molter and R. Koch, *Eur. J. Inorg. Chem.*, 1999, **1999**, 2021–2027.
- 214 P. P. Power, *Chem. Rev.*, 1999, **99**, 3463–3504.
- 215 S. Schulz, *Coord. Chem. Rev.*, 2001, **215**, 1–37.
- 216 K. Knabel, H. Nöth and T. Seifert, *Z. Naturforsch. B*, 2002, **57**, 830–834.
- 217 R. C. Fischer and P. P. Power, *Chem. Rev.*, 2010, **110**, 3877–3923.
- 218 H. Nöth, *Angew. Chem. Int. Ed. Engl.*, 1988, **27**, 1603–1623.
- 219 H. Nöth, *Angew. Chem.*, 1988, **100**, 1664–1684.
- 220 A. Yasuda, S. Tanaka, K. Oshima, H. Yamamoto and H. Nozaki, *J. Am. Chem. Soc.*, 1974, **96**, 6513–6514.
- 221 K. Maruoka, M. Oishi and H. Yamamoto, *J. Org. Chem.*, 1993, **58**, 7638–7639.
- 222 J. S. Cha, S. Y. Kwon, O. O. Kwon, J. M. Kim and H. Song, *Bull. Korean Chem. Soc.*, 1996, **17**, 900–905.
- 223 D. Chakraborty and E. Y.-X. Chen, *Organometallics*, 2002, **21**, 1438–1442.
- 224 M. Uchiyama, H. Naka, Y. Matsumoto and T. Ohwada, *J. Am. Chem. Soc.*, 2004, **126**, 10526–10527.
- 225 H. Naka, M. Uchiyama, Y. Matsumoto, A. E. H. Wheatley, M. McPartlin, J. V. Morey and Y. Kondo, *J. Am. Chem. Soc.*, 2007, **129**, 1921–1930.
- 226 S. H. Wunderlich and P. Knochel, *Angew. Chem. Int. Ed.*, 2009, **48**, 1501–1504.
- 227 S. H. Wunderlich and P. Knochel, *Angew. Chem.*, 2009, **121**, 1530–1533.
- 228 R. G. Gordon, D. M. Hoffman and U. Riaz, *J. Mater. Res.*, 1991, **6**, 5–7.
- 229 K. J. L. Paciorek, J. H. Nakahara, L. A. Hoferkamp, C. George, J. L. Flippen-Anderson, R. Gilardi and W. R. Schmidt, *Chem. Mater.*, 1991, **3**, 82–87.
- 230 R. G. Gordon, U. Riaz and D. M. Hoffman, *J. Mater. Res.*, 1992, **7**, 1679–1684.
- 231 J. D. Masuda, A. J. Hoskin, T. W. Graham, C. Beddie, M. C. Fermin, N. Etkin and D. W. Stephan, *Chem. Eur. J.*, 2006, **12**, 8696–8707.
- 232 R. A. Fischer and J. Weiß, *Angew. Chem. Int. Ed.*, 1999, **38**, 2830–2850.
- 233 R. A. Fischer and J. Weiß, *Angew. Chem.*, 1999, **111**, 3002–3022.
- 234 W. E. Buhro, *Polyhedron*, 1994, **13**, 1131–1148.
- 235 United States, US5474591A, 1995.
- 236 A. H. Cowley and R. A. Jones, *Angew. Chem.*, 1989, **101**, 1235–1243.
- 237 R. L. Wells and W. L. Gladfelter, *J. Clust. Sci.*, 1997, **8**, 217–238.
- 238 A. H. Cowley and R. A. Jones, *Angew. Chem. Int. Ed. Engl.*, 1989, **28**, 1208–1215.
- 239 H. M. Manasevit, *J. Cryst. Growth*, 1972, **13–14**, 306–314.
- 240 P. Henke, T. Pankewitz, W. Klopper, F. Breher and H. Schnöckel, *Angew. Chem. Int. Ed.*, 2009, **48**, 8141–8145.
- 241 Y. Takahashi, K. Yamashita, S. Motojima and K. Sugiyama, *Surf. Sci.*, 1979, **86**, 238–245.

## 7. References

- 242 J. F. Janik, R. L. Wells, Young Victor G., A. L. Rheingold and I. A. Guzei, *J. Am. Chem. Soc.*, 1998, **120**, 532–537.
- 243 S. Schulz, in *Advances in Organometallic Chemistry*, Academic Press, 2003, vol. 49, pp. 225–317.
- 244 B. Neumüller and E. Irvani, *Coord. Chem. Rev.*, 2004, **248**, 817–834.
- 245 A. Y. Timoshkin, *Coord. Chem. Rev.*, 2005, **249**, 2094–2131.
- 246 T. J. Clark, K. Lee and I. Manners, *Chem. Eur. J.*, 2006, **12**, 8634–8648.
- 247 A. Staubitz, A. Presa Soto and I. Manners, *Angew. Chem. Int. Ed.*, 2008, **47**, 6212–6215.
- 248 A. Staubitz, A. Presa Soto and I. Manners, *Angew. Chem.*, 2008, **120**, 6308–6311.
- 249 A. Staubitz, A. P. M. Robertson and I. Manners, *Chem. Rev.*, 2010, **110**, 4079–4124.
- 250 H. Westenberg, J. C. Slootweg, A. Hepp, J. Kösters, S. Roters, A. W. Ehlers, K. Lammertsma and W. Uhl, *Organometallics*, 2010, **29**, 1323–1330.
- 251 C. Appelt, J. C. Slootweg, K. Lammertsma and W. Uhl, *Angew. Chem. Int. Ed.*, 2012, **51**, 5911–5914.
- 252 C. Appelt, J. C. Slootweg, K. Lammertsma and W. Uhl, *Angew. Chem.*, 2012, **124**, 6013–6016.
- 253 T. Holtrichter-Rößmann, C. Rösener, J. Hellmann, W. Uhl, E.-U. Würthwein, R. Fröhlich and B. Wibbeling, *Organometallics*, 2012, **31**, 3272–3283.
- 254 S. Roters, C. Appelt, H. Westenberg, A. Hepp, J. C. Slootweg, K. Lammertsma and W. Uhl, *Dalton Trans.*, 2012, **41**, 9033–9045.
- 255 S. Roters, A. Hepp, J. C. Slootweg, K. Lammertsma and W. Uhl, *Chem. Commun.*, 2012, **48**, 9616–9618.
- 256 C. Appelt, H. Westenberg, F. Bertini, A. W. Ehlers, J. C. Slootweg, K. Lammertsma and W. Uhl, *Angew. Chem. Int. Ed.*, 2011, **50**, 3925–3928.
- 257 C. Appelt, H. Westenberg, F. Bertini, A. W. Ehlers, J. C. Slootweg, K. Lammertsma and W. Uhl, *Angew. Chem.*, 2011, **123**, 4011–4014.
- 258 W. Uhl, C. Appelt, J. Backs, H. Westenberg, A. Wollschläger and J. Tannert, *Organometallics*, 2014, **33**, 1212–1217.
- 259 D. W. Stephan, *J. Am. Chem. Soc.*, 2015, **137**, 10018–10032.
- 260 D. W. Stephan, *Science*, 2016, **354**, aaf7229.
- 261 L. Keweloh, H. Klöcker, E.-U. Würthwein and W. Uhl, *Angew. Chem. Int. Ed.*, 2016, **55**, 3212–3215.
- 262 L. Keweloh, M. S. H. Klöcker, E.-U. Würthwein and W. Uhl, *Angew. Chem.*, 2016, **128**, 3266–3269.
- 263 H. S. Zijlstra, J. Pahl, J. Penafiel and S. Harder, *Dalton Trans.*, 2017, **46**, 3601–3610.
- 264 A. R. Jupp and D. W. Stephan, *Trends Chem.*, 2019, **1**, 35–48.
- 265 D. W. Stephan and G. Erker, *Angew. Chem. Int. Ed.*, 2015, **54**, 6400–6441.
- 266 D. W. Stephan and G. Erker, *Angew. Chem.*, 2015, **127**, 6498–6541.
- 267 H. Westenberg, J. C. Slootweg, A. Hepp, J. Kösters, S. Roters, A. W. Ehlers, K. Lammertsma and W. Uhl, *Organometallics*, 2010, **29**, 1323–1330.
- 268 K. M. Waggoner, M. M. Olmstead and P. P. Power, *Polyhedron*, 1990, **9**, 257–263.
- 269 D. R. Armstrong, F. J. Craig, A. R. Kennedy and R. E. Mulvey, *Chem. Ber.*, 1996, **129**, 1293–1300.
- 270 E. K. Styron, C. H. Lake, C. L. Watkins and L. K. Krannich, *Organometallics*, 1998, **17**, 4319–4321.
- 271 E. K. Styron, C. H. Lake, C. L. Watkins, L. K. Krannich, C. D. Incarvito and A. L. Rheingold, *Organometallics*, 2000, **19**, 3253–3256.
- 272 C. C. Wang, M. Zaheeruddin and L. H. Spinar, *J. Inorg. Nucl. Chem.*, 1963, **25**, 326–327.
- 273 H. Sonomura and T. Miyauchi, *Jpn. J. Appl. Phys.*, 1969, **8**, 1263.
- 274 S. Z. Beer, *J. Electrochem. Soc.*, 1969, **116**, 263.
- 275 M. R. Lorenz, R. Chicotka, G. D. Pettit and P. J. Dean, *Solid State Commun.*, 1970, **8**, 693–697.
- 276 O. T. Beachley and C. Tessier-Youngs, *Organometallics*, 1983, **2**, 796–801.
- 277 O. T. Beachley and L. Victoriano, *Organometallics*, 1988, **7**, 63–67.

## 7. References

- 278 S. A. Sangokoya, W. T. Pennington, G. H. Robinson and D. C. Hrcir, *J. Organomet. Chem.*, 1990, **385**, 23–31.
- 279 R. J. Wehmschulte and P. P. Power, *J. Am. Chem. Soc.*, 1996, **118**, 791–797.
- 280 U. Vogel, A. Y. Timoshkin and M. Scheer, *Angew. Chem. Int. Ed.*, 2001, **40**, 4409–4412.
- 281 U. Vogel, A. Y. Timoshkin and M. Scheer, *Angew. Chem.*, 2001, **113**, 4541–4544.
- 282 M. A. K. Weinhart, A. S. Lisovenko, A. Y. Timoshkin and M. Scheer, *Angew. Chem. Int. Ed.*, 2020, **59**, 5541–5545.
- 283 M. A. K. Weinhart, A. S. Lisovenko, A. Y. Timoshkin and M. Scheer, *Angew. Chem.*, 2020, **132**, 5586–5590.
- 284 D. C. Bradley, I. S. Harding, I. A. Maia and M. Motevalli, *J. Chem. Soc. Dalton Trans.*, 1997, 2969–2980.
- 285 S. D. Waezsada, C. Rennekamp, H. W. Roesky, C. Röpken and E. Parisini, *Z. Anorg. Allg. Chem.*, 1998, **624**, 987–990.
- 286 P. Shukla, A. H. Cowley, J. N. Jones, J. C. Gordon and B. L. Scott, *Dalton Trans.*, 2005, 1019–1022.
- 287 K. Yamamoto, Y. Shibata, Y. Kashiwa, A. Kondo, H. Tsurugi and K. Mashima, *Eur. J. Inorg. Chem.*, 2013, **2013**, 3821–3825.
- 288 M. A. Petrie, K. Ruhlandt-Senge and P. P. Power, *Inorg. Chem.*, 1993, **32**, 1135–1141.
- 289 P. J. Brothers, R. J. Wehmschulte, M. M. Olmstead, K. Ruhlandt-Senge, S. R. Parkin and P. P. Power, *Organometallics*, 1994, **13**, 2792–2799.
- 290 I. Krossing, H. Nöth, C. Tacke, M. Schmidt and H. Schwenk, *Chem. Ber.*, 1997, **130**, 1047–1052.
- 291 R. L. Wells, E. E. Foos, A. L. Rheingold, G. P. A. Yap, L. M. Liable-Sands and P. S. White, *Organometallics*, 1998, **17**, 2869–2875.
- 292 K. Knabel, I. Krossing, H. Nöth, H. Schwenk-Kircher, M. Schmidt-Amelunxen and T. Seifert, *Eur. J. Inorg. Chem.*, 1998, **1998**, 1095–1114.
- 293 M. Westerhausen, C. Birg, H. Nöth, J. Knizek and T. Seifert, *Eur. J. Inorg. Chem.*, 1999, **1999**, 2209–2214.
- 294 T. Habereeder, H. Nöth and R. T. Paine, *Eur. J. Inorg. Chem.*, 2007, **2007**, 4298–4305.
- 295 T. Yanagisawa, Y. Mizuhata and N. Tokitoh, *Inorganics*, 2019, **7**, 132.
- 296 F. Hengesbach, X. Jin, A. Hepp, B. Wibbeling, E.-U. Würthwein and W. Uhl, *Chem. – Eur. J.*, 2013, **19**, 13901–13909.
- 297 J. Niesmann, U. Klingebiel, M. Noltemeyer and R. Boese, *Chem. Commun.*, 1997, 365–366.
- 298 J. Niesmann, U. Klingebiel, C. Röpken, M. Noltemeyer and R. Herbst-Irmer, *Main Group Chem.*, 1998, **2**, 297–308.
- 299 J. F. Janik, E. N. Duesler, W. F. McNamara, Matthias. Westerhausen and R. T. Paine, *Organometallics*, 1989, **8**, 506–514.
- 300 M. A. Dureen and D. W. Stephan, *Dalton Trans.*, 2008, 4723–4731.
- 301 F. Dornhaus, S. Scholz, I. Sängler, M. Bolte, M. Wagner and H.-W. Lerner, *Z. Anorg. Allg. Chem.*, 2009, **635**, 2263–2272.
- 302 R. J. Wehmschulte, K. Ruhlandt-Senge and P. P. Power, *Inorg. Chem.*, 1994, **33**, 3205–3207.
- 303 R. D. Baechler and K. Mislow, *J. Am. Chem. Soc.*, 1970, **92**, 4758–4759.
- 304 J. M. Lehn, in *Dynamic Stereochemistry*, Springer, Berlin, Heidelberg, 1970, pp. 311–377.
- 305 A. Rauk, J. D. Andose, W. G. Frick, R. Tang and K. Mislow, *J. Am. Chem. Soc.*, 1971, **93**, 6507–6515.
- 306 J. M. Lehn and B. Munsch, *Mol. Phys.*, 1972, **23**, 91–107.
- 307 D. C. Ghosh, J. Jana and R. Biswas, *Int. J. Quantum Chem.*, 2000, **80**, 1–26.
- 308 C. C. Levin, *J. Am. Chem. Soc.*, 1975, **97**, 5649–5655.
- 309 W. Cherry, N. Epiotis and W. T. Borden, *Acc. Chem. Res.*, 1977, **10**, 167–173.
- 310 V. Špirko, S. Civiš, M. Ebert and V. Danielis, *J. Mol. Spectrosc.*, 1986, **119**, 426–432.

## 7. References

- 311 P. Pyykkö and M. Atsumi, *Chem. Eur. J.*, 2009, **15**, 186–197.
- 312 P. Schwerdtfeger, L. J. Laakkonen and P. Pyykkö, *J. Chem. Phys.*, 1992, **96**, 6807–6819.
- 313 J. A. Burrows, *Sci. Educ.*, 1941, **25**, 120–120.
- 314 B. L. Kormos and C. J. Cramer, *Inorg. Chem.*, 2003, **42**, 6691–6700.
- 315 M. A. K. Weinhart, A. S. Lisovenko, A. Y. Timoshkin and M. Scheer, *Angew. Chem. Int. Ed.*, 2020, **59**, 5541–5545.
- 316 C. Tessier-Youngs, C. Bueno, O. T. Beachley and M. R. Churchill, *Inorg. Chem.*, 1983, **22**, 1054–1059.
- 317 D. A. Atwood, L. Contreras, A. H. Cowley, R. A. Jones and M. A. Mardones, *Organometallics*, 1993, **12**, 17–18.
- 318 Beachley O. T., M. A. Banks, J. P. Kopasz and R. D. Rogers, *Organometallics*, 1996, **15**, 5170–5174.
- 319 F. Thomas, S. Schulz and M. Nieger, *Eur. J. Inorg. Chem.*, 2001, **2001**, 161–166.
- 320 M. Bodensteiner, A. Y. Timoshkin, E. V. Peresyphkina, U. Vogel and M. Scheer, *Chem. Eur. J.*, 2013, **19**, 957–963.
- 321 W. Uhl, J. S. Bruchhage, M. Willeke, A. Hepp and J. Kösters, *Eur. J. Inorg. Chem.*, 2016, **2016**, 2721–2730.
- 322 C.-C. Chang, B. Srinivas, W. Mung-Liang, C. Wen-Ho, M. Y. Chiang and H. Chung-Sheng, *Organometallics*, 1995, **14**, 5150–5159.
- 323 J. Boudreau, M.-A. Courtemanche and F.-G. Fontaine, *Chem. Commun.*, 2011, **47**, 11131–11133.
- 324 H. S. Zijlstra, J. Pahl, J. Penafiel and S. Harder, *Dalton Trans.*, 2017, **46**, 3601–3610.
- 325 T. W. Yokley, H. Tupkar, N. D. Schley, N. J. DeYonker and T. P. Brewster, *Eur. J. Inorg. Chem.*, 2020, **2020**, 2958–2967.
- 326 T. Habereeder, H. Nöth and R. T. Paine, *Eur. J. Inorg. Chem.*, 2007, 4298–4305.
- 327 C. E. Bethley, C. L. Aitken, C. J. Harlan, Y. Koide, S. G. Bott and A. R. Barron, *Organometallics*, 1997, **16**, 329–341.
- 328 G. J. Bullen and N. H. Clark, *J. Chem. Soc. Inorg. Phys. Theor.*, 1970, 992–996.
- 329 R. T. Paine and H. Noeth, *Chem. Rev.*, 1995, **95**, 343–379.
- 330 R. T. Paine and H. Noeth, *Chem. Rev.*, 1995, **95**, 343–379.
- 331 J. Faderl, B. Deobald, R. Guilard, H. Pritzkow and W. Siebert, *Eur. J. Inorg. Chem.*, 1999, **1999**, 399–404.
- 332 D. J. Brauer, H. Bürger, F. Dörrenbach, G. Pawelke and W. Weuter, *J. Organomet. Chem.*, 1989, **378**, 125–137.
- 333 W. Kaminsky, K. Külper, H. H. Brintzinger and F. R. W. P. Wild, *Angew. Chem. Int. Ed. Engl.*, 1985, **24**, 507–508.
- 334 L. Wirtz, W. Haider, V. Huch, M. Zimmer and A. Schäfer, *Chem. Eur. J.*, 2020, **26**, 6176–6184.
- 335 W. Haider, V. Huch and A. Schäfer, *Dalton Trans.*, 2018, **47**, 10425–10428.
- 336 S. Liu, A. M. Invergo, J. P. McInnis, A. R. Mouat, A. Motta, T. L. Lohr, M. Delferro and T. J. Marks, *Organometallics*, 2017, **36**, 4403–4421.
- 337 A. Schäfer, K. Rohe, A. Grandjean and V. Huch, *Eur. J. Inorg. Chem.*, 2017, 35–38.
- 338 P. Perrotin, P. J. Shapiro, M. Williams and B. Twamley, *Organometallics*, 2007, **26**, 1823–1826.
- 339 W. Haider, V. Huch, B. Morgenstern and A. Schäfer, *ChemistryOpen*, 2020, **9**, 1095–1099.
- 340 See experimental section for further details, .
- 341 D. J. Liptrot and P. P. Power, *Nat. Rev. Chem.*, 2017, **1**, 1–12.
- 342 C. Müller, A. Stahlich, L. Wirtz, C. Gretsche, V. Huch and A. Schäfer, *Inorg. Chem.*, 2018, **57**, 8050–8053.
- 343 S. Danés, C. Müller, L. Wirtz, V. Huch, T. Block, R. Pöttgen, A. Schäfer and D. M. Andrada, *Organometallics*, 2020, **39**, 516–527.
- 344 S. P. Green, C. Jones and A. Stasch, *Science*, 2007, **318**, 1754–1757.

## 7. References

- 345 S. J. Bonyhady, C. Jones, S. Nembenna, A. Stasch, A. J. Edwards and G. J. McIntyre, *Chem. Eur. J.*, 2010, **16**, 938–955.
- 346 S. J. Bonyhady, D. Collis, G. Frenking, N. Holzmann, C. Jones and A. Stasch, *Nat. Chem.*, 2010, **2**, 865–869.
- 347 W. Haider, D. M. Andrada, I.-A. Bischoff, V. Huch and A. Schäfer, *Dalton Trans.*, 2019, **48**, 14953–14957.
- 348 A. D. Russell, J. B. Gilroy, K. Lam, M. F. Haddow, J. N. Harvey, W. E. Geiger and I. Manners, *Chem. Eur. J.*, 2012, **18**, 8000–8003.
- 349 P. Jutzi and N. Burford, *Chem. Rev.*, 1999, **99**, 969–990.
- 350 W. Strohmeier, H. Landsfeld and F. Gernert, *Ber. Bundesges. Phys. Chem.*, 1962, **66**, 823–827.
- 351 B. O. Wagner and H. F. Ebel, *Tetrahedron*, 1970, **26**, 5155–5167.
- 352 R. E. Dinnebier, U. Behrens and F. Olbrich, *Organometallics*, 1997, **16**, 3855–3858.
- 353 M. Mocker, C. Robl and H. Schnöckel, *Angew. Chem. Int. Ed. Engl.*, 1994, **33**, 862–863.
- 354 M. Mocker, C. Robl and H. Schnöckel, *Angew. Chem.*, 1994, **106**, 946–948.
- 355 C. Klemp, C. Üffing, E. Baum and H. Schnöckel, *Z. Anorg. Allg. Chem.*, 2000, **626**, 1787–1791.
- 356 K. S. Klimek, C. Cui, H. W. Roesky, M. Noltemeyer and H.-G. Schmidt, *Organometallics*, 2000, **19**, 3085–3090.
- 357 Y. Zhao, Y. Liu, L. Yang, J.-G. Yu, S. Li, B. Wu and X.-J. Yang, *Chem. Eur. J.*, 2012, **18**, 6022–6030.
- 358 W. Chen, Y. Zhao, W. Xu, J.-H. Su, L. Shen, L. Liu, B. Wu and X.-J. Yang, *Chem. Commun.*, 2019, **55**, 9452–9455.
- 359 Y. Zhao, Y. Liu, L. Yang, J.-G. Yu, S. Li, B. Wu and X.-J. Yang, *Chem. – Eur. J.*, 2012, **18**, 6022–6030.
- 360 W. Chen, Y. Zhao, W. Xu, J.-H. Su, L. Shen, L. Liu, B. Wu and X.-J. Yang, *Chem. Commun.*, 2019, **55**, 9452–9455.
- 361 W. Uhl and F. Hannemann, *Eur. J. Inorg. Chem.*, 1999, **1999**, 201–207.
- 362 C. Müller, D. M. Andrada, I.-A. Bischoff, M. Zimmer, V. Huch, N. Steinbrück and A. Schäfer, *Organometallics*, 2019, **38**, 1052–1061.
- 363 J. Hey, D. M. Andrada, R. Michel, R. A. Mata and D. Stalke, *Angew. Chem. Int. Ed.*, 2013, **52**, 10365–10369.
- 364 P. Pyykkö, *J. Phys. Chem. A*, 2015, **119**, 2326–2337.
- 365 A. L. Allred, *J. Inorg. Nucl. Chem.*, 1961, **17**, 215–221.
- 366 Y. Apeloig and M. Karni, *J. Am. Chem. Soc.*, 1984, **106**, 6676–6682.
- 367 L. Andersen, M. Dabney and H. A. Harris, *Main Group Met. Chem.*, 1994, **17**, 403–408.
- 368 G. Kuchenbeiser, M. Soleilhavoup, B. Donnadieu and G. Bertrand, *Chem. Asian J.*, 2009, **4**, 1745–1750.
- 369 D. A. Foucher, B. Z. Tang and I. Manners, *J. Am. Chem. Soc.*, 1992, **114**, 6246–6248.
- 370 A. S. Abd-El-Aziz, *Macromol. Rapid Commun.*, 2002, **23**, 995–1031.
- 371 R. A. Musgrave, R. L. N. Hailes, A. Schäfer, A. D. Russell, P. J. Gates and I. Manners, *Dalton Trans.*, 2018, **47**, 2759–2768.
- 372 T. Winter, W. Haider, A. Schießler, V. Presser, M. Gallei and A. Schäfer, *Macromol. Rapid Commun.*, 2021, **42**, 1–6.
- 373 M. Gallei, S. Tockner, R. Klein and M. Rehahn, *Macromol. Rapid Commun.*, 2010, **31**, 889–896.
- 374 M. Mazurowski, M. Gallei, J. Li, H. Didzoleit, B. Stühn and M. Rehahn, *Macromolecules*, 2012, **45**, 8970–8981.
- 375 C. Tonhauser, M. Mazurowski, M. Rehahn, M. Gallei and H. Frey, *Macromolecules*, 2012, **45**, 3409–3418.
- 376 J. D. Dunitz, L. E. Orgel and A. Rich, *Acta Crystallogr.*, 1956, **9**, 373–375.
- 377 P. F. Eiland and R. Pepinsky, *J. Am. Chem. Soc.*, 1952, **74**, 4971–4971.
- 378 F. Takusagawa and T. F. Koetzle, *Acta Crystallogr. B*, 1979, **35**, 1074–1081.



## 7. References

- 379 D. L. Zechel, D. A. Foucher, J. K. Pudelski, G. P. A. Yap, A. L. Rheingold and I. Manners, *J. Chem. Soc. Dalton Trans.*, 1995, 1893–1899.
- 380 D. E. Herbert, J. B. Gilroy, W. Y. Chan, L. Chabanne, A. Staubitz, A. J. Lough and I. Manners, *J. Am. Chem. Soc.*, 2009, **131**, 14958–14968.
- 381 C. Rüttiger, V. Pfeifer, V. Rittscher, D. Stock, D. Scheid, S. Vowinkel, F. Roth, H. Didzoleit, B. Stühn, J. Elbert, E. Ionescu and M. Gallei, *Polym. Chem.*, 2016, **7**, 1129–1137.
- 382 D. Scheid, G. Cherkashinin, E. Ionescu and M. Gallei, *Langmuir*, 2014, **30**, 1204–1209.
- 383 G. Mera, M. Gallei, S. Bernard and E. Ionescu, *Nanomaterials*, 2015, **5**, 468–540.
- 384 J. Elbert, H. Didzoleit, C. Fasel, E. Ionescu, R. Riedel, B. Stühn and M. Gallei, *Macromol. Rapid Commun.*, 2015, **36**, 597–603.
- 385 P. Nguyen, P. Gómez-Elipse and I. Manners, *Chem. Rev.*, 1999, **99**, 1515–1548.
- 386 G. Masson, P. Beyer, P. W. Cyr, A. J. Lough and I. Manners, *Macromolecules*, 2006, **39**, 3720–3730.
- 387 G. E. Southard and M. D. Curtis, *Organometallics*, 2001, **20**, 508–522.
- 388 D. L. Schmidt and E. E. Flagg, *Inorg. Chem.*, 1967, **6**, 1262–1265.
- 389 P. Andrews, C. M. Latham, M. Magre, D. Willcox and S. Woodward, *Chem. Commun.*, 2013, **49**, 1488–1490.
- 390 R. E. Ireland and D. M. Walba, *Org. Synth.*, 1977, **56**, 47–48.
- 391 D. W. Piotrowski, in *Encyclopedia of Reagents for Organic Synthesis*, American Cancer Society, 2001.
- 392 N. Kuhn and T. Kratz, *Synthesis*, 1993, **1993**, 561–562.
- 393 J. S. DePue and D. B. Collum, *J. Am. Chem. Soc.*, 1988, **110**, 5524–5533.
- 394 R. Jazzar, R. D. Dewhurst, J.-B. Bourg, B. Donnadiou, Y. Canac and G. Bertrand, *Angew. Chem.*, 2007, **119**, 2957–2960.
- 395 R. Jazzar, R. D. Dewhurst, J.-B. Bourg, B. Donnadiou, Y. Canac and G. Bertrand, *Angew. Chem. Int. Ed.*, 2007, **46**, 2899–2902.
- 396 V. Lavallo, Y. Canac, C. Präsang, B. Donnadiou and G. Bertrand, *Angew. Chem.*, 2005, **117**, 5851–5855.
- 397 V. Lavallo, Y. Canac, C. Präsang, B. Donnadiou and G. Bertrand, *Angew. Chem. Int. Ed.*, 2005, **44**, 5705–5709.
- 398 G. M. Sheldrick, *Acta Crystallogr. A*, 2008, **64**, 112–122.
- 399 W. Finckh, B. Z. Tang, D. A. Foucher, D. B. Zamble, R. Ziembinski, A. Lough and I. Manners, *Organometallics*, 1993, **12**, 823–829.
- 400 Gaussian 09 Revision D.01, M. J. Frisch, G. W. Trucks, H. B. Schlegel, G. E. Scuseria, M. A. Robb, J. R. Cheeseman, G. Scalmani, V. Barone, B. Mennucci, G. A. Petersson, H. Nakatsuji, M. Caricato, X. Li, H. P. Hratchian, A. F. Izmaylov, J. Bloino, G. Zheng, J. L. Sonnenberg, M. Hada, M. Ehara, K. Toyota, R. Fukuda, J. Hasegawa, M. Ishida, T. Nakajima, Y. Honda, O. Kitao, H. Nakai, T. Vreven, J. A. Montgomery, Jr., J. E. Peralta, F. Ogliaro, M. Bearpark, J. J. Heyd, E. Brothers, K. N. Kudin, V. N. Staroverov, T. Keith, R. Kobayashi, J. Normand, K. Raghavachari, A. Rendell, J. C. Burant, S. S. Iyengar, J. Tomasi, M. Cossi, N. Rega, J. M. Millam, M. Klene, J. E. Knox, J. B. Cross, V. Bakken, C. Adamo, J. Jaramillo, R. Gomperts, R. E. Stratmann, O. Yazyev, A. J. Austin, R. Cammi, C. Pomelli, J. W. Ochterski, R. L. Martin, K. Morokuma, V. G. Zakrzewski, G. A. Voth, P. Salvador, J. J. Dannenberg, S. Dapprich, A. D. Daniels, O. Farkas, J. B. Foresman, J. V. Ortiz, J. Cioslowski, D. J. Fox, Gaussian, Inc., Wallingford CT, **2013**.
- 401 a) A. D. Becke, *J. Chem. Phys.* 1993, **98**, 5648–5652; b) C. Lee, W. Yang, R. G. Parr, *Phys. Rev. B* 1988, **37**, 785–789; c) S. H. Vosko, L. Wilk, M. Nusair, *Can. J. Phys.* 1980, **58**, 1200–1211; d) P. J. Stephens, F. J. Devlin, C. F. Chabalowski, M. J. Frisch, *J. Phys. Chem.* 1994, **98**, 11623–11627; e) S. Grimme, J. Antony, S. Ehrlich, H. Krieg, *J. Chem. Phys.* 2010, **132**, 154104.

## 7. References

- 402 a) F. Weigend, R. Ahlrichs, *Phys. Chem. Chem. Phys.* 2005, **7**, 3297-3305; b) F. Weigend, *Phys. Chem. Chem. Phys.* 2006, **8**, 1057-1065.